HAL
archives-ouvertes.fr

Strategy for Selecting Input Ground Motion for Structural Seismic Demand Analysis

Levent Isbiliroglu

▶ To cite this version:

Levent Isbiliroglu. Strategy for Selecting Input Ground Motion for Structural Seismic Demand Analysis. Earth Sciences. Université Grenoble Alpes, 2018. English. NNT : 2018GREAU009 . tel-01809010

HAL Id: tel-01809010
https://tel.archives-ouvertes.fr/tel-01809010

Submitted on 6 Jun 2018

HAL is a multi-disciplinary open access archive for the deposit and dissemination of scientific research documents, whether they are published or not. The documents may come from teaching and research institutions in France or abroad, or from public or private research centers.

L'archive ouverte pluridisciplinaire **HAL**, est destinée au dépôt et à la diffusion de documents scientifiques de niveau recherche, publiés ou non, émanant des établissements d'enseignement et de recherche français ou étrangers, des laboratoires publics ou privés.

Communauté
UNIVERSITÉ Grenoble Alpes

THÈSE

Pour obtenir le grade de

DOCTEUR DE LA COMMUNAUTE UNIVERSITE GRENOBLE ALPES

Spécialité : **Sciences de la Terre, de l'Univers et de l'Environnement**

Arrêté ministériel : 25 mai 2016

Présentée par

Levent ISBILIROGLU

Thèse dirigée par **Philippe GUEGUEN** et
co-encadrée par **Maria LANCIERI**

préparée au sein de **l'Institut de Radioprotection et Sûreté Nucléaire (IRSN)** et **l'Institut des Sciences de la Terre (ISTerre)**
dans **Terre Univers Environnement**

Strategy for Selecting Input Ground Motion for Structural Seismic Demand Analysis*

Thèse soutenue publiquement le **01 mars 2018**,
devant le jury composé de :

M. Stéphane GRANGE
Professeur à l'INSA de Lyon, Président du Jury
M. John DOUGLAS
Maitre de conférences à l'University of Strathclyde, Rapporteur
M. Roberto PAOLUCCI
Professeur au Politecnico di Milano, Rapporteur
M. Luis-Fabian BONILLA
Directeur de recherche (DR) à l'IFSTTAR, Examinateur
M. Philippe GUEGUEN
DR à l' Communauté Université Grenoble Alpes, Directeur de thèse
Mme. Maria LANCIERI
Chargé de recherche, IRSN, Co-encadrante de thèse

*Élaboration de Stratégies de Sélection de Signaux Accélérométriques pour le Calcul du Comportement des Structures

SINAPS@
Séisme et Installations Nucléaires, Améliorer et Pérenniser la Sûreté

IRSN
INSTITUT DE RADIOPROTECTION ET DE SÛRETÉ NUCLÉAIRE

ISTerre
Institut des Sciences de la Terre

ABSTRACT

The observed variability is very large among the natural earthquake records. The earthquake record variability can be important to select and modify the input ground motions (GMs) for nonlinear dynamic analyses to obtain the engineering demand parameters (EDPs). In the current practice, the input spectral variability is minimized through the ground motion modifications because of the cost and the duration of the analyses, yet without clear impact on the output structural responses. The study, herein, aims at quantifying the impact of large spectral variability on the distribution of the EDPs. The following questions are discussed in the thesis:

What is the level of variability in the natural and the modified GMs?

What is the impact of the input GM variability on the EDPs of various structural types?

For a given deterministic earthquake scenario, we use a magnitude-distance bin (M7.0R40) to collect the unscaled earthquake records. A variety of ground motion prediction equations (GMPEs) is used to define the target spectra, which are necessary for the GM selection and modification. The GM modifications are applied over the unscaled earthquake records to collect (1) the linearly scaled earthquake GMs, (2) the loosely spectrum-matched GMs, and (3) the tightly spectrum-matched GMs. The nonlinear dynamic analyses of simple and complex structural models are then performed with the GM families. The EDPs, namely, the roof displacements, the base shear forces, the interstory drift ratios, and the global damage indices are gathered. The changes triggered by the GM modifications are evaluated relative to the unscaled earthquake records through the record-to-record comparison.

The response spectrum compatible selection is then performed to select five GMs, i.e., a GM set, from the magnitude-distance bin. Two types of set variability are considered in this study: (1) the intraset variability relates to the dispersion in a given set, and (2) the interset variability relates to the existence of multiple sets compatible with the target spectrum. The gathered input and output set distributions of the modified GMs are compared to the observed distributions of the unscaled earthquake records.

This thesis demonstrates that a single GM set, commonly used in the practice, is not sufficient to obtain an assuring level of the EDPs regardless of the GM selection and modification methods, which is due to the record and the set variability. The unscaled real records compatible with the scenario are discussed to be the most realistic option to use in the nonlinear dynamic analyses, and the ‘best’ GM selection and modification method is demonstrated to be specific to the EDP, the objective of the seismic analysis, and the structural model. It is pointed out that the choice of a GMPE can provoke significant differences in the GM characteristics and the EDPs. It can even overshadow the differences imposed by the GM modifications.

Keywords: accelerogram selection, dynamic analysis, seismic hazard, response spectrum, spectrum matching, linear scaling

RESUME

Les amplitudes spectrales des signaux accélérométriques enregistrés lors de l'occurrence d'un séisme présentent une forte variabilité ; telle variabilité n'est pas prise en compte dans l'analyse dynamique de la tenue des structures. En effet, la pratique courante est de minimiser (voir supprimer) la variabilité du mouvement sismique. Toutefois, les conséquences d'une telle opération sur la distribution des réponses de la structura ne sont pas clairement décrites. La présente étude a pour but la quantification de l'impact des méthodes de sélection et modification des accélérogrammes sur les résultats de l'analyse dynamique des structures (exprimée en termes d'engineering demand parameters EDPs). En particulier les questions suivantes sont investiguées : quel est le niveau de variabilité des accélérogrammes réels et comment ce niveau est modifié par les techniques couramment utilisées ? Quelle est l'impact de la variabilité sur la réponse de plusieurs types de structures ?

Pour un scénario déterministe de l'aléa, le spectre cible est défini sur la base d'équations de prédiction du mouvement sismique (GMPEs). Les accélérogrammes sont sélectionnés pour constituer des jeux de signaux de cinq accélérogrammes chacun, sur la base d'un critère de distance au spectre cible. La sélection est effectuée à partir de quatre familles d'accélérogrammes : les réels (tel qui enregistrés lors de l'occurrence du séisme); ceux mis à l'échelle linéairement ; ceux calés au spectre cible avec une tolérance large ; ceux calés au spectre cible avec une tolérance étroite. Deux sources de variabilité caractérisent les jeux de signaux : la variabilité au sein de chaque jeu de données (variabilité intraset), et la variabilité entre les différents jeux de données compatibles avec le même spectre cible (variabilité interset). Les analyses basées sur les signaux réels sont utilisées comme repère afin d'évaluer de combien la distribution des EDPs (exprimée en termes de valeur moyenne et écart type) est modifiée par les différentes méthodes testées. De plus nous avons investigué l'impact des hypothèses émises lors de la sélection des jeux d'accélérogrammes : la définition des plages de tolérance pour la définition de la distance au spectre cible, le nombre d'accélérogrammes constituant chaque jeu d'accélérogrammes, le nombre même de jeux d'accélérogrammes utilisés, ainsi que la cible de l'analyse structurale par rapport à la distribution d'EDP (moyenne, moyenne plus une fraction de l'écart type). Une attention particulière est portée à l'étude de sensibilité des résultats vis-à-vis du modèle de structure, allant du simple oscillateur à un degré de liberté à des structures aux géométries complexes. Dans l'étude nous investiguons également l'impact des GMPEs utilisées pour définir le spectre cible.

Ce travaille nous conduit à conclure que un seul jeu d'accélérogramme, tel qu'utilisé dans la pratique courante, est insuffisant pour estimer correctement la distribution d'EDPs. Cette conclusion est indépendante de la méthode de modification utilisée car aucune ne garde la variabilité des accélérogrammes réels. Si le but de l'analyse est d'estimer le niveau moyen de l'EDP, les quatre familles de signaux donnent des résultats équivalents. Si le but de l'analyse est d'estimer la moyenne des EDP plus une fraction de l'écart type, alors les signaux réels représentent l'option à privilégier. Si l'application d'une méthode de modification du signal s'avère nécessaire elle devrait être choisie en fonction du niveau d'EDP visé et de la complexité du modèle de structure. Finalement, le choix de la GMPE, utilisée pour définir le spectre cible, a un impact significatif sur les caractéristiques des mouvements sismiques et sur la distribution des EDPs. Dans certains cas, la variabilité des EDPs liée aux GMPEs couvre celle liée à l'utilisation des différentes techniques de modification.

Mots clés: Sélection d'accélégrammes, aléa sismiques analyse dynamique, spectre de réponse, calage spectral, mise à l'échelle lineaire

ACKNOWLEDGEMENTS

Doktora çalışmam boyunca, tek bir gün olsun desteğini eksik etmeyen biricik aileme: çok şanslıyım ve bu tez sizsiz mümkün olamazdı. (In English) This thesis would not be possible without the faith, the love, and the support of my parents, Sevim and Murat İşbiliroğlu, and my brother, Yigit Deniz İşbiliroğlu, who have been inspirational in the academic endeavor. Their faith and love have helped me to remain dedicated and motivated during my adaptation to the French culture and the language, the long-hours of study and data processing, and the uncomfortable moments before the tight deadlines.

This thesis would not be possible without the guidance, the encouragement, and the patience of my advisors, Maria Lancieri and Philippe Guéguen. I would like to thank to Maria Lancieri, my primary advisor, who had been supportive, committed, and concerned since my arrival to France. She taught me both the essential technical part (including Python) and the necessary background on the seismology to make a bridge with my structural engineering background. I would like to thank Philippe Guéguen for his supervision especially during my 8-month-long stay in Grenoble. He helped me to focus on the philosophical question out of the large data and the details. The balanced collaboration greatly reinforced the quality of the research.

This thesis would not be possible without the collaboration of Fernando Lopez-Caballero and Julien Clement. I am grateful to them as they shared their structural models (FLC for S1, S2, S3, S4, S9; and JC for S5) and helped me to collect the structural responses.

I really appreciate the valuable comments of Oona Scotti, Christophe Clement, and the BERRSIN team. It was a pleasure to be a part of such an inspirational and a good-humored équipe and the ‘office du banana’.

I am thankful to my supportive friends from Ankara, Auburn, ISTerre, and Paris. I was fortunate to share meaningful memories involving picnics in the lovely gardens and along the Seine, unfinished bottles of French wine, visits around the city, and the hiking in the charming Alpes.

The constructive suggestions of the thesis committee are appreciated as they improved the quality of the thesis.

I would like to extend my gratitude to SINAPS@ Project (ANR-11-RSNR-0022) for the main financial support (39 months) and IRSN for the complementary financial support.

TABLE OF CONTENTS

LIST OF ABBREVIATIONS

Δtop	Lateral (roof) displacements
ε	Epsilon, number of standard deviation
μ	Ductility demand with respect to roof displacements
σ	One standard deviation
Arias	Arias intensity (Arias, 1970)
ASCE	American Society of Civil Engineers
ASN	Autorité de Sûreté Nucléaire (The French Nuclear Safety Authority)
ASI	Acceleration Spectral Intensity (Von Thun et al., 1988)
ATC	Applied Technology Council
CESMD	Center for Engineering Strong Motion Data
COV	Coefficient of Variation
DI	Damage Index (Park and Ang, 1985)
EC8	Eurocode 8 (Eurocode 8, 2004)
EDP	Engineering Demand Parameter
EQ	Earthquake
EPRI	Electric Power Research Institute
FEMA	Federal Emergency Management Agency
GM	Ground Motion
GMPE	Ground Motion Prediction Equation
GMSM	Ground Motion Scaling and Modification
Housner	Housner intensity (Housner and Jennings, 1964)
IDR	Interstory Drift Ratio
IRSN	Institut de Radioprotection et de Sûreté´ Nucléaire (Institute for Radiation Protection and Nuclear Safety)

M	Magnitude
M7.0R40	Moment magnitude of 7.0 and hypocentral distance of 40 km
MA	Method A, Unscaled Earthquake Record-Based Method
MB	Method B, Linear Amplitude Scaling to Natural Frequency of a Structure
MC	Method C, Loosely Spectrum Matching
MD	Method D, Tightly Spectrum Matching
MDOF	Multi Degree of Freedom
NEHRP	National Earthquake Hazards Reduction Program
NIST	National Institute of Standards and Technology
ORFEUS	Observatories & Research Facilities for European Seismology
PEER	Pacific Earthquake Engineering Research Center
PGA	Peak Ground Acceleration
PGD	Peak Ground Displacement
PGV	Peak Ground Velocity
PSA	Pseudo-Spectral Accelerations
PSA (f0)	Pseudo-Spectral Accelerations at natural frequency (first mode) of a structure
R	Distance to the fault
RC	Reinforced Concrete
RESORCE	Reference Database for Seismic Ground-Motion Prediction in Europe
RFS	Règle Fondamentale de Sûreté (Basic Safety Rule)
RSPMatch09	Non-Stationary Spectral Matching Program (Al Atik and Abrahamson, 2010)
SCAV	Standardized cumulative absolute velocity (EPRI, 1991)
SDOF, SDF	Single Degree of Freedom
SEI	Structural Engineering Institute
SHA	Seismic Hazard Assessment
STD	Standard Deviation
Vbase	Base shear force
Vs30	Average shear-wave velocity of top 30 m of soil layer
Vs450	Average shear-wave velocity of top 30 m of soil layer for 450 m/s

GENERAL INTRODUCTION

The seismic analysis of structures is a chain of analyses ranging from the identification of a region's seismicity level to the estimation of the impact on the structures. It urges a bridge study between the seismology and the structural engineering; therefore, it is essential to integrate the seismic hazard assessment (SHA), the selection and modification of ground motions, and the numerical analysis of structures—herein, nonlinear dynamic analyses—as sketched in Figure 0.1. Finallly, th engineering demand parameters (EDPs) are collected to analyze the decisions about the structures (i.e., the design verification, the retrofit, the feasibility of a civil project, the demolition of a structure, etc.).

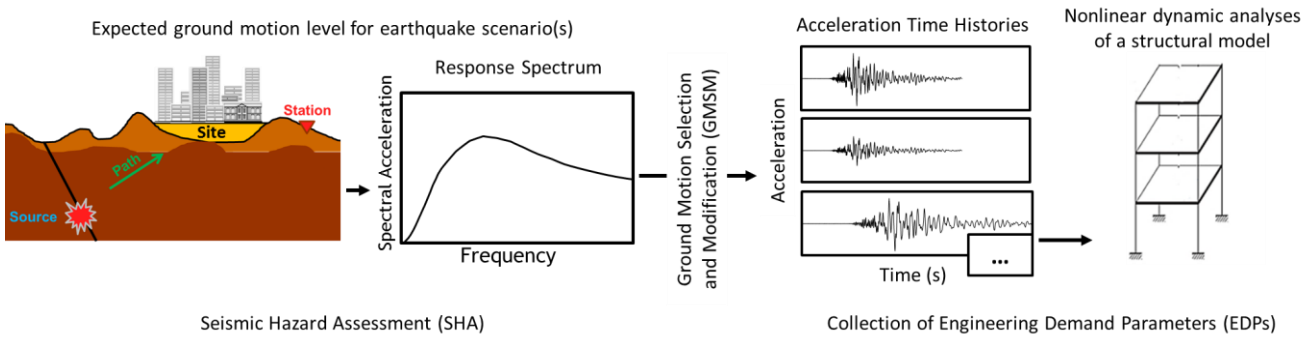

Figure 0.1: Sketch of the possible steps in the seismic analysis of structures

The SHA, the starting point of the seismic analysis, is the estimation of the expected ground motion level at a given site and is mainly performed by the seismologists. It can be deterministic (e.g., RFS 2001-01, 2001), probabilistic (e.g., ASCE/SEI 43-05), or code-based (e.g., Eurocode 8, 2004; ASCE/SEI 7, 2010). In general, the SHAs provide a smoothed response spectrum by the use of ground motion prediction equations (GMPEs) or design (or code) spectra.

A response spectrum, common in the engineering applications, is the collection of peak responses of elastic single-degree-of-freedom oscillators under a particular accelerogram for given oscillation frequencies and a damping ratio (Chopra, 2012). The smoothed response spectrum is the consequence of the fitting of numerous response spectra from recorded or generated data. The response spectrum representing the SHA is taken as a target to select the input seismic loading. The target response spectrum has typically large variability. It does not include the phase content of an accelerogram, which is necessary to retrieve a unique acceleration time history. In fact, a wide range of accelerograms can be possible for a given response spectrum and its variability. It means that the output of the SHA is not compatible alone with the engineering needs to retrieve ground motions (GMs, also referred as earthquake records, accelerograms, time histories, and waveforms), which are the necessary inputs of the nonlinear dynamic analyses.

The question on how to retrieve the GMs in compliance with the SHA has emerged the ground motion selection and modification (GMSM) methods. In the literature, there are at least forty methods to select and scale GMs (Haselton et al., 2009), and there has not been a consensus among the engineers and the seismologists on which method offers the best solution for the structural demand analyses.

The real earthquake records are the natural observations during an earthquake and are recorded by the seismograms. GM characteristics, such as the duration, the number of cycles, and the frequency and energy content, stem from a real earthquake event. The unscaled earthquake records preserve the natural characteristics, and they reveal the most realistic ground motions (e.g., Lai et al., 2012; Bommer and Acevedo, 2004).

The real earthquake records are available via the strong ground motion databases such as the Engineering Strong Motion database hosted by ORFEUS (Luzi et al., 2016), Resorce 2013 (Akkar et al., 2014), CESMD (Haddadi et al., 2012), and PEER NGA Databases (PEER, 2013; PEER, 2014). The real earthquake records can be selected in two main categories (Katsanos et al., 2010):

(A.1) Selection based on a refinement of earthquake records by ground motion database search

(A.1.1) With magnitude (M) and distance (R), i.e., a magnitude-distance bin
(A.1.2) With M, R and site-specific characteristics
(A.1.3) With intensity measures (IMs)

(A.2) Response spectrum compatible selection with real earthquake records (following Category A.1)
(A.2.1) Unscaled earthquake records (also referred as natural or original records)
(A.2.2) Linearly scaled earthquake records
(A.2.2.1) To structure-dependent IMs, i.e., PSA at the natural frequency of a structure (f0)
(A.2.2.2) To other reference IMs

The selection in Category A.1 represents the refinement of accelerograms based on a given earthquake scenario(s). There have been suggestions on the selection of a magnitude-distance range or site-specific GMs (Bommer and Acevedo, 2004; Katsanos et al., 2010) in Categories A.1.1 and A.1.2, but the impact of such suggestions have not been extended to the impact on structural responses.

The scalar and vector intensity measures (IMs) can be employed to search the strong motion database in Category A.1.3. The commonly used scalar IMs are peak ground acceleration (PGA), peak ground velocity (PGV), peak ground deformation (PGD), Arias intensity (Arias, 1970), standardized cumulative absolute velocity (SCAV; EPRI, 1991), acceleration spectral intensity (ASI; Von Thun et al., 1988), Housner intensity (Housner and Jennings, 1964), and pseudo-spectral acceleration (PSA). The commonly used vector IM is the combination of the PSA at the natural frequency of a structure with the number of standard deviation (i.e., epsilon). Some studies (e.g., Zhai et al., 2013; De Biasio et al., 2014; Lancieri et al., 2015; Kohrangi et al., 2016) have shown a good correlation between the certain IMs and the seismic behavior of structures, which motivate the use of IMs in the GM selection.

The unscaled records may not be available for some earthquake scenarios, such as the near-field events with large magnitudes (i.e., the moment magnitude greater than 5.5). They can also exhibit large variability and necessitate a good number of nonlinear dynamic analyses for a stable statistical distribution. The main drawback of the nonlinear dynamic analyses is the cost and the computational duration; thus, the selection by ground motion database search (i.e., Category A.1) is not directly preferred in the current practice.

The spectrum compatibility is commonly used to select a small number of GMs—in time-domain—by comparing their fitness with the target spectrum—in frequency-domain. Several building codes (e.g., Eurocode 8, 2004; ASN/2/01, 2006, ASCE/SEI 7, 2010) provide some guidance on the GM selection criteria. The studies have considered the effect of record-to-record and set-to-set variability (e.g., Sextos et al., 2011), and have proposed the metrics to quantify how well GM spectra match the target spectra (e.g., Ambraseys et al., 2004; Iervolino et al., 2010b). Generally, the decisions on how to tune the variability and which matching criteria to use are left to the engineers.

The spectrum compatible selection is exemplified in Figures 0.2.a and 0.2.b for (1) the unscaled earthquake records of Category A.2.1 and (2) the linearly scaled records of Category A.2.2, respectively. Each method attains goals from preserving the spectral variability to minimizing the spectral variability at a single frequency. The linear scaling of GMs (in Figure 0.2.b and Category A.2.2) improves the fitness of a spectrum relative to the target and may produce GMs for the rare earthquake events. The linear scaling can be performed with respect to the reference IMs (A.2.2.2) such as the PGA, PGV and PGD, and the structure-dependent IMs (A.2.2.1) such as the spectral amplitudes (PSA) at the natural frequency, f0, of a structure, PSA(f0).

Generating synthetic accelerograms, another axis of ground motion modification, can be categorized into four groups (Douglas and Aochi, 2008):

(B.1) Physics-based waveforms,

(B.2) Pure stochastic waveforms,

(B.3) Hybrid waveforms, and

(B.4) Spectrum-matched waveforms (illustrated in Figure 0.2.c).

The physics-based methods, in Category B.1, analytically model the fault rupture and the wave propagation. The pure stochastic methods, in Category B.2, calibrate the model parameters empirically. The hybrid methods, in Category B.3, can be the combination of the physics-based, stochastic, and real earthquake-based methods. The synthetic methods are mainly developed by the seismologists expect for the spectral matching in Category B.4, which is developed by the engineers.

The spectrum matching modifies the synthetic or real GMs by adjusting them in the frequency or time domain to match to a given target spectrum. It is one of the frequently used methods along with the pure stochastic method. The response spectrum compatible selection with the spectrum-matched waveforms is illustrated in Figure 0.2.c. It has a goal of minimizing spectral variability along a frequency range.

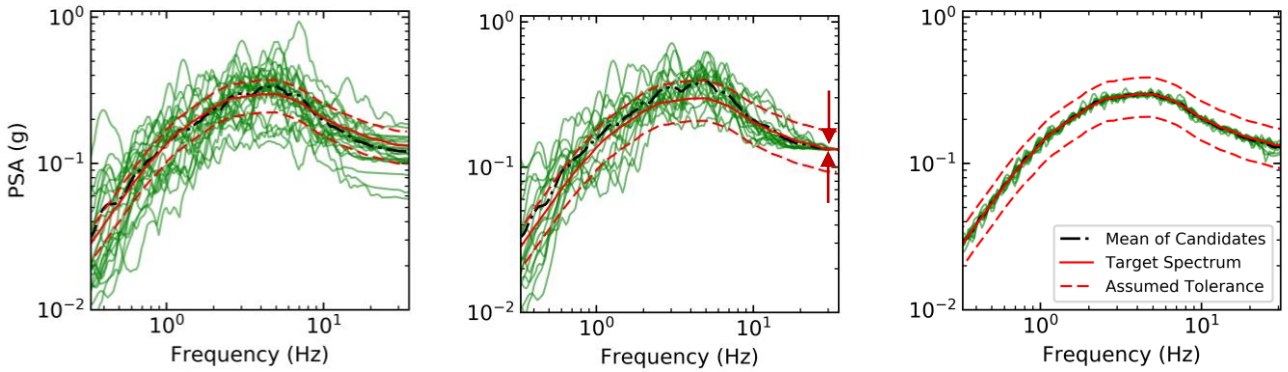

(a) Unscaled Earthquake Records (b) Linearly Scaled Records at PGA (c) Spectrum Matched Waveforms

Figure 0.2: Illustration of ground motion modification and selection. The GMs in (a) are unscaled earthquake records, the GMs in (b) are linearly scaled earthquake records, and the GMs in (c) are tightly matched waveforms. Response spectra of GMs are plotted with the green lines. The target spectrum is shown with the solid red line. The averages of the GM spectra, which are drawn with the dashed black lines, are within the (assumed) tolerances around the target spectrum, i.e., the red dashed lines. It means that the GMs in each case can be used. In the practice, the unscaled records preserving the spectral variability are not preferred due to its large variability.

In addition to the above-mentioned GMSM methods, the recent studies proposed alternative methods to cover the GM variability for the structural analyses despite the tendency of minimizing it. They have proposed approaches to capture the average and the variability of a target scenario(s). Jayaram et al. (2011) proposed the conditional spectrum that provides an expected response spectrum and its dispersion (by conditioning the occurrence of a target PSA at a single frequency instead of all frequencies as in the uniform hazard spectrum). Wang (2011) developed a method conditioning the conditional mean spectrum (Baker, 2011) on the specified seismological features such as the earthquake magnitude, the rupture distance, the type of the faulting, and the site conditions (by scaling GMs to the corresponding target spectra).

Ay and Akkar (2012) introduced a method that scales the GMs in a way to preserve the aleatory variability of GMs (rather than scaling them to a single spectral acceleration). Zentner (2014) introduced a pure stochastic method to generate artificial waveforms that capture the statistical distribution of target response spectrum by combining the methods of Baker (2011) and Wang (2011) and considering the reference power spectral density model.

After the collection of GMs in compliance with the SHA, the structural engineers perform the nonlinear dynamic analyses (also referred as response-history analysis). The outputs of the dynamic analysis are engineering demand

parameters (EDPs), such as lateral roof displacements, base shear forces, interstory drift ratios, element forces, and floor spectra.

The EDPs can be composed of a large volume of data, which necessitates the statistical analysis regarding the objective. Some objectives are the design, the probabilistic assessment, and the performance-based analysis of civil engineering buildings (NIST, 2011). The objective of the engineering application can require the use of (1) the mean (or median) of the EDP distribution (e.g., Eurocode 8, 2004; ASCE/SEI 7, 2010), (2) some higher tendencies (e.g., mean-plus-some-standard deviation in ASN/2/01 [2006]), or (3) the complete EDP distribution (e.g., ATC-58-1, 2011). The EDP distribution can be utilized to obtain the critical displacements and forces in a design project or to derive the curves (fragility) representing the probability of exceeding a performance level.

The primary challenge of the thesis is on how to select and modify accelerograms coherently with the prescribed seismic hazard analysis and suitably with the objective of nonlinear dynamic analyses. The studies in the literature have not converged to a common consensus on the 'best' strategy for selecting input accelerograms for a structural seismic demand analysis since they were limited to the specific scenarios, the structural models, the EDPs, and the objectives.

To illustrate, different conclusions are available for the impact of the linear scaling method on the nonlinear structural demands. Some studies have favored the use of the linear scaling. Shome et al. (1998) published one of the earliest studies broadening the perspectives in this field. They concluded that proper scaling does not introduce any bias and can reduce the number of dynamic analyses by a factor of about 4. Iervolino and Cornell (2005) found that a careful site-specific record selection is not necessary and the scenario-to-scenario record scaling does not cause any concerns for the GMs scaled to the target response spectrum.

The certain studies have shed lights on the importance of the level of linear scaling. Watson-Lamprey and Abrahamson (2006) showed that the limits on the linear scaling factor could be necessary if the GM selection depends on the magnitude, distance, and site condition. Also, the limits on the amplitude-scaling factor can be lifted whether the selection criteria are based on the characteristics of (scaled) ground motion or not. Luco and Bazzurro (2007) delivered similar conclusions based on the nonlinear structural drift responses of the single-degree-of-freedom oscillators and a multi-degree-of-freedom model. Huang et al. (2011) showed that the linear scaling at the natural frequency of the single-degree-of-freedom models provides unbiased estimates of the median responses.

Ay and Akkar (2013) compared three alternatives of linear amplitude-scaling methods such as (1) scaling to the target spectra by preserving the inherent uncertainty (Ay and Akkar, 2012), (2) scaling to the spectral ordinates of the conditional mean spectrum (Baker, 2011), and (3) scaling to the inelastic target level (Kalkan and Chopra, 2011). The former two methods showed similar performances relative to the benchmark and the latter one showed the least dispersion for the probabilistic damage states, which can be significant upon the objective.

Haselton et al. (2009) investigated a wide range of the real earthquake-based methods (in five main categories) and the MDOF structural models representing residential buildings designed in compliance with the US building codes. The linear scaling to the fundamental frequency was concluded to be the least accurate (i.e., the farthest from the benchmark) but the most precise (i.e., the least dispersed) method. Seifried and Baker (2016) evaluated the median EDPs of the single-degree-of-freedom models and a multi-degree-of-freedom model with the linear scaling and the spectrum matching. They concluded that the linear scaling can introduce bias regarding the conditional spectral variability, which can be due to the asymmetry of conditional spectral amplitudes at frequencies affecting the inelastic response.

Besides the linear amplitude scaling, there have been studies questioning the use of the spectrum matching. Heo et al. (2011) compared the impact of the linear scaling and the spectrum matching on the reinforced concrete moment frames. They showed that the linear scaling is less stable than the spectrum matching due to the bias and the dispersion of the EDPs. ATC (2011) investigated the GMSM methods based on the conditional spectrum and the spectrum matching; and the effects of near-fault GMs, and fault-rupture directivity. The results showed that the

spectrum-matched GMs do not introduce unconservative bias in the EDPs. The existing scaling methods were found inappropriate for the pulse-type motions.

Some of the studies have been skeptical on the spectrum matching. Carballo and Cornell (2000) investigated the displacement demands with the spectrum matching (for an earthquake scenario) and showed that the spectrum-matched waveforms can lead unconservative results. Iervolino et al. (2010a) observed underestimations of the peak displacement responses with the synthetic accelerograms based on the single-degree-of-freedom models. Huang et al. (2011) concluded that the spectrum matching underpredicts the median displacement demand and eliminates the dispersion relative to the benchmark based on a large family of the single-degree-of-freedom models. Seifried and Baker (2016) also concluded that the spectrum matching can introduce bias due to the asymmetry of spectral amplitudes of the structure's interest.

Causse et al. (2013) concluded that the variability in the structural responses is significant for the real earthquake records and the synthetic waveforms, even if the spectral accelerations are similar. They recommended keeping the variability of the ground motion characteristics (i.e., Arias and relative significant duration) for the synthetic waveforms. Also, Sextos (2014) pointed out that the findings on the GMSM methods are not reflected in the modern seismic codes.

In the practice, the input GM variability is reduced drastically to manage the cost and the project deadline. This study aims at quantifying the impact of large spectral variability in GM selection on the engineering demand parameters (EDPs). We analyze a deterministic seismic hazard assessment as a function of the ground motion prediction equations (GMPEs), the amplitude tolerances, the number of records used in a set, the input ground motion modifications, the objective of a structural analysis, and the structural models. The following questions are mainly discussed:

What is the level of variability in the natural and modified ground motions?

What is the impact of the input variability on the EDPs of various structural types?

The scope of the study is sketched in Figure 0.3. It includes four main categories: (1) gathering ground motions (with four methods), (2) conducting nonlinear dynamic analyses (with five complex and five simple structural models), (3) performing the spectrum compatible selection (with seven target spectra and various amplitude tolerance types), and (4) carrying out the statistical analyses (of input GM characteristics and output EDPs) for two objectives.

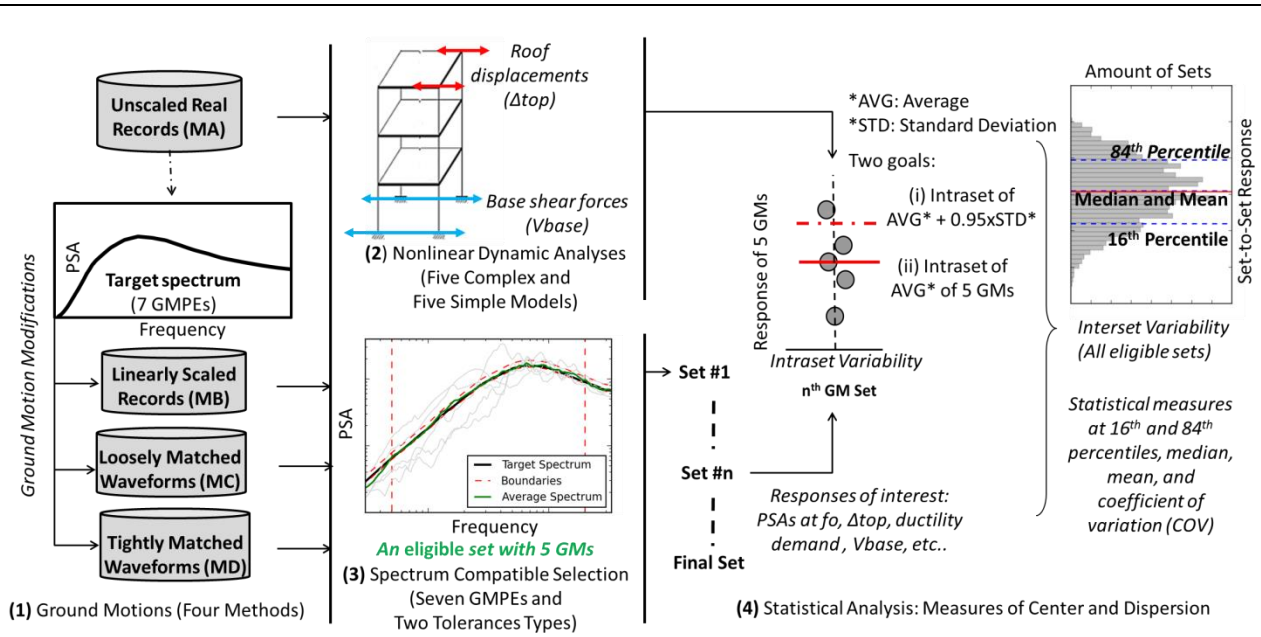

Figure 0.3: Scope of the thesis

In Part 1, we consider the unscaled earthquake records on the bases of the record and set variability with a simple structural model. We demonstrate the selection of unscaled earthquake records (Method A) and the response spectra for the scenario of moment magnitude 7.0, source-to-site distance 40.0 km, average 30-m shear wave velocity (Vs30) 450 m/s, and normal fault. We define the target spectra by seven GMPEs with the equivalent input parameters in compliance with the earthquake scenario. We then test the variability among the unscaled earthquake GMs and their impact on a single structural model. The effects of the site-specific characteristics such as the focal mechanism, the site conditions, and the limiting intensity measures are also presented. We perform the response spectrum compatible ground motion selection with various upper and lower amplitude tolerances (sigma-based tolerances, symmetric tolerances, and asymmetric tolerances), and the number of GMs and GM sets. Part 1 ends with the discussion on the impact of unscaled earthquake records on a single-degree-of-freedom model with the set-to-set variability.

In Part 2, we compare the GMSM methods on the response of simple and complex structural models through the record-to-record variability. Part 2 does not include the spectrum compatible selection (i.e., the set-to-set comparison). In Part 2, we define (1) the linearly scaled earthquake records, (2) the loosely spectrum-matched waveforms, and (3) the tightly spectrum-matched waveforms. We consider the 8-, 7-, 2-, and 1-story reinforced concrete models, the 2-story masonry model, and the five simple structural models with a fundamental frequency ranging from 0.6 Hz to 5.7 Hz. We perform the nonlinear dynamic analyses to obtain the EDPs. Part 2 ends with the discussion on the impacts of the GM modifications on the EDPs in comparison with the unscaled EQ records.

In Part 3, we extend the comparisons of the GMSM methods on the structural models through the set-to-set variability. We obtain the set-to-set distributions of the GM characteristics, the structural displacements (Δtop), the interstory drift ratios (IDR), the base shear forces (Vbase), and the global damage indices. We quantify the differences in the EDP distributions of the modified GMs and the unscaled EQ records upon two objectives such as the mean and the mean-plus-some-sigma (i.e., the criteria of ASN/2/01, 2006).

In Part 4, we present the key conclusions and general discussions as well as a practical integration of the conclusions. Also, we present the limitations of the thesis and possible future work.

This page is intentionally left blank.

PART 1

ANALYSIS OF VARIABILITY ON STRUCTURAL RESPONSES: UNSCALED EARTHQUAKE RECORDS

1.1 Introduction

The unscaled accelerograms are the natural observations of the ground shaking related to the earthquakes and reveal the most realistic time histories for the nonlinear dynamic analysis. The observed variability is large among the earthquake (EQ) records, which can be important in the decisions acquired by a seismic analysis of structures. However, such variability is minimized in the nonlinear dynamic analyses that are time-consuming to avoid the dispersion of the structural responses.

The accelerograms are selected according to the seismic hazard assessment (SHA) that provides the expected ground motion (GM) level. The SHA can be deterministic, probabilistic, or the combination of them with diverse definitions and approaches in the literature (Bommer, 2002). In the deterministic SHA, the earthquake (EQ) scenario controlling the hazard level is defined by the magnitude and the source-to-site distance possibly with the site conditions and the style-of-faulting (Krinitzsky 1995; Bommer, 2002; Wang, 2010). In the probabilistic SHA, the seismologists integrate the combinations of earthquake-related parameters. The controlling EQ scenario(s) is then obtained by the deaggregation of the hazard curve. The probabilistic SHA provides extra information on the number of standard deviation(s) (i.e., epsilon) of the earthquake-related parameters (Reiter, 1990; McGuire, 1995; Bommer, 2002; Wang, 2010).

The parameters characterizing the EQ scenario(s) enable the search of earthquake records (e.g., time histories, accelerometric data, and ground motions) in the strong-motion databases (e.g., Resorce 2013 [Akkar et al., 2014], CESMD [Haddadi et al., 2012], and PEER NGA Databases [PEER, 2013; PEER, 2014]). The common criteria are the earthquake magnitude and the source-to-site distance (i.e., the magnitude-distance bin).

Some studies have demonstrated the zero-to-low dependence of the magnitude-distance bin on the structural responses in general (Bazzurro and Cornell, 1994a; Bazzurro and Cornell, 1994b) or particularly on the maximum lateral displacements and the interstory drift ratios (Iervolino and Cornell, 2005), and the deformation-based damage indices (Shome et al., 1998). However, some structural responses were shown to be sensitive to the magnitude-distance bin (Shome and Cornell, 1998; Baker and Cornell, 2005; Bradley et al., 2010; Katsanos et al., 2010). Records from the similar earthquake magnitudes (such as 0.2 unit range in Bommer [2002]) can be selected with a wide range of the source-to-site distance to retrieve sufficient records (Bommer and Acevedo, 2004, Katsanos et al., 2010) but with a narrower range for the near-source scenarios (Stewart et al., 2001).

In addition to the magnitude-distance bin, the soil profile can be used for selecting the EQ records. The average of the top-30-meter shear wave velocity (Vs30), which is a commonly used metric to define the soil profile, is found representative of the structural damage distribution (e.g., Kanli et al., 2006) but lacks reflecting the deep soil profile alone (e.g., Abrahamson et al., 2014, Campbell and Bozorgnia, 2014, and Chiou and Youngs, 2014). If the selection with Vs30 is not possible, the site (soil) classification (e.g., EC8, NEHRP) can be alternatively used to refine the records from the same site classification (Bommer and Acevedo, 2004). Additional criteria such as the seismic source environment, the type of faulting, the source path, the directivity of seismic waves, and the location of earthquakes can be defined. Overall, a single EQ event should not dominate the record bin (Bommer and Acevedo, 2004).

The parameters expressed as a function of the EQ scenarios such as the strong-motion duration, the acceleration-to-velocity ratio (a/v), and other intensity measures (IMs) can also allow the selection of the records. The studies have also shown (1) the dependence of the absorbed hysteretic energy and the fatigue damages on the strong motion duration (Bommer and Acevedo, 2004; Katsanos et al., 2010); and (2) the dependence of a/v on some structural demands (Zhu et al., 1988; Kwon and Elnashai, 2006). Therefore, the signal characteristics should be considered as the secondary parameter to select the records (e.g., Hancock and Bommer, 2006), as the signal characteristics are the consequences of the complex integration of the geophysical properties (e.g., the source, the propagation, and the site effect).

Response spectrum compatibility is the predominant approach to select the records (i.e., a ground motion set) that are compatible with the elastic target spectrum along a frequency range. There are different ways to determine the target

(i.e., reference) spectrum, which can be design-recommended, or solely observed, or predicted (i.e., expected, estimated) based on the type of the SHA and the goal of the seismic analysis. For example, the target spectrum can be obtained by (1) the seismic code regulations partially representing the rate of exceedance (e.g., Eurocode 8, ASCE/SEI 7-10), (2) the ground motion prediction equation(s) (GMPE) representing the controlling EQ scenario (e.g., RFS 2001-01, 2001, Berge-Thierry et al., 2017), (3) the uniform hazard spectrum giving the uniform rate of exceedance for spectral accelerations at each frequency (e.g., Abrahamson et al., 2004; Trifunac, 2012), and (4) the conditional mean spectrum giving the rate of exceedance conditioned to the spectral acceleration at the frequency of interest (e.g., Baker, 2011).

The response spectrum has been discussed to relate well to some structural responses but with several limitations on (1) the nonlinear responses of structural systems, (2) the effects of soil-structure interaction, (3) the structures with higher mode effect, and (4) the effect of signal's energy content history (Trifunac, 2003).

The spectrum-compatible selection can reveal numerous GM sets (Katsanos et al., 2010; Lai et al., 2012; Sextos et al., 2011). There is a limited research on the impact of the most favorable ground motion set, the variability within a set, and the variability between the sets. Also, the decision on the allowed frequency range, the amplitude tolerances, and the number of records are mostly left to the practicing engineer due to the vague guidance of the building codes (e.g., Eurocode 8, 2004; ASN/2/01, 2006) and the limited research.

The accelerograms exhibit large variability due to, on one side, the complexity behind the earthquake source, the wave propagation, and the site conditions, and, on the other side, its randomness in the process (e.g., Singh, 1985). Besides the GM variability, a large number of GMPEs exists in the literature to obtain the target spectrum, and its choice can be the source of the large variability. In fact, response spectrum of GMPEs with the same dataset and the same input parameters can differ significantly (Douglas et al., 2014).

The GMPEs give the standard deviation (i.e., sigma) around the median prediction to describe the variability. In fact, in the deterministic approaches, the scatter of spectral amplitudes can be ignored with the median (50^{th} percentile) spectrum (e.g., Krinizsky, 1995; ASN/2/01, 2006) or it can be taken into account by the use of the median-plus-one-standard deviation (84^{th} percentile) spectrum (Krinizsky, 2002).

Overall, in the seismic analysis, seismologists prefer conserving the natural variability of the records; whereas, the engineers prefer limiting the record variability in favor of reducing the dispersion of structural responses. Nonetheless, there has been limited research on the impact of permitting larger spectral variability on the structural responses.

In Part 1, the goal is to quantify the variability in the unscaled earthquake GMs and GM sets as well as their impact on the simple structural model. In Section 1.2, the developed procedure for the spectrum compatible selection is introduced. In Sections 1.3 and 1.4, a deterministic SHA is used to select the EQ records according to the requirements of the French nuclear safety guide (ASN/2/01, 2006) and the current practice. In Section 1.5, the GMPEs are utilized to define the target spectrum, which adds the probabilistic elements to the study. From Sections 1.6 to 1.12, the structural responses of a simple model in Section 1.5 are used to analyze the impact of the target spectrum, the amplitude tolerances, the amount of GMs, and the additional elements of the spectrum compatible selection.

1.2 Spectrum Compatible GM Selection

The response spectrum compatibility is a method to select a small number of ground motions (GMs), over a magnitude-distance bin, with an average response spectrum lying within the upper and lower tolerance bounds around a target response spectrum along a frequency range.

Variety of software for the response spectrum compatible selection is available: Rexel (Iervolino et al., 2010b), ASCONA (Lai et al., 2012), ISSARS (Katsanos and Sextos, 2013), REXEL-DISP (Smerzini et al., 2014), and the online PEER Ground Motion Database tool (adapted from Wang et al., 2015). However, a new tool for spectrum compatible selection has been necessary since the available tools were not practical enough for the framework of the thesis (due to the

limitations on changing the source code, the number of GMs, updating the internal strong motion database, amplitude tolerance types, and etc.).

1.2.1 Developed Procedure

The developed procedure is overviewed in Figure 1.2.1 for the spectrum compatible selection of the deterministic SHA. The end user defines the EQ scenario in Box (a1) with the information about the EQ magnitude, the distance, the style-of-faulting, and the site conditions. The IMs (such as strong motion duration, a/v ratio, peak ground amplitudes, etc.) can be optionally used to refine the GM selection in Box (a). The upper and lower amplitude tolerances are user-inputs in Box (2) along with the frequency range. Another user-input is the number of GMs (which forms a set) in Box (d) and should be equal or above the limit in a seismic regulatory code (e.g., Eurocode 8, ASN/2/01, ASCE/SEI 7-10).

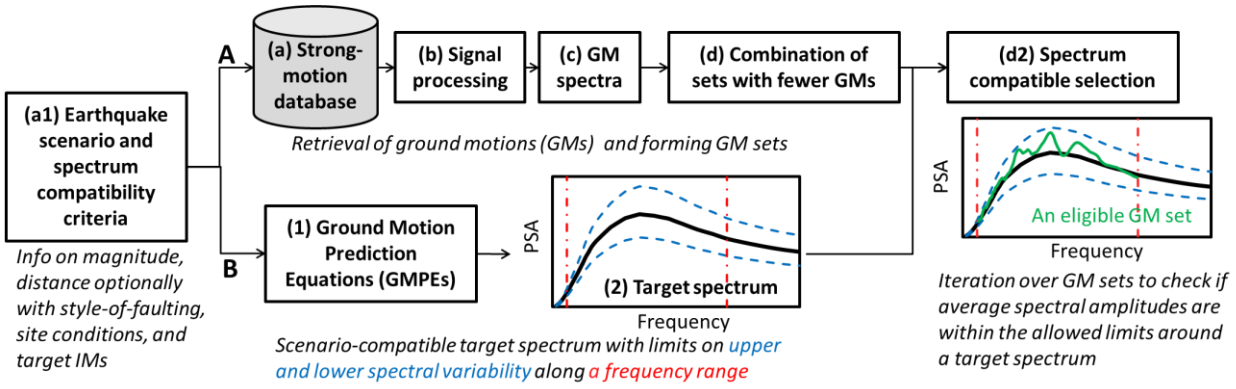

Figure 1.2.1: Overview of spectrum compatible record selection used in the Python tool. Following the definition of the earthquake scenario in Box (a1), Branch A includes the strong-motion database search in Box (a), the signal processing of time histories in Box (b), obtaining the response spectra of GMs in Box (c), and combining GM sets in Box (d). The tool in Box (a) is developed to make a connection with an offline strong motion database (Collection of Databases) that includes about 36 000 worldwide EQ records from Resorce 2013 (Akkar et al., 2014) and CESMD (Haddadi et al., 2012) as explained in Appendix A.1. Also, the tools are developed to perform the signal processing in Box (b) and obtain the response spectra in Box (c). The GM sets are combined for each possibility in Box (d).

Branch B is the definition of the target spectrum with the limits on the spectral variability. For the given scenario, the GMPE is calculated in Box (1). The spectral shapes of GMPEs are obtained integrally by the open-source software, OpenQuake Hazard Library v0.21.0 (Pagani et al. 2014). The output of Branch B is schematized in Box (2). Eligible GM sets (shown in green line) are obtained in Box (d2) if the average spectrum of a GM set is within limits (shown by the blue and red dashed lines).

The spectrum compatible GM selection in Box (d2) requires the combination of GM sets in Box (d) as in Equation 1.2.1:

$$\forall GM^{set,i} \; with \; i \; \in \left[0, \frac{r!}{n_{set}!\,(r-n_{set})!}\right] \qquad \textbf{Equation 1.2.1}$$

where n_{set}, is the number of GMs per set and r is the number of GMs in the magnitude-distance bin[1].
An eligible GM set, $GM^{set,i}$, is determined with respect to the target spectrum, PSA^{target}, if the criteria are satisfied in Equation 1.2.2:

$$Tol_{low}(f) \leq \overline{PSA^{set,i}(f)} \Big/ PSA^{target}(f) - 1.00 \leq Tol_{up}(f), \qquad \forall f \; \in \; [f_1, f_2, \dots, f_N] \qquad \textbf{Equation 1.2.2}$$

[1] The procedure is time consuming. For example, for a search of 5-record sets, 60 time-histories can be combined with 5.5 million different ways, each of which is necessary to be iterated for the spectrum compatibility.

where Tol_{low} is the lower spectral amplitude tolerance (negative), and Tol_{up} is the upper spectral amplitude tolerance (positive) at the frequency, f. f_1 is the minimum frequency; f_N is the maximum frequency. The average response spectra of GMs, $\overline{PSA^{set,i}(f)}$, is given in Equation 1.2.3:

$$\overline{PSA^{set,i}(f)} = \frac{1}{n_{set}} \sum_{j=1}^{n_{set}} PSA_j^{set,i}(f), \qquad \forall f \in [f_1, f_2, \dots, f_N] \qquad \textbf{Equation 1.2.3}$$

where $PSA_j^{set,i}(f)$ is the response spectrum at a frequency , f, of the j[th] GM.

The output of the procedure can bring a large number of eligible GM sets. All GM sets are collected, and the sets which include the same-event and same-station GMs (x-y components of an EQ record) are removed. The developed procedure is utilized to evaluate the impact of GMPEs, upper and lower amplitude tolerances, and the number of GMs.

1.2.2 Intraset and Interset Variability

A GM selection that is compatible with the response spectrum compatible can bring about two types of variability: intraset and interset as given in Figure 1.2.2. The variability relates to the input GMs and output structural responses.

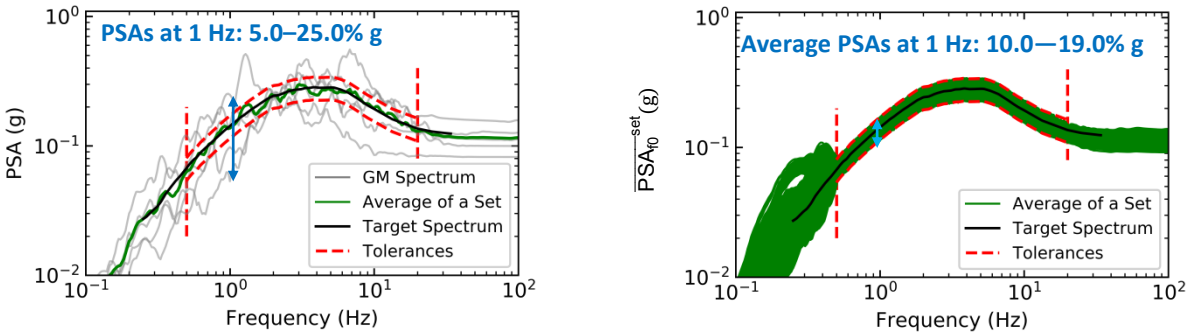

(a) An eligible set (b) 7 000 eligible sets

Figure 1.2.2: Spectral variability in a single set in (a) and average spectral variability between eligible sets in (b). A target spectrum is shown with a thick black line. The spectrum of GM is shown with a grey line. A set that consists of 5 GMs is eligible if the average spectrum (shown with green lines) is inside the amplitude and frequency tolerances (the red dashed lines). In this example, the lower and upper amplitude tolerances are 70% and 130% of the target spectrum, and the frequency range is between 0.50 and 20.0 Hz. For five records in an eligible set, the pseudo-spectral accelerations (PSAs) at 1 Hz range from 5.0% to 25.0% g in (a), which is the *intraset* variability. For 7 000 sets (each including 5 GMs), the average PSAs at 1 Hz range from 10.0% to 19.0% g, which is the *interset* variability.

The intraset variability (Figure 1.2.2.a) is the record-to-record variability within a GM set. Some approaches do not account for the intraset variability by using the central measures (median or mean), and others include the intraset variability by considering the spread of measures (such as standard deviation over the mean) as listed below:

(1) average (AVG) of values in a GM set, $\overline{\text{Val}}^{\text{set}}$, representing input GM characteristics and the output structural responses as given in Equation 1.2.4:

$$\overline{Val}^{set} = \frac{1}{n_{set}} \sum_{j=1}^{n_{set}} Val_j \qquad \textbf{Equation 1.2.4}$$

where Val_j is the value of the j[th] GM, and n_{set} is the number of GMs in a set.

(2) standard deviation (STD) of values in a GM set, $\sigma_{\text{Val}}^{\text{set}}$, as given in Equation 1.2.5:

$$\sigma_{Val}^{set} = \sqrt{\frac{1}{n_{set}-1}\sum_{i=1}^{n_{set}}(Val_j - \overline{Val}^{set})^2} \qquad \textit{Equation 1.2.5}$$

(3) average-plus-some-standard deviation of values in a GM set: $(\overline{\mathrm{Val}} + \lambda\sigma_{\mathrm{Val}})^{\mathrm{set}}$, where λ is the number of standard deviation. In the practice, the intraset variability of AVG is used for the input GM selection. The intraset variability of average-plus-some-standard deviation is used for the output structural responses.

The interset variability (Figure 1.2.2.b) is the variability from one to another eligible GM set and is also called *set-to-set* variability. Analogously, if a GM set represents the selection done by a virtual engineer performing a seismic analysis, the difference in the final values determined by several virtual engineers is the *interset* variability.

The interset variability depends on intraset variability. If the intraset variability is not taken into account, the interset variability is the distribution of the average values in each set ($\overline{\mathrm{Val}}^{\mathrm{set}}$). If the intraset is taken into account, the interset variability is the distribution of the average values plus a fraction of standard deviation in each set $(\overline{\mathrm{Val}} + \lambda\sigma_{\mathrm{Val}})^{\mathrm{set}}$.

A single GM set is used in the practice and the interset variability is not taken into account. The building codes (e.g., Eurocode 8, ASN/2/01, ASCE/SEI 7-10) are not strict on which GM set to choose; in the literature, various metrics have been proposed to define the most suitable GM set (e.g., Ambraseys et al., 2004; Naeim et al., 2004; Kottke and Rathje, 2008; Youngs et al., 2007; Beyer and Bommer, 2007; Iervolino et al., 2010b; Buratti et al., 2011, Smerzini et al., 2012; Katsanos and Sextos, 2013; Wang et al., 2015, Baker and Lee, 2017).

1.2.3 French Nuclear Safety Guide (ASN/2/01)

The French nuclear safety guide, ASN/2/01 (2006), presents a deterministic approach for the consideration of the seismic risk for the design of civil engineering buildings of the nuclear plants (not covering the long duration radioactive wastes disposal). Certain requirements are imposed for the response spectrum compatible selection in Section 2.2 of ASN/2/01. The code requirements that are related to the thesis scope are listed below:

- Using at least 3 GMs for the linear structural analysis and at least 5 GMs for the nonlinear structural analysis,
  - where the GMs can be natural or artificial, and
  - the GMs are 'preferentially' chosen from French Basic Safety Rule (Règle Fondamentale de Sureté), the RFS 2001-01 (2001) database,
- Selecting a 'representative' (i.e., eligible) GM set
  - whose average spectrum (with 5% of damping ratio) is equal to or larger than the target spectrum obtained from RFS 2001-01, which then refers to the GMPE of Berge-Thierry et al. (2003),
- Using a GM with a time-step less than or equal to 0.01 second,
- Calculating the average spectral accelerations for a sufficient number of the frequency points
  - in compliance with 'envelop character' (referring to RFS 2001-01 that provides the spectral amplitudes for a frequency range between 0.25 and 33.0 Hz)
  - with a discretization of $10^{0.03N}$, where N is an integer varying from -33 and 50,
- Ensuring that the intensity measures (IMs) such as strong motion duration, peak ground velocity (PGV), peak ground displacement (PGD), acceleration-to-velocity ratio (a/v), Arias intensity, and cumulative absolute velocity (CAV) are compatible with the scenario (in terms of earthquake magnitude and source-to-site distance), and
- Verifying the selection of statistically independent GMs (the inter-correlation function of two GMs is less than 0.3 and with a mean value less than 0.2).

The intraset variability is considered on the output of the nonlinear dynamic analysis by adding a fraction of the standard deviation to the average structural response, $(\overline{\mathrm{EDP}} + \lambda\sigma_{\mathrm{EDP}})^{\mathrm{set}}$, where the EDP is the engineering demand parameter, and λ is the fraction of the standard deviation as defined in Equation 1.2.6:

$$\lambda = \frac{t_{0.05,n_{set}-1}}{\sqrt{n_{set}}} \qquad \textit{Equation 1.2.6}$$

where n_{set} is the number of GMs in a set, and $t_{0.05,n_{set}-1}$ is the Student variable corresponding to 95% confidence level (unilateral), or equivalent of 90% confidence interval (bilateral). To illustrate, for 5, 7, 11, 13, 19, 23, and 29 GMs per set, λ become 95%, 73%, 55%, 49%, 38%, 34%, and 34%, respectively.

Following the guidance of ASN/2/01, the elements involved in the spectrum compatible GM selection are evaluated in the thesis. For a given EQ scenario, the tests are performed with the target spectra defined by the additional GMPEs. The effect of the flexible amplitude tolerances is evaluated in comparison with the tight amplitude tolerances (such as ±5% for 5% damping and ±10% for greater damping ratios in the current application, which are not necessarily required by ASN/2/01). The effect of the number of GMs in a set is also tested. The interset variability and the intraset variability are utilized for quantifying the natural variability of the GMs and its uncertainties.

1.3 Retrieval and Process of Earthquake Records

This section shows the accelerogram selection with the developed procedure in Section 1.2 (i.e., Boxes a1, a, and b in Figure 1.2.1). An earthquake scenario is chosen with a moment magnitude (Mw) of 7.0 and a hypocentral distance (Rhypo) of 40.0 km (abbreviated as M7.0R40). It is selected in a way to retrieve sufficient GMs since the GMs are scarce for the large-magnitude and short-distance events (M>5.0 and R<10.0 km as demonstrated in Figure A.1.1 in Appendix A.1). The database search retrieves 92 free-field GMs (i.e., not structure-related records) from Collection of Databases as provided in Table 1.3.1. The metadata of the GMs is collected from the related databases except for Vs30 in Resorce 2013, which are updated according to Engineering Strong Motion database hosted by ORFEUS (Luzi et al., 2016) as discussed in Appendix A.1.

The raw earthquake records can contain errors due to the noise and the baseline offsets. It can root in the tilting and the transducer response under a strong shaking; thus, the raw earthquake records must be corrected for the use of the engineering applications by filtering and the baseline correction (Boore, 2001; Boore and Bommer, 2005; Burks and Baker, 2014; Burks and Baker, 2016).

The approach developed for the signal processing includes two phases: (1) the inspection, and (2) the process of each signal (which is not automated by a script) with a goal to optimize the loss of the accelerometric data as described in Appendix A.2.1. The number of the GMs passing the inspection (i.e., first phase) and the number of the processed GMs (i.e., second phase) are summarized in Table 1.3.2 with the list of the GMs in Table A.2.2 (Appendix A.2.4).

The GMs from Resorce 2013 are already processed, and the GMs from CESMD are raw. The first phase inspects the processed records (i.e., Resorce 2013) for whether (1) they have zero-units at the ends of the acceleration, the velocity and the displacement time histories, (2) they have the velocity and displacement time histories starting synchronously with the acceleration time history and (3) they conserve the spectral amplitudes in the frequency range of interest (0.5 to 20.0 Hz) after the signal processing. In total, 17 processed records have satisfactorily passed the first phase.

In the second phase, the records that fail the inspection in the first phase are signal-processed (by the use of the raw records). Errors due to the noise and the baseline offset are corrected by applying a combination of the time windowing, the tapering, the padding, the detrending and the Butterworth bandpass filtering, respectively. The time windowing enables the analysis of a smaller subset of the accelerometric data rather than the use of the extensive pre- and post-event accelerometric data, which is critically important for the total duration of the nonlinear dynamic analysis. The tapering, which is applied to a cosine function, is used to ensure the time histories' smoothly approaching to zero at its ends. The zero padding on the acceleration time history is used as a pre-processor for the signal detrending and the filtering (Boore and Akkar, 2003). The signal detrending removes the existing trend in the raw signals to correct the baseline offset. The signal detrending is applied over the acceleration, the velocity, and the

displacement time histories. If the records have errors even after the signal detrending, the Butterworth bandpass filtering is applied over the acceleration, the velocity, and the displacement time histories with the corner frequencies (fmin and fmax) to remove the low- and high-frequency noises.

Table 1.3.1: Selected earthquake events and GMs for M7.0R40

	Event Date yyyymmdd_hhmm	Location and State/Country	Fault Type	Mw	Station ID [Rhypo, Vs30]	# GMs
CESMD	19891017_1704	Loma Prieta, California	Oblique	6.9	47006[34, 730], 47179[50, 271], 47379[34, 1428], 47380[35, 271], 47381[36, 278], 57066[44, 264], 57191[41, 282], 57217[35, 597], 57382[37, 222], 57383[40, 663], 57425[44, 334], 57504[36, 215], 58065[33, 381]	26
	19920425_1806	Petrolia, California	Reverse	7.0	89509[39, 519], 89530[36, 337]	4
	19920728_0457	Landers, California	Strike-slip	7.3	12025[44, 312], 22161[45, 635], 22561[47, 430], 12630[44, 524]	8
	19991016_0246	Hector Mine, California	Strike-slip	7.1	21081[49, 383]	2
	20061015_0707	Hawaii	Strike-slip	7.1	02810[35, N/A], 02849[46, N/A]	4
RESORCE 2013	19760517_0258	NW Uzbekistan	Reverse	6.8	27[32, 121]	2
	19801123_1834	Irpinia, Italy	Normal	6.9	ALT[30, 1018], BSC[31, 976], BRN[46, 403], RNR[37, 539], STR[36, 1122]	10
	19830117_1241	Kefallinia Island, Greece	Reverse	6.9	ARG1[31, 437]	2
	19831030_0412	Pasinler, Turkey	Strike-slip	6.6	2503[37, 316]	2
	19881207_0741	Spitak, Armenia	Reverse	6.8	173[31,278]	2
	19900620_2100	Manjil, Iran	Strike-slip	7.3	6211[41, 621]	2
	19971118_1307	Strofades, Greece	Reverse	6.6	ZAK1[39, 241]	2
	19991112_1657	Duzce, Turkey	Strike-slip	7.1	1401[37, 294], 1406[41, 355], 3102[30, N/A], 3103[31, N/A], 3104[30, N/A], 9900[49, 455], 9901[31, 481], 9904[31, 439], 9902[34, 448], 9906[38, 456], 9907[36, 316],	22
	20031226_0156	Bam, Iran	Strike-slip	6.6	3599[48, N/A]	2
	20111023_1041	Van, Turkey	Reverse	7.1	6502[41, 293]	2

Table 1.3.2: Amount of GMs that are manually processed or removed

Case	Database	# of Records Retrieved	First Phase*	Second Phase**	# of Records Removed	# of Records Used	Total # of Records
M7.0R40	Resorce 2013	48	17	27	4	44	88
	CESMD	44	–	44	0	44	

* Amount of the 'already' processed GMs satisfying the conditions of the first phase.

** Amount of the GMs that are signal processed and then satisfied the conditions in the first phase.

The second phase is repeated to minimize the loss of the accelerometric data. The narrower tapering window and the extended cutoff frequencies along with the less zero-padding amount are used. The raw records for the EQ events in Resorce 2013 are retrieved from Engineering Strong Motion (Luzi et al., 2016). In total, 71 records are signal-processed to satisfy the requirements in the first phase. Figure 1.3.1 illustrates an example of the signal processing with the description and the comparison, and the additional examples can be found in Appendix A.2.3.

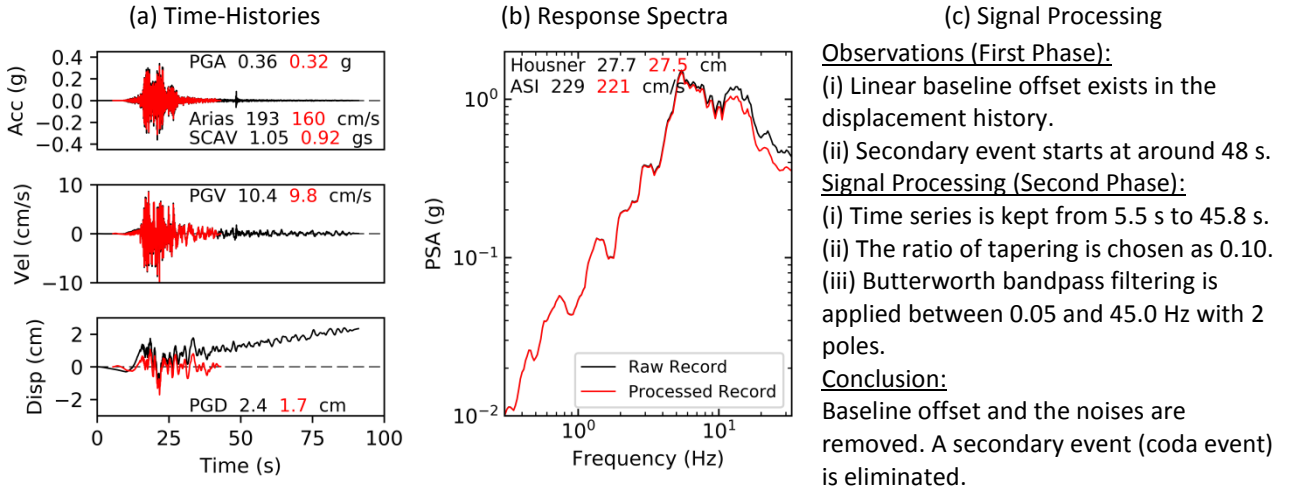

Figure 1.3.1: Time- and frequency-domain characteristics of the raw and processed record. The record is from the Hawaii earthquake (station no 02849) with Mw 7.1 and R_{hypo} 46 km. Column (a) shows the acceleration, velocity, and displacement time-histories of the raw record in black and the processed record in red. For the main event, the signal processing results in a slight change in the acceleration and velocity time histories, and the significant change in the displacement time history. In column (b), the comparison of the spectral shapes is shown. The spectral amplitudes differ slightly after 10.0 Hz in (b) due to the removal of the coda-event. The amplitude-based IMs (i.e., PGA, PGV, and PGD) and the duration-based IMs (i.e., Arias and SCAV) decrease moderately. The frequency-based IMs (i.e., Housner and ASI) slightly decrease. In column (c), the signal processing is explained.

The reason why the available records in the database (i.e., Resorce 2013) do not satisfy the requirements of the first phase is the difference in the corner frequencies and the one-by-one signal processing. The use of an automated approach instead of one-by-one signal processing does not optimize the loss of data and can overlook some issues as illustrated in Appendix A.2.2. Also, different number precisions are used to verify the zero-unit ending of time histories.

If the time histories fail the requirements of the inspection even after the signal processing, the records—the four of them in this case—are eliminated. They are likely to indicate a problem related to the quality of the accelerometric data as discussed in Appendix A.2.2 along with the additional observations (e.g., the insufficient pre-main event data, the difference in the sampling time, and the polarity of the records).

1.4 Target Spectra

In the deterministic SHA, a single ground motion prediction equation (GMPE) is used to define the target spectrum in compliance with a given EQ scenario. As the amount of the modern seismic networks has increased, the earthquake catalogs have expanded regarding the number of GMs and the availability of the metadata, which has enabled the development of the GMPEs (e.g., Douglas, 2017).

The classical (basic) GMPEs characterize the fault as a point source and require about four input parameters such as the earthquake magnitude, the distance, the soil conditions, and the style of faulting. The complex GMPEs characterize the source as an extended rupture and require around 13 input parameters (Pagani et al. 2014) as shown in Figure 1.4.1. They necessitate detailed information about (i) the rupture properties such as dip angle (δ), source-to-site azimuth (ϒ), depth to top of rupture (ztor), down-dip rupture width (w); (ii) the distance metrics such as source-to-hypocentral distance (Rhypo), horizontal distance to the surface projection of the rupture (Rjb), slant distance to the closest point on the rupture plane (Rrup), hanging/foot-wall flag, and horizontal distance to the surface projection of the top edge of the rupture measured perpendicular to the fault strike (Rx); and (iii) the site properties such as Vs30, the depth where shear wave velocity is equal to 1.0 km/s (Z1.0), and the depth where shear wave velocity is equal to 2.5 km/s (Z2.5).

In ASN/2/01, the median spectra provided by the Berge-Thierry et al. (2003) GMPE is suggested as the target spectrum. In order to quantify the variability of the GMPEs for the impact on structural responses, four classical and three

complex GMPEs are used as given in Table 1.4.1. For the EQ scenario of M7.0R40, Vs30 450 m/s (Vs450), and normal fault are assumed, and the equivalent input parameters for each GMPE are selected as illustrated in Figure 1.4.1.

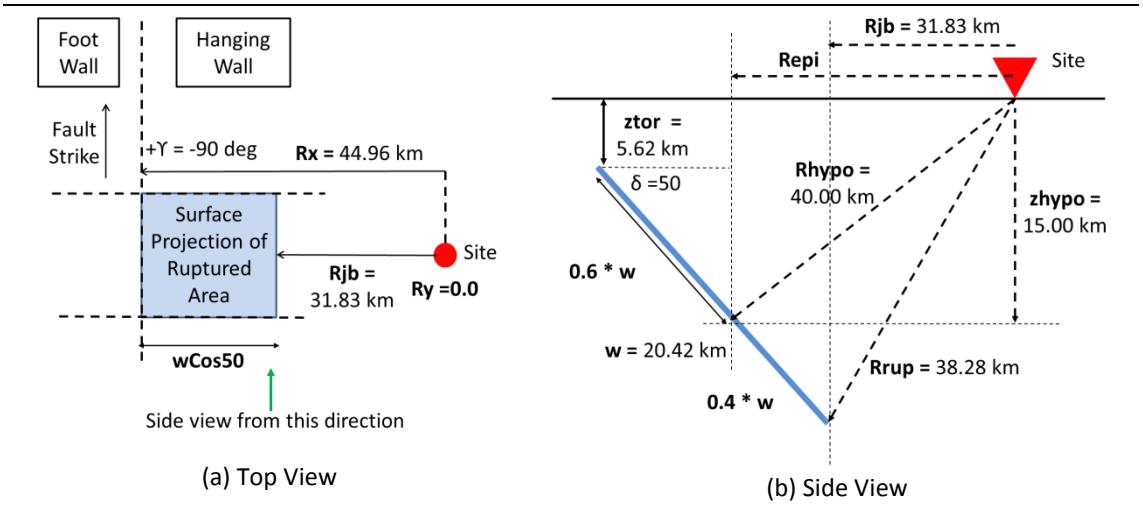

Figure 1.4.1: Top and side view of assumed fault geometry and site position (not in scale)

Table 1.4.1: GMPEs used in this study

	GMPE	Abbreviation
CLASSICAL	Akkar et al. 2014 (considering the erratum)	AK2014
	Boore and Atkinson 2008 and Atkinson and Boore 2011	BA2011
	Berge-Thierry et al. 2003	BT2003
	Bindi et al. 2014	BD2014
COMPLEX	Abrahamson et al. 2014	AB2014
	Campbell and Bozorgnia 2014	CB2014
	Chiou and Youngs 2014	CY2014

The source-to-site azimuth (γ) of 90˚ is assumed, which implies that the site resides on the hanging wall. The hypocentral depth (Zhypo) is roughly estimated with the linear relationship given by Scherbaum et al. (2004) to have Zhypo within the given standard deviation. Rest of the necessary rupture properties such as the dip angle, the rake, and the down-dip rupture width (W) are determined after the relationships reviewed in the technical notes by Kaklamanos et al. (2011). Accordingly, the hypocenter is assumed to locate 60% down the fault width. The surface magnitude for the use of BT2003 is back-calculated based on Mw from the linear relationship by Scordilis (2006). The depth to the top of the rupture (Ztor), the horizontal distance to the surface projection of the rupture (Rjb), and the slant distance to the closest point on the rupture plane (Rrup) are calculated according to the geometric interdependence.

The depth at shear wave velocity (Vs) being equal to 1.0 km/s (Z1.0) is estimated with the AS08 relationship as 0.25 km for AB2014 and with the CY08 relationship as 0.16 km for CY2014 (Kaklamanos et al. 2011). The depth at Vs being equal to 2.0 km/s (Z2.5) is estimated with the extrapolation of Z1.0 from the AS08 relationship as 1.41 km (Kaklamanos et al. 2011). The equivalent input parameters for each EQ scenario are tabulated in Appendix A.3.

The scenario is assumed with the precise fault geometry and the site position; however, large uncertainty exists in defining some of the input parameters in the real-life application. The change in the AK2014's median spectrum is illustrated in Figure A.3.2 along with the spectral distributions of the EQ records. The median spectrum is sensitive to the input parameters (at various levels). For the complex GMPEs, there can be a good number of combinations of input parameters that are not considered in the classical GMPEs. For the sake of brevity, the earthquake scenario with the above-mentioned parameters is used in this study.

1.5 Structural Models

Once the multiple GM sets are selected, the impact of the input variability on the structural responses can be quantified. A single-degree-of-freedom (SDOF) oscillator is modeled with a natural frequency of 1.00 Hz, a 5%-damping ratio, and an elastic-plastic strain hardening behavior, 5% of the initial stiffness. It is modeled with a fixed base. The stiffness of the SDOF model is 100 000 kN/m with a mass of 2 533 tonnes. The elastic strength demand is calculated by multiplying the SDOF's mass and the average of seven GMPEs' spectral accelerations at 1.00 Hz (0.118 g). Therefore, the elastic strength demand is 2 926 kN (= 2 533 tonne x 0.118 g x 9.81 m/s^2). The design strength is obtained according to the equal-displacement concept: the elastic strength demand is divided by the strength reduction factors, R, to permit the seismic energy absorption through yielding by assuming that the structural system has the sufficient capacity (Chopra, 2012).

Four design strengths with R1, R2, R4, and R8 are tested as shown in Figure 1.5.1. The observed dispersion of the structural displacements (Δtop) is large. The ductility demand (μ) is the ratio between ultimate Δtop and yield Δtop (i.e., the level of inelastic response) and is utilized to decide the SDOF design. The R4 and R8 designs result in high ductility demands (>12.0); therefore, the R1 and R2 designs are used in this study. The yielding limits are 2.92 cm and 1.46 cm for the R1 and R2 designs, respectively. The Δtop estimates are not capped (i.e., thresholds are not applied).

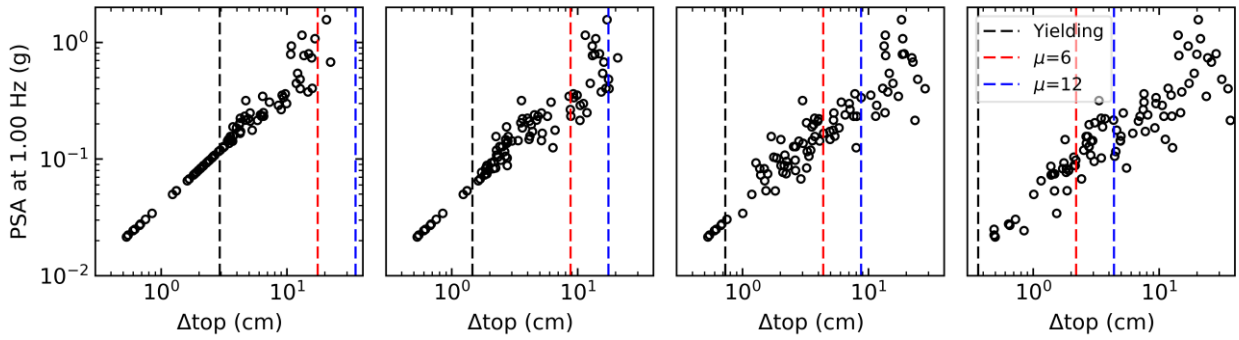

(a) SDOF-R1 (b) SDOF-R2 (c) SDOF-R4 (d) SDOF-R8

Figure 1.5.1: Structural responses of the SDOF model at 1.00 Hz under unscaled earthquake records. The structural responses are shown with black circles. The logarithmic x-axis shows the maximum absolute of the lateral structural displacements (Δtop). The logarithmic y-axis shows PSAs at 1.00 Hz of accelerograms. There are 88 processed GMs from the database search of M7.0R40. The yielding and the displacement ductility levels, μ, of 6 and 12 are plotted with the vertical dashed lines. The maximum ductility demand (μ) is 8 for the R1 design, 15 for the R2 design, 30 for the R4 design, and 60 for the R8 design. The R1 and R2 designs are preferred in this study.

1.6 Impact of Signal Processing

The signal processing is a key step in the process of the accelerogram selection. Here, the impact of signal processing on the input signal characteristics is compared relative to the raw accelerogram. The effect of the signal processing is exemplified for a single GM in Figure 1.6.1. The signal processing eliminates the baseline offset in the velocity history and results in a significant decrease of PGV. Δtop and Vbase also decrease largely after the signal processing.

The change in the signal characteristics and the structural responses of SDOF-R1 and SDOF-R2 are plotted in Figure 1.6.2. After the signal processing, PGV, PGD, Arias, and SCAV change significantly and have large dispersion. The structural responses remain unaffected on average regardless of the SDOF design level, but the dispersion can be observed to a more considerable extent in Δtop than Vbase. An additional test is extended to the effect of the different signal processing approaches as provided in Appendix A.2.5. The signal processing can be the source of the variability for the signal characteristics and the structural responses.

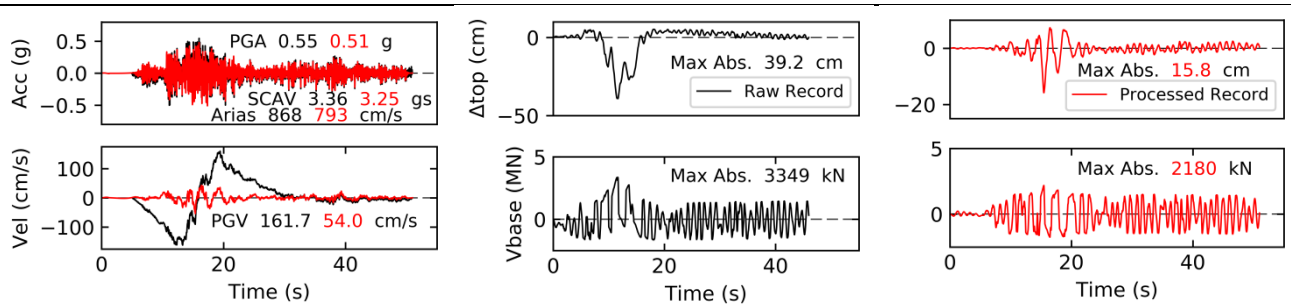

(a) Signal Processing (b) Response of Raw Record (c) Response of Processed Record

Figure 1.6.1: Effect of signal processing on time histories and response histories of SDOF-R2 at 1.00 Hz. The solid black line represents the time and response histories of the raw record. The solid red line represents the time and response histories of the signal-processed record. Acceleration and velocity time histories are shown in (a). The lateral displacements (Δtop) and the maximum base shear force (Vbase) are shown in (b) for the raw record and in (c) for the signal-processed record. The record is from the Iranian earthquake (19900620_210008, station 6211) with Mw 7.3, Rhypo 41 km, and Vs30 621 cm/s. The signal processing includes tapering with a ratio of 0.05, padding with the zeros for 5.0 seconds, detrending, and Butterworth bandpass filtering between 0.10 and 50.0 Hz with two poles.

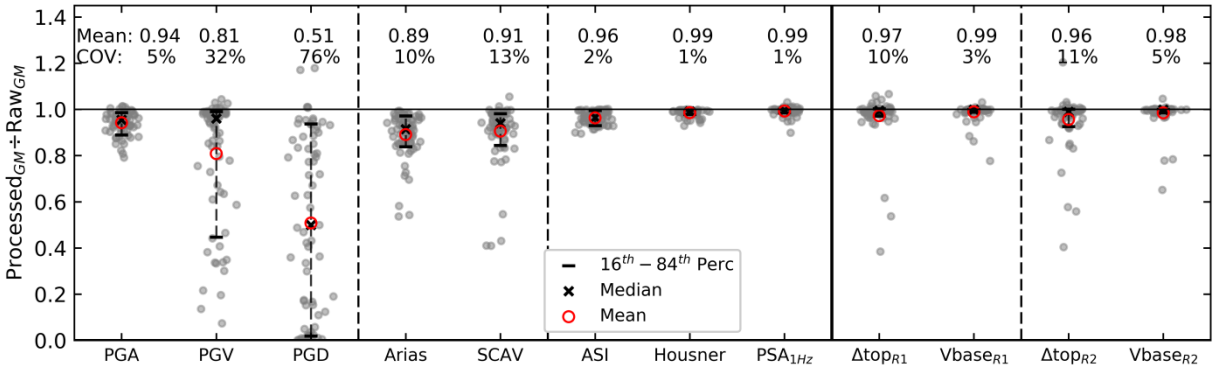

Figure 1.6.2: Impact of signal processing on signal characteristics and structural responses of the simple models. Each grey dot represents the ratio of a value before and after the signal processing of 71 records. Ratios lower than 1.0 signifies a decrease in the value and vice-versa. Mean of the ratios is shown with the red unfilled circle. Median of the ratios is shown with the black cross marker. The 16th and 84th percentiles are shown with the black horizontal bars. The mean and the coefficient of variation (COV) are provided. PGA, PGV, and PGD are amplitude-based IMs. The mean decrease is 0.81 in PGV and 0.51 in PGD, which can be explained by the fact that single and double integrations of raw acceleration-time histories augment the errors in velocity and displacement histories. Duration-based IMs, Arias, and SCAV, experience a mean decrease of about 0.90. The frequency-based IMs (such as ASI, Housner, and PSAs) are slightly affected. Lateral displacements (Δtop) and base shear forces (Vbase) are the responses of SDOF-R1 and SDOF-R2. On average, the structural responses decrease after the signal processing with a mean ratio of around 2-3%. COVs of structural estimates are 11% for displacements and 5% for base shear forces.

For the engineering purposes, the spectra of the accelerograms are inspected in detail. The signal processing and its different approaches result in variability of the GM characteristics regarding the acceleration, velocity, and displacement time histories. Consequently, the variability in the structural responses is provoked. The results signify the importance of the inspection of the acceleration, velocity, and displacement time histories.

1.7 Refinement of Record Selection

Following the GM selection with the EQ magnitude and the source-to-site distance, the GMs can be refined with the additional parameters (the soil conditions, the style-of-faulting, the event dominancy, the IMs, and etc.).

1.7.1 Metadata-Based Refinement

This subsection questions the impact of the metadata-based refinement on the input PSAs at 1.00 Hz and the output Δtop estimates for the EQ scenario of interest. In Figure 1.7.1, the metadata is separated in terms of the soil conditions

and the style-of-faulting. PSAs and Δtop scatter largely. Based on the limited data, the style-of-faulting and the soil conditions do not affect the PSA, and Δtop scatters. The record selection with a site-specific parameter results in fewer records and large dispersion, i.e., it does not necessarily reduce the variability of Δtop as given in Table 1.7.1.a.

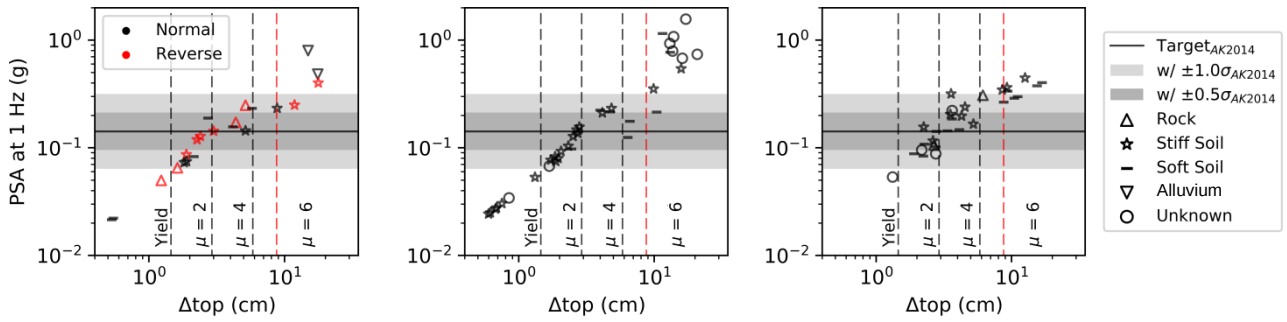

(a) Normal and Reverse (b) Strike-Slip (c) Oblique

Figure 1.7.1: Distributions of PSAs at 1.00 Hz and lateral displacement responses (Δtop) of SDOF-R2 at 1.00 Hz with respect to style-of-faulting, and EC8 soil categories. The y-axis presents the PSAs at 1.00 Hz, and the x-axis shows the corresponding Δtop. The results are for the normal fault (in black) and the reverse fault (in red) in (a), the strike-slip fault in (b), and the oblique fault in (c). Markers represent the EC8 soil condition. The yielding limit and ductility demands (μ) are shown with the vertical dashed lines. The black horizontal line shows the median PSA of AK2014 at 1.00 Hz. The 0.5 and 1.0 standard deviations around the median are shown with the shaded grey. PSAs at 1.00 Hz vary between 0.02 g and 1.56 g; Δtop estimates vary between 0.5 cm and 21.0 cm. The records below the target's 0.5σ-plus-median PSA are also below μ of 6. The records above the target's one-sigma-plus-median PSA are above μ of 6.

Another way to refine the GMs is the homogenization of event dominance. In the magnitude-distance bin (Table 1.3.1), the records are dominantly from three EQ events: Loma Prieta (30% of total records), Duzce (25%), and Irpinia (11%). The homogenous bin is formed in Table 1.7.1. It includes two GMs per EQ event (out of 14 events). For the same-event multiple-station records, the priority is given to the records from the different stations with Vs30 close to 450 m/s.

The homogenous bin does not have a significant effect on the mean PSAs and slightly decreases the standard deviation; subsequently, the distribution of Δtop remains unaffected relative to the reference distribution of Δtop. The mean PSA at 1.00 Hz for the Duzce event is the greatest (0.45 g) and results in Δtop of 7.5 cm (i.e., μ of around 4.0). The analyses compromising other IMs also confirm the existence of the significant variability (relatively less for Vbase), which is mainly for the Duzce event as given in Appendix A.4.

Table 1.7.1: Record variability in terms of PSAs at 1.00 Hz and lateral displacements (Δtop) of SDOF-R2.

	Record Bins	Number of Records	PSA at 1.00 Hz (g) Mean[6]	PSA at 1.00 Hz (g) STD[6]	$\Delta top_{R2,1.00\ Hz}$ (cm) Mean[6]	$\Delta top_{R2,1.00\ Hz}$ (cm) STD[6]
	All (Reference)[1]	88	0.250	0.274	5.8	5.2
(a) Site Specific	Normal Fault (NF) [2]	10	0.166	0.107	5.2	5.4
	Vs450[3]	30	0.147	0.104	4.0	4.0
	NF + Vs450[4]	6	0.188	0.118	6.5	6.7
(b) Event Dominancy	Homogenous	28	0.206	0.183	5.7	5.3
	Loma Prieta[5]	26 (30%)	0.228	0.109	6.2	4.3
	Duzce[5]	22 (25%)	0.450	0.466	7.5	6.6
	Irpina[5]	10 (11%)	0.166	0.107	5.2	5.4

[1]The All bin represents the magnitude-distance bin. [2]The Normal Fault (NF) bin selects the records with the normal fault from the All bin. [3]The Vs450 bin selects the records with Vs30 between 350 and 550 m/s from the All bin. [4]The NF and Vs450 bin represent the intersection of the two bins. [5]The rest of the bins include the specific event records. The amount of records in each bin is given. [6]Mean, and standard deviation (STD, for unbiased sample) of PSAs at 1.00 Hz and Δtop are also shown.

For the scenario of M7.0R40, Vs450, and normal fault, the metadata-based refinement (i.e., style-of-faulting, soil conditions, and event dominancy) does not necessarily improve the variability level (of the GM characteristics and the structural responses) but reduces the number of GMs. Therefore, the reference (i.e., magnitude-distance) bin is used.

1.7.2 IM-Based Refinement

An additional way of the GM refinement can be done regarding the IMs. We may eliminate some GMs by comparing the spectra of the GMs with the target spectra and the IMs of the GMs with the average IMs of the magnitude-distance bin. To illustrate, the GMs which exhibit PSAs greater than 0.5σ-over-median spectra (AK2014) are identified (15 out of 88 GMs) in Figure 1.7.2.a. One of the identified GMs with the greatest Arias intensity is plotted in Figure 1.7.2.b. They reveal IMs and structural responses 'significantly' greater (3 to 7 times except for Vbase) than the rest of the GMs.

The refinement can be useful to reduce the computational duration related to the iterations in the spectrum compatible selection (i.e., the number of combinations can be reduced according to Equation 1.2.1). It is interesting to note that if such refinement is not considered, the spectrum compatibility does not select, at least, 15 GMs. In other words, they never occur in the eligible sets (i.e., Equation 1.2.2). This observation is verified through the spectrum compatible selection with different target spectra (AK2014, BA2011, and BT2003) as given in Appendix A.5.4. The Arias intensity gives an apparent difference between the refined and discarded GMs.

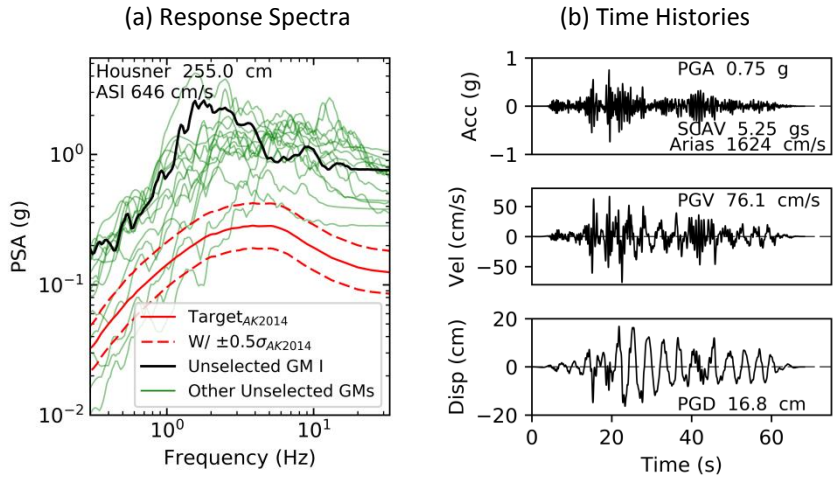

Figure 1.7.2: Response spectra of GMs above the half-sigma-over-median target spectra in (a) and time histories of the GM (GM I) with greatest Arias intensity in (b). Response spectra are shown in (a) for GM I with the black line and other GMs with the green lines. The spectral shape of target spectra, AK2014, is shown in solid red line and the half-sigma-around-median spectra are shown with the dashed red lines. GM in (b) is from the Duzce event (station 3103) with Mw 7.1, R 31 km, and unknown Vs30. Acceleration, velocity, and displacement time histories are given in (b). IMs of GM in (b) are also noted. PGA of GM I is 0.75 g, where target PGA is 0.11 g. The spectral amplitudes are mainly above the target spectra particular at frequency ranges above 2 Hz.

1.8 Impact of Spectrum Compatible GM Selection on GM Set Variability

This subsection presents the results of the spectrum compatible GM selection performed with the tool in Section 1.2.1 over the selected EQ records in Section 1.3 for the assumed EQ scenario in Section 1.4. The tight tolerances (i.e., ±5% around the target) are used in the current practice but do not permit any sets that consist of the unscaled EQ records.

The spectral variability is extended to the half-sigma-around-median spectrum of AK2014 to select the unscaled GMs in Figure 1.8.1. The half-sigma range covers the central 38% of the observations (i.e., expected fraction of the population in a normal distribution). The spectrum compatible is then performed for a set compromising five GMs and the frequency range from 0.50 to 20.0 Hz after the discussion given in Appendix A.5.1. In total, 982 535 GM sets are collected.

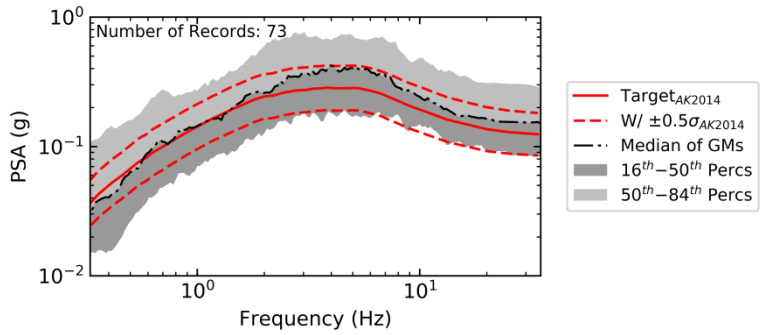

Figure 1.8.1. Response spectrum of GMs and the target with permitted spectral variability (dashed red lines) in spectrum compatible selection.

1.8.1 Single versus Eligible GM Sets

This subsection provides the comparison of the results obtained by all eligible sets and a single GM set, which is used in the current practice. Among the eligible GM sets, a GM set is selected with the least distance described in Equation 1.8.1 (adapted from Iervolino et al., 2010b):

$$\delta^{set,i} = \sqrt{\frac{1}{N}\sum_{k=1}^{N}\left(\frac{\overline{PSA^{set,i}(f_k)} - PSA^{target}(f_k)}{PSA^{target}(f_k)}\right)^2} \qquad \textit{Equation 1.8.1}$$

where N is the number of spectral accelerations within the frequency range. $\overline{\mathrm{PSA}_{\mathrm{j}}^{\mathrm{set,i}}(\mathrm{f_k})}$ is the average pseudo-acceleration from the ith set at a frequency f_k, and $\mathrm{PSA}_{\mathrm{reference}}(\mathrm{f_k})$ is the spectral acceleration of the target spectrum at $\mathrm{f_k}$.

The distributions of single sets (the set with the least metric distance, $\delta^{\mathrm{set,i}}$, from 0.5 to 20.0 Hz and four randomly selected sets) are shown in terms of PSAs at 1.00 Hz in Figure 1.8.2.a and output Δtop in Figure 1.8.3.a. 5 GMs in each set reveal dispersed values (i.e., intraset variability). The last set reveals a large standard deviation due to a single GM, which is one of the possible outcomes of the spectrum compatibility.

All GM sets are considered with the set's average in Figure 1.8.2.b. The mean of all $\overline{\mathrm{PSA}_{\mathrm{fo}}}^{\mathrm{set}}$ is 0.138 g with a coefficient of variation (COV) of 16%. The intraset variability is included in Figure 1.8.2.c. The mean of all $(\overline{\mathrm{PSA}_{\mathrm{fo}}}+0.95\sigma_{\mathrm{PSA}})^{\mathrm{set}}$ is 0.213 g with a COV of 18%. The distribution of the lateral structural displacements, $\overline{\Delta\mathrm{top}}^{\mathrm{set}}$, has a mean of 3.3 cm with a COV of 20% in Figure 1.8.3.b. The single sets of $\overline{\Delta\mathrm{top}}+0.95\sigma_{\Delta\mathrm{top}}$ in Figure 1.8.3.a cover a big portion of all-set-distribution, all $\overline{\Delta\mathrm{top}}^{\mathrm{set}}$, in Figure 1.8.3.b.

The way of treating intraset variability depends on the objective of a seismic analysis and the engineer's point of view. If the objective necessitates the use of ASN/2/01 (or the engineers aim at imparting conservatism), the intraset variability with $0.95\sigma_{\Delta\mathrm{top}}$ results in 55% increase in the mean of all $\overline{\Delta\mathrm{top}}^{\mathrm{set}}$. A tail-like distribution is observed when $(\overline{\Delta\mathrm{top}}+0.95\sigma_{\Delta\mathrm{top}})^{\mathrm{set}}$ is larger than 6.0 cm. There may not be sufficient amount of GM sets resulting in this range. The way of treating intraset variability impacts the ductility demand and the possible final decisions about the structures (i.e., resizing the structural elements, the feasibility of a project, etc.). Therefore, the calculations for two types of intraset variability are performed in the thesis.

The spectral variability of 0.5σ around the target spectrum is permitted to select unscaled real records, which is not typical in the practice. The spectrum compatible ground motion selection brings the intraset and the interset variability. The intraset variability is regarded partially in the seismic regulatory codes. The interset variability has not been considered, and a single ground motion set is commonly used in the practice. Large dispersion is observed due to all GM sets. It suggests that a good number of GM sets is needed to obtain an assuring level of mean and its variability in

the spectrum compatible selection. In other words, each virtual engineer selecting a different GM set can come up with very different structural displacement estimates. A single set regardless of its being the closest to the target (Equation 1.8.1) results in the estimates that fail representing the distribution of all GM sets. A single set with $\overline{\Delta\text{top}}+0.95\sigma_{\Delta\text{top}}$ may serve a shortcut to cover the interset variability of all $\overline{\Delta\text{top}}^{\text{set}}$.

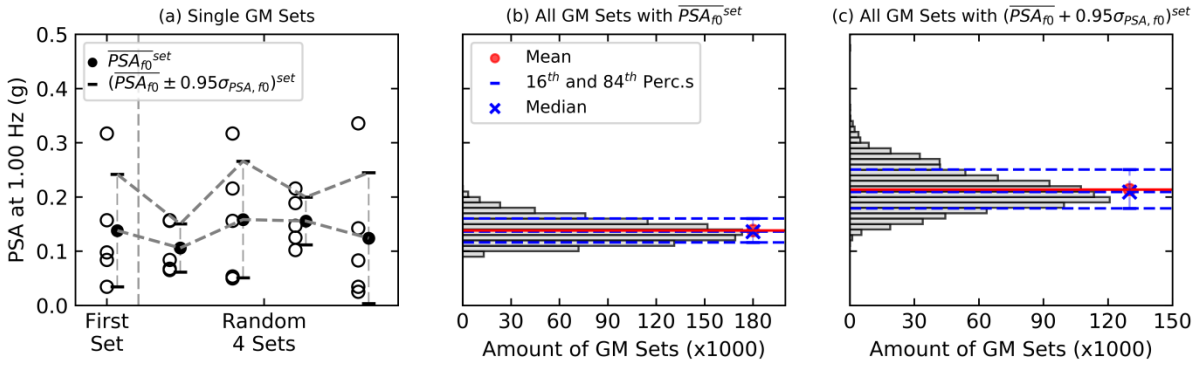

Figure 1.8.2 Distributions of PSAs at 1.00 Hz with GM selection using spectrum compatibility. The y-axis shows the PSA at 1.00 Hz. The GM selection is performed with the median of AK2014 for the scenario of M7.0R40, Vs30 450 m/s, and normal fault. The distributions of single sets are shown in (a). The first set is the most favorable set calculated according to Equation 1.8.1. The value of a GM is shown with the unfilled black circle. Average of a set is given by the filled black circle. Average-plus-minus-95%-standard-deviation (STD) of a set is drawn with the horizontal bars.

In total, there are 982 535 GM sets. Set-to-set distribution of GM sets is shown with the intraset variability of average, $\overline{\text{Val}}^{\text{set}}$, in (b) and the intraset variability of average plus 95% standard deviation, $(\overline{\text{Val}}+0.95\sigma_{\text{Val}})^{\text{set}}$, in (c). Mean of the distribution is plotted with a filled red circle. The median value of the distribution is demonstrated with a blue cross marker. 16th and 84th percentiles of the distribution are given with blue horizontal lines.

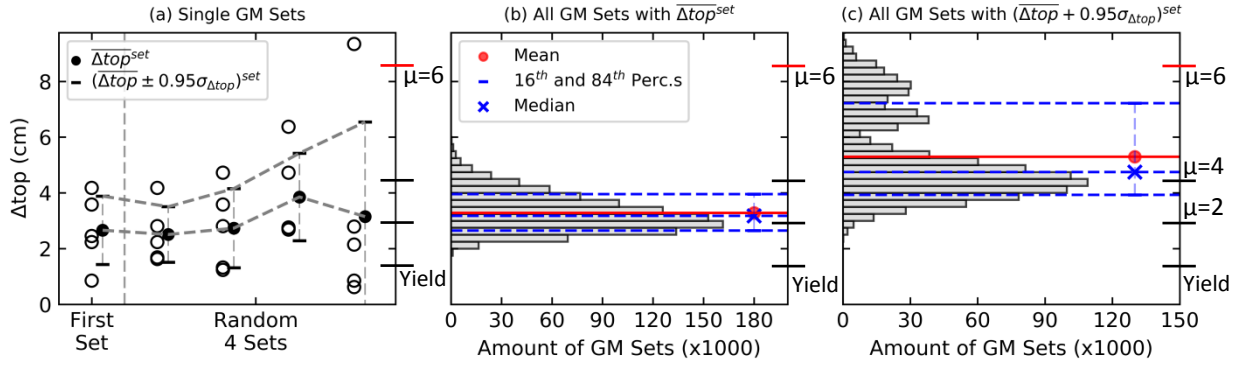

Figure 1.8.3: Distributions of lateral displacement responses (Δtop) of SDOF-R2 at 1.00 Hz with GM selection using spectrum compatibility. Similar graphical elements with Figure 1.8.2 are used here. The ductility demands, μ, and yielding points are marked.

1.8.2 Use of Site-Specific or Event-Dominant Record Bin

The record-to-record variability in the magnitude-distance bin is shown to scatter widely even if the bin is refined by the site-specific settings and the event dominance in Section 1.7. In order to evaluate its impact on the spectrum compatibility, the records with various type-of-faulting, soil conditions, and events are removed from all eligible sets in Figure 1.8.4. The B1 bin on the x-axis represents the magnitude-distance bin. The labels from -B2 to -B8 represent the removal of the site-specific bins. The labels from -B9 to -B12 represent the removal of the event-dominant bins.

The site-specific and the event-dominant bins are shown to cause unimportant differences for the distribution of all $\overline{\Delta\text{top}}^{\text{set}}$. It suggests that the spectrum compatibility is a satisfactory tool to reveal stable set distribution even if the bin includes non-site specific and event dominant GMs. The same conclusion can be extended to $(\overline{\Delta\text{top}}+0.95\sigma_{\Delta\text{top}})^{\text{set}}$, the IMs, and Vbase as well as other GMPEs (BA2011 and BT2003) in Appendix A.5.2. Therefore, the magnitude-distance bin is used without further refinement.

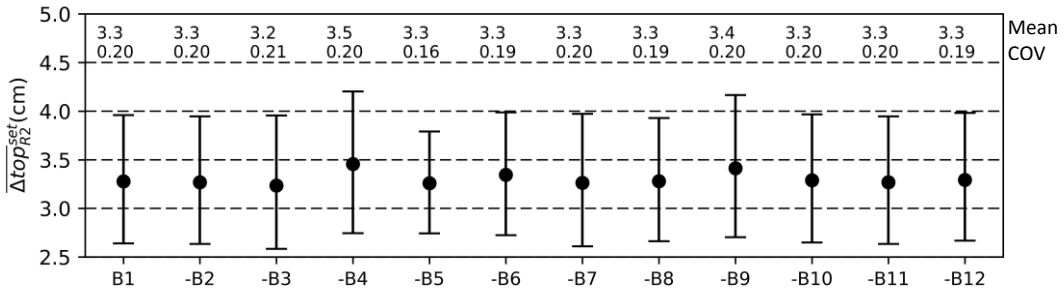

Figure 1.8.4: Effect of removing site-specific and even dominant records on lateral displacement responses (Δtop) of SDOF-R2 at 1.00 Hz. The spectrum compatible selection is explained in the caption of Figure 1.8.2. The distribution of each set's average, $\overline{\Delta\text{top}}^{\text{set}}$, is shown on the y-axis. Bin 1 (B1) in the x-axis represents the distribution of sets with magnitude-distance bin. The next rows represent the distributions when the GMs are removed from B1. The mean and the COV are noted on the figure.

The bins and the number of GMs are given as: B1: All (88); B2: Normal Fault (10); B3: Reverse Fault (12) ; B4: Oblique Fault (30); B5: Strike-Slip F. (36); B6: Vs450 (30); B7: Vs800+ (6); B8: Normal+Vs450 (6); B9: Loma Prieta (26); B10: Duzce Event (20); B11: Irpina Event (10); B12 Landers Event (8).

For example, The -B2 bin removes the records with the normal fault from the GM sets. The -B6 bin removes the records with Vs30 between 350 and 550 m/s. The -B7 bin removes the records with Vs30 greater than 800 m/s.

Using 'statistically independent' GMs in a set is another criteria suggested by the building codes (e.g., ASN/2/01, 2006). In order to evaluate the effect of interdependence that exists in a set, the tests are performed by separating (i) the sets without same EQ event and (ii) the sets with same-event and same-station records as provided in Appendix A.5.3. Accordingly, their impacts are shown to be insignificant on the distribution of the IMs and the structural responses, if all eligible GM sets are considered.

1.9 Impact of GMPEs used as Target Spectra

This subsection presents the impact of the chosen GMPE on the structural responses. The GMPEs are utilized to obtain the spectra with the equivalent input parameters as explained in Section 1.4. The median spectra of the GMPEs and their standard deviation (i.e., the sigma) are provided in Figure 1.9.1. There is a significant difference in the median spectra. The dispersion of the spectrum (i.e., one sigma of a GMPE) is large as a function of the frequency.

The spectrum compatible selection is then performed with the tool with 0.5σ around the target in Section 1.2.1. All GM sets are collected for each GMPE. The difference due to the choice of the GMPEs is as large as 0.04 g in PGA, 8.4 cm/s in PGV, 18.3 cm/s in Arias, 0.12 gs in SCAV, 34 cm/s in ASI, and 25.5 cm in Housner. BD2014 reveals the highest mean, and BA2011 reveals the least mean of all $\overline{\text{IM}}^{\text{set}}$ (i.e., the IM's distribution with each set's average). The IM distributions are tabulated in detail in Table A.6.1 (Appendix A.6).

In Figure 1.9.1, the distributions of PSAs at 1.00 Hz and Δtop of the SDOF-R2 model are compared. The choice of GMPE causes the means of all $\overline{\text{PSA}_{1.00\text{Hz}}}^{\text{set}}$ ranging from 0.09 g to 0.14 g (i.e., +55% of the former) and the means of all $\overline{\Delta\text{top}}^{\text{set}}$ ranging from 2.0 cm to 3.2 cm (i.e., +60% of the former). A similar trend can be traced in the distribution of all $(\overline{\Delta\text{top}}+0.95\sigma_{\Delta\text{top}})^{\text{set}}$ in Figure 1.9.2.b.

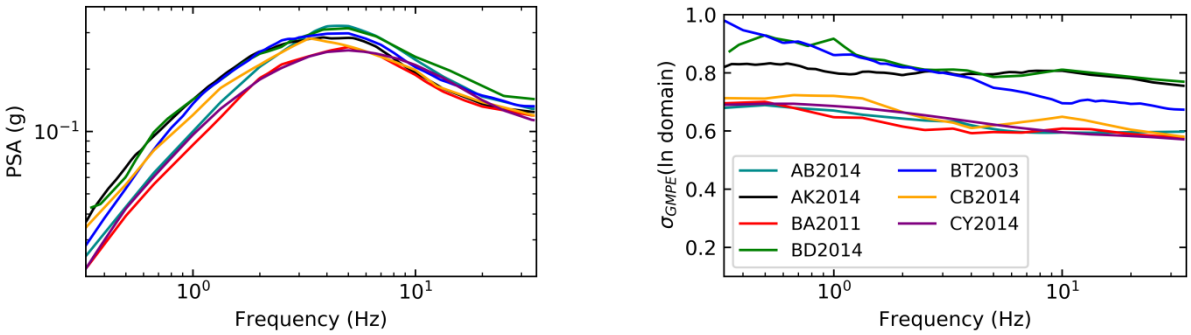

(a) Median spectra of GMPEs (b) One-sigma spectra of GMPEs

Figure 1.9.1: Median spectral shapes of GMPEs and their standard deviations. The median spectra are shown in (a), and one-standard-deviation (sigma) spectra are shown in natural logarithmic scale in (b). The spectra are obtained with the equivalent parameters for the scenario of M7.0R40, Vs450, and normal fault as discussed in Section 1.4. BT2003 uses basic parameters with soil and rock classifications. BD2014, AK2014, and BA2011 require basic input parameters with a bit more detail. AB2014, CB2014, and CY2014 characterize the source as an extended fault and require detailed information about the site. PSAs at 1.00 Hz vary between 0.09 g and 0.14 g. PGAs vary between 0.11 g and 0.14 g. The standard deviations of GMPEs exhibit a decreasing trend from the low to high frequencies.

The inclusion of $(0.95\sigma_{\Delta\text{top}})^{\text{set}}$ elevates the means of all $\overline{\Delta\text{top}}^{\text{set}}$ about 60% regardless of the GMPE, which impacts the acquired decisions from such analyses. The distributions of Δtop are more dispersed than the distributions of all $\overline{\text{PSA}_{1.00\text{Hz}}}^{\text{set}}$. The spread of the structural response distribution is affected by the choice of a GMPE, which can be explained by the difference in the PSA levels and the structural demand level.

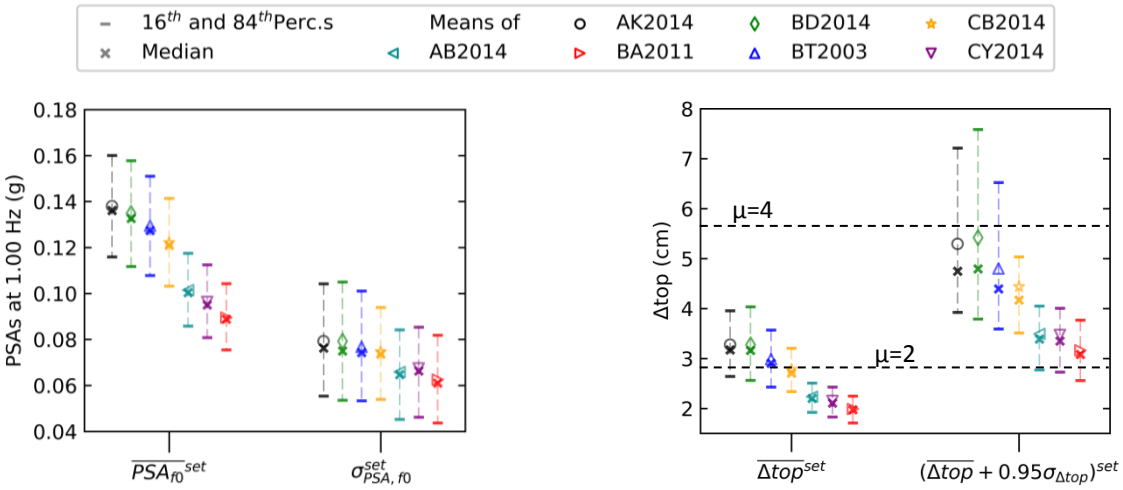

(a) PSAs at 1.00 Hz (b) Δtop of SDOF-R2 at 1.00 Hz

Figure 1.9.2: Impact of GMPEs on the distributions of PSAs at 1.00 Hz and Δtop of SDOF-R2. The upper and lower amplitude tolerances are defined with 0.5σ of the GMPE around its median spectra. The frequency tolerance is from 0.50 Hz to 20.0 Hz. Five GMs per set are used. 16^{th} and 84^{th} percentiles are plotted with horizontal line markers. Medians are shown with cross markers. Means are demonstrated with the markers and colors in the legend box for corresponded GMPEs. The average of 5 GMs per set is shown. The average with 95% of standard deviation per set is also shown. PSAs at 1.00 Hz in (a) represent the elastic spectral accelerations at the fundamental frequency of SDOF-R2 in (b). Data can be found in Table A.6.2 (Appendix A.6).

In the DSHA, a single GMPE is used without considering the spectral variability and the GMPE-based variability. It is shown that the GMPEs can significantly impact the distribution of the IMs and the structural responses (slightly less for Vbase as summarized in Table A.6.2). This conclusion is specific to the EQ scenario and the precise input parameters.

1.10 Impact of Upper and Lower Amplitude Tolerances

The upper and lower amplitude tolerances are used as a way to tune the spectral variability. The sigma-based tolerances provide a certain level of the observed spectral variability in the dataset of the GMPE but are not preferred in the current practice. The linear amplitude tolerances such as linear-symmetric or linear-asymmetric are preferred. The symmetric tolerance expands the upper and lower tolerances equally. The asymmetric tolerance, which is required in ASN/2/01 (2006), expands the upper amplitude tolerance (with a constant lower tolerance) to impart conservatism.

The equivalency between the sigma-based and the linear tolerances is shown in Figure 1.10.1 and for the other GMPEs in Figure A.6.1 (Appendix A.6). The linear tolerances correspond to the non-uniform level of the observed PSAs in the dataset of the GMPE (i.e., epsilon). To illustrate, in AK2014, linear tolerance of +50% has an equivalent epsilon ranging between 0.5 and 0.6. In BT2003, linear tolerance of +50% has an equivalent epsilon ranging between 0.4 and 0.6.

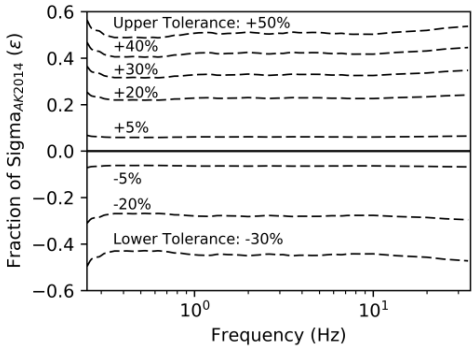

Figure 1.10.1: Equivalent epsilons of linear tolerances (in the natural logarithmic base). The spectrum is AK2014 for the scenario of M7.0R40, Vs30 450 m/s, and normal fault. The equivalent fraction of sigma (ε) is calculated with the ratio of linear tolerances in natural logarithm and sigma of GMPE. The dashed lines are the linear tolerances.

In Figure 1.10.2, the sigma-based, the linear-symmetric and the linear-asymmetric tolerances are analyzed for their impact on Δtop. The symmetric tolerances reveal comparable means with respect to the sigma-based tolerances. The asymmetric tolerances reveal mostly greater means (i.e., imparting conservatism) than the sigma-based tolerances. Tightening the tolerances in the sigma-based and the linear-symmetric tolerances reveal precise estimates (for the interest of the mean and median). Tightening the asymmetric tolerances can cause a significant decrease in the mean and median estimates. The choice of the GMPE results in large differences independent of the tolerance type. The same conclusions can be extended to PSAs at 1.00 Hz and $(\overline{\Delta\text{top}}+0.95\sigma_{\Delta\text{top}})^{\text{set}}$ as provided in Appendix A.6.

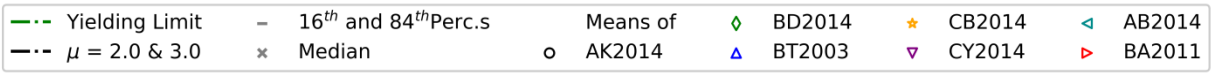

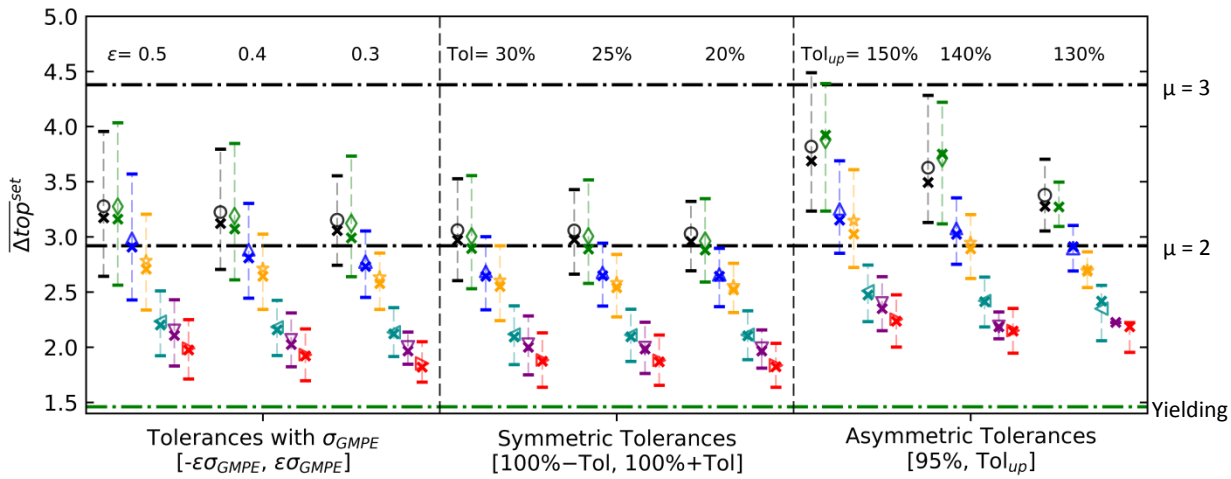

Figure 1.10.2: Distribution of Δtop of SDOF-R2 at 1.00 Hz with different upper and lower amplitude tolerances.

(continued) The GM selection is performed for the scenario of M7.0R40, Vs30 450 m/s, and normal fault. Results with the intraset approach of the average of 5 GMs are shown in cm. Means are demonstrated with the markers and colors in the legend box for each GMPE. Medians are shown with the cross markers. The 16th and 84th percentiles are plotted with the horizontal bars. The horizontal lines show the yielding and ductility demands (μ).

1.11 Shrinking GM Set Amount

We demonstrated that all GM sets need to be collected in the spectrum compatible selection. Yet, the collection of all GM sets may not be possible due to the technical limitations (i.e., if there are many GMs in the magnitude-distance bin and many GMs per set). For example, the selection of 13 GMs among 73 records purges the number of iterations about 6 million times relative to the selection of 5 GMs (see Equation 1.2.1). This section empirically evaluates how to shrink the amount of the GM sets by conserving the arrangement of the GM sets and the interset variability.

1.11.1 Number of GM Sets

In the practice, the GM sets that are close to the target spectrum is preferred. Figure 1.11.1 shows the change of Δtop for the first 250 sets according to the metric defined in Equation 1.8.1. The mean Δtop estimates increase with the inclusion of more GM sets and do not reveal stabilized distribution even if the first 250 GM sets are included.

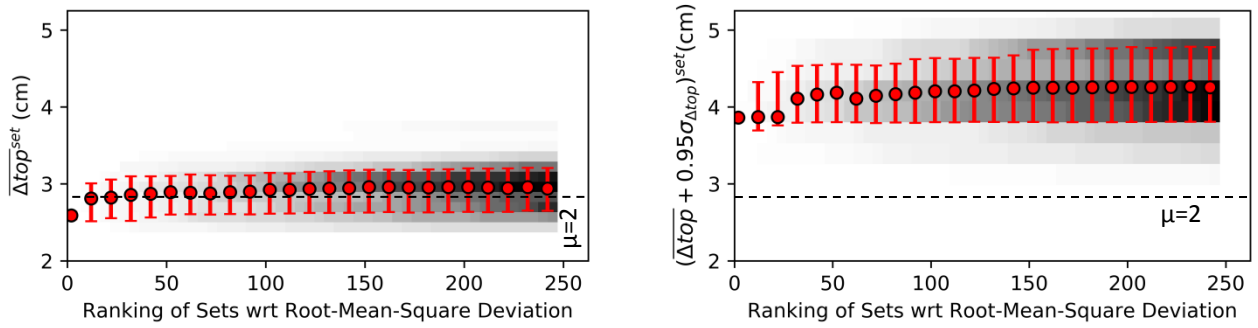

(a) Intraset Approach of Average

(b) Intraset Approach of Average-Plus-95%-St.Deviation

Figure 1.11.1: Change in set-to-set distributions of Δtop of SDOF-R2 at 1.00 Hz. The spectrum compatible selection is performed with AK2014 and 0.5σ-around-median spectra. Along the x-axis, the ranking of each set (Equation 1.8.1) is shown, which is adapted from Iervolino et al. (2010b). Along the y-axis, the set-to-set distribution of Δtop is shown for the related intraset approach. The shades of black indicate how often Δtop estimates are in the range. The darker the shade is, the more the data can be observed. 250 GM sets are shown and are sampled at every 10 GM sets.

The distribution in Figure 1.11.1 is compared with the all-GM-set distribution in Figure 1.11.2. The random selection of the GM sets is also included. First set, first 100 sets, and first 250 sets underestimate Δtop and are not sufficient to capture the interset variability regardless of the intraset approaches. Randomly selected 100 sets that are composed of less than 44 GMs (60% of all GMs) underestimate the structural responses and their dispersion. Randomly selected 100 sets that are composed of at least 50 GMs (75% of all GMs) closely represent the whole distribution. The similar observations are made for PSAs at 1.00 Hz and Vbase in Appendix A.7.1. For the clarity, randomly selected sets are referred as semi-random in the figures due to their refinement regarding the number of GMs.

1.11.2 Arrangement of GM sets

Among a group of sets, the GMs are repeated at different rates. If the repetitions of GMs are normalized, we will refer them as 'reoccurrence frequencies' of each GM in the thesis. The recurrence frequency gives the weight of each GM on the final structural estimate. For example, a single set that consists of 5 GMs has an equal recurrence frequency (i.e., weight) of 20% (one over five GMs) on the final estimate.

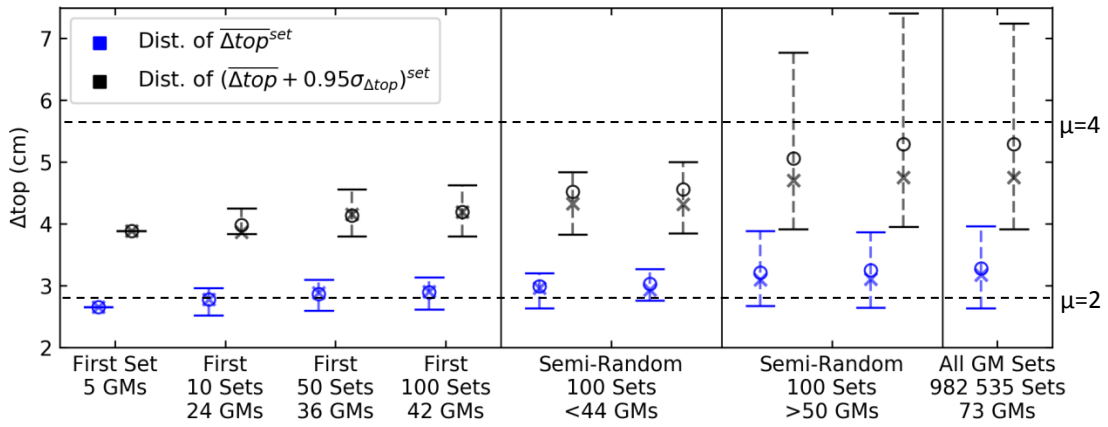

Figure 1.11.2: Distributions of Δtop of SDOF-R2 at 1.00 Hz with the inclusion of various amount and combination of GM sets. First set, first 10 sets, first 50 sets, and first 100 sets are taken from the previous graph. They have 5 GMs, 24 GMs, 36 GMs, and 42 GMs, respectively. All GM sets have 982 535 GM sets and use 73 GMs. There is a difference in the amount of GMs and the distribution of GM sets. As a result, two different approaches are used to retrieve four semi-random 100 GM sets. The first approach is to select two semi-random 100 sets having less than 44 GMs, which cover 60% of all GMs. The second approach is to select two semi-random 100 sets with at least 50 GMs, which cover 75% of all GMs.

The recurrence frequencies are plotted for the above-mentioned semi-random approaches in Figures 1.11.3.a and 1.11.3.b, and for all GM sets in Figure 1.11.3.c. In Figure 1.11.3.a, there are 42 GMs, and three GMs reoccur more than 7.5%, which is inadequately higher than the rest. It means that these three GMs are likely to govern the final Δtop.

In Figure 1.11.3.b, the recurrence frequencies are more homogenously distributed, and 59 GMs reoccur less than 5.0%. Figure 1.11.3.c shows the recurrence frequencies of all GM sets and the recurrence frequencies are less than 3.0%. Also, there are several GMs reaching over the ductility demand of 6 in Figures 1.11.3.b and 1.11.3.c, which are not present in Figure 1.11.3a.

The semi-randomly selected 100 GM sets consist of more than 75% of GMs (no outliers) can reveal similar set-to-set distribution (i.e., interset variability) to the all-GM-set distribution. All GM sets should be considered when a precise study on the interset variability is required.

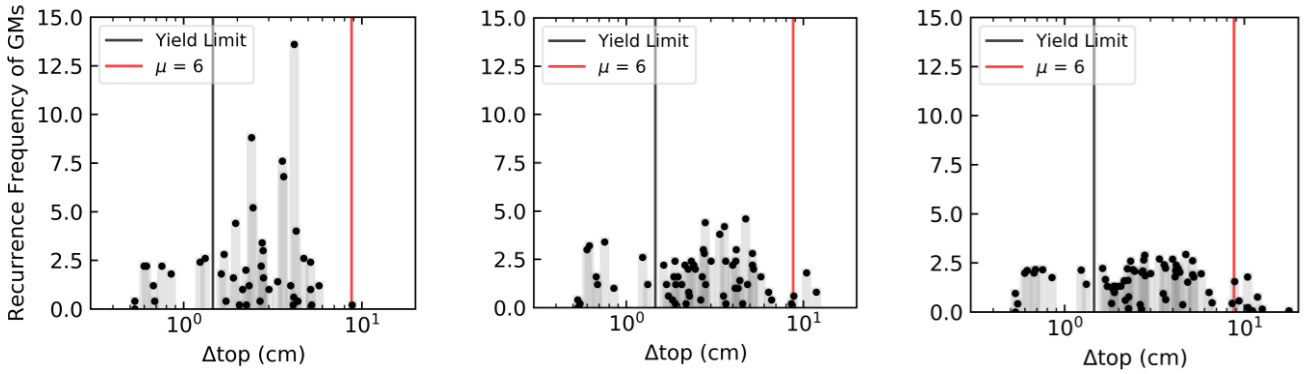

(a) First 100 sets with 42 GMs (b) 100 sets with 59 GMs (c) 982 535 sets with 73 GMs

Figure 1.11.3: Comparison of recurrence frequencies (%) of Δtop for SDOF-R2 at 1.00 Hz for different groups of GM sets. Δtop is given along the x-axis. Recurrence frequencies of GMs are given in percentage along the y-axis. Yielding limit and ductility demand of 6 are plotted with vertical lines. Δtop of each record is plotted with the black marker, and its recurrence frequency is highlighted with the grey line.

1.11.3 Approach to Avoid GM Dominancy with Partial GM Sets: Cycle-and-Shift Algorithm

A stable set distribution of structural responses can be represented by fewer GM sets if they are combined in a particular way to avoid the dominance of GMs in sets (i.e., large recurrence frequency). Three components are found to be essential to represent the interset variability sufficiently with fewer sets:

- Amount of the records with respect to all records
- Recurrence frequencies of the records, and
- Amount of the records recurring equally and greatly

These components are then integrated to develop the 'cycle-and-shift' algorithm. It expedites the run time of spectrum compatible GM set selection, overcomes the technical limitations due to a large amount of GM sets, and avoids the biased GM set selection relative to the results obtained by all GM sets. The cycle-and-shift algorithm includes cycles at a defined limit and shifts with a certain amount of GMs in the following cycle. It is applicable only if

(a) the ground motions (GMs) are compatible with the target spectra, i.e., there are no outliers that are out of the M&R bin and that do not give extremely high IMs than the observed population in the M&R bin (Section 1.7.2),
(b) the amount of GMs per set is at least 5, and
(c) the amount of GMs is equal to and larger than three times the amount of the GMs per set.

The algorithm is sketched in Figure 1.11.4 and is explained in Steps 1 to 9 below:

(1) Sort ground motions, GMs, with an increasing metric in accordance with Equation 1.11.1 (Iervolino et al. 2010b):

$$\delta^{GM,i} = \sqrt{\frac{1}{N}\sum_{k=1}^{N}\left(\frac{PSA^{GM,i}(f_k) - PSA^{target}(f_k)}{PSA^{target}(f_k)}\right)^2} \qquad \textit{Equation 1.11.1}$$

where N is the number of spectral accelerations within the frequency range. $PSA^{GM,i}(f_k)$ is the average pseudo-acceleration from the j[th] GM at a frequency f_k. $\mathrm{PSA}_{\mathrm{reference}}(\mathrm{f_k})$ is the spectral acceleration of the target spectrum at $\mathrm{f_k}$.

(2) Combine the GM sets which consist of the amount of GMs per set, *nset,* by respecting the order of sorted GMs as explained in Equations 1.2.1, 1.2.2, and 1.2.3,
(3) Stop the iterations after
  (i) collecting a certain amount of eligible GM sets, M_{set} or
  (ii) exceeding the allowed maximum duration, t_{max}
(4) Collect the eligible GM sets at the end of a cycle
(5) Eliminate the GM sets if they are repeated in the previous cycles
(6) Go to Step (1) to start another cycle by shifting a certain amount of GMs, r_{shift}, from the beginning of the sorted order while N_{GM} is equal to and larger than GMs per set, *k*
(7) Calculate the amount of unique GMs among the collected sets, $N_{GM,used}$
(8) Calculate the repetition amount (recurrence) of GMs among the collected sets and its recurrence frequencies, $R_{GM,i}$
(9) While (i) $N_{GM,used} < 0.75N_{GM}$ where N_{GM} is the total number of GMs), and
  (ii) $R_{GM,i} > min\left(1/k, 0.075\right)$ where $1 \le i \le N_{GM,used}$, repeat the algorithm with different r_{shift} or N_{set} or t_{max}

For the discussion in the following sections, r_{shift} is 3, N_{set} is 2500, and t_{max} is 90 minutes. These values are obtained after a trial-and-error procedure. It is also observed that if two consecutive cycles do not return any GM sets, the subsequent cycles do not return any GM sets.

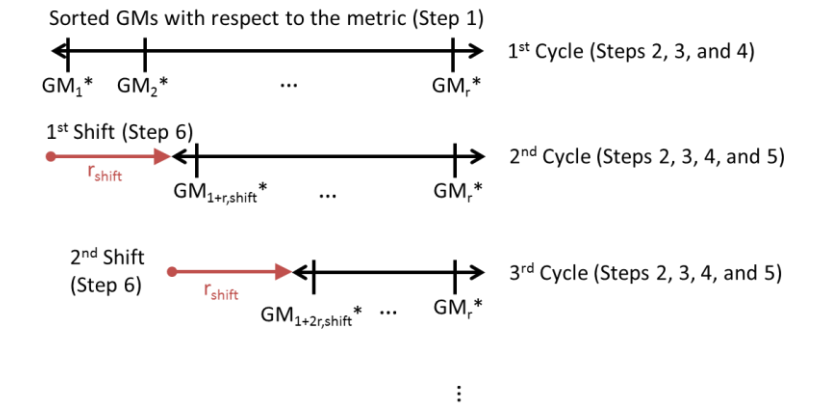

Figure 1.11.4: Sketch of the cycle-and-shift algorithm. *GMs are sorted in an increasing metric value, i.e., GM_1 gives the least metric distance.

The sets collected by the cycle-and-shift algorithm are compared with the sets obtained by one cycle set selection (i.e., no shifts) in Figure 1.11.5. First 100 000 sets with 56 GMs meet the criteria of using 75% of the GMs (56 GMs out of 73 GMs); however, several GMs reach over the defined recurrence limit of 7.5%. The recurrence frequency of 7.7% implies that each GM is repeated within the 100 000 GM sets since their recurrence frequency is equal to 1/13, 7.7%. In other words, they have a high weight on the final structural estimates.

In Figure 1.11.5.b, the cycle-and-shift algorithm is used to collect 31 911 GM sets. There are 69 GMs, and each has homogeneously distributed recurrence frequencies, which are less than 2.6%. The cycle-and-shift algorithm reveals the mean of 2.7 cm with a COV of 14% for $\overline{\Delta\text{top}}^{\text{set}}$. They are exactly same as the all-GM-set distribution. It suggests that the sets obtained by the cycle-and-shift algorithm can optimize the GM set selection (the duration and the technical limitations) and represent the all-GM-set distribution. The same conclusions can be extended to the distributions of PSAs, Δtop, and Vbase with other GMPEs in Appendix A.7.2. For the future use of the cycle-and-shift algorithm, we suggest the verification of r_{shift}, N_{set}, and t_{max} specific to the case.

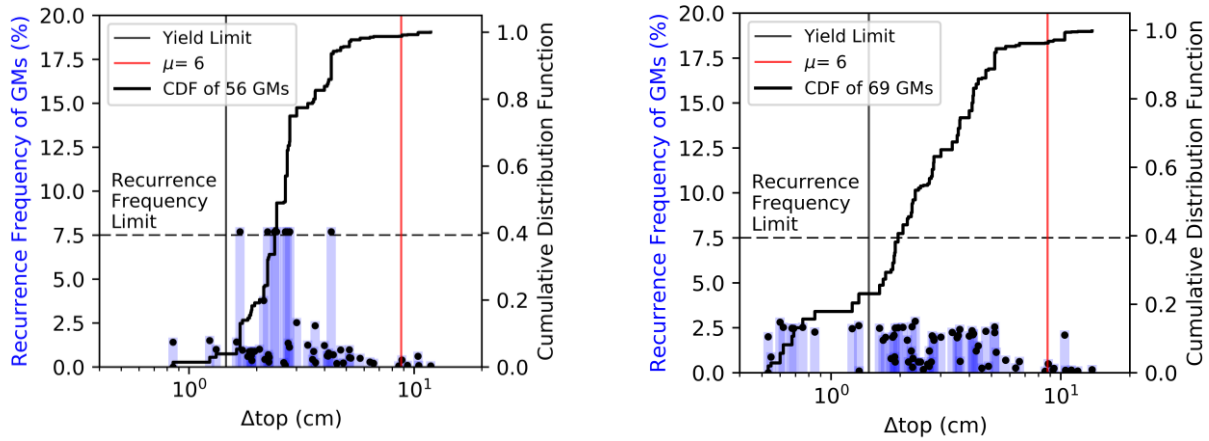

(a) First 100 000 Sets with 56 GMs

(b) 31 911 sets with 69 GMs using cycle-and-shift algorithm

Figure 1.11.5: Recurrence frequencies (%) of GMs with (a) insufficient interset variability and (b) sufficient interset variability for 13 GMs per set. The target spectrum is obtained from BT2003 for the earthquake scenario of M7.0R40 and soil site. Spectral variability is limited with symmetric tolerances between 70% and 130%. Recurrence frequency of GMs among sets is shown along the left y-axis. Cumulative distribution function (CDF) is shown on the right y-axis. It is a curve representing how broad the structural estimates are.

1.12 Impact of GM Amounts per Set

The cycle-and-shift algorithm is used to collect sets with different amount of GMs per set. The computational duration is drastically improved. For example, the selection of 23 GMs per set takes about 10 hours with the cycle-and-shift algorithm; whereas, the developed procedure (in Section 1.2.1) takes at least 2 weeks (not possible to complete).

The impact of GMs per set on the Δtop distribution is given in Figure 1.12.1. First sets underpredict Δtop with respect to the mean of all sets except for the case with 7 GMs per set. The use of more GMs per set tends to decrease the dispersion of Δtop estimates, which is also observed for PSAs at 1.00 Hz and Vbase in Appendix A.8.

The mean of all $\overline{\Delta\text{top}}^{\text{set}}$ in 1.12.1.a increases from 2.6 to 3.1 cm with more GMs per set. The mean of all $(\overline{\Delta\text{top}} + 0.95\sigma_{\Delta\text{top}})^{\text{set}}$ decreases from 4.2 to 3.7 cm with more GMs per set. A similar trend is also observed for the distribution of PSAs at 1.00 Hz and Vbase in Appendix A.8. ASN/2/01 (2006) suggests increasing the average of structural responses by a factor of standard deviation based on a number of GMs, which is shown to level the final structural responses.

The findings imply that the use of more GMs per set does not change the average structural responses (with an exception of 7 GMs/set). The results show that a single GM set is neither sufficient nor stable to capture the average responses from all set distribution.

All set distribution requires the use of at least 60 GMs in each case with different number of GMs per set. Each GM has then different recurrence frequencies. Based on the cycle-and-shift algorithm, the GMs per set is a source of uncertainty in the spectrum compatible selection. Using more GMs per set tends to reveal less dispersed distribution. The results are based on the symmetric boundaries and the simplified structural model.

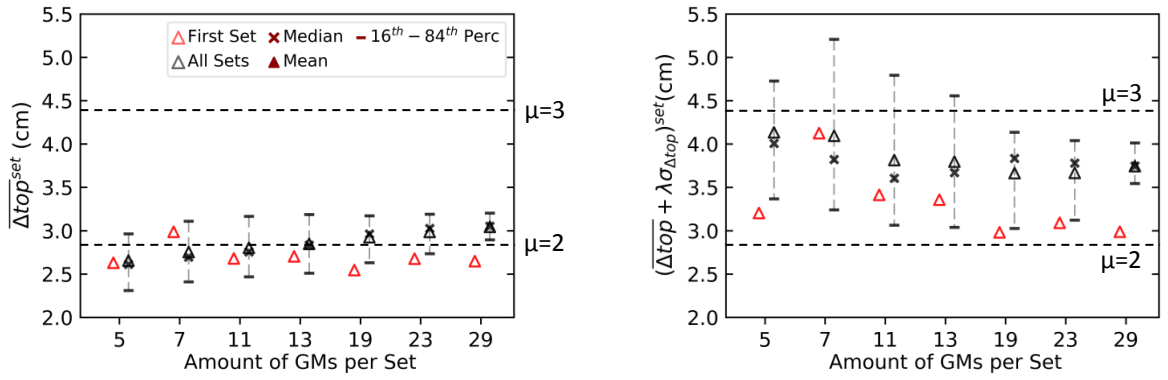

(a) Intraset of average

(b)Intraset of average-plus-λ-standard-deviation

Figure 1.12.1: Impact of the amount of GMs per set on Δtop estimates of SDOF-R2 at 1.00 Hz. 5, 7, 11, 13, 19, 23, and 29 GMs/set are selected with a target spectrum of BT2003 and ±30% symmetric tolerances. The mean Δtop estimates of the first set are shown in red color. The distribution of the Δtop estimates of all sets is shown in black color. The medians are shown with the cross markers. The means are shown with the triangle markers. The 16th and 84th percentiles are marked with the horizontal bars.

The same-event and same-station records in a set are allowed because there are not any available sets for 11 GMs per set and more. The intraset approach in (b), average plus λ of the standard deviation, is determined according to ASN/2/01 (2006). λ is calculated according to the Fisher's student method. λ is 95%, 73%, 55%, 49%, 38%, 34%, and 34% for 5, 7, 11, 13, 19, 23, and 29 GMs per set, respectively.

1.13 Conclusion

The unscaled accelerograms are the natural observations exhibiting large variability, which can be important in the decisions acquired through the seismic analysis. However, such variability is minimized in the current practice due to the time and budget constraints.

In Part 1, the impact of spectrum compatible selection with the use of unscaled real records on structural responses is studied by testing various sources of uncertainty and introducing large spectral variability in the spectrum compatible selection. Based on the unscaled earthquake records for a single earthquake scenario and their impact on structural responses of SDOF-R2 at 1.00 Hz, we draw the following conclusions:

- The signal processing and its technique can be the source of the uncertainty for the ground motion characteristics and the structural responses. The uncertainty can be improved by inspecting the acceleration, velocity, and displacement time histories for the baseline offset and the noises in a way to respect the specific needs of a seismic analysis (e.g., the frequencies of interests, the residual values).

- The chosen magnitude-distance bin has large record-to-record variability. The refinement of the site-specific parameter results in few records and large dispersion as well. In the spectrum compatible selection, the refinement of the magnitude-distance bin (i.e., with the site-specific conditions or the event dominance) slightly affects the final set-to-set distribution of ground motion characteristics and structural displacements. Therefore, the magnitude-distance bin is used.

- In the spectrum compatible selection, some ground motions can be refined based on the comparison of the spectral amplitudes with the target amplitude and the IMs (such as Arias intensity) with the average of the magnitude-distance record bin. Indeed, the spectrum compatible selection does not select those ground motions.

- The spectrum compatible ground motion selection reveals two types of variability: the intraset variability, i.e., the record-to-record variability within a ground motion set, and the interset variability, i.e., the variability from one to another ground motion set. The intraset variability may be regarded partially in the seismic regulatory codes. The interset variability has not been considered, and a single ground motion set is commonly used in the current practice. A single ground motion set is concluded to be insufficient to represent a stable structural response regarding all ground motion sets. The use of more sets is shown to be necessary for a stable distribution of the estimates. Three factors are shown to be important to replicate the interset variability with a small number of sets: (1) the number of records with respect to all ground motions, (2) the recurrence frequency of ground motions, and (3) the number of ground motions with a relatively large recurrence frequency. Accordingly, the cycle-and-shift algorithm is developed to integrate three factors. The algorithm has the advantage of revealing a stable distribution of structural responses with fewer ground motion sets and enhancing the technical limitations (i.e., memory and duration problem).

- The sigma-based tolerances (i.e., using the sigma of a GMPE) represent a certain level of observed spectral variability in the dataset of a smoothed spectrum obtained by a GMPE. It can be reasonable to use in the current practice. Tightening the tolerances in the sigma-based and the linear symmetric tolerances reveal precise estimates. Tightening the asymmetric tolerances can cause a significant decrease in the central measures.

- In the spectrum compatible selection, the number of ground motions in a set can be the source of uncertainty. ASN/02/1 (2006) suggests escalating the average of structural responses by a factor of standard deviation based on a number of ground motions, which is demonstrated to level the final structural responses. Also, using more GMs per set tends to decrease the dispersion.

- Among the investigated elements, the target spectrum obtained by the GMPEs results in significant differences in the ground motion characteristics and the structural responses. This conclusion is limited to the scenario and the assumed equivalent parameters (i.e., fault geometry, the site position).

This page is intentionally left blank.

PART 2

IMPACT OF ACCELEROGRAM VARIABILITY ON STRUCTURAL RESPONSES: COMPARISON OF LINEARLY SCALED AND SPECTRUM-MATCHED GROUND MOTIONS

2.1 Introduction

The unscaled earthquake (EQ) records are the most realistic option for the nonlinear dynamic analyses, but the modified ground motions (GMs) are rather preferred in the current engineering practice. Part 2 extends the research work to the GM selection and modification (GMSM) methods as well as the nonlinear dynamic analyses of the simple and the complex structural models. The goal in Part 2 is to compare the characteristics of the modified ground motions and the corresponding structural responses.

There are at least forty GMSM methods in the literature (Haselton et al., 2009) from the linearly scaled GMs to the generated synthetic waveforms. A consensus on how to select and scale GMs for the nonlinear dynamic analysis has not been reached since the 'best' strategy depends on the availability of the EQ records, the purpose of the analysis, the engineering demand parameter (EDP), the structural model, etc. The on-going debate can be grouped in two poles as summarized in Figure 2.1.1. On one side, the so-called 'naturalists' promote conserving the natural GM characteristics and the inherent variability; on the opposite side, the so-called 'pragmatics' promote the GM modifications to reduce the variability with respect to the target spectra.

The naturalists claim that the unscaled real records preserve the seismological properties and the natural variability. They favor the approaches lying on the zero-level record modification axis (left side, Fig. 2.1.1). One of the concerns of the pragmatics is the cost and the duration of the nonlinear dynamic analyses. They prefer reducing input GM variability to satisfy the budget and the time constraints. Also, the records of the near-fault and the large magnitude earthquake events are scarce in the database, and they can be generated with the pragmatic methods. The tightly spectrum-matched waveforms placed on the extreme of the record-modification axis (right side, Fig. 2.1.1). The linearly scaled EQ records and the loosely matched waveforms lie in the middle of the record-modification axis (Fig. 2.1.1).

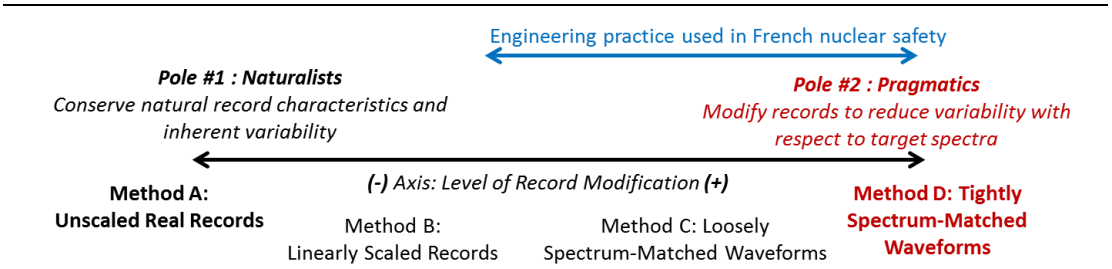

Figure 2.1.1: Two poles of discussions on ground motion selection and modification

The linear amplitude scaling (Method B, Fig. 2.1.1) is a commonly used method to adjust the spectral amplitudes at the frequency of interest such as the natural frequency of a structure, f0, (Shome et al., 1998) to the target spectral amplitude. The spectral variability at the frequency of interest is forced to be zero. The question whether linear amplitude scaling results in biased structural estimates or not has been discussed widely. Some studies have argued that the scaling factors should be limited, and the record bin (magnitude and distance) should be selected with the caution in order not to disturb the observed signal characteristics and introduce any biased structural responses (e.g., Bommer and Acevedo, 2004; Watson-Lamprey and Abrahamson, 2006, Luco and Bazzurro, 2007; Baker, 2007; Kwong and Chopra, 2015). Some researchers have claimed that the linear scaling should not be used due to the questionable structural estimates (Grigoriu, 2010). On the contrary, some studies have debated that linear scaling can be used even without a careful site-specific record selection, i.e., no limitation on scaling factors, (Iervolino and Cornell, 2005) and the scaling does not cause any bias in the nonlinear structural estimates for the far-field records (Iervolino and Cornell, 2005, Huang et al., 2011).

The spectrum matching (Methods C and D, Fig. 2.1.1) is a pragmatic approach that generates synthetic waveforms by adjusting the synthetic and the real accelerograms in the frequency domain (Rizzo et al., 1975) or the time domain (Kaul, 1978). The frequency-domain spectrum matching involves the adjustment of the Fourier amplitudes with the

target amplitudes and their inversion into the time domain. RASCAL (Silva and Lee, 1987) and SIMQKE (Gasparini and Vanmarcke, 1976) are the readily available tools to perform the frequency-domain spectrum matching. The frequency-domain spectrum matching has been shown to result in a significant manipulation of the records (Hancock et al., 2006), i.e., not a preferred method (Seifried, 2013).

The time-domain spectrum matching alters the response spectrum by adding wavelets into the acceleration time history to satisfy the defined spectral amplitude tolerance within the frequency range. Therefore, the non-stationary characteristics, Arias intensity, and the strong motion duration of the record can be better conserved (Lilhanand and Tseng, 1988; Seifried, 2013). Following the development of the algorithm (Abrahamson, 1992; Hancock et al., 2006; Al Atik and Abrahamson, 2010), RSPMatch09 (Al Atik and Abrahamson, 2010) has been made available to perform the time-domain spectrum matching, which is used in this study. Generally, the tight spectrum matching (i.e., small tolerance range around the target spectrum) is used to reduce the spectral discrepancy relative to the target spectra.

Several studies have argued that the time-domain spectrum-matched waveforms reveal biased structural estimates, which are mostly unconservative and a function of ductility (Carballo and Cornell, 2000; Bazzurro and Luco, 2006; Huang et al., 2011). On the other hand, the researchers have not reported any biased estimates with the time-domain spectrum-matched waveforms (Hancock et al., 2008; Iervolino et al., 2010a; Heo et al., 2011; Grant and Diaferia, 2013).

Some of the pragmatic methods are permitted by the building guidelines (Eurocode 8, 2004; ASCE/SEI 43-05, 2005; ASN/2/01, 2006; ASCE/SEI 41-06, 2007; AASHTO LRFD, 2010; ASCE/SEI 7, 2010). The pragmatic methods can have the following underlying assumptions: (1) the variability in the target spectra obtained from seismic hazard assessment (SHA) is negligible (NIST, 2011), which is a deterministic SHA approach, (2) the structural response variability under GMs of similar spectral shapes is minimal (NIST, 2011; Seifried and Baker, 2016), and (3) the elastic spectral shape is sufficient to select and modify GMs for the nonlinear dynamic analyses (ATC-19, 1995; Haselton et al., 2009).

The aim, herein, is to compare the impact of the pragmatic GMSM methods such as the linearly scaled and the spectrum-matched GMs relative to the naturalist method (i.e., the unscaled real records) on the signal characteristics and the structural responses of the simple and complex models. The spectrum compatible GM selection is not performed in Part 2. The GM modifications are done with Method B (MB), Method C (MC), and Method D (MD) in Section 2.2 and their impacts on the intensity measures are discussed in Section 2.3. Then, the GM families are used as inputs for the simple and complex structural models in Section 2.4. The impacts on structural responses are presented as a function of the modification degree in Section 2.5, and with respect to the structural model in Sections 2.6 and 2.7.

2.2 Ground Motion Selection and Modification Methods

Three GMSM methods are defined in Figure 2.2.1 to obtain horizontal single-direction GMs. Following the definition of the earthquake (EQ) scenario (M7.0R40, Vs450, and normal fault), the EQ records are retrieved from the strong motion database. They are then signal-processed to obtain the unscaled real records in Method A (MA) as explained in Part 1. The modifications are applied over the magnitude-distance record bin in MA.

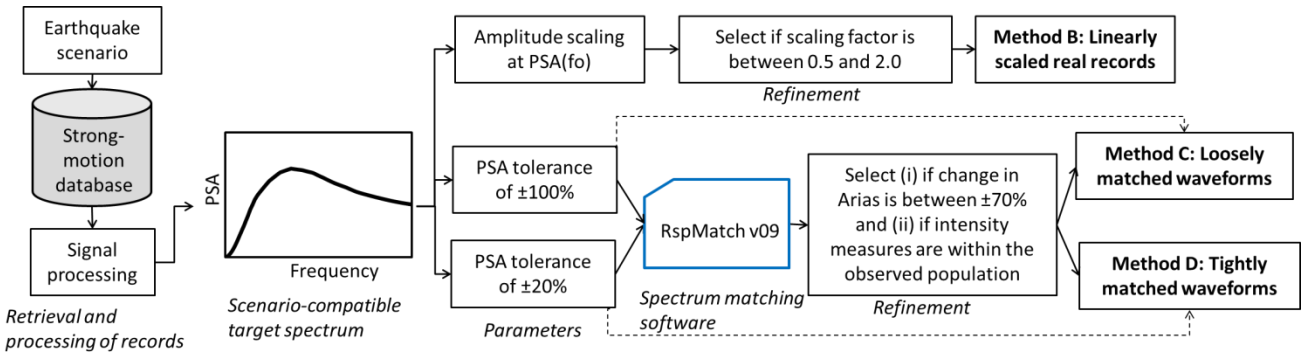

Figure 2.2.1: Ground motion selection and modification methods in Part 2.

The investigated elements are summarized in Table 2.2.1, and further information about the EQ scenario and the GMPEs can be found in Part 1.

Table 2.2.1: Elements investigated in Part 2

EQ Scenario	Target Spectra (Median GMPEs)	GMSM Methods	Structural Models
M7.0R40, Vs450, Normal Fault (88 GMs)	AB2014, AK2014, BA2011, BT2003, BD2014, CB2014, and CY2014	MB (linearly scaled GMs), MC (loosely matched GMs), and MD (tightly matched GMs)	8-/7-/2-/1-story RC buildings, 2-story masonry building, and five simple models

2.2.1 Method B: Linearly Scaled Earthquake Records

MB is the linear amplitude scaling method, which modifies the response spectra of the real record to the target PSA with a scaling factor (SF). SF is obtained by the ratio of the PSA of the record at f0, $PSA_{f0,GM}$, and the target PSA at f0, $PSA_{f0,Target}$, as given in Equation 2.2.1:

$$SF = PSA_{f0,GM}/PSA_{f0,Target} \qquad \textbf{Equation 2.2.1}$$

SF being greater than the unity signifies an increase in the PSA and vice versa. The aim is to improve the fit of a record to the target spectra and minimize the spread of the spectral amplitudes at a given frequency. SFs should be allowed in a way not to result in the large modifications and the unrealistic GM characteristics in comparison with the observed characteristics of the unscaled real records (Bommer and Acevedo, 2004, Lai et al., 2012,). Luco and Bazzurro (2007) quantified the biases in the median nonlinear structural responses to reveal the tolerable scaling factors as a function of f0, the strength of a structure, and the higher mode dominance.

In this study, the SF is limited to be between 0.5 and 2.0. The GMs are eliminated if the scaling factor is out of this limit. Lastly, a sufficient number of GMs (>45 for each target) is obtained. Figures 2.2.2 shows an example of the linearly scaled record to the target PSA at 1.00 Hz.

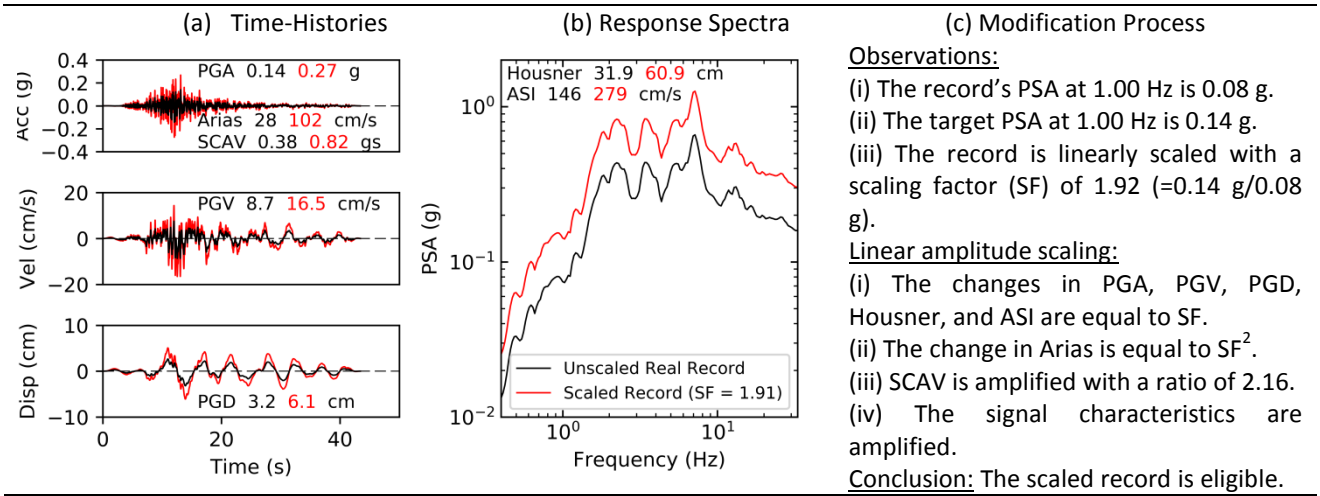

Figure 2.2.2: Time- and frequency-domain characteristics of the unscaled earthquake record and the linearly scaled GM in Method B. Method B linearly scales the unscaled real record to the target PSA at 1.00 Hz. The target is the median of AK2014 for the scenario of M7.0R40 and Vs450. The acceleration, velocity, and displacement time-histories in (a) present the unscaled GM in black and the scaled GM in red. The time histories are linearly amplified with the scaling factor. The spectral shape in (b) is amplified with the scaling factor. The modification process in (c) explains the justification of the scaling. The record is from the Kefallinia Island earthquake (ARG1 station) in Greece with Mw 6.9, R_{hypo} 31 km, and Vs30 437 m/s.

2.2.2 Method D: Tightly Spectrum-Matched Waveforms

The spectrum-matched waveforms are obtained by the nonlinear modification of a GM under the given parameters in RSPMatch09 (Al Atik and Abrahamson, 2010), which optionally linearly scales the GM to the target PGA prior to the spectrum matching.

Some studies (Hancock et al., 2006; Al Atik and Abrahamson, 2010; Grant and Diaferia, 2013; Seifried, 2013; Seifried and Baker, 2016) have utilized criteria on whether to accept or reject a spectrum-matched waveform based on the comparison of the acceleration, the velocity, and the displacement time-histories as well as the comparison of Arias intensities to justify that the original signal characteristics are conserved. However, there has not been a widely acknowledged technique, and the decision is upon the judgment of the engineer or the seismologist (Seifried, 2013).

In this study, the goal of Method D is to generate a waveform of whose spectrum is within the ±20% tolerances around the target spectrum, i.e., reducing the spectral variability significantly. Following the discussions (Seifried, 2013) and the requirements (ASN/2/01, 2006), four types of tests are utilized to judge the use of the generated waveforms:

1. Convergence test

The spectrum matching is an iterative process, and there can be non-converged waveforms for the defined tolerances around the target spectra. If the convergence criterion is not satisfied, the generated waveforms are eliminated.

2. Zero-unit check

Prior to the use of RSPMatch09, the records are ensured to have zero-units at both ends of the acceleration, the velocity, and the displacement time-histories. Having zero-units is essential for the nonlinear dynamic analysis of the far-field EQ records. The spectrum matching can reveal residual acceleration, velocity, and displacement at both ends of the time-histories.

3. Level of change in Arias intensity

The spectrum-matched waveforms are modified with respect to the frequency-domain properties, which can be essential to judge its consequences on the duration- and the amplitude-based GM characteristics. The change in Arias intensity, a duration-based IM, is imposed on remaining within ±70% of the unscaled EQ record. The rest is eliminated. The limit is optimized with a trial-and-error approach to retrieve the sufficient GMs.

4. Comparison with the observed intensity measures (IMs)

The spectrum-matched waveforms are further checked whether (i) strong motion duration (Dobry et al., 1978), (ii) peak ground velocity (PGV), (iii) peak ground displacement (PGD), (iv) Arias intensity, and (v) cumulative absolute velocity (CAV) are within the compatible range of the predicted scenario as required by ASN/2/01 (2006). The standardized cumulative absolute velocity (SCAV) is used instead of CAV due to its conservatism in a long shaking duration with the low-amplitude cycles (EPRI, 2006). Two standard deviations from the mean (95.4%) of the observed IMs in unscaled earthquake records (MA) are used to define the limiting characteristics (optimized to return a sufficient amount of GMs). The outliers (15 out of 88 GMs as explained in Section 1.7.2) are not considered.

- The observed strong-motion durations are between 5.5 and 50.2 seconds,
- The observed PGVs are between 3.3 and 51.3 cm/s,
- The observed PGDs are between 0.8 and 27.4 cm,
- The observed Arias intensities are between 4.3 and 227.1 cm/s, and
- The observed SCAVs are between 0.09 and 1.58 gs (i.e., g times seconds).

For illustrating the effect of the tests, the spectrum matching is performed to the median of AK2014 (for the scenario of M7.0R40, Vs450, and normal fault). 2 out of 88 GMs are eliminated in the convergence test, 53 GMs are removed in the zero-unit check, and 19 GMs are removed due to the large change in the Arias intensity. The rest of 14 GMs are within the observed intensity measures and are kept.

RSPMatch09 is shown to result in residual time-history values (mostly residual displacement) for a large number of GMs. An example is provided in Figure B.1.1 (Appendix B.1). The precision used in the zero-unit check (5 cm/s^2 to check the residual acceleration, 0.75 cm/s to check the residual velocity, 0.3 cm to check the residual displacement) can be stretched if more GMs is necessary. In that case, 15 more spectrum-matched waveforms (also satisfying the IM-based tests) become eligible.

Figure 2.2.3 shows an example of a tightly spectrum-matched waveform. An example of an unsatisfactory spectrum-matched GM is given in Figure B.1.2.

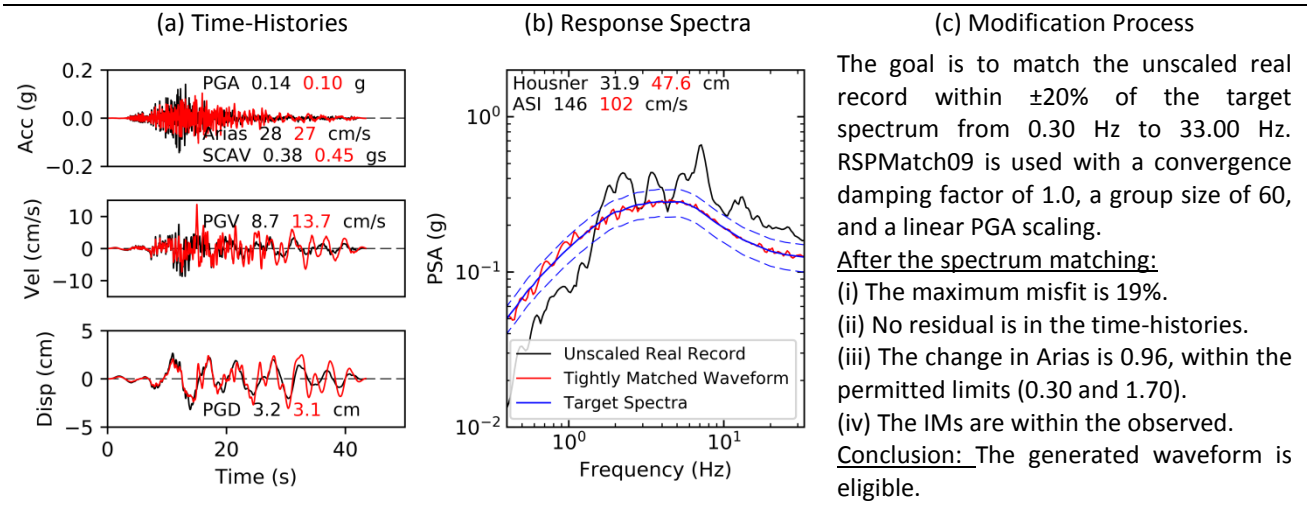

Figure 2.2.3: Time- and frequency-domain characteristics of the unscaled earthquake record and the tightly spectrum-matched GM in Method D. The record is from the Kefallinia Island earthquake (ARG1 station) in Greece with Mw 6.9, R_{hypo} 31 km, and Vs30 437 m/s. Method D modifies the GMs with respect to the target, which is the median of AK2014 for the scenario of M7.0R40 and Vs450. Column (a) shows the acceleration, velocity, and displacement time-histories of the unscaled record in black and the spectrum-matched waveform in red. In column (b), the manipulation of the spectral shape is shown. The wavelets that are added by the software explain the significant change in the acceleration and velocity histories. The reason why the displacement history is slightly affected is the frequency content of the displacement history (0.10—0.20 Hz) being below the lower limit. In column (c), the modification process is explained along with the justification.

2.2.3 Method C: Loosely Spectrum-Matched Waveforms

MC is defined in this thesis and proposes a new test with the spectrum matching of greater spectral variability. MC applies the loose spectrum matching with a goal to generate a waveform of whose spectrum is between -20% and +100% tolerances of the target spectrum. The technical difference between MC and MD is due to the parameters such as the convergence tolerance and the convergence damping in RSPMatch09.

RSPMatch09 lacks alternative ways to define an asymmetric tolerance. The tolerance of ±100% is used, which allows any PSAs below 100%-above-target spectrum. Therefore, a test is applied to limit vis-à-vis PSAs to 20% of the target PSAs. For the loosely spectrum-matched waveforms, the same refinements in Section 2.2.2 are applied.

For the target spectrum of AK2014 (for the scenario of M7.0R40, Vs450, and normal fault), 19 out of 88 GMs are eliminated in the convergence test. 9 GMs are removed in the zero-unit check, and 34 GMs are removed due to the large change in Arias intensity. Rest of the 24 GMs is within the observed IM range and is kept. Figure 2.2.4 demonstrates an example of a loosely spectrum-matched waveform. An example of an unsatisfactory spectrum-matched GM is given in Figure B.1.3 (Appendix B.1). An example input of RSPMatch09 is provided in Appendix B.2.

(a) Time-Histories

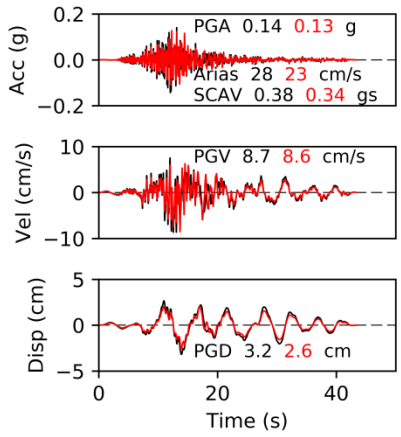

(b) Response Spectra

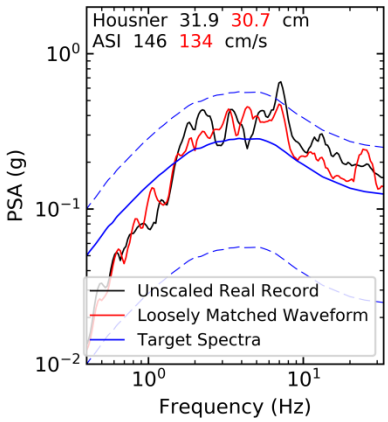

(c) Modification Process

The goal is to match the unscaled real record between 20% and 200% of the target from 0.30 Hz to 33.00 Hz. RSPMatch09 is used with a convergence damping factor of 0.15, a group size of 60, and a linear PGA scaling.

After the spectrum matching:

(i) The spectrum is within the allowed PSAs (blue dashed lines).

(ii) No residual is in the time-histories.

(iii) The change in Arias is 0.82.

(iv) The IMs are within the observed.

Conclusion: The generated GM is eligible.

Figure 2.2.4: Time- and frequency-domain characteristics of the unscaled earthquake record and the loosely spectrum-matched GM in Method C. The record is from the Kefallinia Island earthquake (ARG1 station) in Greece with Mw 6.9, R_{hypo} 31 km, and Vs30 437 m/s. Methods C modifies the GMs with respect to the target, which is the median of AK2014 for the scenario of M7.0R40 and Vs450. The allowed PSAs are plotted with the blue dashed lines. Column (a) shows the acceleration, velocity, and displacement time-histories of the unscaled record in black and the spectrum-matched waveform in red. In column (b), the spectral shapes are compared. The changes in spectra and time-histories are slight; in other words, the characteristics of the unmodified GM are conserved. In column (c), the modification process is explained.

2.3 Impact of GMSM on Intensity Measures

The objective of this section is to evaluate how the modifications in Method B (MB), Method C (MC), and Method D (MD) change the signal characteristics with respect to the unscaled real records. MB, MC, and MD are obtained from 88 GMs (without GM refinement based on the IMs explained in Section 1.7.2). The PSA distributions for MA, MB, MC, and MD are shown in Figure 2.3.1. The observed spectral variability is consistently wide in MA. The spectral variability in MB is the smallest at 2.5 Hz and purges as distancing away from 2.5 Hz. The spectral variability in MC is larger in the low frequencies than in the high frequencies, which is due to the PGA scaling. MD reveals smoothed spectra with a minimized spectral dispersion from the target spectra. The observed spectral variability (MA) is partially conserved in MB and MC but reduced in MD.

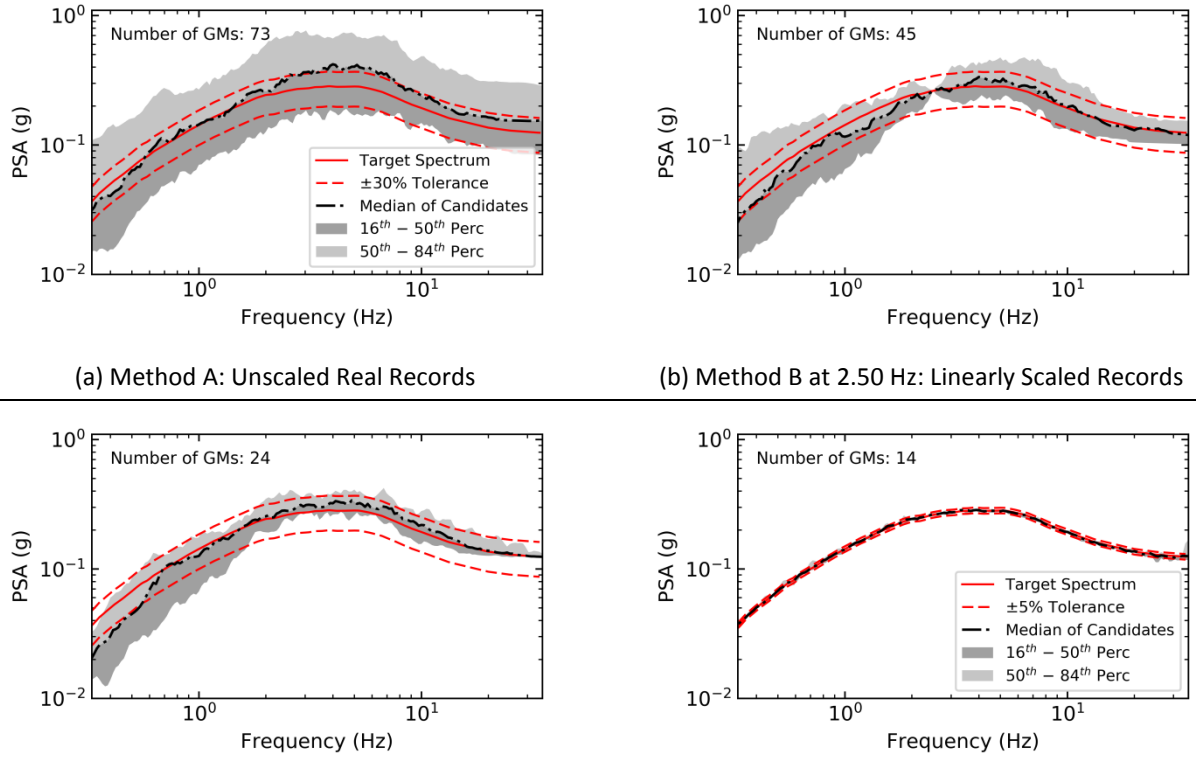

(a) Method A: Unscaled Real Records

(b) Method B at 2.50 Hz: Linearly Scaled Records

(c) Method C: Loosely Matched Waveforms

(d) Method D: Tightly Matched Waveforms

Figure 2.3.1: The median of AK2014 for the defined scenario and the 16th, 50th and 84th percentiles of pseudo-spectral accelerations (PSAs) of ground motions (GMs) in Methods A, B, C, and D. The modifications in Methods B, C, and D are applied according to the target, which is the median of AK2014 for the earthquake scenario of M7.0R40, Vs450, and normal fault. The red dashed lines show ±30% around the median of AK2014 in Methods A, B, and C; and ±5% around the median of AK2014 in Method D. Method B at 2.50 Hz scales GMs to the target PSA at 2.50 Hz. The amount of GMs is given for the methods. Method A does not include outliers as explained in Section 1.7.2.

The median spectrum in Method A is around the target from 0.30 Hz to 2.00 Hz and above the target along the rest of the frequencies. The median spectrum in Method B is less than the target from 0.3 Hz to 2.5 Hz and close to the target along the rest of the frequencies. Method C results in the median spectra below the target from 0.3 Hz to 0.7 Hz and close to the target. Method D reveals the closest spectra to the target.

The IM distributions are given in Figure 2.3.2 for MA, MB, MC, and MD when they are refined with respect to PSA at 2.50 Hz. The GMSM methods (except for MB at 2.50 Hz) generally reveal less IMs on average than the observed IMs in MA. MB reveals the comparable dispersion with MA except for PSAs at the scaling frequency. The effect of MB on the IMs is upon the scaling frequency. On the other hand, MD has minor variability for the frequency-based IMs but considerable variability for the amplitude- and duration-based IMs. The IM distributions without the PSA refinement are provided in Table B.3.1 (Appendix B.3).

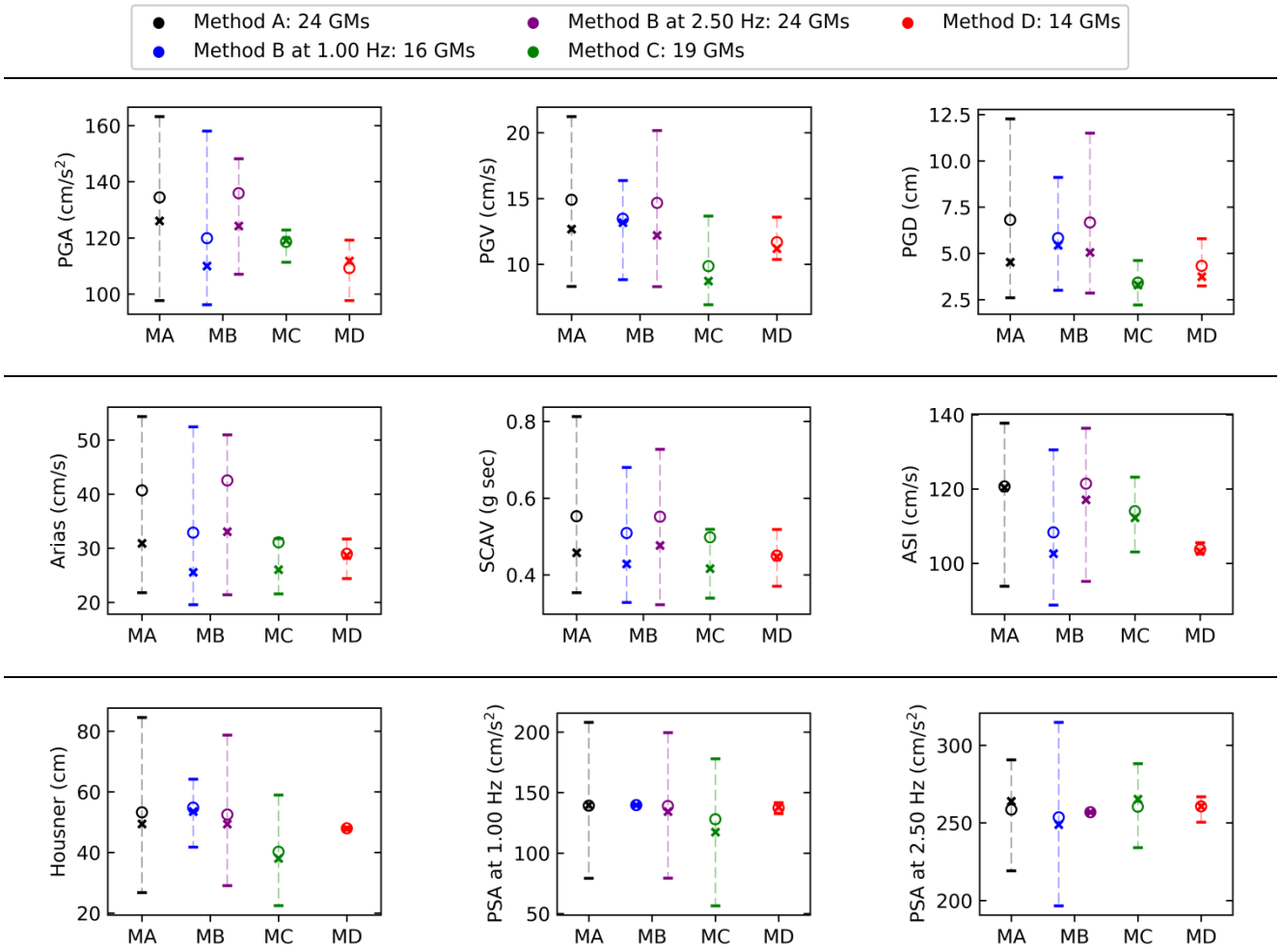

Figure 2.3.2: Intensity measures obtained by Methods A, B, C, and D. The y-axes plot intensity measures (IMs). The x-axes plot Method A (MA), Method B (MB), Method C (MC), and Method D (MD) with the colors given in the legend. The 16th and 84th percentiles of the distributions are shown with the horizontal bars. The mean of the distribution is shown with the unfilled circle. The median is plotted with the cross marker. The target is the median of AK2014 for the scenario of M7.0R40, Vs450, and normal fault. MB at 1.0 Hz is scaled to the target PSA at 1.0 Hz. MB at 2.5 Hz is scaled to the target PSA at 2.5 Hz. GMs in MA, MB at 1.00 Hz and MC are selected if they are within ±30% of the target PSA at 2.50 Hz. GMs in MB at 2.50 Hz are refined to have a scaling factor between 0.7 and 1.3. GMs in MD have PSAs at 2.50 Hz between ±20% of the target PSA at f0. The amount of data is given in the legend. PGAs are calculated at 35.0 Hz. The dispersion in MD can be observed since the spectrum matching range between 0.33 and 33.00 Hz.

The changes in the IMs, $Val_{Mx,change}$, are then calculated for each GM in MB, MC, and MD as given in Equation 2.3.1:

$$Val_{Mx,change} = \frac{Val_{Mx,i}}{Val_{MA,i}} \qquad \textit{Equation 2.3.1}$$

with $Val_{MX,i}$ being an intensity measure (IM) or an engineering demand parameter (EDP) corresponding to the i^{th} GM in MB, MC, or MD, and $Val_{MA,i}$ being the IM or the EDP corresponding to the i^{th} unscaled earthquake record (MA).

The distribution of the changes in IMs is given in Figure 2.3.3. For MB, the changes in PGA, PGV, ASI, Housner, and PSAs are equal to the scaling factor, which is between 0.50 and 2.00. The change in Arias is equal to the square of the scaling factor for MB. The GMs for MC and MD are limited to have a change of Arias intensity within ±70% of the unscaled GM. The central tendency (mean and median) is between 0.70 and 1.20. One sigma (16^{th}–84^{th} percentiles) remains mostly within 0.50 and 2.00 except for the Arias intensity. In general, MB, MC, and MD cause a slight change of the signal characteristics. The observations are valid for another GMPE (BA2011) used as a target spectrum in Figure B.3.1.

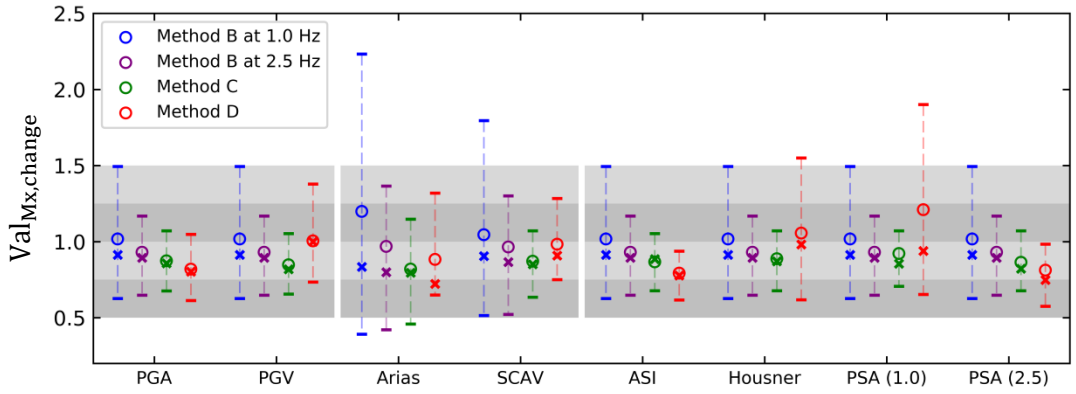

Figure 2.3.3: The change of intensity measures (IMs) in Methods B, C, and D with respect to Method A. The change is defined as a ratio of IMs of the modified ground motion (GM) and the unmodified GM. Values greater than the unity represents an increase in IM and vice versa. The 16th and 84th percentiles of the distribution are shown with the horizontal bars. The median and the mean of the distribution are shown with the cross marker and the unfilled circle, respectively. The color code represents the method in the legend. The target is the median of AK2014 for the scenario of M7.0R40, Vs450, and normal fault. There are 52 GMs in Method B at 1.00 Hz (scaling to the target PSA at 2.50 Hz), 45 GMs in Method at 2.50 Hz (scaling to the target PSA at 2.50 Hz), 24 GMs in Method C, and 14 GMs in Method D.

The medians of the distributions are below the unity, i.e., more than half of the modified GMs experience a decrease. The means of the distributions are between 0.80 and 1.20. Method C causes the most reduction in the duration-based IMs such as Arias and SCAV. Generally, the change scatters the most in Method B at 1.00 Hz. Method C reveals the most consistent dispersion of the change in IMs.

The total amount of GMs, and, therefore, the expected duration of the nonlinear structural analyses are the least in MA and the most in MB. MA, the pure naturalist method, does not depend on the structural model and the target spectra. MB depends on the target spectra and the structure's f0. For a single structural model and a single GMPE, there are about 50 GMs in MB. For 7 GMPEs and 8 fundamental frequencies, there are around 2800 GMs in MB. The modifications in MC and MD depend on target spectrum. MC has around 25 GMs per target spectrum, and there are 151 GMs in total. In MD, there are about 15 GMs per target spectrum and 98 GMs in total.

2.4 Structural Models

This section introduces the structural models in Table 2.4.1 in order to extend the tests on the changes in engineering demand parameters (i.e., $\mathrm{Val}_{\mathrm{Mx,change}}$) in the subsequent sections. In this study, five complex and the five simple structural models, with natural frequencies (f0) ranging from 0.60 Hz to 5.68 Hz, are used. These characteristics are previously considered to apply the linear amplitude scaling (MB).

2.4.1 Simple Structural Models

The single-degree-of-freedom (SDOF) oscillators are referred by their strength reduction factor (R1 or R2), and the oscillation frequency, f0, as listed in Table 2.4.1 with an ID from S6 to S9. The models are based on the elastoplastic strain hardening behavior (i.e., uniaxial bilinear kinematic hardening). The models dissipate the seismic energy after yielding.

Table 2.4.1: List of complex and simple structural models.

ID	Structure	Modeling	f0[(1)] (Hz)	f1[(2)] (Hz)	Height (m)	R[(3)]	Yielding Δtop[(4)] (cm)	Yielding Vbase[(5)] (kN)
S1	8-Story RC	2D Frame	1.00	3.00	28.0	N/A	2.4	300
S2	7-Story RC		1.32	4.35	20.1		4.0	700
S3	2-Story RC		4.17	—	4.2		1.0	200
S4	2-Story Mas.		4.34	—	5.4		0.6	90
S5	1-Story RC	3D	5.68	18.8	1.7	N/A	0.4	25
S6	SDOF-R2	SDOF	0.60	N/A	N/A	2.0	2.3	11 465
S7	SDOF-R2		0.80			2.0	1.8	10 884
S8a	SDOF-R1		1.00			1.0	2.9	2 924
S8b	SDOF-R2		1.00			2.0	1.5	1 462
S9	SDOF-R2		2.50			2.3	0.5	140

[(1)]f0 is the natural oscillation frequency. [(2)]f1 is the second-mode oscillation frequency. [(3)]R is the strength reduction factor. [(4)]Δtop represents roof displacement for the complex models (S1, S2, S3, S4, and S5), and lateral structural displacements for the simple models (S1, S2, S3, S4, and S5). [(5)] Base shear forces are denoted by Vbase.

In Figure 2.4.1, the material behavior model is shown. The S6, S7, S8a, and S8b models use a linear increase in their strain hardening part, which is 5% of the initial stiffness as referred to Rule 1. The S9 model with Rule 2 can absorb slightly more energy due to the larger area under the force-displacement curve.

The equal displacement concept is also given in the figure. It is utilized to design the strength of the SDOF models commonly by the practicing engineers in the seismic-resistant design of the residential buildings. Significant nonlinear behavior with permanent damage is expected. The aim of this approach is to control the damage by detailing the structural systems adequately (i.e., supplying a ductility demand, μ) and ensuring the life safety performance under the maximum considered earthquake level (ATC-19, 1995; Chopra, 2012; FEMA, 2012).

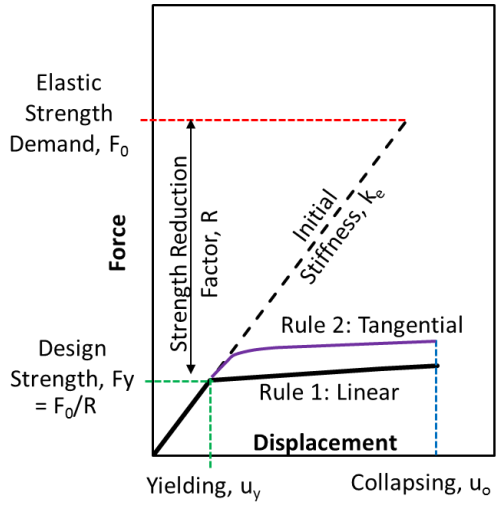

Figure 2.4.1: Material behavior models of simple models and the employed design concept.

Table 2.4.2 presents the characteristics of SDOFs. The lateral stiffness, k, and the mass, m, are obtained by Equation 2.2.1:

$$f0 = \frac{1}{2\pi}\sqrt{\frac{k}{m}} \qquad \textit{Equation 2.2.1}$$

The k and m parameters impact the amplitude of the resulted force. However, they are not important when comparing the relative effect of the input GMs.

The S8a and S8b models (described in Section 1.5) have the same material behavior model and the same f0. The S8a model is designed to resist the seismic forces linearly. The S8b model is designed for half of the seismic forces and is expected to exhibit more inelastic behavior.

The structures are modeled with a fixed base. The damping ratio is 5% for the simple structural models. The S6, S7, S8a, and S8b models are analyzed with OpenSees v2.4.6 (Mazzoni et al., 2006). The S9 model is analyzed with GEFDyn (Aubry et al. 1986, Aubry and Modaressi 1996).

Table 2.4.2: Characteristics of simple models.

ID	Label	**f0** (Hz)	**Lateral Stiffness** (kN/m)	**Mass** (tonne)	**Target PSA(f0)**[(1)] (m/s^2)	**Elastic Strength Demand, ESD**[(2)] (kN) = Mass X PSA(f0)	**Strength Reduction Factor, R**	**Design Strength**[(3)] (kN) =ESD/R
S6	SDOF-R2	0.60	500 000	35 217	0.65	22 930	2.0	11 465
S7	SDOF-R2	0.80	600 000	23 771	0.92	21 767	2.0	10 884
S8a	SDOF-R1	1.00	100 000	2 536	1.15	2 924	1.0	2 924
S8b	SDOF-R2	1.00	100 000	2 536	1.15	2 924	2.0	1 462
S9	SDOF-R2	2.50	33 523	136	2.36	321	2.3	140

[(1)] Target PSAs at f0 are the averages of the median spectra of the GMPEs for the earthquake scenario (M7.0R40, Vs450, and normal fault) as given in Section 1.4. [(2)]Elastic strength demand, ESD, is estimated by multiplying mass and average PSA at f0. [(3)]ESD is then divided by strength reduction factor, R, to obtain the design strength.

2.4.2 Complex Structural Models

The complex structural models have the IDs ranging from S1 to S5. They are labeled with the number of stories and the type of the material as given in Table 2.4.1. The S1, S2, S3, and S4 models are two-dimensional (2D) models. S5 is a three-dimensional (3D) model which is modeled with the frame depth.

The S1 model is an 8-story reinforced concrete (RC) model that represents a dwelling typical from French Antilles in 1970. There are four 4-meter long bays in the longitudinal direction (moment resisting frame), and the height of the stories is about 3.4 m. It is noted that the irregularities exist in the stiffness distribution, which induces torsion. An equivalent two-dimensional model of the three-dimensional model was obtained, and it was shown to be sufficiently accurate (Saez, 2009; Saez et al., 2011). The modal mass contribution is 90% in the first mode of 1.00 Hz, and 7% at the second mode of 3.00 Hz.

The S2 model is a 7-story RC model and consists of four 4-meter wide bays with a height of about 2.6 meters. The structural elements are modeled by the plastic hinge beam-columns elements, which is referred as ‘b02’ in the reference (Marante et al., 2005; Saez, 2009; and Saez et al., 2013).

The S3 model is a 2-story RC model and is composed of a single 4-meter wide bay with an average height of 2.1 meters, which is referred as ‘b01’ in the reference (Marante et al., 2005; Saez, 2009; Saez et al., 2013).

The S4 model is a 2-story masonry model and has a single 4-meter long bay with an average height of 2.1 m. The model includes beam-column elements and diagonal struts for the structural behavior with zero-strength solid elements for the structural mass. The detailed information of this model can be found in the references (Lopez-Caballero et al., 2011; Ferrrario et al., 2017).

This S1, S2, S3, and S4 models are analyzed with GEFDyn (Aubry et al., 1986; Aubry and Modaressi, 1996). The S2, S3, and S4 models are defined with the two-component model (Giberson, 1969) and the modifications (Prakash et al., 1993) to account for the axial force and bending moment interaction. The damping ratio is between 1% and 6% for the S1, S2, S3, and S4 models. The damping evolutions are exemplified under a single GM in Figure B.4.10 (Appendix B.4).

The S5 model is a 1-story RC model with a single 3-meter long bay and a height of 1.7 meter. The model is constructed for the shaking table test. Later, the numerical model is done according to the experimental results (CEA Report, 2007). The nonlinear dynamic analyses are completed in Cast3M v15 (CEA, 2015).

The lateral-force-resisting system is the moment resisting frame in the S1, S2, S3, and S5 models. The yielding limits (for the roof displacements, Δtop, and the base shear forces, Vbase) are given in Table 2.4.1. They are the approximate values obtained after analyzing the response time-histories and the push-over curves for Δtop and Vbase. Due to the various cyclic motions of the input GM, the yielding limits may vary. There can be critical elements which may yield

before the defined limits. The structural models are modeled with a fixed base (i.e., soil effect is not considered). The geometry, the mechanical properties, and additional information are provided in Appendix B.4. An example response history for the complex models is given in Figure B.4.13.

2.5 Impact of Modification Degree on Structural Responses

This section evaluates the impact of the modification degree in the GM characteristics (i.e., the scaling factor for MB and the change in Arias intensity for MC and MD) on the changes in structural responses (i.e., $\mathrm{Val}_{\mathrm{Mx,change}}$). The impact of the scaling factors (SF) on structural responses of complex models is shown in Figure 2.5.1. If the SF is outside 0.50 and 2.00, the structural responses deviate from the original structural responses (i.e., unscaled EQ record). The changes in the structural responses scatter from the 1:1 line especially at the low SFs. If the SF is between 0.50 and 2.00, the corresponding structural responses are between 0.50 and 2.00 of the observed structural responses, which suggests that the controlled signal modification can result in controlled changes in the structural responses. Similar observations can be made for other complex models in Figure B.6.1 (Appendix B.6), except for the change in Vbase of the S1 model.

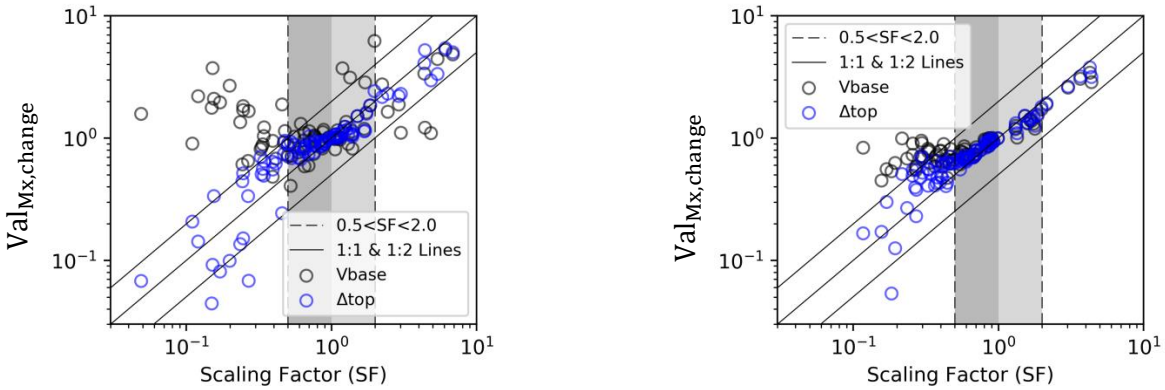

Figure 2.5.1: Comparison of scaling factors (SF) in Method B and the corresponding change in structural responses. The x and y-axes are in logarithmic scale. The base shear forces (Vbase) are obtained at the time of maximum absolute of the roof displacements (Δtop). The change in Vbase at the corresponding SF is plotted with the black circles. The change in Δtop at the corresponding SF is plotted with the blue circles. The 1:1, 1:2, and 2:1 lines are shown with the solid black lines. Each data represents GM scaled to the target PSA at f0. The SF greater than the unity imply an amplification of the signal characteristics and vice versa. The ratio of the response greater than the unity implies an increase in the structural response and vice versa. The change is defined according to Equation 2.3.1. The target is the median of AK2014 for the scenario of M7.0R40, Vs450, and normal fault. The permitted level of SF is between 0.5 and 2.0 as shown with the vertical dashed lines. The S2 and S3 models (described in Section 2.4.2) have f0 of 1.32 Hz and 4.17 Hz, respectively.

The impact of the changes in the Arias intensity by the loose spectrum matching is illustrated in Figure 2.5.2. The restriction in Arias intensity (range of 0.30 and 1.70) prevents the excessive change of the original structural responses, which are between 0.4 and 1.5. The changes in structural responses scatter less if they are within the restricted limits of Arias intensity. The similar observations can be drawn for the tightly spectrum-matched GMs (MD) in Appendix B.5 (Figure B.5.1), except for few GMs (up to 2.5 increase of Δtop even the slight change in Arias intensity).

The GM modification can result in the deviations from the observed structural responses of the original EQ records. If the level of GM modifications is restricted, the deviation from the observed structural responses can also be restricted.

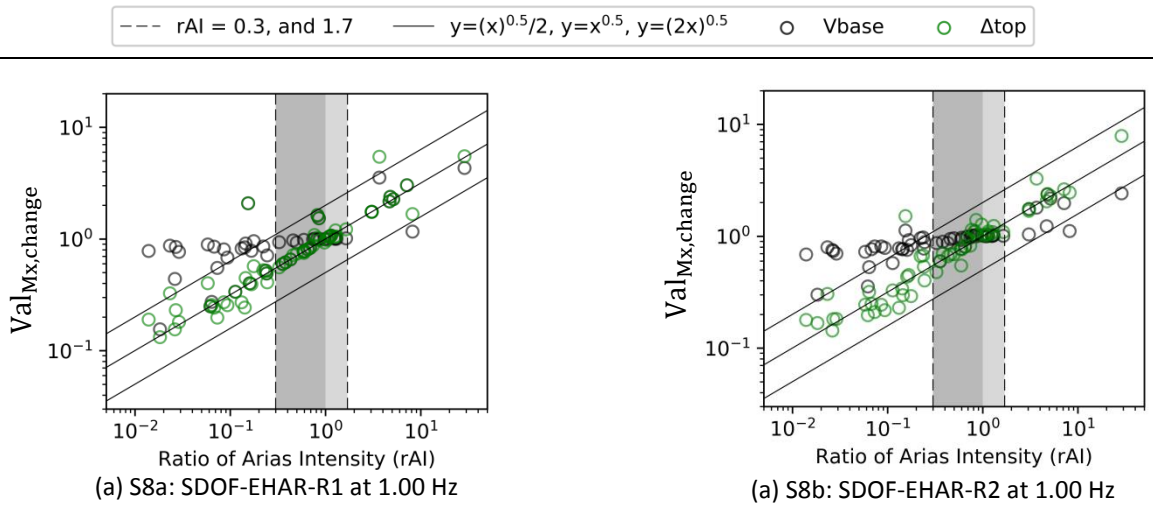

Figure 2.5.2: Comparison of the ratio of Arias intensity (rAI) in Method C and the corresponding change in structural responses. The x and y-axes are in the logarithmic scale. The change in the base shear forces (Vbase) at the corresponding rAI is plotted with the black circles. The change in the roof displacements (Δtop) at the corresponding rAI is plotted with the green circles. The change is defined according to Equation 2.3.1. rAI greater than the unity implies an amplification of the Arias intensity and vice versa. The ratio of the response greater than the unity implies an increase in the structural response and vice versa. Each data represents a loosely spectrum matched GM according to the target, which is the median of AK2014 for the scenario of M7.0R40, Vs450, and normal fault. The permitted level of rAI is between 0.3 and 1.7. The S8a model is designed to resist the lateral design forces linearly. The S8b model is designed for half of the lateral design forces and exhibits more inelastic behavior.

2.6 Impact of GMSM Methods on Structural Responses of Simple Models

2.6.1 Change in Structural Responses of Simple Models

The GMs in Figure 2.6.1 are used as inputs for the S8b model, and the structural response histories are compared in Figure 2.6.2. The change in the GM characteristics results in differences in the Δtop and Vbase demands. In MA, MB, MC, and MD, PSAs at 1 Hz are 0.075 g, 0.145 g (+93% of MA), 0.115 g (+53% of MA), and 0.153 g (+104% of MA), respectively. The Δtop demands are 1.9 cm, 3.3 cm (+74% of MA), 2.7 cm (+42% of MA), and 3.9 cm (+107% of MA) in MA, MB, MC, and MD, respectively. It implies that the change in the PSAs at f0 is related to the change in Δtop.

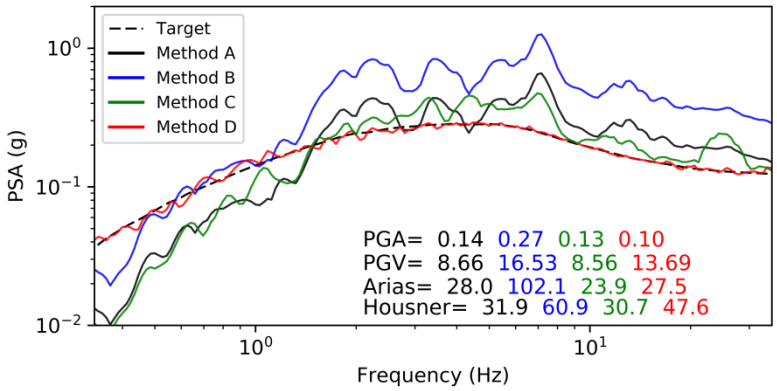

Figure 2.6.1: Spectra of the input GMs obtained by Methods A, B, C, and D. The record is from the Kefallinia Island Earthquake (ARG1 station) in Greece with Mw 6.9, R_{hypo} 31 km, and Vs30 437 m/s. Methods B, C, and D apply modifications to the unscaled real record in Method A according to the target shown with the dashed black line. The target is median AK2014 for the scenario of M7.0R40 and Vs450. The spectra and IMs follow the same color code in the legend. Method B scales GM to the target PSA at 1.00 Hz with a scaling factor of 1.93, which equally amplifies PSAs and some IMs. Method C slightly affects specific IMs such as PGA, PGV, and Housner but manipulates Arias significantly. The modifications in Method D cause PGV and Housner increasing, but PGA and Arias dropping, which can be related to the amplification of the low-frequency content and the decrease of the high-frequency content.

However, the change in PSAs may not be related to other engineering demand parameters. The GM modification results in the different permanent deformations and the different time point at which the maximum demand occurs. The structural demands in compression (positive sign) and tension (negative sign) are different. The latter difference is not considered for the simple models (since the tensional and compressional demands are assumed to be equal), but could be of high importance of the systems with the different tensional and compressional capacity (e.g., RC members).

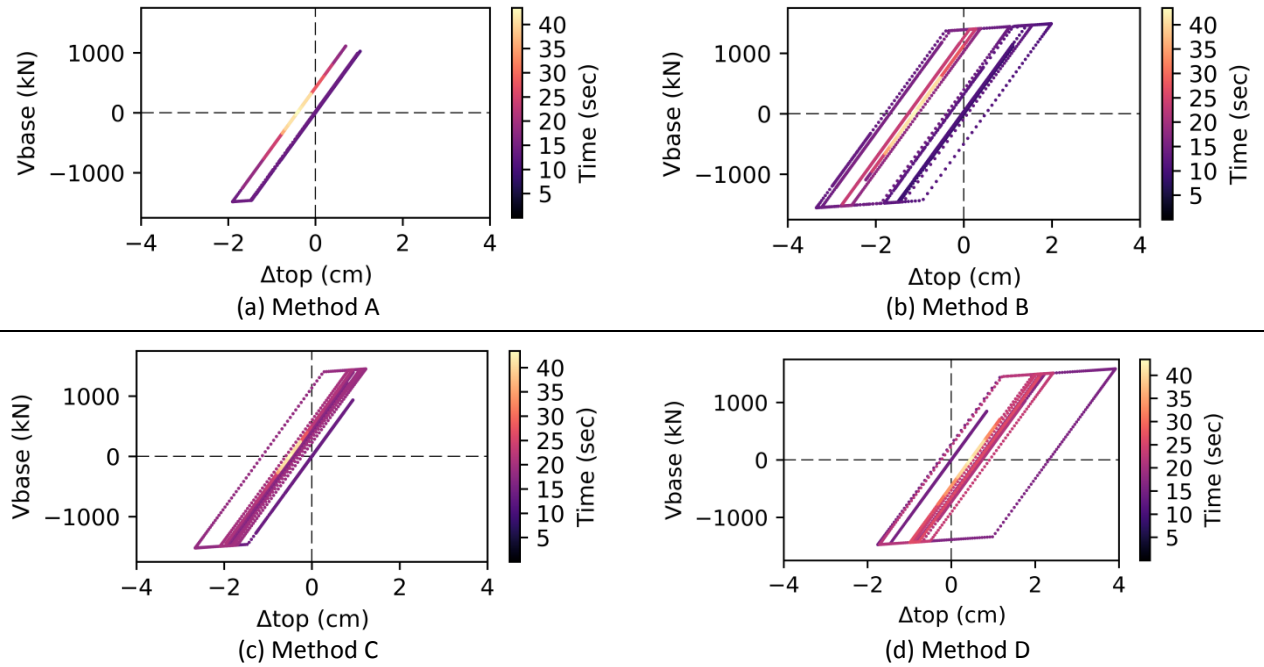

Figure 2.6.2: Response histories of the S8b model under GMs in Methods A, B, C, and D. The x-axis represents the lateral displacements relative to the ground (Δtop). The y-axis is the base shear forces (Vbase). The color of the curve relates to the period of the time given in the legend: the darker colors represent the initial part, and the lighter colors represent the final part. The positive values signify the compression, and the negative values signify the tension on the element. The unscaled record is from the Kefallinia Island earthquake (ARG1 station) in Greece with Mw 6.9, R_{hypo} 31 km, and Vs30 437 m/s. The input GMs are provided in the previous figure. The structural model (described in Section 2.4.1) has a natural frequency of 1.00 Hz.

The response trajectories (thus, seismic energy absorptions), and the residual values in (b), (c), and (d) differ from (a). Maximum absolute of roof displacements (Δtop) are 1.9 cm in (a), 3.3 cm in (b), 2.7 cm in (c), and 3.9 cm in (d). Maximum absolutes of base shear forces (Vbase) are 1484 kN in (a), 1556 kN in (b), 1522 kN in (c), and 1585 kN in (d). The maximum responses occur in tension in (a), (b), and (c); whereas, they happen in compression in (d).

In order to compare the changes in structural responses triggered by the GMSM methods, Figure 2.6.3 is shown for the maximum absolute responses of the simple models under the modified GMs and the unscaled earthquake GMs (MA). The subfigures on the last column demonstrate the statistics of the change in the structural responses, i.e., $\mathrm{Val}_{\mathrm{Mx,change}}$, according to Equation 2.3.1 (horizontal black line represents the equality with the unscaled earthquake record). The central values (mean and median) of the structural responses remain in the close vicinity of MA (within ±25% of MA). The change in Vbase is insignificant for the nonlinearly behaving simple models (i.e., the S6, S7, S8b, and S9 models). MB, MC, and MD are not able to capture the natural variability observed in the structural responses of MA. The unscaled earthquake records causing μ greater than 6 (i.e., the Δtop demand being six times above the yielding limit) are modified in MB and MC to reveal unconservative μ. The GMs in MD does not typically cause μ greater than 6.

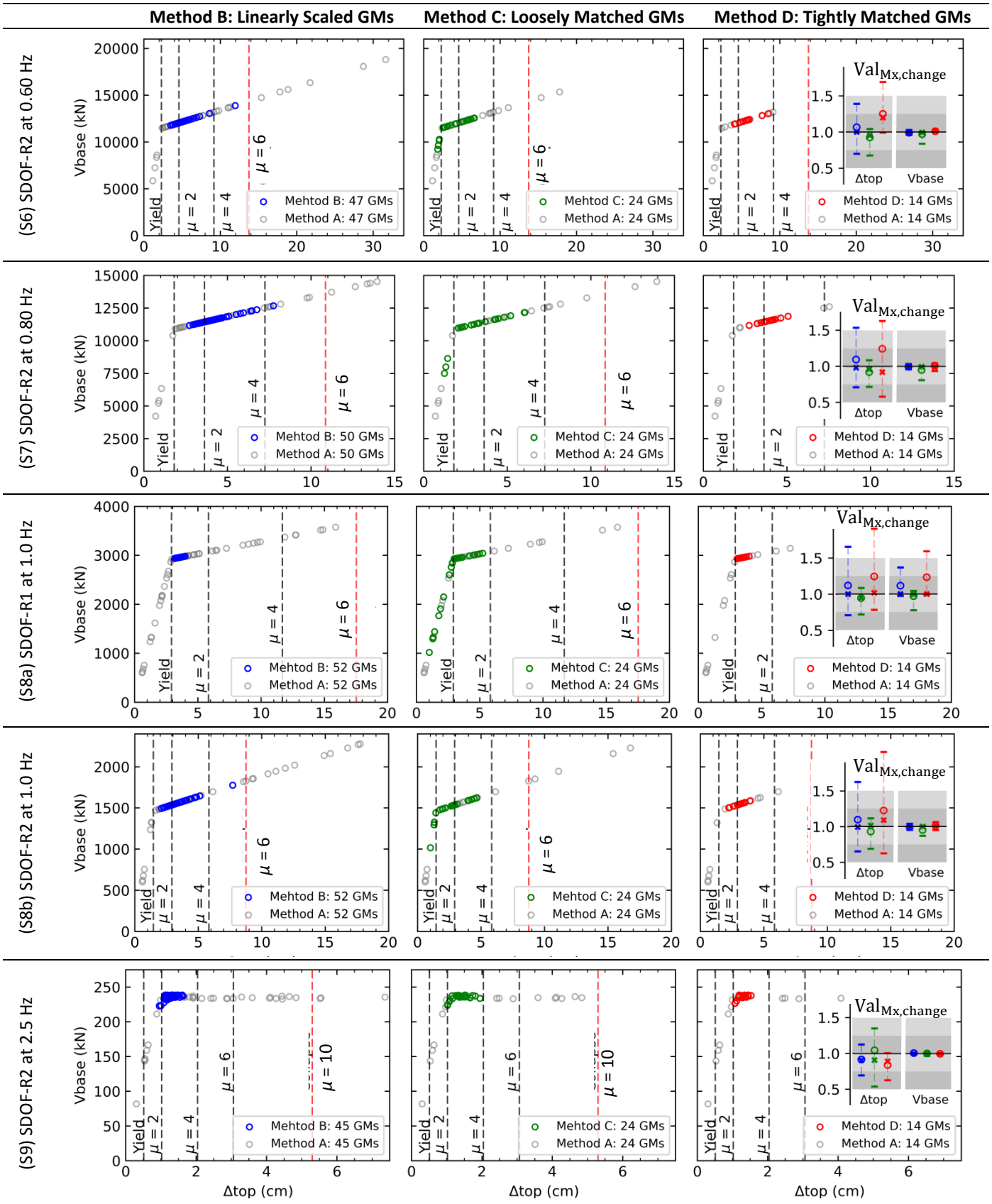

Figure 2.6.3: Structural responses of the simple models under GMs of Methods B, C, and D. Data for Methods B, C, and D are shown with blue, green, and grey, respectively. The corresponding data for the unscaled earthquake records (Method A) are shown with grey. The figures are divided in column-wise according to the method type and in row-wise according to the structural model. The x-axis shows the maximum absolute of the lateral structural displacements (Δtop). (continued)

The y-axis illustrates the maximum absolute of the base shear forces (Vbase). The amount of the GMs is given in the legend box. The yielding limit and ductility levels, μ, at 2, 4, and 6 are plotted with the vertical dashed lines.

The subplots in the last column demonstrate the statistical change as calculated by Equation 2.3.1. The color code indicates the method. The grey shades represent the ratios of 0.50—0.75, 0.75—1.00, 1.00—1.25, and 1.25—1.50, from a lower to an upper shade. The equality is highlighted by the black solid line. The values above it indicate an increase in the structural response with respect to the unscaled earthquake record and vice versa. The 16^{th} and 84^{th} percentiles of the distribution are shown with the horizontal bars. The median and the mean of the distribution are shown with the cross marker and the unfilled circle, respectively.

The target is the median of AK2014 for the scenario of M7.0R40, Vs450, and normal fault. The GM amount decreases from Method B to Method D. Method B and Method D always result in yielding, and MC partially results in yielding.

2.6.2 Dispersion of PSAs and Lateral Displacements of Simple Models

The distribution of PSAs at f0 and the corresponding Δtop estimates are compared as a function of the GMSM methods in Figure 2.6.4. The greater PSA at f0 is expected to cause the greater structural demand; however, this statement is challenged for the Δtop distributions obtained for the S7 and the S8b models. With respect to the observed mean Δtop in MA, the modifications can introduce significant differences (e.g., conservative in the S6 model by MB and MD and unconservative in the S8b model by MC and MD) and slight changes (e.g., in the S7, S8a, and S9 models).

The output (Δtop) demands span along a wide range in the nonlinearly behaving models (the S6, S7, S8b, S9 models) regardless of the choice of the GMSM method, which can cover the great portion of the naturally observed Δtop demands (including the mean). In MB and MD, the variability of PSAs at f0 does not correspond to the variability in the Δtop demands. The conclusions are structure-dependent.

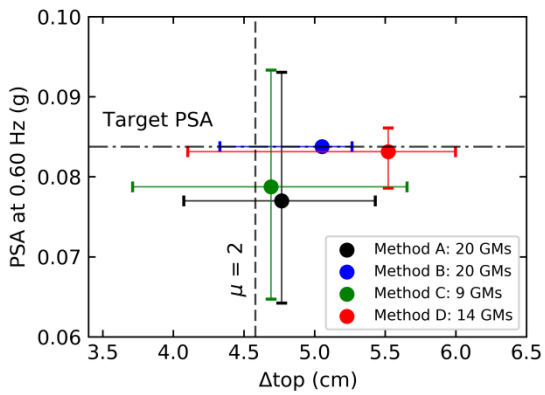

(a) S6: SDOF-R2 at 0.60 Hz

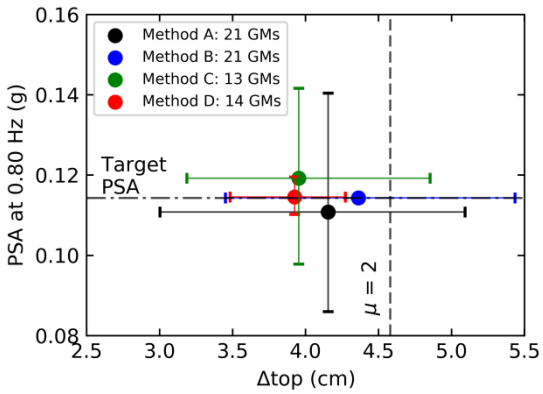

(b) S7: SDOF-R2 at 0.80 Hz

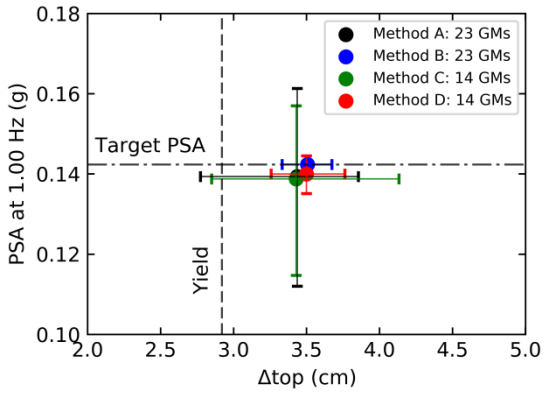

(c) S8a: SDOF-R1 at 1.00 Hz

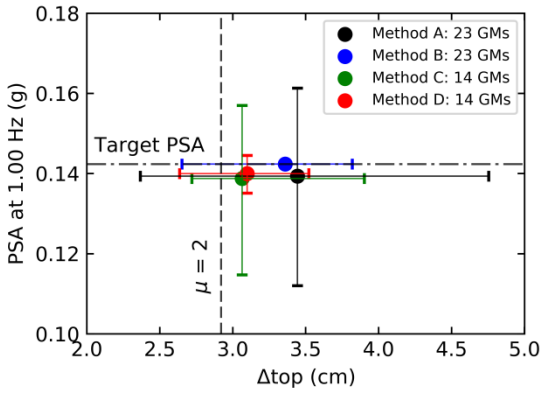

(d) S8b: SDOF-R2 at 1.00 Hz

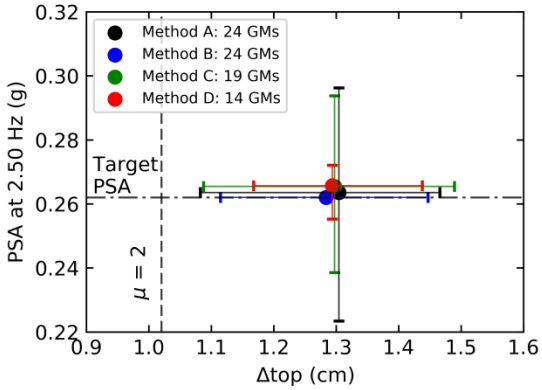

(e) S9: SDOF-R2 at 2.50 Hz

Figure 2.6.4: The distribution of PSAs at f0 in Methods A, B, C, and D and the corresponding lateral displacements (Δtop) of the simple models. PSAs at f0 are shown on the y-axis. The target PSA at f0 is plotted in the horizontal dashed line. The x-axis illustrates the maximum absolute of Δtop. The yielding limit or ductility demand of 2, μ=2, are plotted with the vertical dashed line. The 16th and 84th percentiles of the distributions are shown with the horizontal bars (PSAs at f0) and the vertical bars (Δtop). The mean of the distribution is shown with the filled circle. The target is the median of AK2014 for the scenario of M7.0R40, Vs450, and normal fault. GMs in MA and MC are selected if they are within ±30% of the target PSA at f0 (horizontal dashed line). GMs in MB are refined to have a scaling factor between 0.7 and 1.3. GMs in MD have PSAs at f0 between ±20% of the target PSA at f0.

2.7 Impact of GMSM on Structural Responses of Complex Models

2.7.1 Change in Structural Responses

This section extends the tests in the previous section to the complex structural models. The GMs in Figure 2.7.1 is applied to the S5 model (1-story RC model) in Figure 2.7.2. The GM modifications result in a slight change of certain

PSAs (including 5.68 Hz) and some IMs, unlike the example in Figure 2.6.1. Consequently, the maximum structural demands slightly differ from each other.

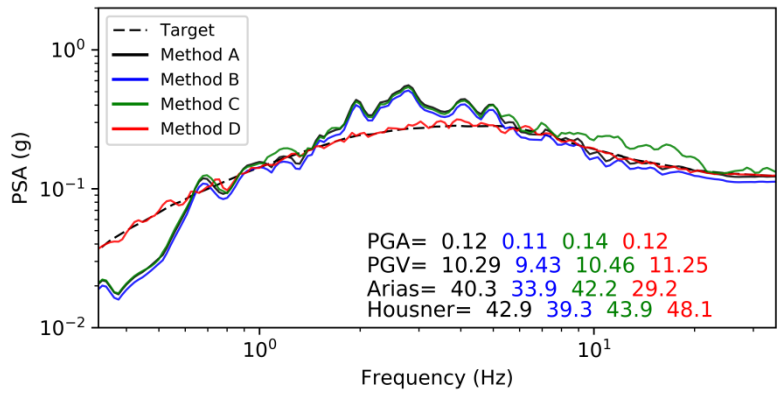

Figure 2.7.1: Spectra and intensity measures obtained by Methods A, B, C, and D, and the target spectra. The record is the Duzce Earthquake (station of 4100_9902) with Mw 7.1, R_{hypo} 34 km, and Vs30 448 m/s. Methods B, C, and D apply the modifications to the unscaled real record in Method A according to the target shown in black dashed line. The target is the median of AK2014 for the scenario of M7.0R40 and Vs450. The spectra and IMs follow the same color code in the legend. Method B scales the GM to the target PSA at 5.68 Hz with a scaling factor of 0.92, which equally reduces PSAs and some IMs. Method C amplifies PSAs from 6.00 Hz to 35.0 Hz. Method D amplifies PSAs from 0.30 Hz to 0.60 Hz and reduces them from 1.50 Hz to 5.00 Hz. MD reveals the greatest PGV and Housner and the least Arias.

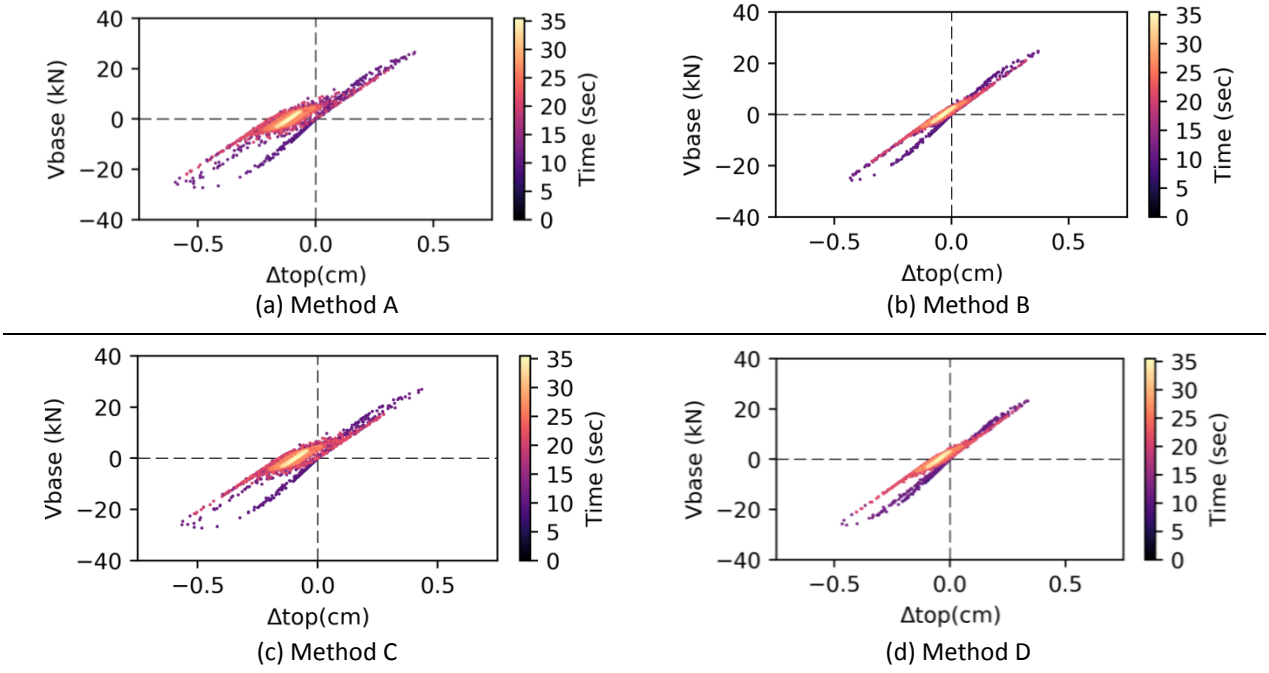

Figure 2.7.2: Response histories of the S5 model under GMs in Methods A, B, C, and D. The x-axis represents the roof displacements relative to the ground (Δtop). The y-axis is the sum of base shear forces (Vbase). The color of the curve relates to the period of time given in the legend: the darker colors represent the initial part, and the lighter colors represent the final part. Positive and negative values signify the direction of the movement. The record is the Duzce Earthquake (station of 4100_9902) with Mw 7.1, Rhypo 34 km, and Vs30 448 m/s. The input GMs are provided in the previous figure. The structural model (described in Section 2.4.1) has a natural frequency of 5.68 Hz.

Maximum absolute of roof displacements (Δtop) are 0.6 cm in (a), 0.4 cm in (b), 0.6 cm in (c), and 0.5 cm in (d). Maximum absolutes of base shear forces (Vbase) are 27.3 kN in (a), 25.7 kN in (b), 27.3 kN in (c), and 26.2 kN in (d). Method B results in the least structural demands. The changes in the structural demands are insignificant with respect to Method A.

With the intention of comparing the changes in structural responses due to the GM modifications, the ductility demands are plotted for the modified GMs (MB, MC, and MD) and the corresponding unscaled GMs (MA) in Figure 2.7.3. The structural behavior is mostly nonlinear in the S1 model and partially nonlinear for the S2, S3, S4 and S5 models. The changes in the structural demands are calculated according to Equation 2.3.1, and their distribution is given in the subfigures of the last column. The central values (mean and median) of the structural responses are in the near vicinity of MA, i.e., within -25% and +35% of the structural responses by MA. They are comparable to the central values (mean and median) of IMs which are between 0.70 and 1.20 (given in Figure 2.4.2). MB, MC, and MD are not able to capture the natural variability observed in the structural responses of MA. Some extreme structural demands in MA are not reproduced with the modified GMs. The observations from the simple models are mostly confirmed.

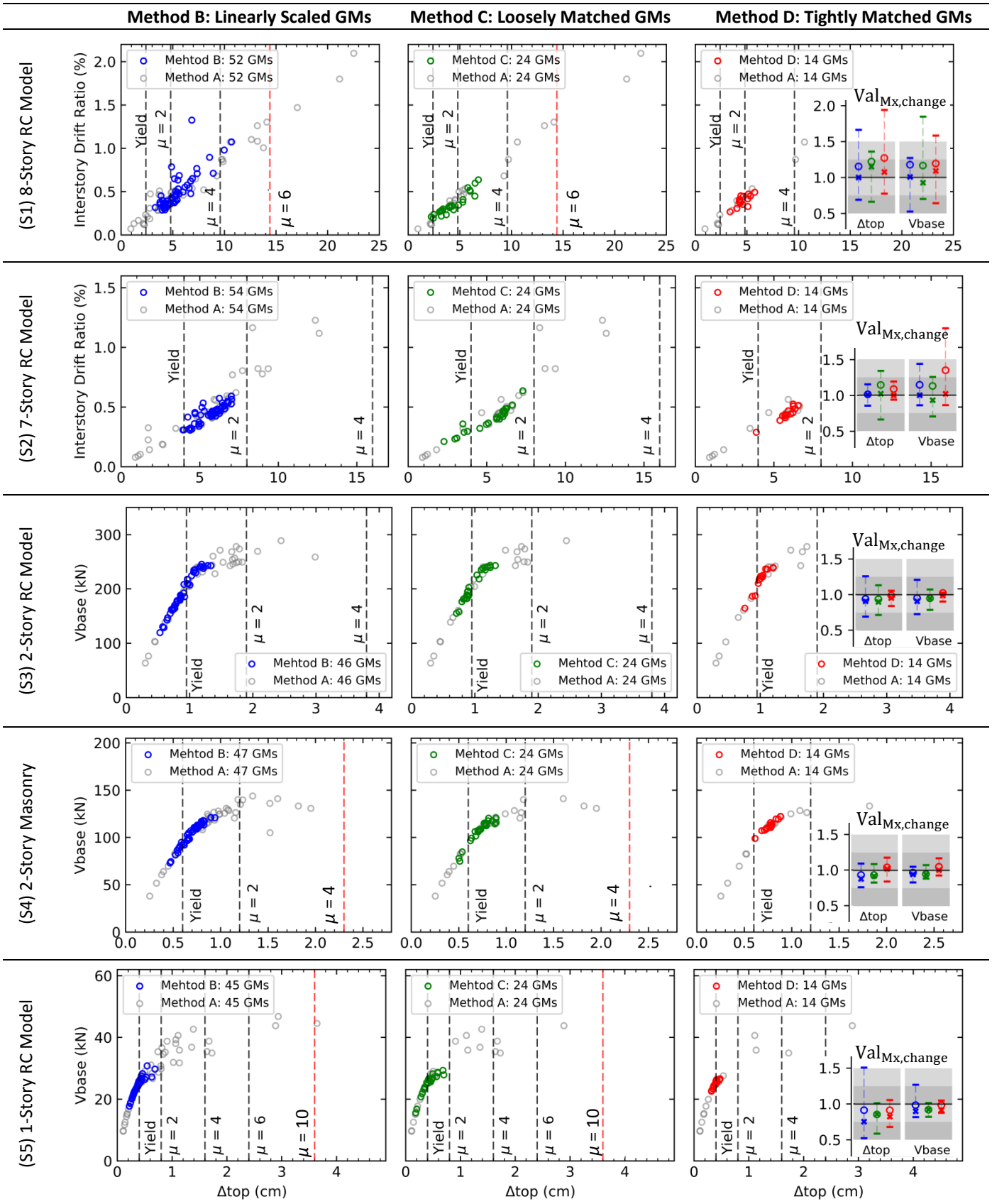

Figure 2.7.3: Structural responses of the complex models under GMs of Methods B, C, and D. Data for Methods B, C, and D are shown with blue, green, and grey, respectively. The corresponding data for the unscaled earthquake record (Method A) are shown with grey. The figures are separated in column-wise according to the method type and in row-wise according to the structural model. The x-axis shows the maximum absolute of the roof displacements (Δtop). (continued)

The y-axis illustrates the interstory drift ratio (IDR) in the S1 and S2 models (not the base shear forces), and the base shear forces (Vbase) in the S3, S4, and S5 models when the maximum absolute of Δtop is obtained. The number of GMs is given in the legend box. The yielding limit and displacement ductility levels, μ, of 2, 4, and 6, and 10 are plotted with the vertical dashed lines.

The subplots in the last column demonstrate the statistical change as calculated by Equation 2.3.1. The color code indicates the method. The equality is highlighted by the black solid line. The values above it indicate an increase in the structural response with respect to the unscaled earthquake record and vice versa. The 16^{th} and 84^{th} percentiles of the distribution are shown with the horizontal bars. The median and the mean of the distribution are shown with the cross marker and the unfilled circle, respectively.

The target is the median of AK2014 for the scenario of M7.0R40, Vs450, and normal fault. The GM amount decreases from MB to MD.

2.7.2 Dispersion of PSAs and Roof Displacements of Complex Models

The input dispersion (PSAs at f0) is compared against the output structural response (Δtop) dispersion of the complex models for a single GMPE in Figure 2.7.4. The output responses by MB and MC span along a wide range, which covers the large portion of the observed output responses in MA. A considerable dispersion of the output responses is also acquired by MD. On the whole, the mean structural responses are in the comparable damaging range (with regard to the yielding line or μ=2) but are not precisely the same regarding the observed mean responses (MA).

When the analyses are extended to six other GMPEs in Appendix B.7, the similar observation on the mean Δtop can be made (in Figure B.7.1). The GMSM methods produce relatively minor differences on the mean Δtop than the changes produced by the GMPEs. Since the dispersions at f0 are small for MB and MD, the additional analyses for the case with the reduced PSA dispersions (in Figure B.7.2) further confirm the observations.

The COVs of the PSAs at f0 and the output Δtop are compared in Figure 2.7.5 for all GMPEs. It is observed that the variability of the model response is (1) in general larger than the variability of the intensity measure of GM; (2) sensitive to the selection of GMPE, except for the S9 model for which the response variability is less than other models; and (3) depend on the GMSM method, with the least variability mostly offered by MD.

It is also important to note that even for MB (no variability in PSAs at f0), the variability of the structural response is not negligible and sometimes the largest (e.g., the S1 model). In comparison with MA, MC provides the same order of the variability of the structural response (except for the S5 and S8b models) regardless of the GMPE. The S9 model is less sensitive to the choice of the GMPE.

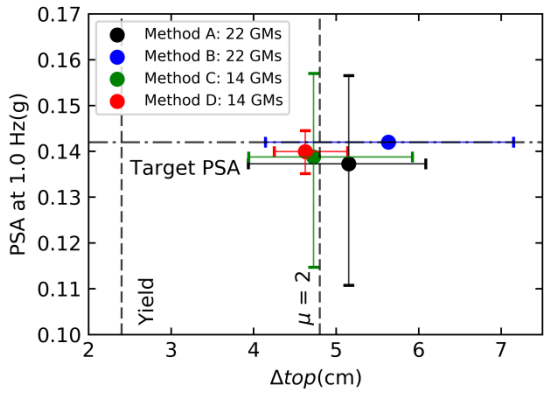

(a) S1: 8-Story RC Model

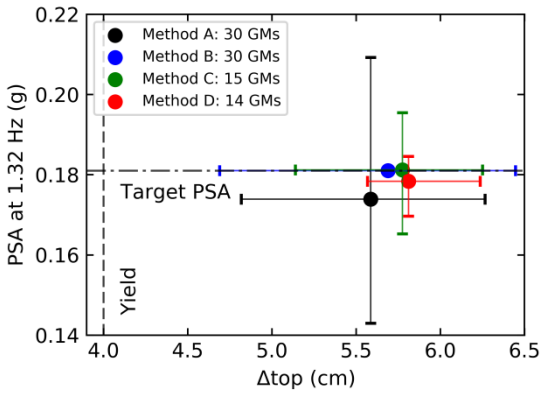

(b) S2: 7-Story RC Model

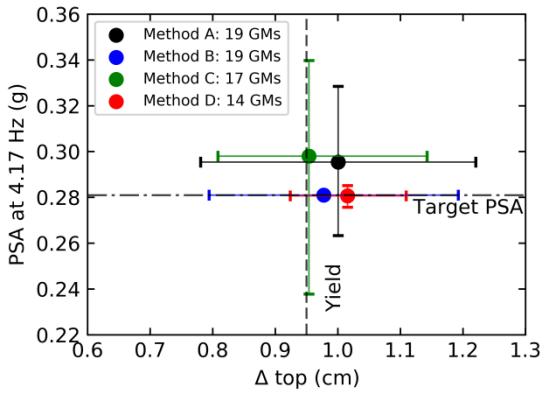

(c) S3: 2-Story RC Model

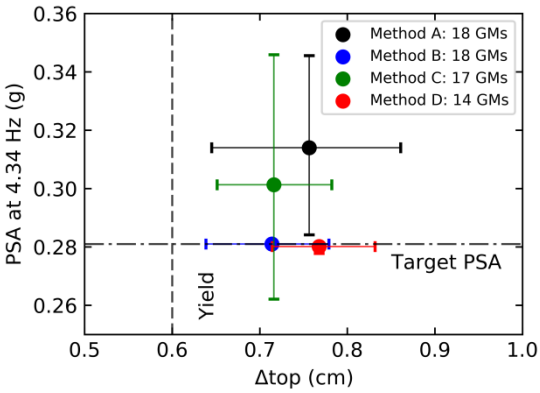

(d) S4: 2-Story Masonry Model

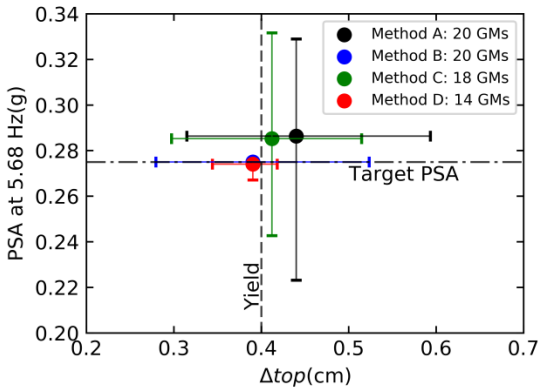

(e) S5: 1-Story RC Model

Figure 2.7.4: Distribution of PSAs at f0 in Methods A, B, C, and D and the corresponding roof displacements (Δtop) of the complex models. PSAs at f0 are shown on the y-axis. The target PSA at f0 is plotted in the horizontal dashed line. The x-axis illustrates the maximum absolute of Δtop. The yielding limit and the ductility demand of 2, μ=2, are plotted with the vertical dashed lines. The 16th and 84th percentiles of the distributions are shown with the horizontal bars (for PSAs at f0) and the vertical bars (for Δtop). The mean of the distribution is shown with the filled circle. The target is the median of AK2014 for the scenario of M7.0R40, Vs450, and normal fault. The color code represents the method as in the legend. GMs in MA and MC are selected if they are within ±30% of the target PSA at f0 (horizontal dashed line). GMs in MB are refined to have a scaling factor between 0.7 and 1.3. GMs in MD have PSAs at f0 between ±20% of the target PSA at f0. The amount of data is given in the legend.

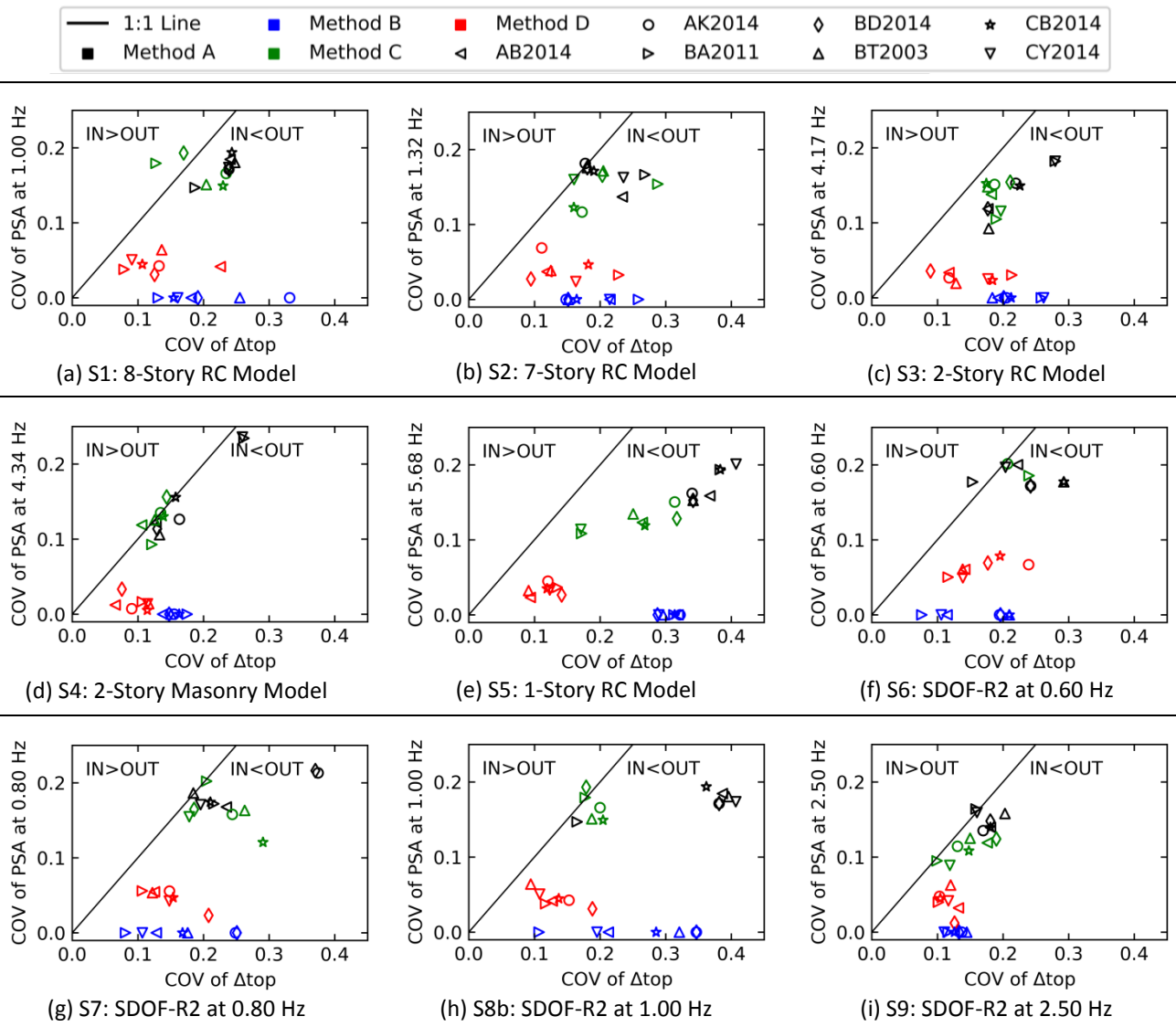

(a) S1: 8-Story RC Model (b) S2: 7-Story RC Model (c) S3: 2-Story RC Model

(d) S4: 2-Story Masonry Model (e) S5: 1-Story RC Model (f) S6: SDOF-R2 at 0.60 Hz

(g) S7: SDOF-R2 at 0.80 Hz (h) S8b: SDOF-R2 at 1.00 Hz (i) S9: SDOF-R2 at 2.50 Hz

Figure 2.7.5: Variability in input PSAs at f0 versus the variability in output lateral structural displacements (Δtop) in Methods A, B, C, and D for seven GMPEs. The x-axis illustrates the coefficient of variance (COV) of maximum absolutes of the output lateral displacements (Δtop). The y-axis illustrates COV of input PSAs at f0. The solid black line is the equality line. The data below the equality line signify that the input variability is less than the output variability (IN<OUT) and vice versa. The earthquake scenario is M7.0R40, Vs450, and normal fault. GMPEs such as AB2014, AK2014, BA2011, BD2014, BT2003, CB2014, and CY2014 are plotted with the markers introduced in the legend. Methods A, B, C, and D are shown with black, blue, green, and red, respectively. The GMs in MA and MC are selected if they are within ±30% of the target PSA at f0. The GMs in MB are refined to have a scaling factor between 0.7 and 1.3. The GMs in MD have PSAs at f0 between ±20% of the target PSA at f0. The COV is shown if there are at least 9 data.

2.8 Perspectives

In Part 2, the linear amplitude scaling is limited with the scaling option at the natural frequency of a structure, f0, (MB). It may be disadvantageous to represent the structure's higher mode effect, elongating period effect due to the nonlinearity, and the equipment responses. Also, it is a structure-dependent method and requires ground motion modification for each structural model. Alternatively, linear amplitude scaling could be applied with respect to (1) the peak ground acceleration (PGA), which is commonly used in the literature, and (2) the average of spectral accelerations (PSAs) at multiple frequencies, which could replicate better the uniform spectral variability observed in the magnitude-distance bin. In both alternatives, the PSA dispersions at structure's f0 and possible frequencies of interest will be preserved, which can suggest that the alternatives of the linear scaling can better replicate structural response

dispersions obtained by the unscaled earthquake records. Specific points are supported by the tests of the alternative amplitude scaling in Section B.8.1 (Appendix B.8).

The loosely-matched waveforms, Method C, have narrower spectral variability at the higher frequencies than the low frequencies. It is due to the PGA scaling prior to the spectrum matching, which is optional in RSPMatch09 (Al Atik and Abrahamson, 2010). If the PGA scaling is not applied, the spectral variability can be more uniform at the higher frequencies, which can likely affect the dispersion of responses of the structural models of high natural frequency (i.e., f0 > 2.00 Hz). Some tests are extended to show the uniformity of the IM dispersion without PGA scaling in Section B.8.2.

2.9 Conclusion

A large number of ground motion selection and modification (GMSM) methods exist in the literature, and there has not been a common consensus on how to select and scale ground motions for the seismic demand analysis. In the current practice, the spectral variability is reduced without evaluating the consequences on the final structural responses. Part 2 aims at comparing the impact of variability by the modified ground motions on the structural responses for the GMSM methods such as the linear amplitude scaling at the natural frequency of a structure, f0, (MB), the loosely spectrum matching (MC), and the tightly spectrum matching (MD). We evaluate the GMSM methods with respect to the unscaled earthquake records (MA) through the record-to-record variability. The main conclusions are listed below:

- The modifications that are applied to the ground motions in the matching magnitude-distance bin can result in large deviations from the observed (i.e., unscaled) structural responses. If the modification degree is restricted (e.g., by bounding the scaling factors in the linearly scaled ground motions and the change in Arias intensity in spectrum-matched ground motions), the deviation from the observed structural responses can be controlled in return. It also reinforces the findings of the previous studies (e.g., Luco and Bazzurro, 2007; Hancock et al., 2008).

- The GMSM methods with an aim to reduce the PSA variability (or discrepancy) at a single frequency (MB) or along a frequency range (MD) show considerable variability in the specific ground motion characteristics, such as PGA, PGV, PGD, Arias intensity, and SCAV, as well as considerable dispersion in the structural responses. The GMSM methods are not able to capture the extreme structural responses observed in the unscaled earthquake records (MA). All in all, for the earthquake design, the selection of the ground motion among the GMSM methods will introduce a wide range of dispersion of the structural responses, limiting the representativeness of the natural ground motion dispersion, which supports the previous findings (e.g., Huang et al., 2012).

- The previous conclusion challenges one of the motivations behind the pragmatic GMSM methods. The assumption that the structural response variability can be reduced by reducing spectral variability is not the case for most of the lateral displacement responses (Δtop) and for the base shear forces (Vbase) of the complex models. In fact, reducing the spectral variability (at f0 in MB or along a frequency range in MD) does not necessarily reduce the variability of the structural responses, which reinforces the findings of the recent studies (e.g., Causse et al., 2013; Seifried and Baker, 2016).

- The GMSM methods (MB, MC, and MD)—which decrease the number of dynamic analyses for a single target—reveal comparable Δtop on average with the benchmark, i.e., the symmetrically refined unscaled earthquake records (MA) around target PSA at f0. The precision of the predictions depends on the structural model. The conclusion implies that, for an objective requiring the central measure (i.e., mean and median) of the structural responses, the GMSM methods can be preferred to predict the final structural response while offering a small number of nonlinear dynamic analyses.

- This study shows that the choice of a ground motion prediction equation (GMPE) can result in significant differences in the mean structural responses, which can overshadow the corresponding differences due to the GMSM methods. The target spectrum is defined by different GMPEs representing the similar earthquake scenario, and the conclusions can have limitations due to the specific scenario and the input parameters.

This page is intentionally left blank.

PART 3

IMPACT OF SET VARIABILITY ON STRUCTURAL RESPONSES: COMPARISON OF LINEARLY SCALED AND SPECTRUM-MATCHED GROUND MOTIONS

3.1 Introduction

The modified ground motions (GMs) are preferred in the current practice for the nonlinear dynamic analyses due to the budget and time constraints, even if the unscaled earthquake (EQ) records with large variability are the most realistic option. The input variability is minimized yet without evaluating its consequences on the output structural responses. There has not been a common consensus on how to select and scale the GMs for the seismic demand analysis.

In Part 3, we present the spectrum compatible ground motion (GM) selection with the modified GMs. We question (1) how similar the set distribution of the modified GMs are relative to the unscaled earthquake records (Method A), and (2) whether or not the unscaled GMs can be replaced by the modified GMs. We quantify the impact of the GM set variability on engineering demand parameters (EDPs) obtained by the linearly scaled records (Method B), the loosely matched waveforms (Method C), and the tightly matched waveforms (Method D) with respect to the unscaled earthquake records (Method A).

The impact of the set variability on the input GM characteristics is presented in Section 3.2. Then, in Section 3.3, the EDP distributions are gathered for the structural models by considering the interset and the intraset variability. Section 3.4 quantifies the differences between the sets of the modified GMs and the benchmark (i.e., sets of unscaled earthquake records). The predictions by the modified GMs are also examined with the use of the asymmetric tolerances in the spectrum compatible selection in Section 3.5.

3.2 Impact of GMSM Methods on Input Ground Motion Characteristics Considering Interset and Intraset Variability

In this section, the spectrum compatible selection is performed to collect all eligible sets for the GMSM methods and for the GMPE (7 times) as summarized in Table 3.2.1 to compare the EDP distributions in the latter sections.

Table 3.2.1: Elements investigated in Part 3

EQ Scenario	Target Spectra (Median GMPEs)	GMSM Methods	Structural Models	Engineering Demand Parameters	Tolerance Type	Intraset Variability
M7.0R40 Vs450 Normal Fault	AB2014, AK2014, BA2011, BT2003, BD2014, CB2014, CY2014	Method A Method B Method C Method D	5 complex and 5 simple models	Ductility demand (μ), roof displacement (Δtop), base shear force (Vbase), interstory drift ratio (IDR)*, and damage index (DI)*	Symmetric: ±30% Asymmetric: -5%, +50%	$\overline{\mathrm{Val}}^{\mathrm{set}}$ and $(\overline{\mathrm{Val}} + \lambda\sigma_{\mathrm{Val}})^{\mathrm{set}}$

*Calculated for some complex structural models

3.2.1 Spectra of Each Set's Average

The spectrum compatible selection is performed to collect all eligible GM sets that consist of 5 GMs for the symmetric tolerances according to Section 1.2.1. The spectral amplitudes for each set's average, $\overline{\mathrm{PSA}_{\mathrm{f0}}}^{\mathrm{set}}$, are shown in Figure 3.2.1.

In Method A (MA), the median of all $\overline{\mathrm{PSA}_{\mathrm{f0}}}^{\mathrm{set}}$ is in the vicinity of the target spectrum with uniform dispersion of the spectral amplitudes. In Method B (MB), the dispersion of all $\overline{\mathrm{PSA}_{\mathrm{f0}}}^{\mathrm{set}}$ is zero at 1.00 Hz, and between the upper and lower tolerances at elsewhere. In Method C (MC), the median of all $\overline{\mathrm{PSA}_{\mathrm{f0}}}^{\mathrm{set}}$ is below the target spectra between 0.5 Hz and 1.7 Hz and above the target at higher frequencies with the eccentric dispersion, i.e., the 16$^{\mathrm{th}}$ and 84$^{\mathrm{th}}$ percentiles are both above the target at higher frequencies. In MD, the median of all $\overline{\mathrm{PSA}_{\mathrm{f0}}}^{\mathrm{set}}$ spectra is smoothed with respect to the target spectrum and attain a local peak between 30 Hz and 40 Hz, which is out of the frequency of interest and can affect peak ground acceleration (PGA). The PGA is calculated at 33.0 Hz in the thesis.

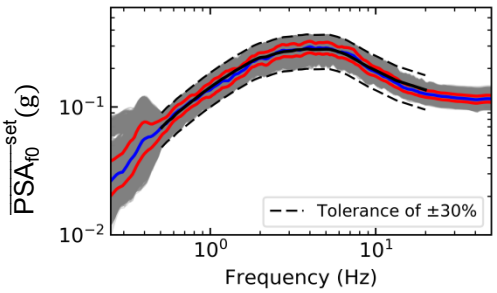

Method A: Unscaled Earthquake Records

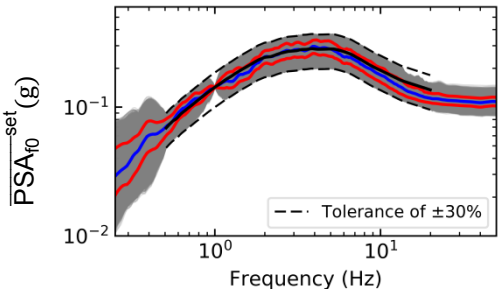

Method B: Linearly Scaled Records to PSA at Method 1.0 Hz

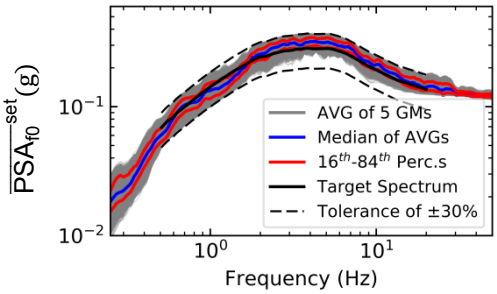

Method C: Loosely Matched Waveforms

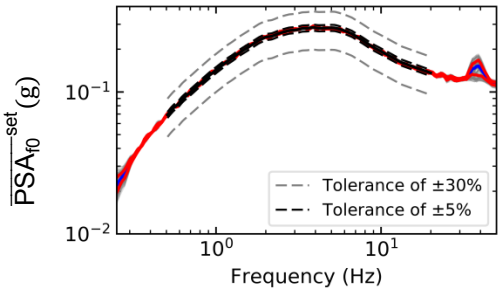

Method D: Tightly Matched Waveforms

Figure 3.2.1: Average spectra of all eligible GM sets with the <u>symmetric</u> tolerances. The target is shown with the solid black line and is the median of AK2014 for the scenario of M7.0R40, Vs450, and normal fault. Each set includes five ground motions. The upper and lower amplitude tolerances are shown with the dashed black lines: -30% and +30% of the target for Methods A, B, and C, and between-5% and +5% of the target for Method D. The frequency range is from 0.50 Hz and 20.0 Hz. Grey lines represent the average spectra of the GM sets, $\overline{\mathrm{PSA}_{\mathrm{f0}}}^{\mathrm{set}}$. The 16$^{\mathrm{th}}$ and 84$^{\mathrm{th}}$ percentiles of eligible GM spectra, $\overline{\mathrm{PSA}_{\mathrm{f0}}}^{\mathrm{set}}$, are shown with solid red lines. The median of all $\overline{\mathrm{PSA}_{\mathrm{f0}}}^{\mathrm{set}}$ is shown with the solid blue line. For Methods A, B, C, and D, there are 203 534, 46 167, 6 807, and 274 GM sets, respectively.

To evaluate whether or not the sets at PSA at 1.00 Hz are similar, the distribution of PSAs at 1.00 Hz is shown in Figure 3.2.2. All methods provide the mean of all $\overline{\mathrm{PSA}_{1.00\mathrm{Hz}}}^{\mathrm{set}}$ close to the target. With respect to MA, the distribution of all $\sigma_{1.00,Hz}^{set}$ is not conserved in MB and MD; whereas, MC partially conserves the observed intraset variability. The dispersion in MA and MC are comparable. MB and MD do not reveal any dispersion. The latter observation stresses the MB's and MD's goal to minimize the spectral variability (at 1.00 Hz in this case).

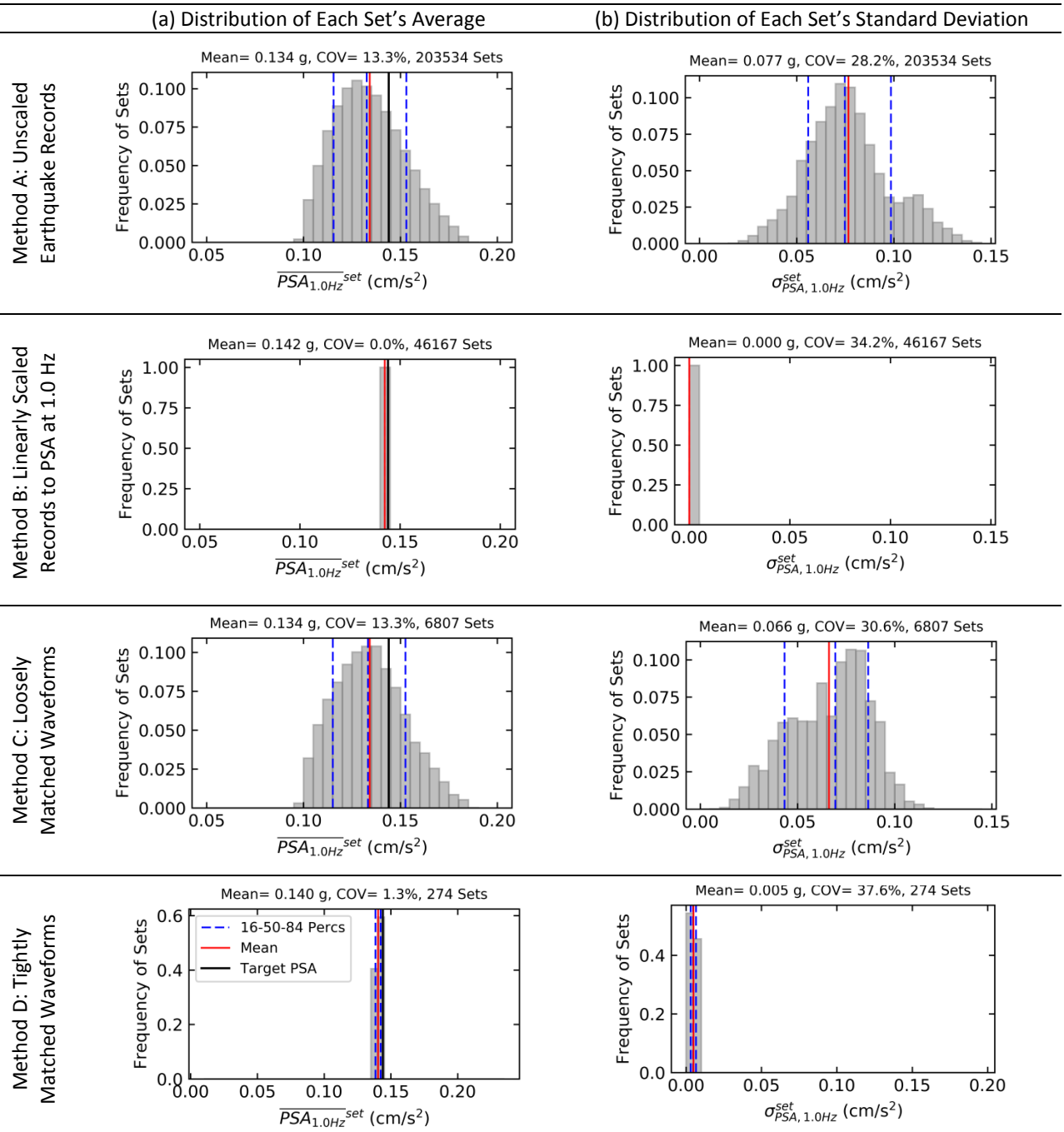

Figure 3.2.2: Distribution of PSAs at 1.00 Hz for each set's average (a) and each set's standard deviation (b) with the symmetric tolerances. The spectrum compatible selection is explained in Figure 3.2.1. Grey lines represent the average spectra of GM sets. The 16th and 84th percentiles and the median of the average spectra of the eligible sets are provided. The mean, COV, and amount of sets are all shown on the title of the subfigures. The coefficient of variation (COV) of all $\sigma^{set}_{PSA,1.00,Hz}$ is around 30% in MA and MC; whereas, MB and MD reveal unimportant COV relative to their mean.

3.2.2 Distribution in Other Intensity Measures

The selection of eligible GM sets has been made according to the frequency-based GM characteristics. In order to evaluate the effect of set variability on other GM characteristics, the distribution of intensity measures (IMs) is provided in Table 3.2.2. The spectrum compatible selection is performed as explained in the caption of Figure 3.2.1. The changes in the means are calculated with respect to MA, and the changes greater than 15% or less than -15% are highlighted with the bold font.

MB reveals similar mean estimates and similar dispersions with respect to the observed GM characteristics in MA. MC reveals a moderate decrease in the mean of all $\overline{\mathrm{PGV}}^{\mathrm{set}}$; moderate increase in the mean of all $\overline{\mathrm{SCAV}}^{\mathrm{set}}$ and $\overline{\mathrm{ASI}}^{\mathrm{set}}$; and a significant decrease in the mean of all $\overline{\mathrm{PGD}}^{\mathrm{set}}$. MD reveals comparable mean estimates except for the large decrease in the mean of all $\overline{\mathrm{PGD}}^{\mathrm{set}}$. MD reveals the least dispersion in the IMs due to the ±5% amplitude tolerances. Overall, the spectrum compatible selection tunes the mean of all $\overline{\mathrm{IM}}^{\mathrm{set}}$ close to the benchmark (i.e., ±15% around MA) except for $\overline{\mathrm{PGD}}^{\mathrm{set}}$ in MC and MD.

Table 3.2.2: All set distribution of intensity measures using each set's average for Methods A, B, C, and D.

Intensity Measures	Method A (203 534 GM Sets)		Method B at 1.00 Hz (46 167 GM Sets)			Method C (6 807 GM Sets)			Method D (274 GM sets)		
	Mean	COV	Mean		COV	Mean		COV	Mean		COV
$\overline{PGA}^{\mathrm{set}}$ (g)	0.11	0.08	0.11	(0%)	0.08	0.12	(9%)	0.03	0.11	(0%)	0.03
$\overline{PGV}^{\mathrm{set}}$ (cm/s)	12.5	0.15	13.1	(5%)	0.14	11.2	(-10%)	0.09	11.4	(-9%)	0.06
$\overline{PGD}^{\mathrm{set}}$ (cm)	5.4	0.29	5.7	(6%)	0.26	3.7	**(-31%)**	0.15	4.3	**(-20%)**	0.11
$\overline{Arias}^{\mathrm{set}}$ (cm/s)	30.5	0.17	27.9	(-9%)	0.18	31.9	(5%)	0.17	29.4	(-4%)	0.06
$\overline{SCAV}^{\mathrm{set}}$ (g sec)	0.44	0.18	0.42	(-5%)	0.20	0.50	(14%)	0.20	0.46	(5%)	0.07
$\overline{ASI}^{\mathrm{set}}$ (cm/s)	102	0.08	103	(1%)	0.07	114	(12%)	0.04	104	(2%)	0.00
$\overline{Housner}^{\mathrm{set}}$ (cm)	47.1	0.09	49.0	(4%)	0.07	45.0	(-4%)	0.07	47.9	(2%)	0.00

Each set's standard deviation is considered, i.e., the distribution of $\sigma_{\mathrm{IM}}^{\mathrm{set}}$, in Table 3.2.3 for evaluating the intraset variability. The changes in the means are calculated with respect to MA, and the changes greater than 15% or less than -15% are highlighted with the bold font. Relative to MA, MB preserves the observed intraset variability of IMs, but to a limited level for $\sigma_{\mathrm{PGV}}^{\mathrm{set}}$ and $\sigma_{\mathrm{Arias}}^{\mathrm{set}}$, and to a significantly less level for $\sigma_{\mathrm{Housner}}^{\mathrm{set}}$. MC does not conserve the observed intraset variability except for $\sigma_{\mathrm{Housner}}^{\mathrm{set}}$, but still conserves some level of the intraset variability for all IMs. MD does not capture the intraset variability with respect to MA but still reveals the intraset variability except for the frequency-based IMs (i.e., ASI and Housner).

Table 3.2.3: All set distribution of intensity measures using each set's standard deviation for Methods A, B, C, and D.

Intensity Measures	Method A (203 534 GM Sets)		Method B at 1.00 Hz (46 167 GM Sets)			Method C (6 807 GM Sets)			Method D (274 GM sets)		
	Mean	COV	Mean		COV	Mean		COV	Mean		COV
σ_{PGA}^{set}(g)	0.04	0.34	0.04	(-12%)	0.41	0.01	**(-81%)**	0.44	0.01	**(-80%)**	0.25
σ_{PGV}^{set}(cm/s)	6.5	0.47	4.6	**(-30%)**	0.43	3.7	**(-43%)**	0.24	1.6	**(-76%)**	0.27
σ_{PGD}^{set} (cm)	3.2	0.51	3.1	(-4%)	0.51	1.5	**(-52%)**	0.39	1.1	**(-67%)**	0.35
σ_{Arias}^{set} (cm/s)	18.8	0.43	15.1	**(-20%)**	0.47	13.0	**(-31%)**	0.62	4.8	**(-74%)**	0.31
σ_{SCAV}^{set}(g sec)	0.23	0.35	0.20	(-14%)	0.52	0.23	(0%)	0.65	0.10	**(-56%)**	0.26
σ_{ASI}^{set} (cm/s)	45	0.35	42	(-8%)	0.39	13	**(-72%)**	0.36	1	**(-98%)**	0.30
$\sigma_{Housner}^{set}$ (cm)	23.1	0.28	11.6	**(-50%)**	0.32	15.5	**(-33%)**	0.21	0.4	**(-98%)**	0.48

3.2.3 Impact of Ground Motion Prediction Equations

To study the impact of the target spectrum, the spectrum compatible selection is performed with other GMPEs. The distribution of the PSAs at 1.00 Hz is illustrated in Figure 3.2.3. The choice of a GMPE impacts the distributions of $\overline{\mathrm{PSA}_{\mathrm{f0}}}^{\mathrm{set}}$ and $\sigma_{\mathrm{f0}}^{\mathrm{set}}$ (except for MB and MD) significantly regardless of the GMSM method. The GMSM methods have a comparable mean of all $\overline{\mathrm{PSA}_{\mathrm{f0}}}^{\mathrm{set}}$ (between -10% and +20% of the benchmark, MA as quantified in Figure C.1.7), and the

distributions of all σ_{f0}^{set} are not preserved in MB and MD but are partially conserved for MC with respect to MA, which can be observed for other natural frequencies of structural models (such as 0.60, 0.80, 1.32, 2.50, 4.17. 4.32, and 5.68 Hz) in Figure C.1.1 (Appendix C.1).

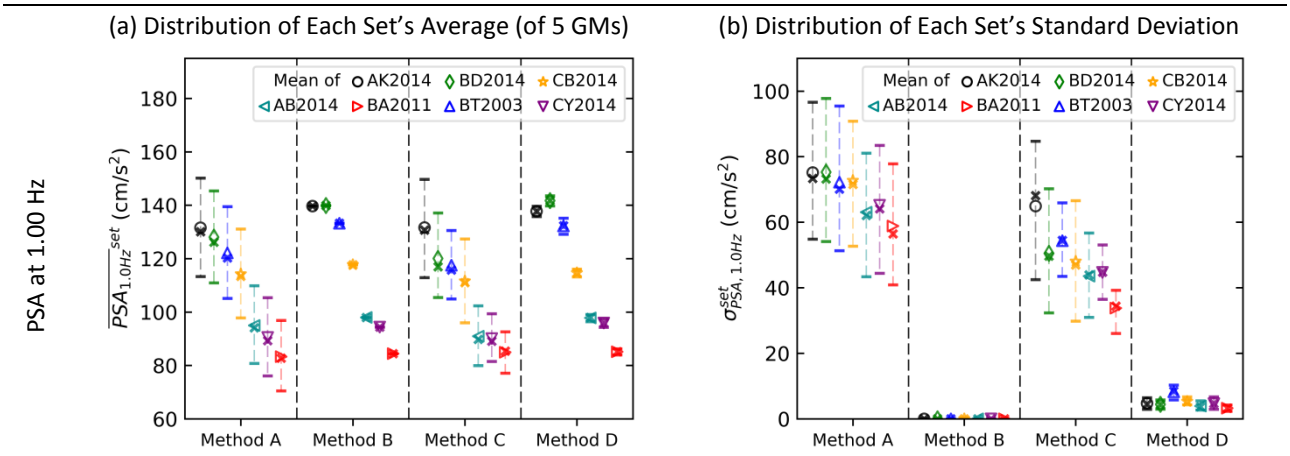

Figure 3.2.3: Distribution of pseudo-spectral accelerations (PSA) at 1.00 Hz with all GM sets considering each set's average in column (a) and each set's standard deviation in column (b) with the symmetric tolerances. Each set includes five ground motions. The upper and lower amplitude tolerances are -30% and +30% of the target for Methods A, B, and C, and between-5% and +5% of the target for Method D. The frequency range is from 0.50 Hz and 20.0 Hz. The target is obtained for the scenario of M7.0R40, Vs450, and normal fault as explained in Section 1.4. Means are demonstrated with the markers and colors in the legend box for the corresponded GMPEs. Medians are shown with the cross markers. The 16th and 84th percentiles are plotted with the horizontal bars.

3.3 Impact of GMSM Methods on Output Structural Responses Considering Interset and Intraset Variability

3.3.1 Impact of Set Variability on Lateral Roof Displacements (Δtop)

This section presents the impact of the GMSM methods on the structural response distributions by considering the interset and the intraset variability. Figure 3.3.1 shows the distribution of the roof displacements (Δtop) for the 8-story RC building. The mean of all $\overline{\Delta\text{top}}^{\text{set}}$ is slightly affected (between -0.1 and +0.3 cm difference in the mean with respect to MA) by the GMSM method, their COVs are reduced with a smaller degree by MB and MC, but with a larger degree by MD. Each GMSM method poses a certain level of the interset variability (i.e., COV of all $\overline{\Delta\text{top}}^{\text{set}}$) despite the minimized interset variability in PSAs at f0 (for MB and MD).

The mean of all $(\overline{\Delta\text{top}} + 0.95\sigma_{\Delta\text{top}})^{\text{set}}$ differs significantly with respect to the benchmark (MA), which is 0.8 cm less by MB, 0.6 cm less by MC, and 1.4 cm less by MD. Each GMSM method underpredicts the benchmark upon the capability of preserving the ground motion variability. Moreover, MD is shown to produce considerable intraset variability (i.e., $\sigma_{\Delta\text{top}}$), which points out the effect of intraset variability in the amplitude- and duration-based IMs (Table 3.2.2).

The tendency in the current practice is to use a single GM set as discussed for a simple structural model in Section 1.8.1. In order to extend the tests to a complex structural model and different GMSM methods, a single GM set is compared against all sets in Figure 3.3.2. The use of a single set does not reveal an assuring distribution of PSAs and Δtop for the complex structural model in MA as well as in MB and MC. For MD, the chances of a single set being close to the mean of all $\overline{\Delta\text{top}}^{\text{set}}$ are higher than other methods, but this observation is limited to the shown structural model for Δtop.

In order to explain the reason why the distribution of all GM sets with MB, MC, and MD deviate from MA, Figure 3.3.3 shows the reoccurrence percentages of GMs and the cumulative distribution functions (CDF) for each method. In other words, it demonstrates how frequent and how spread each Δtop composing GM sets.

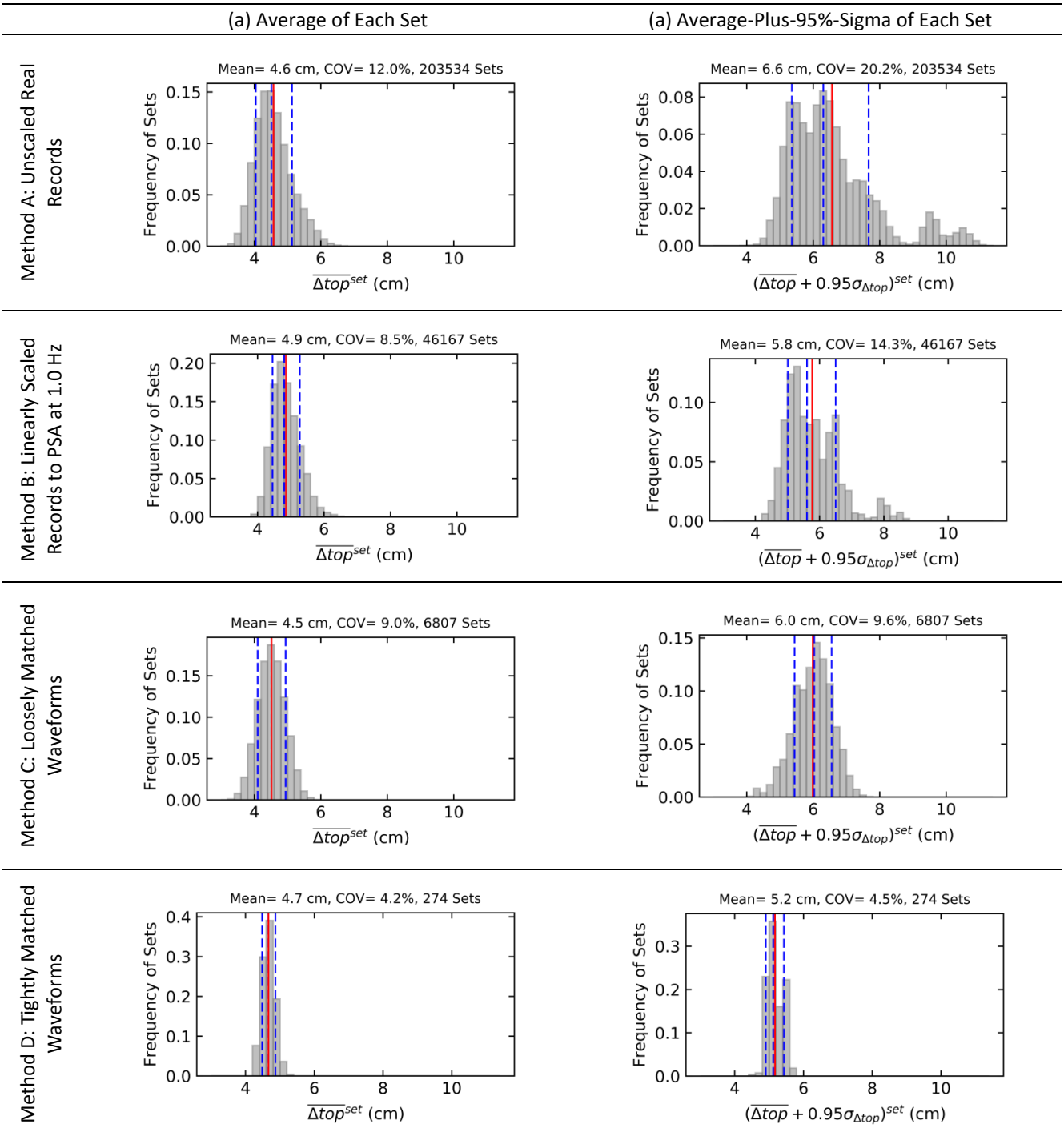

Figure 3.3.1: Distribution of Δtop for each set's average in (a) and each set's average-plus-95%-standard-deviation in (b) with the symmetric tolerances. The spectrum compatible selection is explained in Figure 3.2.1. The structural model is the S1 model, the 8-story RC building. The mean, COV, and amount of sets are shown on the title of the subfigures. The distribution in (b) show tail-like distribution starting at 9.0 cm for Method A, and at 7.0 cm for Method B. The trend is due to the insufficient GM sets resulting in this range.

In MA, there are 60 GMs with the recurrence percentages less than 4%, and the structural responses range from the elastic behavior to μ of 6, which is also observed in the slope of the CDF curve. Relative to the trend in the benchmark (MA), MB, MC, and MD cannot replicate the structural responses at the critical levels and reveal less dispersed (or centralized) structural responses, which, in return, impact the intraset variability. MC keeps some of the non-damaging (i.e., linearly responding) structural responses, which enhances the standard deviation of structural responses relative to MB and MD. It signifies the importance of conserving non-damaging structural responses in the seismic analysis.

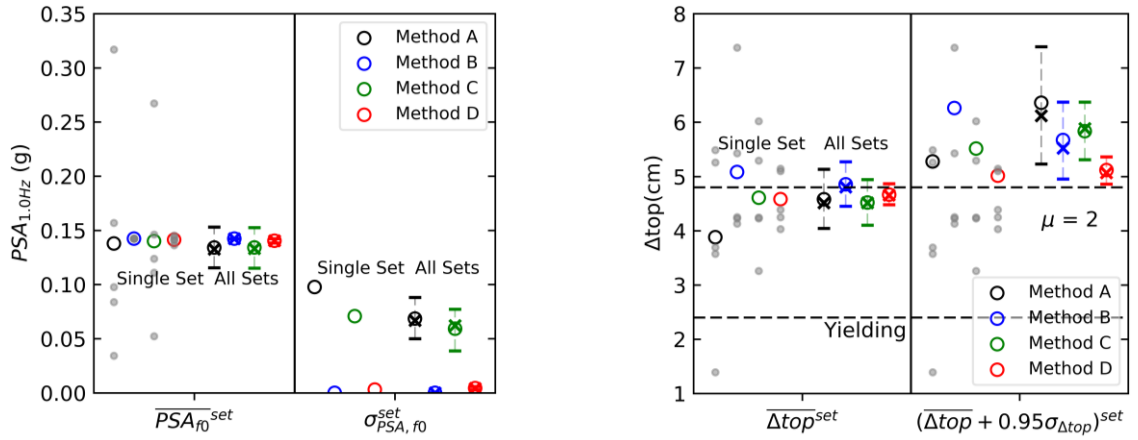

Figure 3.3.2: Distribution of PSAs at 1.00 Hz and Δtop with a single set versus all sets for each GMSM method. The spectrum compatible selection is explained in Figure 3.2.1. Each grey dot shows the value of a GM. The mean of the set distribution is plotted with the unfilled circles. The median is shown with the cross markers. The 16th and 84th percentiles are plotted with the horizontal bars. The color code shows the method in the legend box.

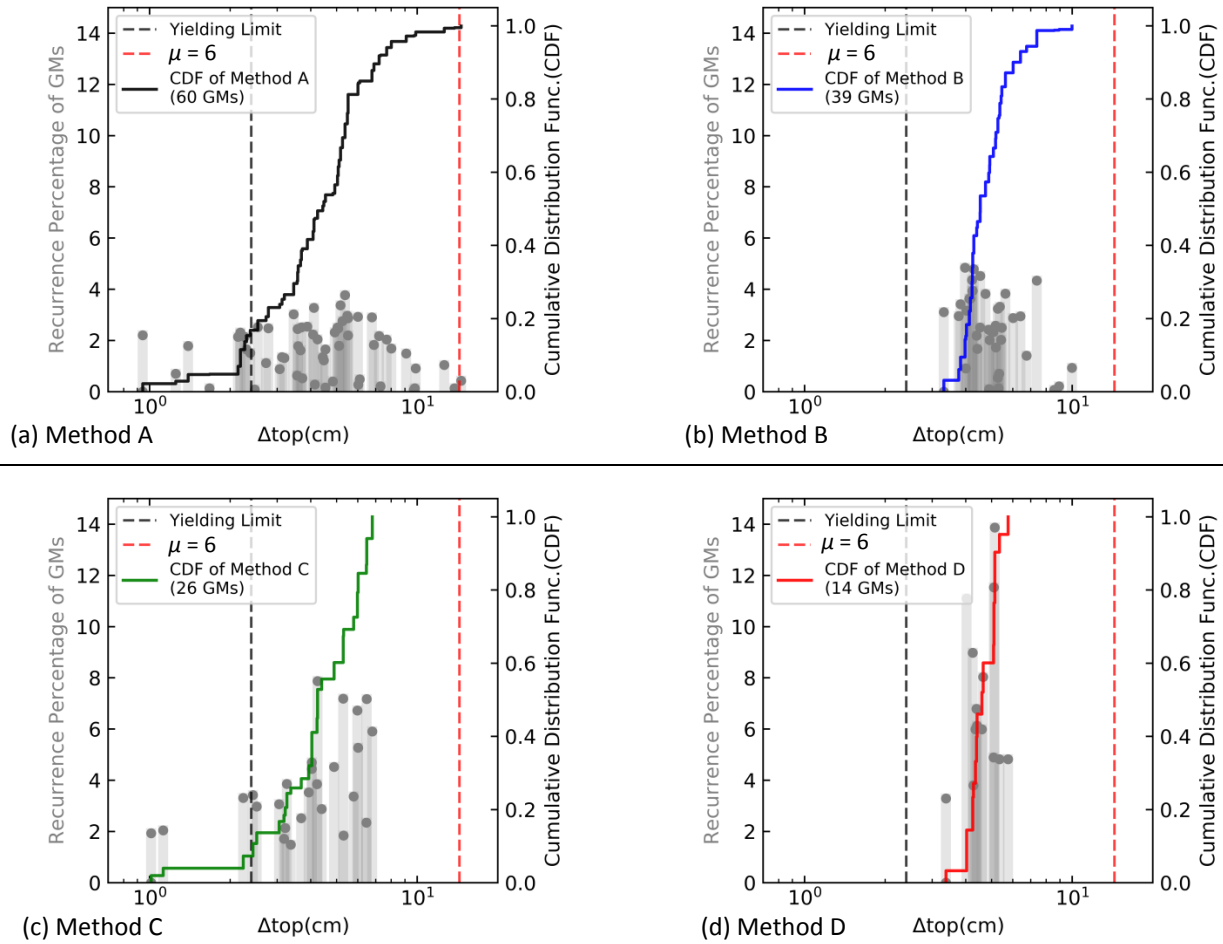

Figure 3.3.3: Comparison of recurrence percentages of GMs and cumulative distribution functions (CDF) for roof displacements (Δtop) of the S1 model, 8-story RC model. The x-axis represents the roof displacements (Δtop) from each GM. Along the left-side y-axis, the reoccurrence percentages of GMs are shown. The vertical grey bars are related to the left-side y-axis. Along the right-side y-axis, cumulative distribution function (CDF) is shown. CDF is the summation of reoccurrence frequencies. The solid lines in black (Method A), in blue (Method B), in green (Method C), and in red (Method D) relate to the right-side y-axis. The yielding limit and ductility demand, μ, of 6 are shown with the vertical dashed lines.

3.3.2 Impact of Ground Motion Prediction Equations

This section evaluates the impact of the GMPEs on the EDP distributions obtained by the sets of modified GMs. The distributions of the roof displacements (Δtop), the base shear forces (Vbase), the interstory drift ratios (IDR), and the global damage indices (DI) are plotted in Figure 3.3.4. DI is a measure of the structural damage calculated for all structural elements by Park & Ang index (Park and Ang, 1985). In the case of DI<0.4, the structural damage is tolerable, and in the case of DI>1.0, the structural collapse is very likely (Park et al., 1987). For each set's average, the distributions of the structural damages are tolerable. For each set's average-plus-95%-sigma, some GMPEs reveal that the 84th percentiles of the structural damages are above the intolerable damage limit, i.e., causing permanent deformations.

The choice of the GMPE results in significant difference in the distributions of DI, Δtop, and IDR, and relatively less difference in the distributions of Vbase regardless of the GMSM method. These observations are supported with other structural models by the distributions of the roof displacements (Δtop) in Figure C.1.2 (Appendix C.1), the base shear forces (Vbase) in Figure C.1.3, the interstory drift ratios (IDR) in Figure C.1.4, and the global damage indices (DI) in Figure C.1.5.

The distribution of some EDPs may exhibit correlation with the differences in the elastic PSAs at f0 (Section 3.2.3). To illustrate, the mean of all $\overline{\mathrm{PSA}_{1.00Hz}}^{\mathrm{set}}$ with AK2014 is 62% larger than its distribution with BA2011 in MD. Consequently, for the S1 model (8-Story RC), it results in 35% larger mean of all $\overline{\Delta\mathrm{top}}^{\mathrm{set}}$. In this case, the difference in PSAs at f0 can be indicative and is not directly related with the level of difference in the EDP. Such a trend may not be observed for some GMPEs (e.g., AB2014 versus CY2014) and Vbase as demonstrated in Section C.1.6, which can be due to the nonlinearity and the higher mode effect.

Interset variability (represented by the one-sigma of the distributions) is influenced by the choice of a GMPE and a GMSM method. MB and MD have almost zero interset variability of PSAs at f0 and result in considerable output interset variability, which highlights that a single GM set is not able to attain an assuring level of the structural response distribution regardless of the GMSM method. Same observations can be drawn for the rest of the structural models in Figures C.1.7 and C.1.8.

In sum, the difference in the target spectrum representing the same EQ scenario can result in significant differences in the structural response distributions. In this study, a target spectrum obtained from a single GMPE is found insufficient to evaluate the seismic behavior of a structure regardless of the GMSM method. However, the analyses may not be sufficient to generalize the conclusion since they are defined by the precise input parameters specific to this study.

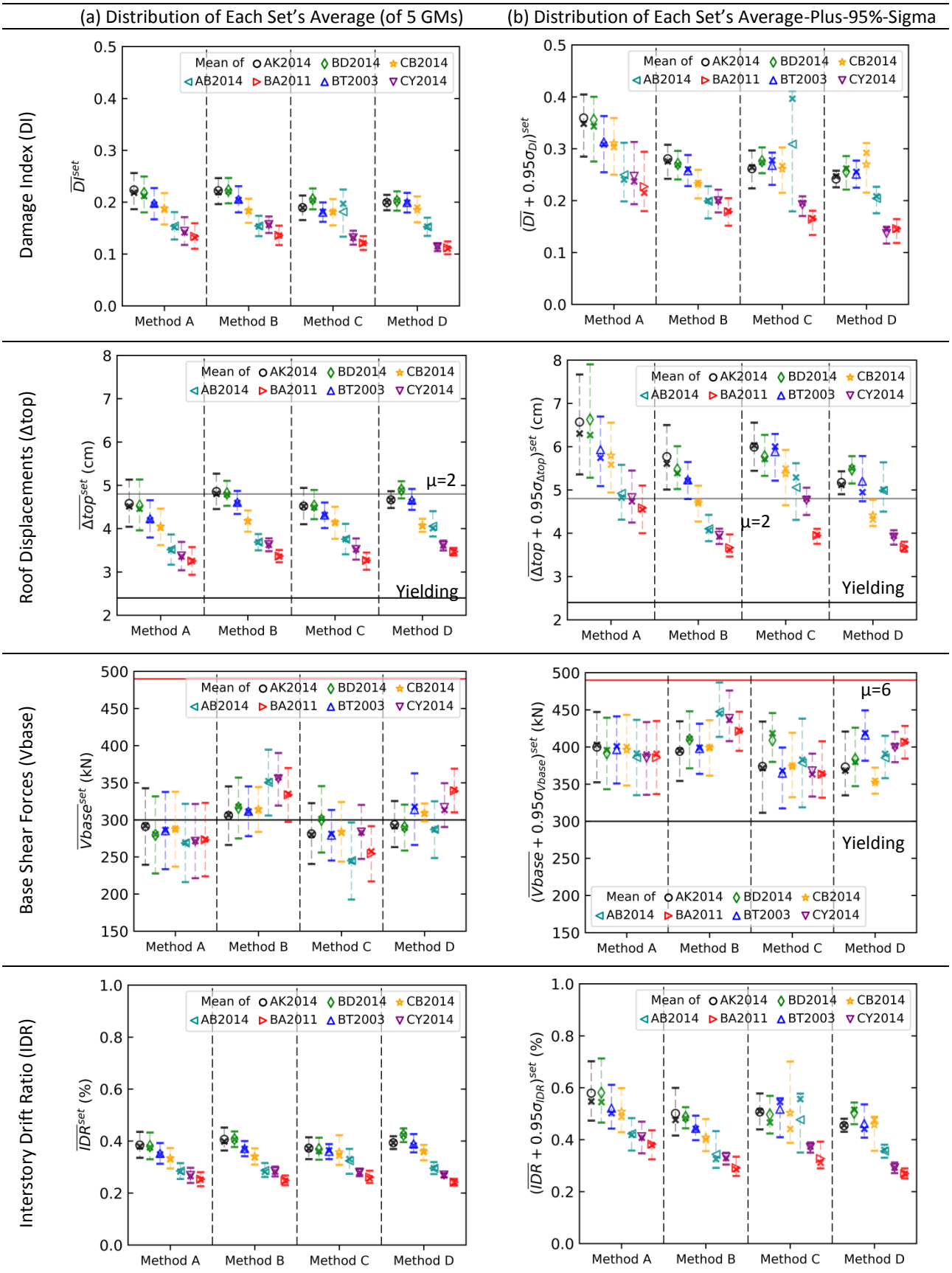

Figure 3.3.4: Distribution of structural response (on column-wise) with all GM sets considering intraset variability with the symmetric tolerances. Each set includes five ground motions. The upper and lower amplitude tolerances are -30% and +30% of the target for Methods A, B, and C, and between-5% and +5% of for Method D. (continued)

The frequency range is from 0.50 Hz and 20.0 Hz. The target is obtained for the scenario of M7.0R40, Vs450, and normal fault as explained in Section 1.4. In column-wise, the distributions of each set's average are shown in (a), and the distributions of each set's average-plus-95%-standard-deviation are shown in (b). In row-wise, the engineering demand parameters are listed. Means are demonstrated with the markers and colors in the legend box for the corresponded GMPEs. Medians are shown with the cross markers. The 16th and 84th percentiles are plotted with the horizontal bars. The structural model is the S1 model, 8-story RC. The yielding limit and ductility demands (μ) of 2, 4, and 6 are shown with a horizontal solid line with black, grey, blue, and red, respectively.

3.3.3 Impact on Ductility Demands (μ)

The previous studies have shown a relation between the increasing nonlinearity level and the bias of the GMSM methods (e.g., Huang et al., 2011). In order to evaluate the nonlinearity level of structural models, the mean of the ductility demand (μ, with respect to the roof displacement) distributions from all GM sets is shown for the GMPEs in Figure 3.3.5. The S1, S6, S7, S8b, S9 models are always over the yielding limit when the mean of all sets is considered. The mean of all $\bar{\mu}^{set}$ is not affected much by the choice of the GMSM method. When the intraset variability is included (i.e., $(\bar{\mu} + 0.95\sigma_{\mu})^{set}$), the mean of the distributions increase (for each GMPE) about 0.5 and 1.0 in MA and MC and less than 0.5 in MB and MD.

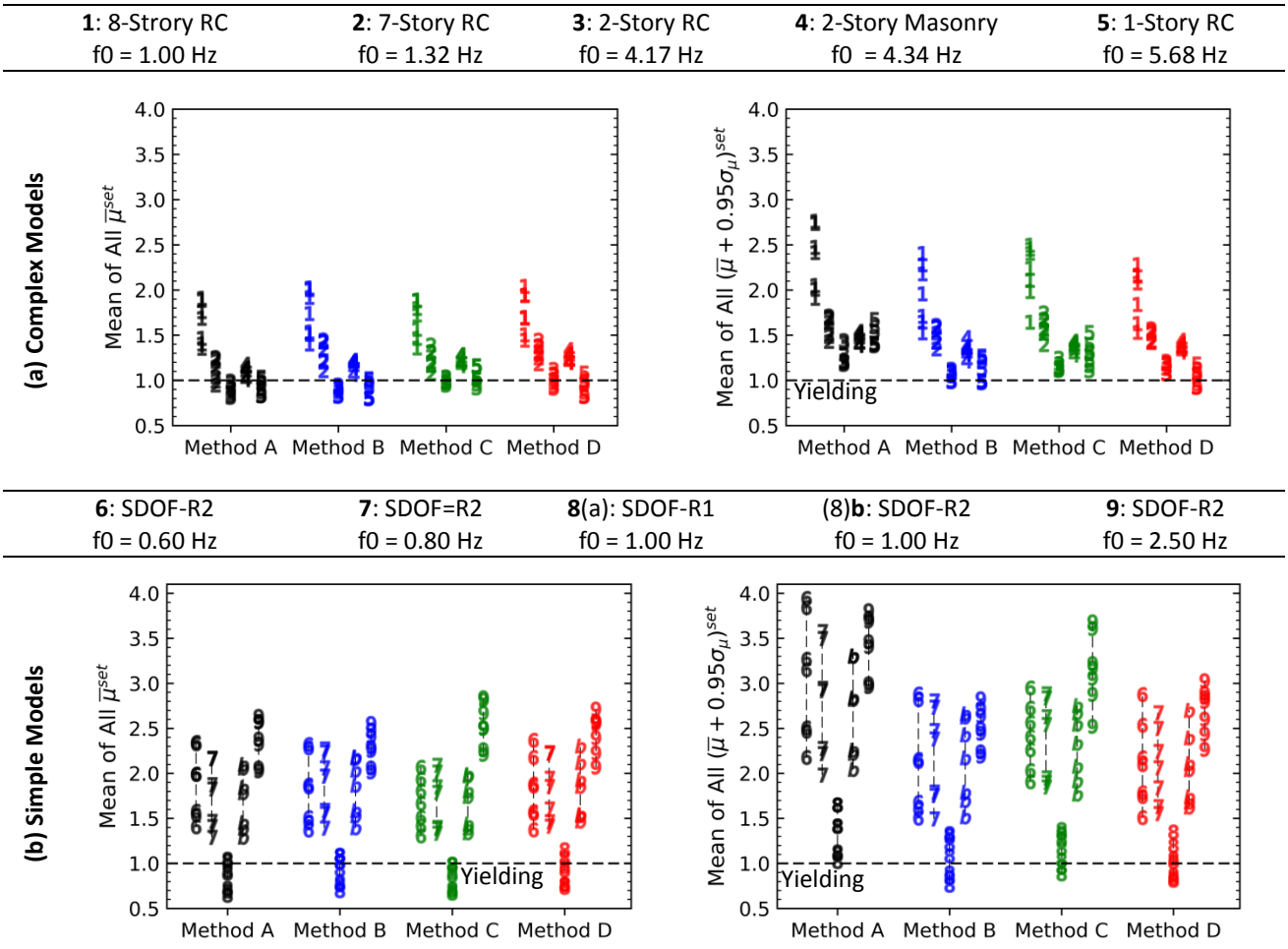

Figure 3.3.5: Comparison of roof displacement ductility demands (μ) considering interset and intraset variability. The spectrum compatible selection is made with each set including five ground motions. The upper and lower amplitude tolerances are -30% and +30% of the target for Methods A, B, and C, and between-5% and +5% of the target for Method D. The frequency range is from 0.50 Hz and 20.0 Hz. The target is obtained for the scenario of M7.0R40, Vs450, and normal fault as explained in Section 1.4. In column-wise, the distributions of each set's average are shown on the left column, and the distributions of each set's average-plus-95%-standard-deviation are shown on right column. In row-wise, the responses of structural models are listed. Each GMPE (7 of them) is plotted for the structural models. The markers are shown with the ID of the structural model given in the legend box. (continued)

Methods A, B, C, and D are shown with black, blue, green, and red, respectively. For the complex structural models, there can be certain structural elements with more critical ductility demands.

3.4 Quantification of Differences between GMSM Methods Considering Interset and Intraset Variability

In the thesis, we have large sets of structural responses (the GMSM methods, the GMPEs, the EDPs, the objectives, and the structural models). The impact of the GMSM methods may not be apparent. Therefore, the quantification metric is defined in this section. It compares the mean of distributions of the EDPs. MA is used as a benchmark to quantify the differences by MB, MC, and MD. The metric to quantify the differences, δ, is given in Equations 3.4.1 and 3.4.2:

$$\delta\left(\overline{Val}^{set}\right) = \frac{1}{Nset_{Mx}} \sum_{j=1}^{Nset_{Mx}} \left(\overline{Val}_{Mx}^{set,j}\right) \Big/ \frac{1}{Nset_{MA}} \sum_{j=1}^{Nset_{MA}} \left(\overline{Val}_{MA}^{set,j}\right) - 1.00 \qquad \textit{Equation 3.4.1}$$

where $\overline{Val}_{Mx}^{set,j}$ is a value from the set's average for Method X (explained in Equation 1.2.4), and $Nset_{Mx}$ is the amount of all eligible sets for Method X.

$$\delta\left(\left(\overline{Val} + \lambda\sigma_{Val}\right)^{set}\right) = \frac{1}{Nset_{Mx}} \sum_{j=1}^{Nset_{Mx}} \left(\left(\overline{Val} + \lambda\sigma_{Val}\right)_{Mx}^{set,j}\right) \Big/ \frac{1}{Nset_{MA}} \sum_{j=1}^{Nset_{MA}} \left(\left(\overline{Val} + \lambda\sigma_{Val}\right)_{MA}^{set,j}\right) - 1.00 \qquad \textit{Equation 3.4.2}$$

where $\left(\overline{Val} + \lambda\sigma_{Val}\right)_{Mx}^{set,j}$ is a value from set's average-plus-some-standard-deviation for Method X (Section 1.2.2).

The metric is visually exemplified in Figure 3.4.1. The differences in Δtop distributions are compared between MA and MD. In Figure 3.4.1.a, the distribution of all $\overline{\Delta top}^{set}$ is shown and the difference between MA and MD is insignificant with $\delta(\overline{\Delta top}^{set})$ of 2%. In Figure 3.4.1.b, the metric for the difference, $\delta\left(\left(\overline{\Delta top} + 0.95\sigma_{\Delta top}\right)^{set}\right)$ is illustrated, and MD considerably underpredicts with the defined metric of -21% if the objective of the seismic analysis is to use each set's average-plus-95%-sigma (i.e., ASN/2/01, 2006).

(a) Distribution of Each Set's Average (of 5 GMs)

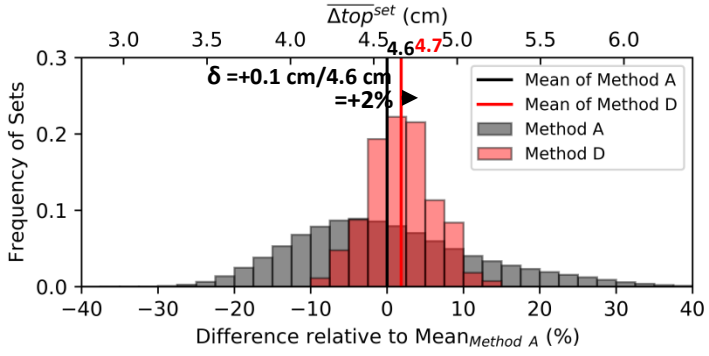

(b) Distribution of Each Set's Average Plus 95% of Sigma

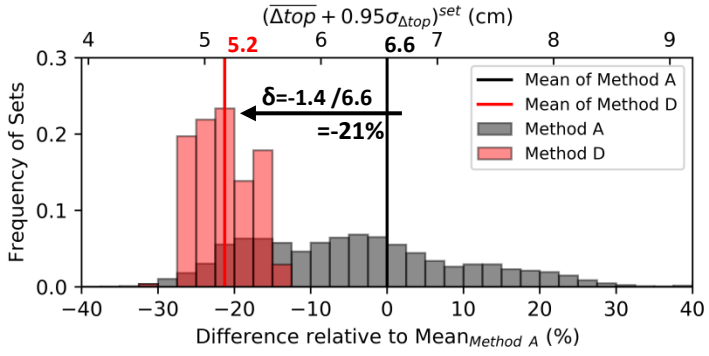

Figure 3.4.1: Quantification of differences in roof displacements (Δtop) due to the GMSM methods. The spectrum selection is made with each set including five ground motions. (continued)

The upper and lower amplitude tolerances are -30% and +30% of the target for Method A and between-5% and +5% of the target for Method D. The frequency range is from 0.50 Hz and 20.0 Hz. The target is AK2014 obtained for the scenario of M7.0R40, Vs450, and normal fault. The distributions of each set's average are shown on row (a), and the distributions of each set's average-plus-95%-standard-deviation are shown on row (b). Methods A and D are shown with black, and red, respectively.

In the example of 3.4.1.b, MD underpredicts the distribution since it minimizes the input variability. The metric, herein, is able to quantify such central difference in the distributions. In the following subsections, the quantification metric is used to quantify the differences as a function of EDPs: the roof displacements (Δtop), the base shear forces (Vbase), the interstory drift ratios (IDR), and the global damage indices (DI).

3.4.1 Differences in Roof Displacements (Δtop)

The spectrum compatible selection is based on the spectra. It is assumed that the (elastic) PSAs relate to the (inelastic) structural responses. To check this assumption, the differences in $\overline{\Delta\text{top}}^{\text{set}}$ are compared with the differences in $\overline{\text{PSA}_{\text{f0}}}^{\text{set}}$. Figure 3.4.2 shows the quantification of the differences for the GMPEs and the structural models. For example, for the S3 and S4 models, MD reveals considerable differences (up to +20%) in $\overline{\Delta\text{top}}^{\text{set}}$despite the insignificant differences in $\overline{\text{PSA}_{\text{f0}}}^{\text{set}}$. It means that $\overline{\Delta\text{top}}^{\text{set}}$ is overpredicted independent of the differences in $\overline{\text{PSA}_{\text{f0}}}^{\text{set}}$.

For other structural models, the differences in $\overline{\Delta\text{top}}^{\text{set}}$ frequently follow a similar trend with the differences in $\overline{\text{PSA}_{\text{f0}}}^{\text{set}}$, which indicates that any GMSM method can be used to obtain comparable $\overline{\Delta\text{top}}^{\text{set}}$ by ensuring compatibility with the target PSAs at f0. However, in the spectrum compatible selection, large spectral variability is permitted as observed in the nature. Then, the collected GM sets are assumed to represent the same EQ scenario regardless of the differences in the PSAs at f0.

If the differences in the mean of all PSAs at f0 (which is less than 20% herein) are tolerated, a positive difference will reflect an overprediction and a negative difference will reflect an underprediction relative to MA. Thus, the differences are mostly overpredicted for MB, MC, and MD with some exceptions (e.g., MB underpredicting the S5, S6 and S9 models; MC underpredicting the S6, S7, and S8b models; and MD underpredicting the S6 model).

Overall, the difference in the GMSM methods is between -10% and +20% for $\overline{\text{PSA}_{\text{f0}}}^{\text{set}}$, and -10% and +25% for $\overline{\Delta\text{top}}^{\text{set}}$. They are considerable but not major. The same test is extended to the differences in the median of all GM sets in Figure C.1.10 (Appendix C.1), and the same conclusion can be drawn.

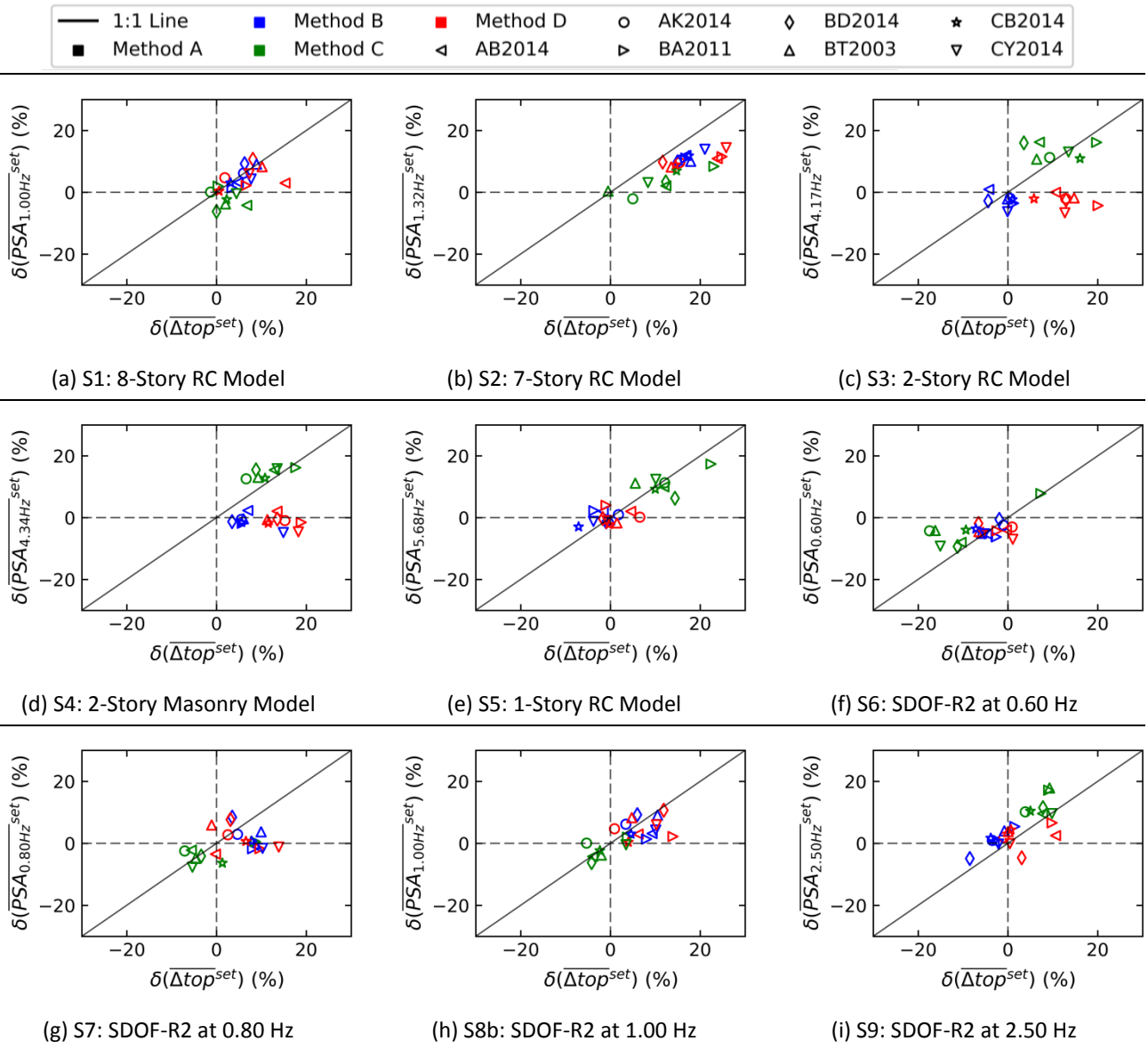

(a) S1: 8-Story RC Model (b) S2: 7-Story RC Model (c) S3: 2-Story RC Model

(d) S4: 2-Story Masonry Model (e) S5: 1-Story RC Model (f) S6: SDOF-R2 at 0.60 Hz

(g) S7: SDOF-R2 at 0.80 Hz (h) S8b: SDOF-R2 at 1.00 Hz (i) S9: SDOF-R2 at 2.50 Hz

Figure 3.4.2: The difference in mean of input PSAs at f0 versus the difference in mean of output lateral structural displacements (Δtop) with respect to Method A for seven GMPEs. The x-axis illustrates the difference in the mean of Δtop distributions. The y-axis illustrates the differences in the mean of input PSAs at f0. The solid black line is the equality line. The earthquake scenario is M7.0R40, Vs450, and normal fault. GMPEs such as AB2014, AK2014, BA2011, BD2014, BT2003, CB2014, and CY2014 are shown with the marker in the legend. Methods B, C, and D are represented with blue, green, and red, respectively. The spectrum selection is made with each set including five ground motions. The upper and lower amplitude tolerances are -30% and +30% of the target for Methods A, B, and C, and between-5% and +5% of the target for Method D. The frequency range is from 0.50 Hz and 20.0 Hz. The negative values represent underprediction relative to Method A and vice versa.

Figure 3.4.3 shows the differences for the mean of all $(\overline{\Delta top} + 0.95\sigma_{\Delta top})^{set}$, which are generally underpredicted to a larger degree by MB and MD, and to a smaller degree by MC. It highlights that MC can produce a larger amount of intraset variability (i.e., $0.95\sigma_{\Delta top}$ per set) than MB and MD; however, it is not sufficient with respect to MA.

The underprediction in the complex structural models (the S1, S2, S3, S4, and S5 models) is less critical than the simple structural models.

The choice of the GMPE can be important especially for some structures, e.g., the analysis of the S4 model with MB, the analysis of the S6 model with MC, and the analysis of the S1 model with MD.

1: 8-Story RC f0 = 1.00 Hz	**2**: 7-Story RC f0 = 1.32 Hz	**3**: 2-Story RC f0 = 4.17 Hz	**4**: 2-Story Masonry f0 = 4.34 Hz	**5**: 1-Story RC f0 = 5.68 Hz

Complex Models

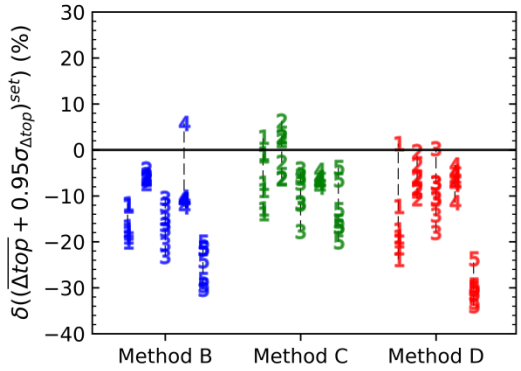

6: SDOF-R2 f0 = 0.60 Hz	**7**: SDOF=R2 f0 = 0.80 Hz	**8**(a): SDOF-R1 f0 = 1.00 Hz	(8)**b**: SDOF-R2 f0 = 1.00 Hz	**9**: SDOF-R2 f0 = 2.50 Hz

Simple Models

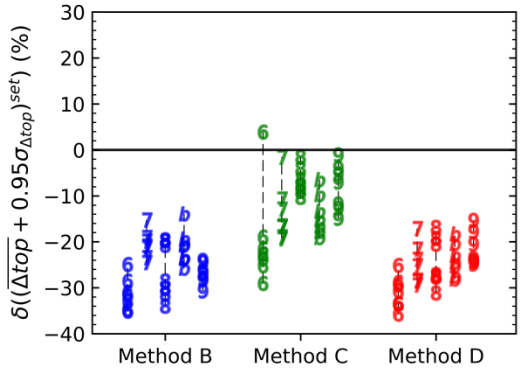

Figure 3.4.3: The difference in mean of lateral structural displacements (Δtop) distributions at each set's average-plus-95%-standard-deviation. The spectrum compatible selection is made as explained in the caption of Figure 3.4.2. The markers are shown with the ID of the structural model given in the legend above the subfigures. The differences are quantified according to Equation 3.4.2. Methods B, C, and D are shown with blue, green, and red colors, respectively. The negative values represent the underprediction relative to Method A and vice versa.

3.4.2 Differences in Base Shear Forces (Vbase)

In Figure 3.4.4, the differences in Vbase are quantified. The means of all $\overline{\text{Vbase}}^{\text{set}}$ are significantly overpredicted relative to MA with some exceptions. The means of all $(\overline{\text{Vbase}} + 0.95\sigma_{\text{Vbase}})^{\text{set}}$ are predicted in the close proximity of MA. In this case, the intraset variability (i.e., $0.95\sigma_{\text{Vbase}}$ per set) is not well reproduced by MB, MC, and MD, but it becomes advantageous to reveal comparable levels in the latter case.

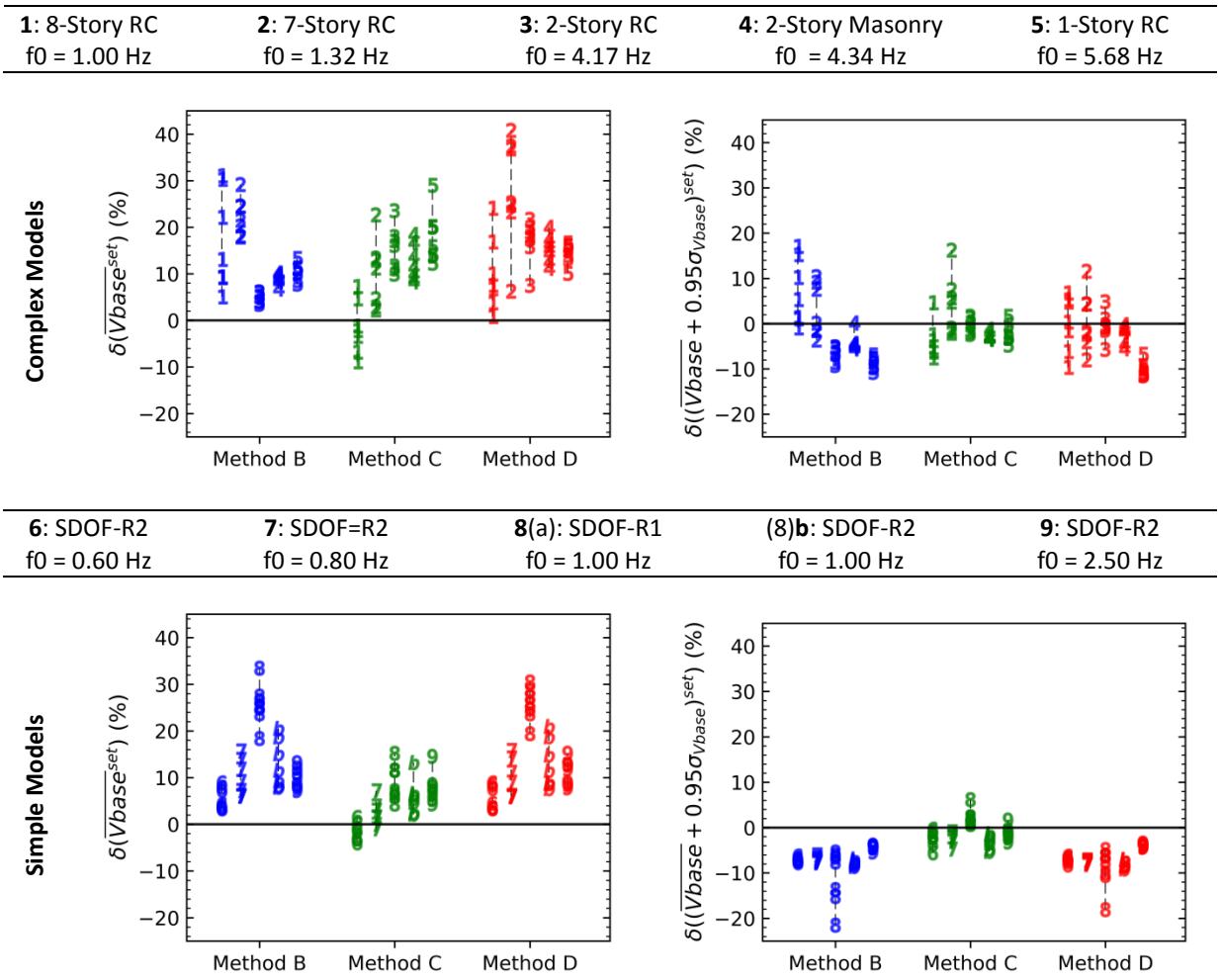

Figure 3.4.4: The difference in mean of base shear force (Vbase) distributions. The differences in distributions of each set's average are shown on the left column, and the differences in distributions of each set's average-plus-95%-standard-deviation are shown on right column. The spectrum compatible selection is made as explained in the caption of Figure 3.4.2. The differences are quantified according to Equations 3.4.1 and 3.4.2. The markers are shown with the ID of the structural model given in the legend above the subfigures. Methods B, C, and D are shown with blue, green, and red colors, respectively. The negative values represent the underprediction relative to Method A and vice versa.

3.4.3 Differences in Interstory Drift Ratio (IDR)

The quantification of IDR is shown in Figure 3.4.5. For the S1 model, the means of all $\overline{\mathrm{IDR}}^{\mathrm{set}}$ are overpredicted to a small degree, less than 10%. For the S2 model, MB, MC, and MD result in overpredictions about 10% with respect to MA.

For the S1 and S2 models, MC predicts the means of all $(\overline{\mathrm{IDR}} + 0.95\sigma_{\mathrm{IDR}})^{\mathrm{set}}$ close to the benchmark. MB and MD underpredict them up to 30% for the S1 model and up to 15% for the S2 model.

The impact of GMPE becomes apparent for the S1 model with MB, MC, and MD, and for the S2 model with MC.

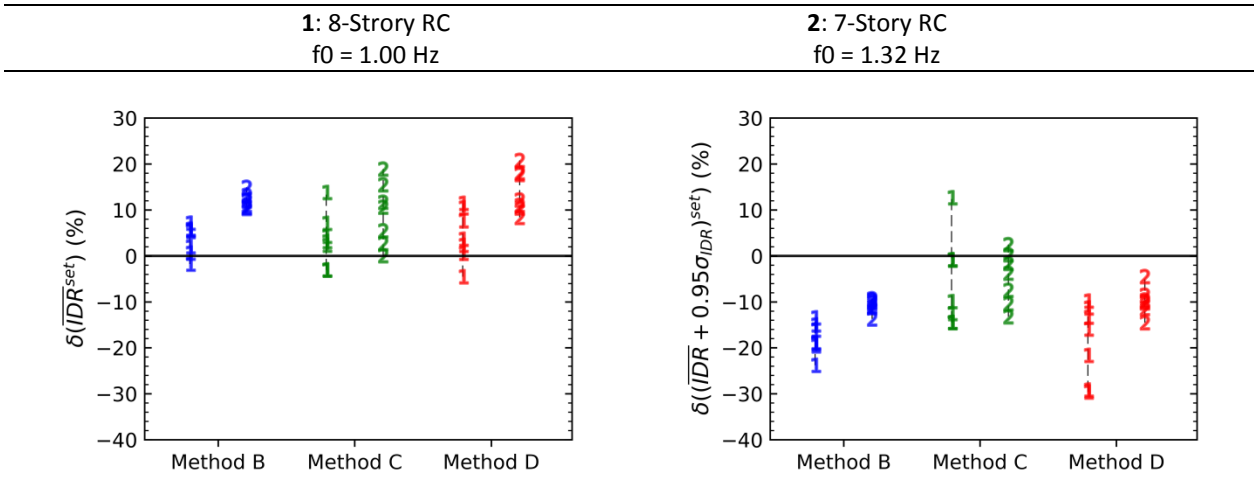

Figure 3.4.5: The difference in mean of interstory drift ratio (IDR) distributions. The differences in distributions of each set's average are shown on the left side, and the differences in distributions of each set's average-plus-95%-standard-deviation are shown on right side. The spectrum compatible selection is performed as explained in the caption of Figure 3.4.2. The differences are quantified according to Equations 3.4.1 and 3.4.2. The markers are shown with the ID of the structural model given in the legend above the subfigure. Methods B, C, and D are shown with blue, green, and red colors, respectively. The negative values represent an underprediction relative to Method A and vice versa.

3.4.4 Differences in Global Damage Index (DI)

The results for the global damage indices (DI) are shown in Figure 3.4.6. DI is a measure of structural damage calculated for all structural elements by Park & Ang index (Park and Ang, 1985). For the S1 model, the means of all $\overline{\mathrm{DI}}^{\mathrm{set}}$ are overestimated slightly by MB, and underpredicted by MC and MD. For the S4 model, MB, MC, and MD result in overprediction up to 33% with respect to MA.

For the S1 model, means of all $(\overline{\mathrm{DI}} + 0.95\sigma_{\mathrm{DI}})^{\mathrm{set}}$ are mostly underpredicted for the S1 model. For the S4 model, the estimates are mostly underpredicted to a smaller degree, less than -20%. The results show dependence on GMPE and the structural model.

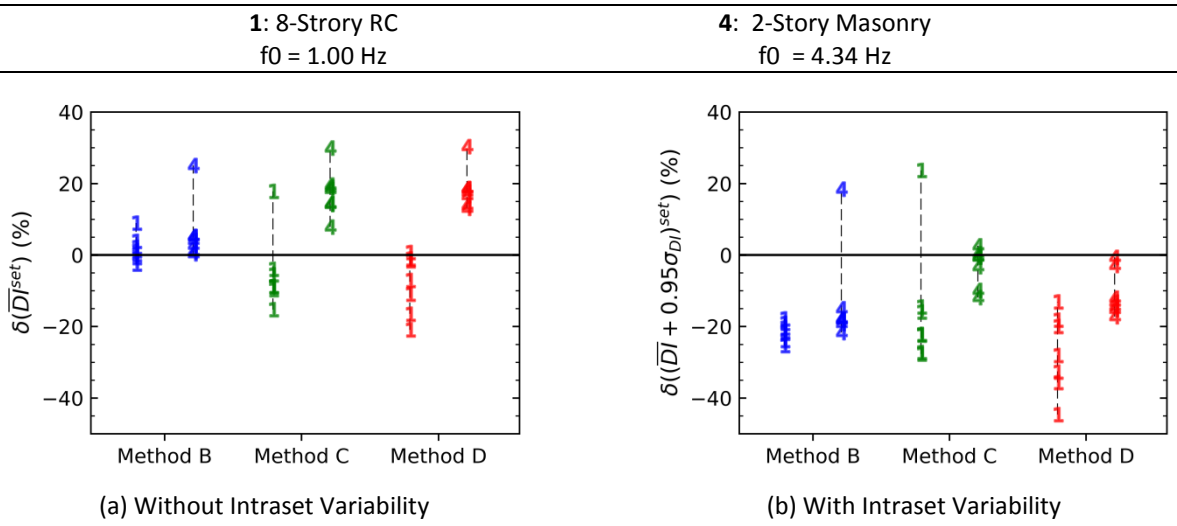

Figure 3.4.6: The difference in mean of global damage index (DI) distributions. The differences in distributions of each set's average are shown on the left column, and the differences in distributions of each set's average-plus-95%-standard-deviation are shown on right column. The spectrum compatible selection is performed as explained in the caption of Figure 3.4.2. The differences are quantified according to Equations 3.4.1 and 3.4.2. The markers are shown with the ID of the structural model given in the legend above the subfigure. Methods B, C, and D are shown with blue, green, and red colors, respectively. The negative values represent the underprediction relative to Method A and vice versa.

3.4.5 Approach to Integrate Differences due to Ground Motion Prediction Equations

In the previous subsections, the quantifications are completed for each GMPE. This section consolidates the effects of GMPEs. In the probabilistic SHA, the logic tree approach is utilized to integrate the differences of the GMPEs. A similar approach is utilized to consolidate the results of the quantification metric (i.e., Equations 3.4.1 and 3.4.2). The weights are given in Table 3.4.1. Option 1 represents the deterministic SHA with RFS 2001-01 (2001) (i.e., the use of BT2003). Option 2 consists of an equal weight of the GMPEs. In Option 3, larger weights are allocated to BT2003 and the GMPEs from Resorce Database. In Option 4, larger weights are given to the complex GMPEs.

Table 3.4.1: Weights used for GMPEs

GMPE	Option 1	Option 2	Option 3	Option 4
AB2014	0	2/14	1/14	3/14
AK2014	0	2/14	3/14	1/14
BA2011	0	2/14	1/14	1/14
BD2014	0	2/14	3/14	1/14
BT2003	14/14	2/14	3/14	2/14
CB2014	0	2/14	1/14	3/14
CY2014	0	2/14	2/14	3/14

In Figure 3.4.7, the results with different weight options are summarized for the complex structural models. Options 2, 3, and 4 reveal a similar level of quantifications. In this specific case, BT2003 reveals similar results with the rest of the options.

The previous conclusions are also verified with the logic tree approach: the results depend on (i) structures, (ii) engineering demand parameter, (iii) the objective of seismic analysis (i.e., the use of whether $\overline{Val}^{set}$ or $(\overline{Val} + \lambda\sigma_{Val})^{set}$), which are also supported by the other structural models and the intraset approaches in Appendix C.1.9. The underpredictions become more critical for the single-degree-of-freedom models when the responses of the complex structural models are underpredicted by the GMSM methods. It implies that the use of a simplified structural model for the comparison of GMSM methods can exaggerate the underpredictions relative to the complex structural models. This may explain the different conclusions in the literature, where some studies are solely based on the single-degree-of-freedom models and the other studies are based on the complex structural models.

S1: 8-Strory RC	**S2**: 7-Story RC	**S3**: 2-Story RC	**S4**: 2-Story Masonry	**S5**: 1-Story RC
f0 = 1.00 Hz	f0 = 1.32 Hz	f0 = 4.17 Hz	f0 = 4.34 Hz	f0 = 5.68 Hz

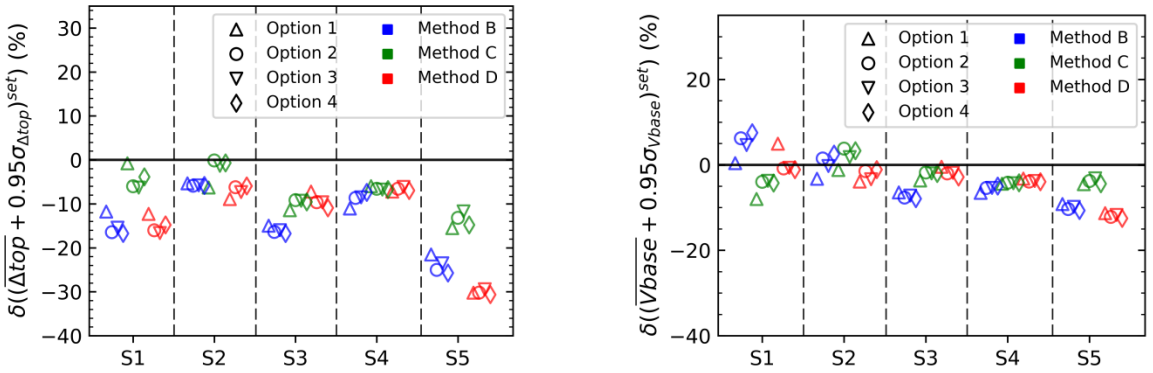

(a) Differences in Roof Displacements (Δtop) (b) Differences in Base Shear Forces (Vbase)

Figure 3.4.7: The difference in the structural response distributions relative to Method A with the logic tree approach and the symmetric tolerances. The differences in distributions of each set's average-plus-95%-standard-deviation are shown. The spectrum compatible selection is done as explained in the caption of Figure 3.4.2. The differences are quantified according to Equation 3.4.2. The labels in the y-axis show the ID of the structural model given in the legend above the subfigure. Methods B, C, and D are shown with blue, green, and red colors, respectively. The negative values represent the underprediction relative to Method A and vice versa. The weights of GMPEs are provided in Table 3.4.1.

3.5 Comparison of GMSM methods with Asymmetric Tolerances

In the current practice with ASN/2/01 (2006), the asymmetric tolerances are suggested. They result in the average spectra being above the target to impart conservatism in the structural responses. It is previously discussed for MA in Section 1.10. This section evaluates the asymmetric tolerances for the impact of the GMSM methods on structural response distributions with the interset and the intraset variability. The amplitude tolerances are 5% below the target spectra and 50% above the target spectra for MA, MB, and MC (MD is already within the tolerances). The same tests in Section 3.2, 3.3, and 3.4 are repeated in Section 3.5.

3.5.1 Impact on Input Ground Motion Sets

For the asymmetric tolerances, the spectral amplitudes for each set's average, $\overline{\mathrm{PSA}_{\mathrm{f0}}}^{\mathrm{set}}$ and the target spectra are shown in Figure 3.5.1. MA reveals greater mean of all $\overline{\mathrm{PSA}_{\mathrm{f0}}}^{\mathrm{set}}$ than MB and MC. Basically, the asymmetric tolerances cause GM sets deviating positively from the target spectra upon the capability of preserving the spectral variability. MB exhibits comparable dispersion with MA except at 1.00 Hz. MC experiences less deviation than MB.

The distribution of PSA at 1.00 Hz is shown in Figure 3.5.2 for other GMPEs. The GMPE results in considerably different PSA levels. The intraset variability in the PSAs (i.e., σ_{f0}^{set}) of MA is greater than the intraset variability of the symmetric tolerances. The observations for the other frequencies in Figures C.2.1 and C.2.2 (Appendix C.2) reinforce the observations.

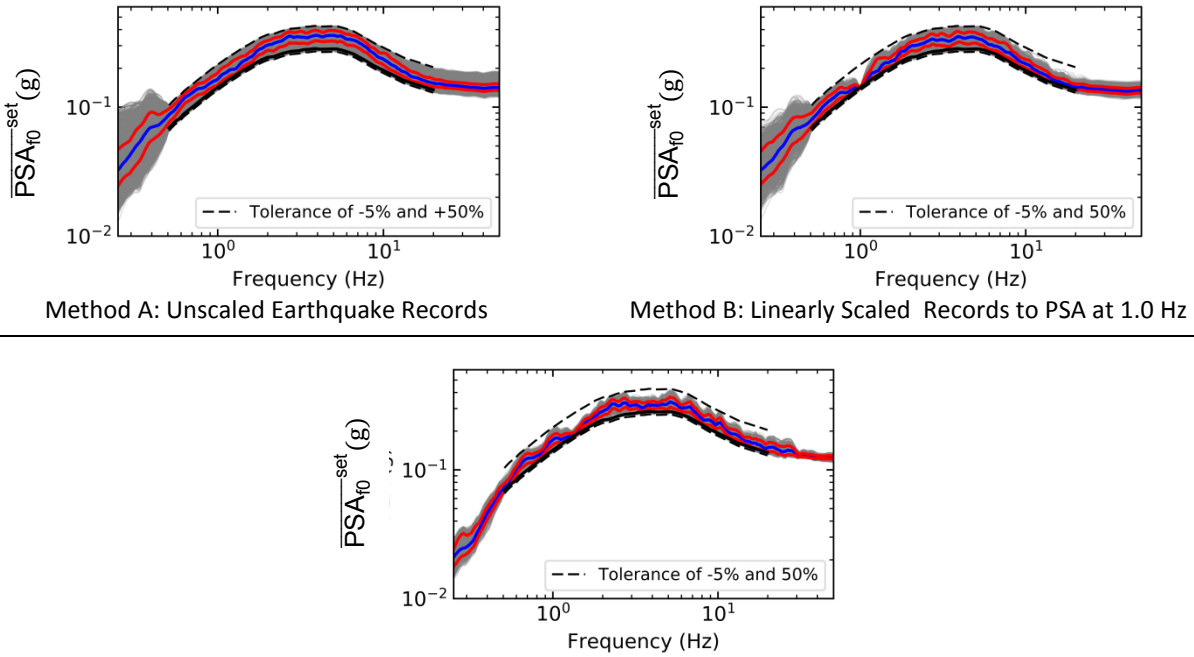

Method A: Unscaled Earthquake Records

Method B: Linearly Scaled Records to PSA at 1.0 Hz

Method C: Loosely Matched Waveforms

Figure 3.5.1: Average spectra of all eligible GM sets with the <u>asymmetric</u> tolerances. The target is shown with a solid black line and is the median of AK2014 for the scenario of M7.0R40, Vs450, and normal fault. Each set includes five ground motions. The upper and lower amplitude tolerances are shown with dashed black lines: -5% and +50% of the target for Methods A, B, and C. The frequency range is from 0.50 Hz and 20.0 Hz. The grey lines represent the average spectra of the GM sets, $\overline{PSA_{f0}}^{set}$. The 16th and 84th percentiles of the eligible GM spectra, $\overline{PSA_{f0}}^{set}$, are shown with the solid red lines. The median of all $\overline{PSA_{f0}}^{set}$ is shown with the solid blue line. For Methods A, B, and C, there are 34 174, 8 647, and 948 GM sets, respectively.

(a) Distribution of Each Set's Average (of 5 GMs) (b) Distribution of Each Set's Standard Deviation

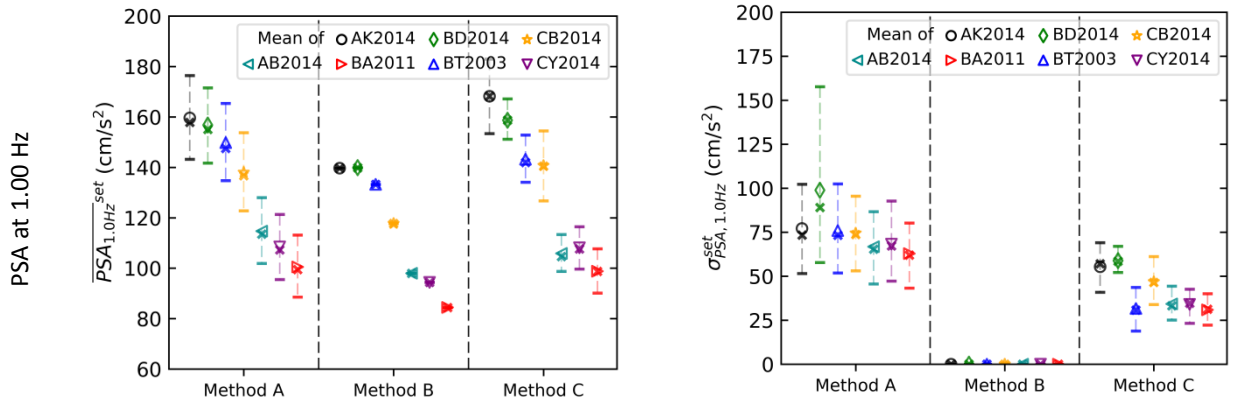

Figure 3.5.2: Distribution of PSAs at 1.00 Hz with all GM sets considering each set's average in column (a) and each set's standard deviation in column (b) with the <u>asymmetric</u> tolerances. The spectrum compatible selection is performed as described in the previous figure. The target is obtained for the scenario of M7.0R40, Vs450, and normal fault as explained in Section 1.4. Means are demonstrated with the markers and colors in the legend box for corresponded GMPEs. Medians are shown with the cross markers. The 16th and 84th percentiles are plotted with the horizontal bars.

3.5.2 Impact on Output Structural Responses

The distribution of Δtop (with all GM sets) is shown in Figure 3.5.3 to test the impact of the asymmetric tolerances on the EDPs. For the selection with AK2014, the mean of all $(\overline{\Delta\text{top}} + 0.95\sigma_{\Delta\text{top}})^{\text{set}}$ increases 23% in MA, 12% in MB, and 5% in MC relative to the symmetric tolerances (in Figure 3.3.2). The change relative to the symmetric tolerances indicates the level of conservatism imparted. However, MB and MC are not able to cause the same level of increase, which is due to the GM modifications' goal of reducing the representativeness of the natural variability. Other structural responses support these findings: for Δtop in Figure C.2.5, Vbase in Figure C.2.6, IDR in Figure C.2.7, and DI in Figure C.2.8.

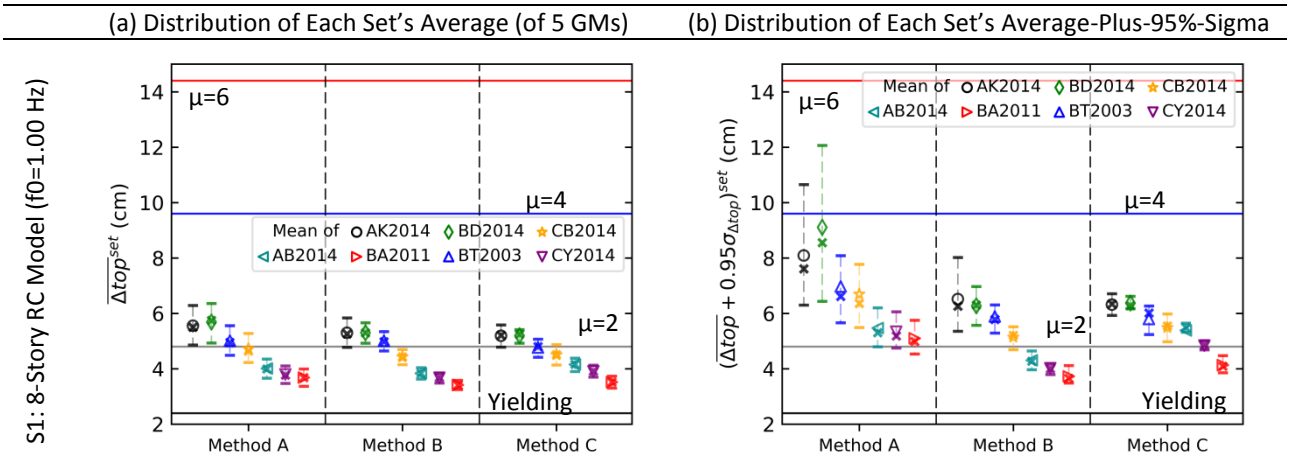

Figure 3.5.3: Distribution of structural response (on column-wise) with all GM sets considering intraset variability with the symmetric tolerances. Each set includes five ground motions. The upper and lower amplitude tolerances are -5% and +50% of the target for Methods A, B, and C. The frequency range is from 0.50 Hz and 20.0 Hz. The target is obtained for the scenario of M7.0R40, Vs450, and normal fault as explained in Section 1.4. In column-wise, distributions of each set's average are shown in (a), and the distributions of each set's average-plus-95%-standard-deviation are shown in (b). Means are demonstrated with the markers and colors in the legend box for the corresponded GMPEs. Medians are shown with the cross markers. The 16th and 84th percentiles are plotted with the horizontal bars. The structural model is the S1 model, 8-story RC. The yielding limit, ductility demands (μ) of 2, 4, and 6 are shown with horizontal solid lines with black, grey, blue, and red, respectively.

3.5.3 Quantification of Differences in Output Structural Responses

The differences in the mean of the structural response distributions are quantified for Δtop in Figures C.2.9 and C.2.10, Vbase in Figure C.2.11, IDR in Figure C.2.12 and DI in Figure C.2.13 according to Equations 3.4.1 and 3.4.2. In Figure 3.5.4, the quantification is integrated for the GMPEs with the logic tree approach in Table 3.4.1. Relative to the symmetric tolerances, the quantification metric, δ, is about 10-20% less in the asymmetric tolerances. Therefore, the conclusions become more critical for the underpredictions (i.e., Δtop, IDR, and DI) and uncritical for the overpredictions (i.e., Vbase), which is also confirmed for the each set's average in Figure C.2.14.

Overall, the use of the asymmetric tolerances in the GM selection causes eccentricity between the GM modification and selection. In other words, the GM modification is applied with respect to the target spectrum, and the asymmetric tolerance results in the benchmark sets' (i.e., the unscaled real records) drifting significantly. However, the GMSM methods do not exhibit the same level of the increase due to the incapability of keeping such input variability.

It also implies that the French nuclear safety guide (ASN/2/01, 2006) can indirectly support the use of the GMSM methods that underpredict critically. Since the guide is not explicit on the expectations behind the asymmetric tolerances as well as the minimum acceptable level of the spectral variability, the GMSM methods that are insensitive to such asymmetry (e.g., tightly spectrum-matched waveforms in this study) will likely reveal less structural demands, therefore, will be favored in the current practice.

S1: 8-Strory RC f0 = 1.00 Hz	**S2**: 7-Story RC f0 = 1.32 Hz	**S3**: 2-Story RC f0 = 4.17 Hz	**S4**: 2-Story Masonry f0 = 4.34 Hz	**S5**: 1-Story RC f0 = 5.68 Hz

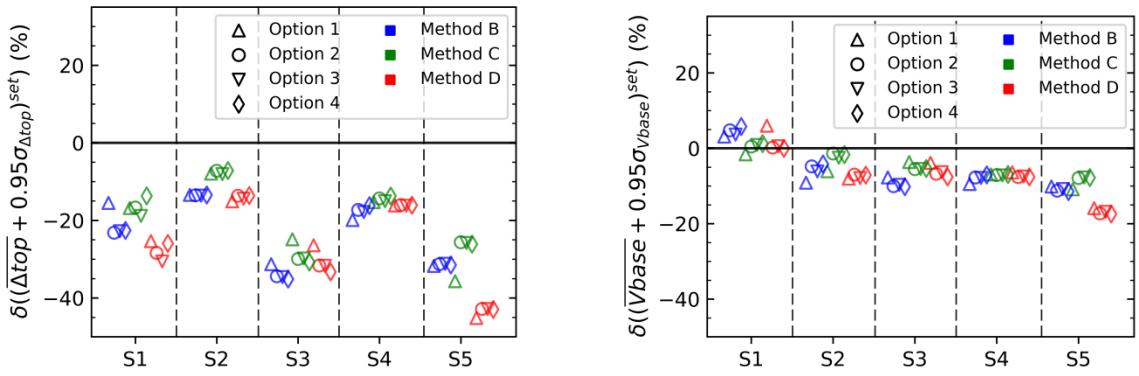

(a) Differences in Roof Displacements (Δtop) (b) Differences in Base Shear Forces (Vbase)

Figure 3.5.4: The difference in structural response distributions relative to Method A with the logic tree approach and asymmetric tolerances. The differences in distributions of each set's average-plus-95%-standard-deviation are shown. The target spectra are obtained for the earthquake scenario is M7.0R40, Vs450, and normal fault with AB2014, AK2014, BA2011, BD2014, BT2003, CB2014, and CY2014 as explained in Section 1.4. The spectrum selection is made with each set including five ground motions. The upper and lower amplitude tolerances are -5% and +50% of the target for Methods A, B, and C, and between-5% and +5% of the target for Method D. The frequency range is from 0.50 Hz and 20.0 Hz. The negative values represent the underprediction relative to Method A and vice versa. Weights of GMPEs are provided in Table 3.4.1.

3.6 Perspective

The code-based design spectra are commonly used in the engineering applications. For example, the EC8 spectrum has a shape based on the PGA level, and the ASCE 7-10 spectrum has a shape based on the PSA at 1.00 Hz and the PSA forming the plateau. The code-based design spectra can give similar amplitudes but non-smoothed shape regarding the GMPE spectrum if the relevant scaling is done. It can suggest that the final structural responses would be in the similar range of the above-mentioned results. A comparison of the AK2014 spectrum and the code-based target spectrum is given in Figure C.3.1 (Appendix C.3).

The conclusions are based on a single scenario of M7.0R40 and Vs450. There can be multiple earthquake scenarios in an engineering project. An earthquake scenario with a moment magnitude of 5.5, a source-to-site distance of 20 km, and Vs30 of 450 m/s (i.e., M5.5R20 and Vs450) is also tested. The structural responses remain in the elastic range and are mentioned in Appendix C.3.2. The GMPE-based variability is shown to be important as well as the type of intraset approaches (i.e., the objective). The results of M5.5R20 and Vs450 are partially given since the linear elastic behavior is not the main scope of the thesis. If there had been other earthquake scenarios with closer magnitude and the distance range (i.e., 6.0<M<6.5 and R<30.0 km), it would be necessary to repeat the analyses for each scenario to determine the critical structural responses in a deterministic SHA.

It is also common to use a median-plus-some-standard-deviation spectrum as the target to cover the various sources of variability in an engineering application. This approach may necessitate the adaptation of a tolerance type in line with the lognormal distribution of the PSAs (i.e., the tolerances covering upper part of the PSA distribution, for example, the 80^{th} to 90^{th} percentiles).

3.7 Conclusion

In Part 3, we present the discussion on the impact of the ground motion (GM) set variability on the engineering demand parameters (EDPs). We compare the linearly scaled records (MB), the loosely matched waveforms (MC), and the tightly

matched waveforms (MD) relative to the unscaled earthquake records (MA). The key conclusions of Part 3 are summarized below:

- In tightly matched waveforms (MD), the GMs have similar spectral shapes, but the output structural responses show a considerable level of the set dispersion, which is likely due to the variability in the time-based ground motion (GM) characteristics. This is also addressed by Causse et al. (2013) and suggests the importance of other GM characteristics in addition to the PSAs, a common parameter (e.g., Kohrangi et al., 2016; Seifried and Baker, 2016).

- Interset variability is calibrated by the upper and the lower amplitude tolerances being symmetric and asymmetric in Part 3, and a single ground motion set is concluded to be insufficient regardless of the ground motion selection and modification (GMSM) method for a stable distribution of the EDPs.

- For the objective of a seismic analysis requiring the each set's average (i.e., $\overline{\mathrm{Val}}^{\mathrm{set}}$), the GMSM methods (MB, MC, and MD) can result in considerable but uncritical differences in PSAs at f0, the roof displacements (Δtop), the interstory drift ratios (IDR), and the global damage indices (DI) and relatively critical overprediction in base shear forces (Vbase) in comparison with the unscaled earthquake records (MA).

- The previous conclusion implies that, for an objective requiring the central measure (i.e., mean and median) of structural responses, the GMSM methods can be preferred to predict the final structural response while offering a small number of the nonlinear dynamic analyses. Among the modified GMs, MD reveals the least dispersed EDP distirbution and is largely preferred in the practice. It brings the on-going questions up for discussion such as:

  (1) how much pragmatism can be accepted in the case of the unnatural ground motion characteristics, such as the modified ground motions with smoothed response spectra and reduced variability, and

  (2) whether or not they can be accepted for the sake of obtaining 'fast' structural responses.

  Also, the conclusions (and most of the previous studies) are based on the global structural responses (e.g., the roof displacements, the base shear forces, etc.), but the local structural responses (e.g., the tensional and compressional demands in the structural members, etc.) can also be important for such a decision.

- For the objective of the seismic analysis requiring the each set's average-plus-some-standard deviation (i.e., $(\overline{\mathrm{Val}} + 0.95\sigma_{\mathrm{val}})^{\mathrm{set}}$), the GMSM methods (MB, MC, and MD) can result in critical underpredictions in PSAs at f0, Δtop, IDR, and DI but the insignificant difference in Vbase relative to the naturalist method.

- The previous conclusions are made for the symmetric tolerances. For the asymmetric tolerances required by the French nuclear safety guide (ASN/2/01, 2006), the GMSM methods (MB and MC) are not able to mimic the same level of increase (i.e., conservatism) in PSAs and the output structural responses of the naturalist method (MA). Thus, the underpredictions are emphasized, and the overpredictions become less critical relative to the symmetric tolerances. The use of asymmetric tolerances causes eccentricity between the GM modification and selection upon the capability of keeping spectral variability. Since the ASN/2/01 guide (2006) is not explicit on the assumptions behind the asymmetric tolerances and the minimum level of acceptable GM variability. The guide may indirectly promote the use of the GMSM methods (e.g., tightly spectrum-matched waveforms) which will likely reveal less structural demands than the unscaled earthquake records.

- The simple structural models (i.e., single-degree-of-freedom oscillators) tend to reveal more critical underpredictions but in a comparable level in the case where the responses of the complex structural models are underpredicted. It implies that the use of a simplified structural model for the comparison of GMSM methods can exaggerate the underpredictions relative to the complex structural models.

- The unscaled earthquake-based method (MA) is the most realistic option to use in the seismic analysis. The 'best' modified GMs depends on the objective of the structural analysis (i.e., the intraset approach), the engineering demand parameter (EDP), and the structural model. This conclusion emphasizes the necessity of a ground motion selection method specific to the objective, the EDP, and the structure.

- Target spectrum obtained by the GMPEs results in significant differences in the structural responses regardless of the GMSM method. The uncertainty in the target spectrum outweighs the differences due to the GMSM methods. The choice of the GMPEs can also be important when it comes to the comparison of the GMSM methods. If a logic tree approach is used to integrate the effect of the GMPEs on the differences (i.e., δ), the options with various weights result in similar conclusions. These findings may not be sufficient to generalize the conclusions for other earthquake scenarios or the cases that combine the possible input parameters of a GMPE.

PART 4

GENERAL CONCLUSIONS, DISCUSSIONS, AND FUTURE WORK

4.1 General Conclusions and Discussions

The observed variability is very large among the natural earthquake records. The accelerogram variability is reduced in the engineering applications because of the cost and the duration of the nonlinear dynamic analyses. Yet, the question of its consequences on the output structural responses has remained unanswered. The study, herein, aims at quantifying the impact of the large accelerogram variability on the GM selection and the engineering demand parameters (EDPs).

In Part 1, we studied the impact of the unscaled earthquake records (MA) on the behavior of the single-degree-of-freedom model (through the record-to-record and set-to-set variability). In Part 2, we compared the ground motion selection and modification (GMSM) methods such as (1) the linearly scaled earthquake records (MB), (2) the loosely spectrum-matched waveforms (MC), and (3) the tightly spectrum-matched waveforms (MD) on the response of the simple and complex structural models through the record-to-record variability. In Part 3, we extended the comparisons of the GMSM methods on the structural models by considering the set-to-set variability, i.e., the response spectrum compatible selection.

The discussions and the conclusions are presented in two aspects: the results regarding (a) the uncertainty and the variability and (b) the comparison of the GMSM methods.

(a) Uncertainty and Variability

On one side, we questioned the impact of the GM (set) variability and the target spectrum variability. The GMs in the chosen magnitude-distance bin (M7.0R40) were shown to reveal large record-to-record variability. The spectrum compatible selection, with an aim of selecting a few GMs, was then performed.

The spectrum compatible selection was demonstrated to give two types of variability: (1) the interset variability, i.e., the variability among the GM sets and (2) the intraset variability, i.e., the record-to-record variability within a GM set. The interset variability has not been considered in the seismic regulatory codes, and a single GM set is used in the practice. The interset variability is allowed by the upper and lower amplitude tolerances. We applied the sigma-based (i.e., using the sigma of a GMPE), the symmetric, and the asymmetric tolerances.

There are different ways to treat the intraset variability of the output EDP: the average of each set, $\overline{\mathrm{EDP}}^{\mathrm{set}}$, and the average with some standard deviation, $(\overline{\mathrm{EDP}} + \lambda\sigma_{\mathrm{EDP}})^{\mathrm{set}}$. The latter approach is supported by some seismic regulatory codes (e.g., ASN/2/01 [2006]) and the engineers that aim at imparting conservatism. We showed that the intraset approach of some standard deviation above the average can increase the Δtop estimations of about 60% on average (in MA). Such difference can impact the final engineering decisions while increasing the cost in a design project and the probability of a damage exceedance in the risk analysis.

We discussed how representative a small GM set can be regarding all eligible GM sets (from a magnitude-distance bin). This study demonstrated that, regardless of the GMSM method, a single set is not sufficient to obtain an assuring distribution of the structural responses (considering all GM sets). In fact, the simplification with a single set causes a lack of information on the EDP distribution. These conclusions are based on the half sigma boundary. For the GM set selection with one (or more) sigma boundaries, the set variability can gain more importance.

We showed that three factors are essential to replicate the set variability with a small number of GM sets: (1) the number of records with respect to all GMs (herein at least 3/4 of the GMs in the magnitude-distance bin are recommended), (2) the recurrence frequency of the GMs in each set, and (3) the number of GMs with a relatively large recurrence frequency. Accordingly, we developed the cycle-and-shift algorithm having the advantage of revealing a stable EDP distribution with fewer sets and overcoming the technical limitations (i.e., the memory and duration problem).

We demonstrated that the target spectrum obtained by different ground motion prediction equations (GMPEs) results in significant differences (about ± 65%) in the GM characteristics and the EDPs. This conclusion is valid for all considered GMSM methods. The uncertainty in the target spectrum overshadows the differences among the GMSM methods.

The GMPEs were defined for the specific input parameters, which may not require further analyses on other earthquake scenarios or the cases that combine the possible parameters of a GMPE. We also performed the analyses of the scenario with a moment magnitude of 5.5, a source-to-site distance of 20 km, and Vs30 of 450 m/s. The results were found in the elastic range. If there had been other earthquake scenarios with closer magnitude and the distance range (i.e., 6.0<M<6.5 and R<30.0 km), it would be necessary to repeat the analyses for each scenario to determine the critical structural responses in a deterministic SHA.

In summary, we underlined that there are significant differences in the structural responses due to the set variability and the various GMPEs. The target spectrum obtained from a single set and a single GMPE may not be sufficient to evaluate the seismic behavior of a structure even in a deterministic SHA. The probabilistic elements can be inserted in the seismic analysis by the logic tree approach or other convenient approaches.

(b) Comparison of Ground Motion Selection and Modification (GMSM) Methods

On the other side, we questioned whether or not the unscaled earthquake records can be replaced by the modified GMs (e.g., MB, MC, and MD). We supported that the unscaled earthquake records (MA) are the most realistic option. We concluded that the modified GMs may replace MA upon the objective of a seismic analysis (i.e., the intraset approach), the engineering demand parameter (EDP), and the structural model. It can also explain why the previous studies, which consider specific objectives, EDPs, and structures, have not reached a universal consensus on which GMSM method is the best for the structural demand analysis.

For the objectives requiring the use of each set's average, i.e., $\overline{\mathrm{EDP}}^{\mathrm{set}}$; the modified GMs (i.e., MB, MC, and MD) can result in considerable but uncritical differences of the roof displacements (Δtop), the interstory drift ratios (IDR), and the global damage indices (DI) in comparison with the benchmark (i.e., MA). They can result in important overpredictions in the base shear forces (Vbase).

For the objectives requiring the use of each set's average-plus-some-standard deviation, i.e.,$(\overline{\mathrm{EDP}} + 0.95\sigma_{\mathrm{EDP}})^{\mathrm{set}}$, the modified GMs do not impose same increase as the benchmark upon their capability of conserving the GM variability (the ranking of increase is Benchmark, MA > MC ≈ MB > MD). Thus, the modified GMs can result in critical underpredictions in PSAs at f0, Δtop, IDR, and DI; but insignificant differences in Vbase relative to the benchmark.

The previous conclusions are valid for the symmetric tolerances. For the asymmetric tolerances, the modifed GMs (i.e., MB and MC) are not able to replicate same level of the increase (i.e., the conservatism) in the EDPs relative to the benchmark (i.e,. MA). Thus, the underpredictions are emphasized and the overpredictions become less critical relative to the symmetric tolerances.

The simple structural models (i.e., the single-degree-of-freedom oscillators) tend to reveal more critical underpredictions relative to the complex structural models for the same observations. It may explain some different conclusions by the previous studies which are solely based either on the simple structural models or on the complex structural models (e.g., the non-converging conclusions on the spectrum matching based on the single-degree-of-freedom models [Huang et al., 2011] and the reinforced concrete models [Heo et al., 2011]).

This study concluded that the modified GMs predict the means of all-set-EDP distribution in the close vicinity of the benchmark if (1) the GM selection and modification is symmetrically performed around the target spectrum and (2) the chosen intraset approach (of the EDPs) is the average. Otherwise, the modified GMs can significantly underpredict the final EDPs.

This study demonstrated that the unscaled earthquake records cause non-damaging to damaging structural responses; the modified GMs (i.e., MB, MC, and MD) also introduce a wide dispersion of the structural responses. The modified GMs are not able to capture the 16^{th} and 84^{th} percentiles from the all-set-EDP distribution (the ranking of representing such percentiles is roughly as Benchmark, MA > MC ≈ MB > MD). Therefore, the modified GMs may not be suitable for the variability studies. The modified GMs keeping spectral variability (such as the loosely spectrum matching without PGA scaling and the linear amplitude scaling at two points in Section 2.8) can be favored.

Our results can be criticized due to the double-counting of the GM variability as the intraset and the interset variability are considered simultaneously. One may support the sufficiency of using either interset or intraset variability. To illustrate, a single set with the intraset approach of each set's average-plus-some-standard deviation may cover the upper portion of the all set distribution with the intraset approach of each set's average (e.g., more than the 84^{th} percentile in Figure 3.3.2 in Section 3.3.1).

On the other hand, one may defend that it is not a double-counting since the spectral variability is introduced symmetrically to collect eligible sets (except the asymmetric tolerances). The intraset approach can then be considered as the final objective (e.g., as we considered in this thesis) based on the project requirement or the choice of an engineer. There will be many 'virtual' engineers (i.e., the sets) reporting a wide range of structural responses regardless of which intraset approach is used. The discussion on the double-counting of GM variability is an open debate.

Overall, our results can have strong implications for the seismic regulatory codes (e.g., Eurocode 8, 2004; ASCE/SEI 41-06, 2007; AASHTO LRFD, 2010; ASCE/SEI 7, 2010) and particulary for the French nuclear safety guide (ASN/2/01, 2006), which allows a single set with the asymmetric tolerances and the each set's average-plus-some-standard deviation.

The motivation of such criteria in ASN/2/01 is not explicitly stated. Assuming that ASN/2/01 suggests them as a shortcut to cover the 'implicit' uncertainties and natural variability, the modified GMs can result in critical underpredictions (of the EDPs) relative to the benchmark (i.e., MA). The guide may also involuntarily motivate the use of the modified GMs revealing less structural responses instead of the unscaled earthquake records.

At this point, the seismic regulatory guides (as well as the engineers' choice) need to be more transparent on the implicit assumptions behind the use of a single set, the asymmetric tolerances and the intraset approach along with the acceptable level of the minimum input GM variability.

The conclusions about the importance of the GM and set variability are valid for the deterministic SHA and can have some implications for the probabilistic SHA (PSHA). A wide range of earthquake-related parameters is integrated in the framework of the PSHA. After deriving the controlling earthquake scenario(s) by the deaggregation, the target spectra can include some standard deviation, i.e., epsilon, above the median. Indeed, the GM variability is not kept for the uniform hazard spectrum (e.g., Abrahamson et al., 2004) by applying spectrum matching as the GM variability is assumed to be considered in the process. Another study showed the importance of keeping the GM variability for the condional spectrum (Seifried and Baker, 2016). Our conclusions can partially contribute to the open debate in the PSHA.

4.2 Discussion on Engineering Demand Parameter, Objective, and Structure Specific Ground Motion Selection

In the current practice, the spectral shape is utilized to select and modify the GMs regardless of the engineering demand parameters (EDPs), the structural models, and the objective of the seismic analysis. In fact, our conclusions were in contrary to this approach. Our results can imply that the all-set-EDP distribution (specific to the structure and the objective) needs to be inspected prior to the GM selection. However, it may not be possible to obtain it since the nonlinear dynamic analyses can be costly and time-consuming as a function of the complexity of a structural model.

The question on how to select and modify the GMs by integrating the variability (i.e., due to the interset variability, the intraset approach, and the choice of a GMPE) and respecting the budget and time constraints can add new perspectives in the deterministic SHA. A five-step (from a to e) strategy is tested in this subsection with about 60 unscaled earthquake records on the S5 model (i.e., 1-story RC model) for two EDPs (i.e., story drift and base shear forces).

In step (a), the complex structural models are simplified as opposed to simplifying the seismic loading (e.g., selecting a set of 5 GMs with response spectrum compatibility, and modifying GMs to reduce spectral variability). The spectrum compatible selection is performed with the unscaled earthquake records to collect all GM sets in step (b). The logic tree approach is employed in step (c) to integrate the GMPE-based variability. Based on the EDP distribution's level (such as, median, mean, and 84th percentile), the GMs close to the 'damaging' level are selected based on the EDP distribution of the simplified model in step (d). The selected GMs are then applied to the complex structural model to have accurate responses in step (e).

(a) Dynamic Analyses with Simplified Structural Model

The simplification is done with the equivalent single-degree-of-freedom (eSDOF) model and the pushover curve of the S5 model (i.e., 1-story RC model) as shown in Figure 4.2.1. The story drifts are overestimated by the simplified model, and the base shear forces (Vbase) are found comparable.

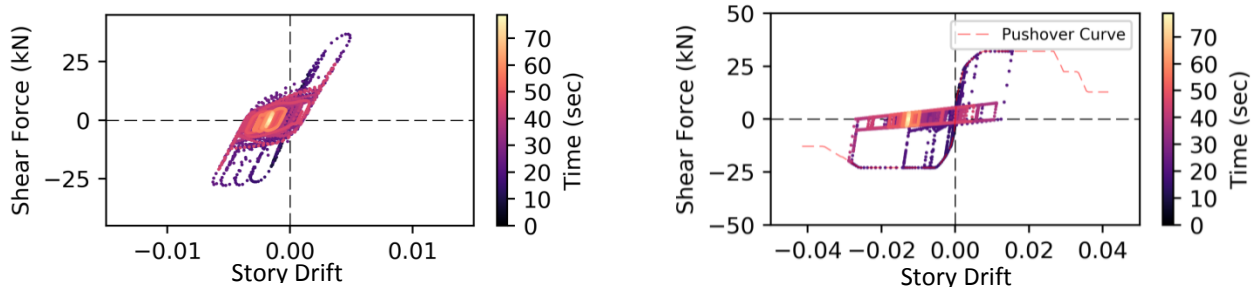

(a) S5: 1-Story R/c Model (3D Model) (b) eSDOF of S5 with pushover curve

Figure 4.2.1**: **Response histories of the S5 model and its simplified model (eSDOF). The x-axis represents the lateral displacements relative to the ground (Δtop). The y-axis is the base shear forces (Vbase). The color of the curve relates to the period of time given in the legend: the darker colors represent the initial part, and the lighter colors represent the final part. The sign represents the direction of the movement. The unscaled record is from the Duzce earthquake (3104 station). The structural model (described in Section 2.4.2) has a natural frequency of 5.68 Hz.

(b) Spectrum Compatible Selection with GMPEs

The spectrum compatible GM selection is performed by permitting large spectral variability to obtain all GM sets with the unscaled EQ records (in Section 1.3) obtained for the scenario of M7.0R40, Vs450, and normal fault. The spectrum compatible GM selection is repeated seven times for each GMPE (in Section 1.4). All eligible GM sets (about 100 000 sets for each GMPE) are collected to obtain the recurrence frequencies of the GMs (i.e., how many times the GMs repeat as explained in Section 1.11.2). It constitutes the effect of the interset variability.

The nonlinear dynamic analyses are then performed to obtain the distribution of the story drifts and base shear forces (Vbase) according to the recurrence frequencies of the GMs. Using different GMPEs do not imply more nonlinear dynamic analyses (in the unscaled earthquake records) but imply different distributions.

(c) Logic Tree Approach to Account for GMPE-based Variability

The recurrence frequencies of the GMs are weighed by the logic tree approach to integrate the effect of the GMPE-based variability. The weights of GMPEs are 3/14 for AB2014, 1/14 for AK2014, 1/14 for BA2011, 1/14 for BD2014, 2/14 for BT2003, 3/14 for CB2014, and 3/14 for CY2014 (i.e., Option 4 in Section 3.4.6).

The integration of set distributions can be considered as a single set that consists of about 60 GMs. Each GM has different contribution to the final EDP. The recurrence percentages of the GMs cover the interset variability and the GMPE-based variability of the final story drifts in Figure 4.2.2.a and the final Vbase in Figure 4.2.2.b

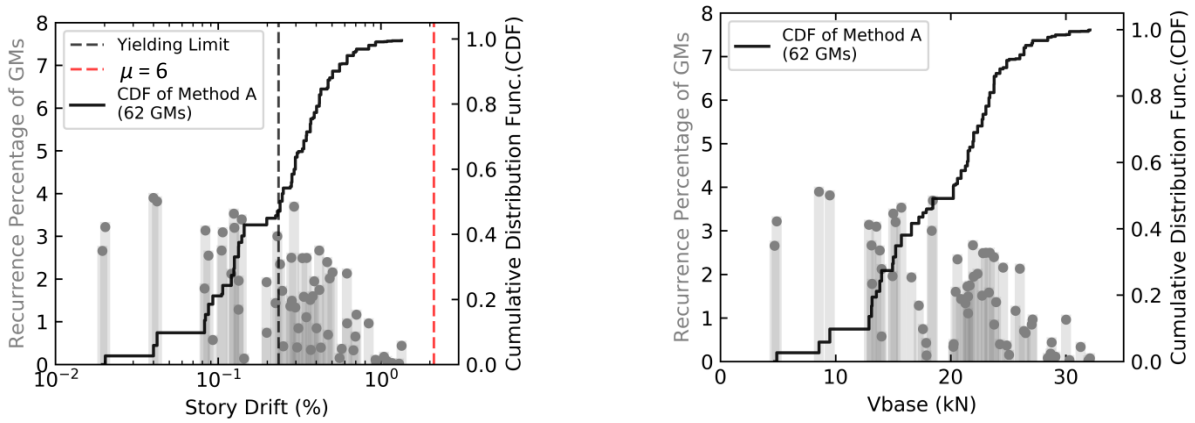

(a) Recurrence Percentages of Story Drift Responses (b) Recurrence Percentages of Base Shear Forces (Vbase)

Figure 4.2.2: Recurrence percentages of GMs and cumulative distribution functions (CDF) for story drift and base shear forces (Vbase) of the e-SDOF of S5 model. The spectrum compatible selection is made with the upper and lower amplitude tolerances are -30% and +30% of the targets for unscaled earthquake records (Methods A). The targets are obtained for the scenario of M7.0R40, Vs450, and normal fault as explained in Section 1.4. Each set includes five ground motions, and the frequency range is between 0.50 Hz and 20.0 Hz. The frequencies of each GM repeating among all GM sets are collected. The spectrum compatible GM selection is repeated seven times for each GMPE. The recurrence frequencies are weighted according to the GMPE with Option 4 in Section 3.4.6.

The x-axis represents the story drift on the left figure and Vbase from each GM on the right figure. Along the left-side y-axis, the recurrence percentages of GMs are shown. The vertical grey bars are related to the left-side y-axis. Along the right-side y-axis, cumulative distribution function (CDF) is shown. CDF is the summation of recurrence frequencies. The yielding and sing limits of the S5 model is shown with the vertical black dashed lines and the vertical red dashed lines, respectively. The amount of GMs is noted in the legend box.

(d) Selection of Fewer GMs Specific to the EDP and the Objective

Based on the objective and the EDP, the GMs close to the distribution's level (such as, median, mean, and 84th percentile) can be identified. From the distribution of the sets and the logic tree approach, the following responses are obtained from the eSDOF model:

- The mean of all $\overline{\text{StoryDrift}}^{\text{set}}$ is 0.26%,
- The mean of all $(\overline{\text{StoryDrift}} + 0.95\sigma_{\text{StoryDrift}})^{\text{set}}$ is 0.45%,
- The mean of all $\overline{\text{Vbase}}^{\text{set}}$ is 17.9 kN, and
- The mean of all $(\overline{\text{Vbase}} + 0.95\sigma_{\text{Vbase}})^{\text{set}}$ is 23.9 kN.

Six GMs in the vicinity of each objective and EDP are identified from Figure 4.2.2. They are noted for their recurrence frequencies, Ri, in Tables 4.2.1, 4.2.2, 4.2.3, and 4.2.4. The identified GMs constitute about 10% of the whole distribution. They are different for each objective and each EDP.

(e) Dynamic Analyses with Complex Structural Model

The identified GMs are then applied to the complex structural model. They are then multiplied by the normalized recurrence frequencies, Ri_{norm}. The details of the proposed method are given in Tables 4.2.1, 4.2.2, 4.2.3, and 4.2.4. The GMs with small Ri (i.e., Ri_{norm} <5%) could have been replaced with the GMs with larger Ri.

Table 4.2.1: Selection of 6 GMs in the proximity of mean of all $\overline{StoryDrift}^{set}$.

GM Label	Ri	Ri_{norm}	eSDOF Model		3D Model	
yyyymmdd_hhss_station_comp	Recurrence Percentage	Ri/ ΣRi	Story Drift (%)	Ri_{norm} x Story Drift	Story Drift (%)	Ri_{norm} x Story Drift
19801123_1834_RNR_h2	3.0%	26.4%	0.23	0.06	0.25	0.07
19971118_1307_ZAK1_h2	2.3%	20.7%	0.24	0.05	0.32	0.07
19891710_1704__57383__Chan02_0	1.7%	15.2%	0.25	0.04	0.26	0.04
19830117_1241_ARG1_h1	0.4%	3.7%	0.25	0.01	0.27	0.01
19801123_1834_BRN_h2	1.4%	12.0%	0.28	0.03	0.47	0.06
19971118_1307_ZAK1_h1	2.5%	22.0%	0.28	0.06	0.21	0.05
Σ	**11.4%**	**100.0%**	**Σ**	**0.25%**	**Σ**	**0.28%**

Table 4.2.2: Selection of 6 GMs in the proximity of mean of all $(\overline{StoryDrift} + 0.95\sigma_{StoryDrift})^{set}$.

GM Label	Ri	Ri_{norm}	eSDOF Model		3D Model	
yyyymmdd_hhss_station_comp	Recurrence Percentage	Ri/ ΣRi	Story Drift (%)	Ri_{norm} x Story Drift	Story Drift (%)	Ri_{norm} x Story Drift
19891710_1704__57217__Chan02_195	1.7%	18.5%	0.42	0.08	0.27	0.05
19891710_1704__57383__Chan00_90	0.4%	4.2%	0.43	0.02	0.60	0.03
19891710_1704__22561__Chan02_360	2.4%	25.5%	0.47	0.12	0.31	0.08
20061510_0707__02810__Chan01_360	0.7%	7.4%	0.47	0.04	0.47	0.03
20111023_1041_6502_h2	2.0%	21.4%	0.48	0.10	0.16	0.03
19991112_165721.4100_9902_h2	2.2%	22.9%	0.50	0.12	0.51	0.12
Σ	**9.4%**	**100.0%**	Σ	**0.47%**	Σ	**0.34%**

Table 4.2.3: Selection of 6 GMs in the proximity of mean of all $\overline{\mathrm{Vbase}}^{set}$.

GM Label	Ri	Ri_{norm}	eSDOF Model		3D Model	
yyyymmdd_hhss_station_comp	Recurrence Percentage	Ri/ ΣRi	Vbase (kN)	Ri_{norm} x Vbase (kN)	Vbase (kN)	Ri_{norm} x Vbase (kN)
19891710_1704__57191__Chan02_0	1.3%	13.8%	17.2	2.4	22.5	3.1
19831030_0412_2503_h1	0.7%	8.0%	17.6	1.4	25.4	2.0
19830117_1241_ARG1_h1	0.4%	4.6%	17.9	0.8	27.6	1.3
19831030_0412_2503_h2	0.1%	1.5%	17.9	0.3	31.2	0.5
19801123_1834_RNR_h2	3.0%	32.3%	18.3	5.9	27.0	8.7
19991112_165721.4100_9907_h2	3.7%	39.8%	18.4	7.3	25.1	10.0
Σ	**9.3%**	**100.0%**	**Σ**	**18.1**	**Σ**	**25.6**

Table 4.2.4: Selection of 6 GMs in the proximity of mean of all $(\overline{Vbase} + 0.95\sigma_{Vbase})^{set}$.

GM Label	Ri	Ri_{norm}	eSDOF Model		3D Model	
yyyymmdd_hhss_station_comp	Recurrence Percentage	Ri/ ΣRi	Vbase (kN)	Ri_{norm} x Vbase (kN)	Vbase (kN)	Ri_{norm} x Vbase (kN)
19801123_1834_RNR_h1	1.5%	11.7%	22.7	2.6	27.8	3.2
19991112_165721.4100_9906_h2	2.5%	19.2%	22.8	4.4	25.8	5.0
19971118_1307_ZAK1_h1	2.5%	19.2%	23.0	4.4	23.9	4.6
19991112_165721.4100_9904_h2	1.6%	12.2%	23.3	2.8	28.4	3.5
19991112_165721.4100_9904_h1	2.5%	19.2%	23.4	4.5	32.2	6.2
19891710_1704__22561__Chan02_360	2.4%	18.5%	23.7	4.4	27.5	5.1
Σ	**13.0%**	**100.0%**	**Σ**	**23.2**	**Σ**	**27.5**

Table 4.2.5 shows the summary of the proposed GM selection method specific to the EDP, objective, and structure. The nonlinear dynamic analyses are performed with Cast3M v15 (CEA, 2015) in serial over 12 CPU cores (Intel Xeon(R) E5-2667) with the memory of 128GB RAM.

The first approach shows the approach of the eSDOF model. The nonlinear dynamic analyses last about 0.4 days. The second approach is the proposed method, and the nonlinear dynamic analyses take about 3.4 days (for each EDP and each objective). The third approach demonstrates the results of the 3D model. It lasts about 36.5 days.

The eSDOF approach gives the fastest results by overestimating the story drifts and underestimating Vbase. The proposed method reveals relatively fast solutions in the vicinity of the results obtained by the 3D model.

Table 4.2.5: Summary of proposed method specific to the EDP, objective, and structure

Approach	Approx. Duration (days)	$\overline{\text{StoryDrift}}^{\text{set}}$ (%)	$(\overline{StoryDrift} + 0.95\sigma_{StoryDrift})^{set}$ (%)	$\overline{\text{Vbase}}^{set}$ (kN)	$(\overline{Vbase} + 0.95\sigma_{Vbase})^{set}$ (kN)
(1) eSDOF Model	0.4	0.26	0.45	17.9	23.9
(2) eSDOF and 3D Models	**3.4**	**0.28**	**0.34**	**25.5**	**27.6**
(3) 3D Model	36.5	0.22	0.35	23.9	28.9

One of the drawbacks of using a pushover curve in the eSDOF is that the structural responses obtained from eSDOF and 3D reveal different rankings of the EDPs (i.e., how large an EDP is obtained from one GM relative to another GM in Tables 4.2.1, 4.2.2, 4.2.3, and 4.2.4). This trend can be improved with a material behavior including pinching effect, the in-cycle stiffness losses, the strength degradation, etc. (e.g., FEMA, 2009).

In this example, the tests are limited to the unscaled earthquake records, the earthquake scenario, and an eSDOF model representing the 1-story RC model without considering the higher modes. The use of the eSDOF may not be practical for the structures with higher mode effects, the local EDPs (such as element forces and displacements), and the structures with the fragile equipment.

All in all, the EDP distribution can be obtained by the simplified structural model. The ground motions can be selected based on the 'damaging' level of interest (specific to the engineering demand parameter, the objective, and the structure). This approach is more in line with the thesis' findings than the usual approach of simplifying the input seismic loading.

4.3 Limitations and Future Work

The conclusions herein can have some limitations, such as, the limited earthquake scenario, the engineering demand parameters (EDPs), and the structures. The future studies can be necessary to validate some conclusions.

The magnitude-distance of M7.0R40 was considered since it retrieves sufficient unscaled earthquake records. The ground motion selection and modification (GMSM) methods were utilized to apply modifications to the same magnitude-distance bin with the earthquake scenario. It can be practical to test the credibility of using unlike magnitude-distance bin (in the GM modifications) especially for the near-fault events which are scarce in the database.

The structural models were single-mode dominated fixed base systems with a natural frequency ranging from 0.6 Hz to 5.7 Hz. The complex models comprised the moment frame reinforced concrete (RC) models and the masonry model. Different lateral load resisting systems, such as the braced frames, the shear walls, and the dual systems, and different structural materials, such as the steel, the prestressed concrete, the high-performance concrete, and the hybrid materials, can also be studied. The structural models with higher mode effects as well as the soil structure interaction can be tested.

In this study, the engineering demand parameters (base shear force, roof displacement, interstory drift ratio, and global damage index) were related to the global behavior of a structure. The effects of the GMSM methods on the local structural members (i.e., regarding the tensional and compressional demands), the connections, the fragile equipment, and the residual structural responses can also be of high importance. The ductility demands (of the complex models) under the given earthquake scenario were between 1.0 and 3.0. The earthquake scenarios requiring larger demands can also be studied.

Data points in a GM (i.e., the sampling time and the duration) are one of the factors specifying the total duration of the nonlinear dynamic analyses. The consequences of removing a portion of the accelerometric data can be researched for the seismic demand analysis.

Typically, a single ground motion prediction equation (GMPE) is used in the deterministic seismic hazard assessment (SHA), but the impact of the GMPEs on the structural responses were emphasized to be significant. A suitable way (such as a logic tree approach in Section 4.2) to integrate the GMPE-based variability can be further evaluated. The question on how to represent the GM variability in the target spectrum (i.e., the use of a median-plus-standard-deviation spectrum) can be discussed.

The stochastic methods are also common and can be the subject of a future study. The studies evaluating the multi-component GM selection and modification methods can be of high importance.

The eccentricity (of the PSA levels) between the GM modification and selection was discussed to be one of the likely reasons for the poor predictions by the GMSM methods. The question on how to imitate the eccentricity to improve the predictions by the GMSM methods can also be studied. The alternative GMSM methods that keep the observed spectral shape and its variability (such as the loosely spectrum matching and linear amplitude-scaling at two points) can be researched further.

The future studies can further focus on a GM selection method (such as the approach in Section 4.2) that is specific to the engineering demand parameter, the objective of the seismic analysis, and the structure.

This page is intentionally left blank.

APPENDIX A

ADDITIONAL ELEMENTS FOR PART 1

A.1 Collection of Databases

EQ records from two strong-motion databases are compiled together in a new database called as Collection of Databases. One of the databases in Collection of Databases is Resorce (Reference database for Seismic grOund-motion pRediction in Europe) 2013, which was developed for the EDF Sigma Project (Akkar et al., 2014). It includes the EQ records from Pan-European region. Due to the fact that Resorce 2013 does not include strong GMs of other regions such as California and New Zealand, the GM records from CESMD (Center for Engineering Strong Motion Data) (Haddadi et al., 2012) were included in Collection of Databases. In the case of common earthquake records in both databases, records from Resorce 2013 are taken into account. Records from Resorce 2013 are not raw GMs but processed GMs. A careful inspection is recommended especially for the records retrieved from Resorce 2013 due to the observed oddities. CESMD records are raw GMs. Figure 2.1 shows the distribution of hypocentral distances (km) versus moment magnitudes of 35 997 GM records in Collection of Databases. EQ records with moment magnitude smaller than M_w of 4 belong to Resorce 2013.

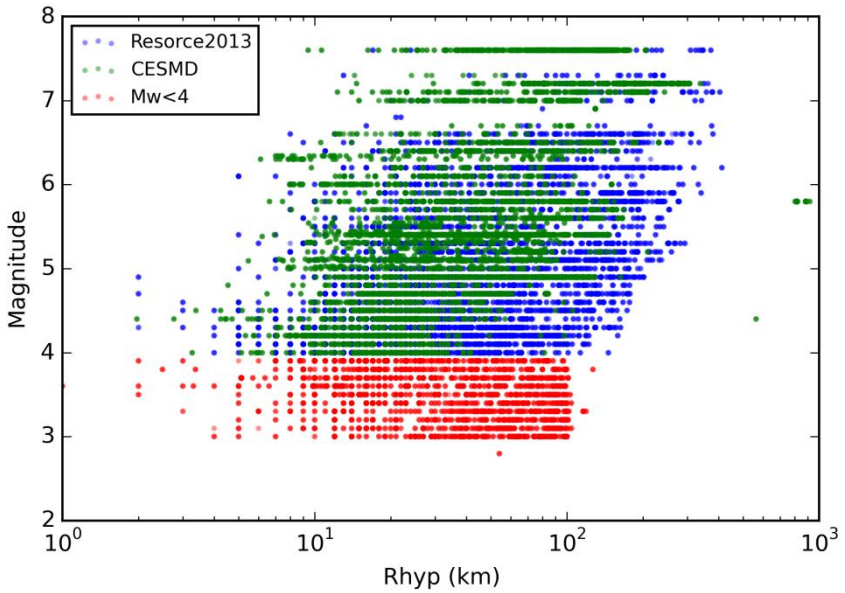

Figure A.1.1: Collection of Databases

Figure A.1.2 shows the country distribution of EQ records in Collection of Databases. Data of pan-European regions are obtained from Resorce 2013, and the rest are collected from CESMD. It also separates the records based on the level of peak ground acceleration (PGA) in order to provide an insight into the amount of 'strong' EQ records in Collection of Databases. Italian, Turkish, and Greek EQ records contribute the most to the amount of EQ records having a PGA larger than 0.20g in Resorce 2013. CESMD records enormously contribute to the total amount of EQ records having a PGA larger than 0.20g.

The metadata for Resorce 2013 and ORFEUS (Luzi et al., 2016) exhibits some differences in the soil conditions of some seismic stations. The soil conditions of ORFEUS are used. Sturno (STR) is updated from 1122 to 382 m/s, Brienza (BRN) is updated from 506 to 403 m/s, Auletta (ALT) is updated from 1122 to 1018 m/s, and the station in Abbar, Iran (ID 6211) is updated from 723 to 621 m/s.

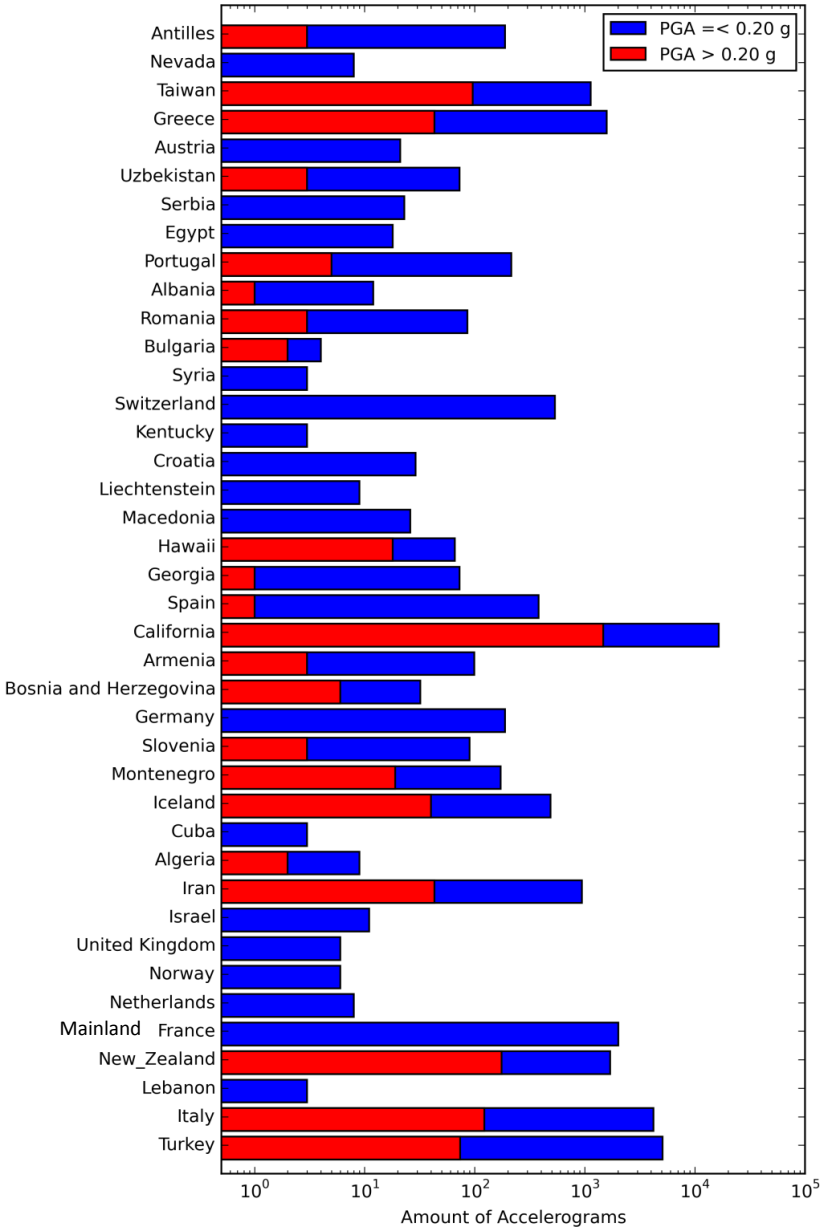

Figure A.1.2: Country and state distribution of records in Collection of Databases

A.2 Signal Processing

A.2.1 Signal Processing in this Study

Errors due to noise and baseline offset are corrected in this study by applying a combination of filtering and baseline removal. Figure A.2.1 shows the algorithm used to perform signal processing. It includes a visual inspection of time histories both over time and frequency domains and iterations of parameters to minimize the loss of accelerometric data. A raw EQ record is used as an input along with various parameters such as:

- The starting and ending time points for performing time windowing
- The ratio of tapering for smoothing both ends in the time domain
- The length of padding with zero in seconds
- The cutoff frequencies for Butterworth bandpass filtering (f_{min} and f_{max})

Time windowing allows analyzing a smaller subset of accelerometric data rather than including extensive pre- and post-event accelerometric data around main strong motion. Windowing is very favorable to reduce the total calculation time of nonlinear structural analysis utilizing time-step approach. It is performed manually by specifying the time of signal cut and automatically by noise threshold check. Tapering with cosine function is used to ensure time histories smoothly approaching to zero at its ends. Padding acceleration time history with zero is found to be useful as a pre-process for detrending and filtering. Detrending subtracts an offset (i.e., removes the trend) from raw signal and is the function correcting baseline offset. Detrending is applied over acceleration, velocity, and displacement time histories. Then, the casual Butterworth bandpass filtering is used with corner frequencies (f_{min} and f_{max}) to eliminate low and high-frequency noises. It is applied to acceleration, velocity, and displacement time histories.

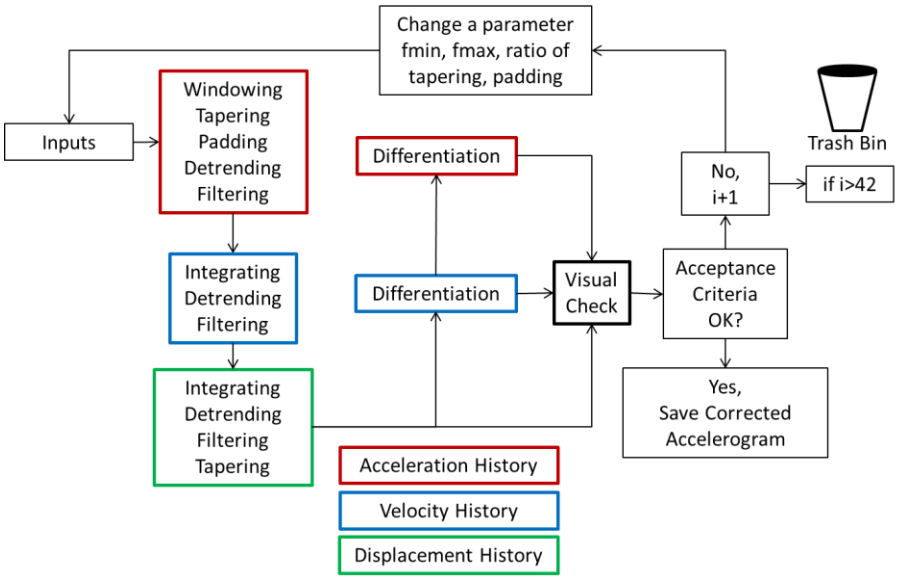

Figure A.2.1: Algorithm used for signal processing

Table A.2.1 shows the parameters used in signal processing. Parameters yield 6 options without filtering and 36 options with filtering. For each record, parameter combinations are iterated up to 42 times, which is the total of options with and without filtering (the exceptional parameters pointed with stars are not counted). The parameters are given in the same order of trial-error application. The frequency interval of our interest is between 0.5 and 20.0 Hz; therefore, the cutoff frequencies are chosen as large as possible outside this interval. Low-frequency cutoff, f_{min}, is selected with respect to the seismological theory which states that the Fourier amplitude spectrum, FAS, of acceleration decays according to f^2 at low frequencies. Accordingly, the allowed f_{min} values for the case of M_w 7.0 are less than the allowed f_{min} values for the case of M_w 5.5. High-frequency cutoff values are chosen out of the frequency of interest and are

further tweaked to find the precise frequency. Later, the records are visually inspected whether the errors due to baseline offset and noise are corrected or not. The raw records that cannot be corrected are removed.

Table A.2.1: Parameters used in signal processing

Case	Noise threshold windowing	Ratio of Tapering	Padding with zero (sec)	Butterworth Bandpass Filter		
				f_{min} (Hz)	f_{max} (Hz)	# of poles
M7.0 R40	0.1 cm/s^2	0.05, 0.10	0, 3, 5	0.05, 0.10, 0.15*	50.0, 40.0, 25.0	2

*Parameters are applied for few records.

A.2.2 Some Issues Observed in Earthquake Records

In this subsection, the issues observed in some GMs are discussed. Following the inspection of earthquake records, four records such as (i) the horizontal components of Duzce Earthquake (Turkey, 19991112_1657) recorded by the station 1406 and (ii) horizontal components of Spitak Earthquake (Armenia, 19881207_0741) recorded by the station 173 are found susceptible. The GMs in (i) are susceptible to insufficient pre-main event accelerometric data before the main strong motion as discussed in Figures A.2.2 and A.2.3. The GMs in (ii) are not possible to be fixed the errors for the baseline offset in displacement time-history as shown in Figure A.2.4.

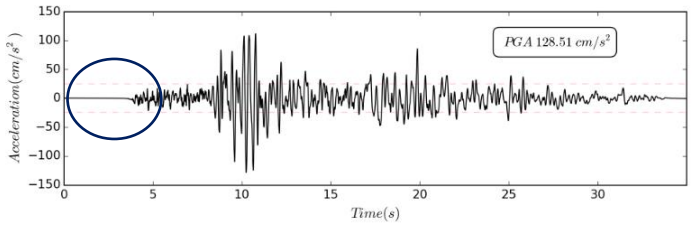

(a) Record in station no 9906

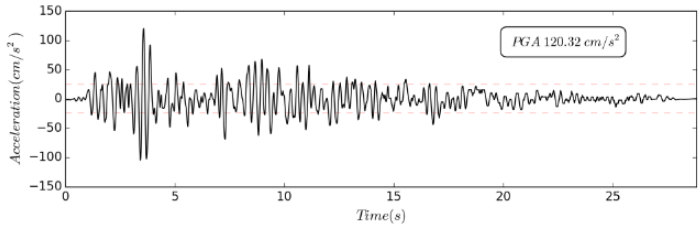

(b) Record in station no 1406

Observations:

Two records from the Duzce Earthquake (Turkey, 19991112_1657) are shown. The event recorded by station no 9906 has pre-main event accelerometric data. The starting point of the main event can be observed in the upper figure. However, the time-history of station no 1406 causes ambiguity to locate the start of the main event. There is a possibility that the record of station no 1406 is missing a part of the accelerometric data which can be necessary for the GM selection and structural responses.

Figure A.2.2: GM susceptible to insufficient accelerometric data before P-wave arrival.

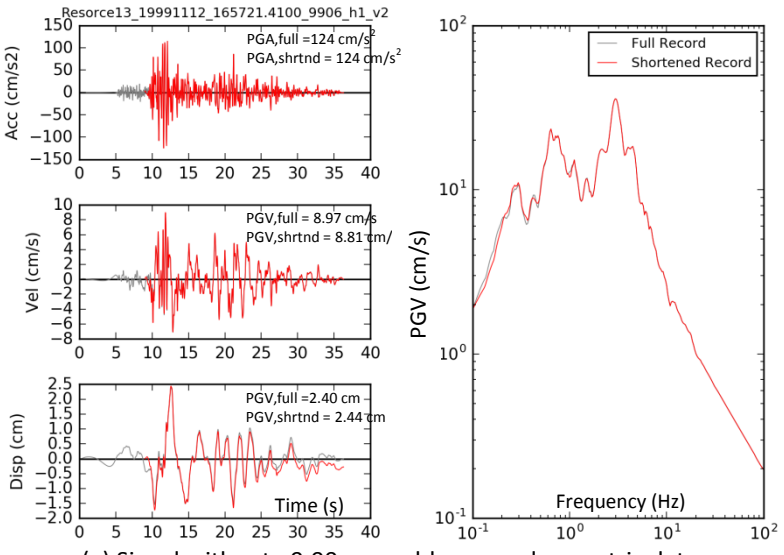

(a) Signal without +9.00 second-long accelerometric data

In order to understand the effect of missing pre-event accelerometric data, two cases are assumed with a missing part of data at their start. In Case a, it is assumed that the part of GM is available after +9.00 seconds. In the second case, it is assumed that the GM is available after +10.55 seconds. Each case is then manually processed. They are also compared to the complete GM.

Observations:

(i) Peak ground accelerations (PGA), velocities (PGV), and displacements (PGD) are mostly changed: more significantly in Case b.

(Cont'd)

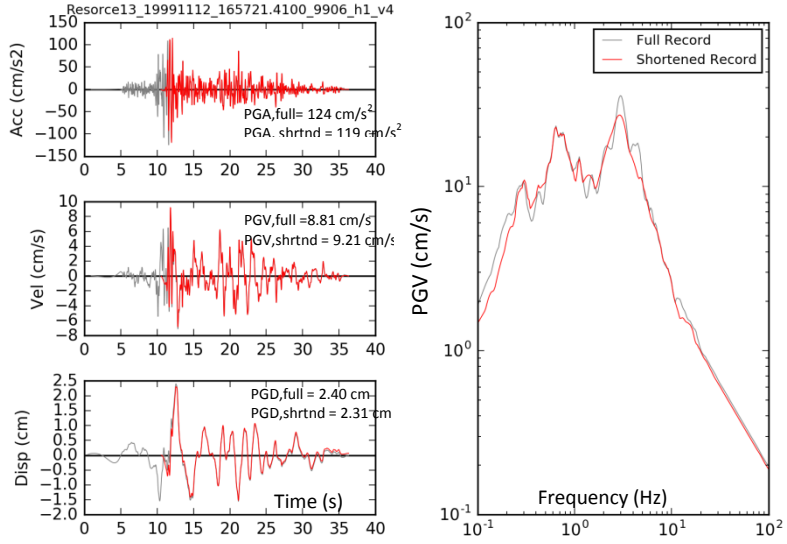

(b) Signal without +10.55 second-long accelerometric data

(Cont'd)
(ii) Shortened signals had an effect on response spectra. In Case a, the low-frequency PSA values are affected. In Case b, full spectral shape is affected.

Conclusion:
The loss of pre-main event accelerometric data before the main event can impact the response spectrum based on the length of data loss. It is not easy to detect the length of accelerometric loss in the EQ records. Therefore, GMs suspected of accelerometric data loss are removed.

Figure A.2.3: Effect of pre-event accelerometric data on spectral velocities and intensity measures.

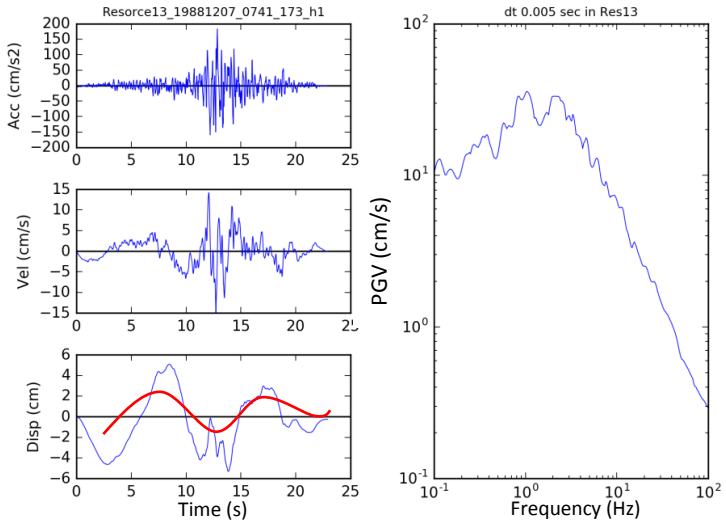

Observations:

The given record is processed with the allowed parameters outside the frequencies of our interest (i.e., 0.5 Hz to 20.0 Hz), but it has baseline offset shown with a red curve in the displacement time history. The displacement time history evolves approximately around the red curve rather than the zero axis of displacement history. In structural analysis, it is important to remove the baseline offset in acceleration, velocity, and displacement time histories except for the near-source records; therefore, the record has been eliminated.

Figure A.2.4: GM having baseline offset which cannot be fixed for the permitted signal processing parameters

GMs are compared with the corresponding GMs in ORFEUS database. In the Iranian Earthquakes (19900620_2100 station 6211, and 20031226_0156 station 3599), the different sampling time is observed as shown in Figure A.2.5.

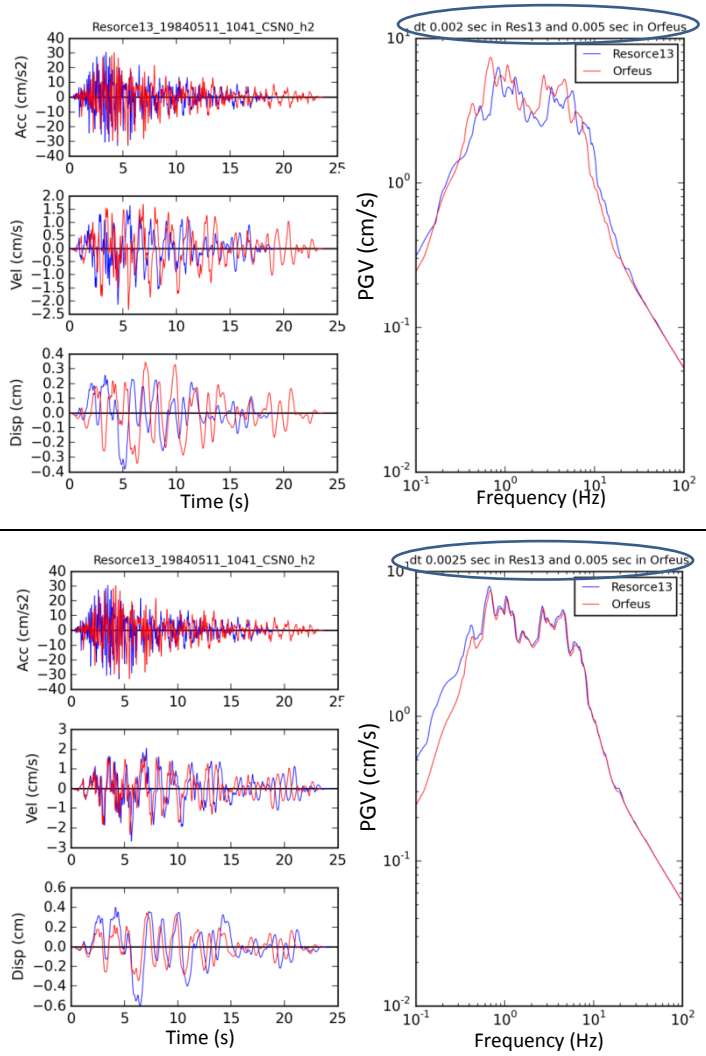

Observations:

The difference in spectra of the identical GMs is observed between Collection of Databases shown with the blue curve, and ORFEUS is shown with the red curve. In the upper graph, the original sampling time, 0.002 sec, is used from Collection of Databases.

In the lower figure, the sampling time of the record in Collection of Databases is changed to 0.0025 sec. The sampling time causes the shift in spectral shapes of the identical records. The spectral shapes do not precisely coincide due to the signal processing. In such cases, the records from ORFEUS are used.

Figure A.2.5: Examples of the GM with the difference in sampling time

In a comparison of the record in Collection of Databases and ORFEUS, the polarity of some records such as Pasinler Earthquake (Turkey, station 2503) is found dissimilar as illustrated in Figure A.2.6.

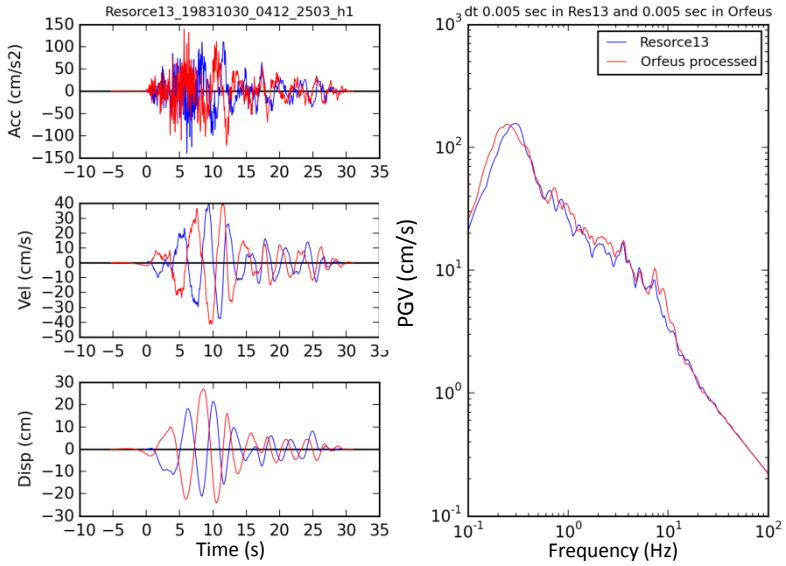

Observations:

The figures on the left compare the record in Collection of Databases and ORFEUS. The records have similar amplitudes and spectral shapes but their time histories have polarity issues. In such cases, the records from ORFEUS are used.

Figure A.2.6: Examples of the GMs with the difference in polarity

A.2.3 Examples of GM Signal Processing

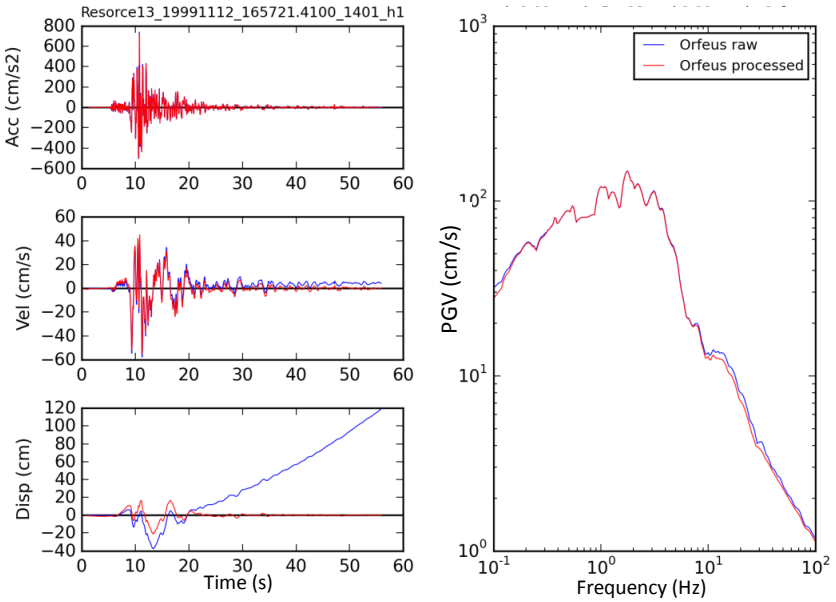

Observations (First Phase):
(i) Baseline offset exists in the velocity and displacement time histories
(ii) Linear baseline offset exists in the displacement history.
Signal Processing (Second Phase):
(i) The ratio of tapering is 0.05.
(ii) Butterworth bandpass filtering is applied with 0.05 and 45.0 Hz and two poles.
Conclusion:
Baseline offset and noises are removed, and the processed signal has passed the second phase.

Figure A.2.7: Time- and frequency-domain characteristics of the raw and processed record. The record is from the Duzce earthquake (station no 1401) with Mw 7.1, R_{hypo} 37 km and Vs30 294 m/s. Column (a) shows the acceleration, velocity, and displacement time-histories of the raw record in blue and the processed record in red. In column (b), the comparison of the spectral shapes is shown. In column (c), the signal processing is explained.

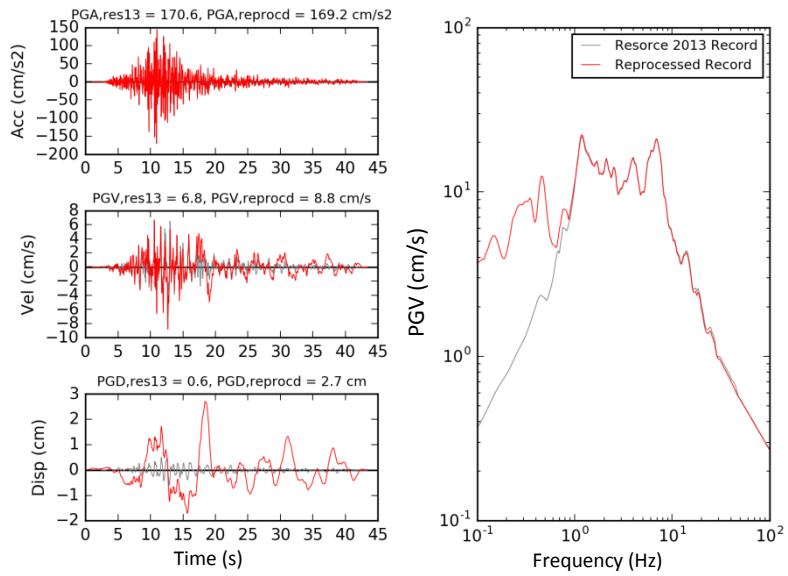

Comparison of Signal Processing:
(i) Signal processing of the record in Collection of Databases:
Removal of the leading and trailing zeros and Butterworth bandpass filtering between 0.60 and 50.0 Hz with n_{poles} of 4.

(ii) Signal processing used in this study:
Baseline correction in acceleration, velocity and displacement time histories and Butterworth bandpass filtering between 0.10 and 50.0 Hz with n_{poles} of 2.

Observations:
PGD and spectral velocities on low frequencies change significantly.

Figure A.2.8: Time- and frequency-domain characteristics of the differently processed records. The record is from the Kefallinia Island earthquake (station ARG1) with Mw 6.9, R_{hypo} 31 km and Vs30 437 m/s. Column (a) shows the acceleration, velocity, and displacement time-histories of the processed record in Collection of Databases in grey and the processed record in this study in red. In column (b), the comparison of the spectral shapes is shown. In column (c), the signal processing is explained.

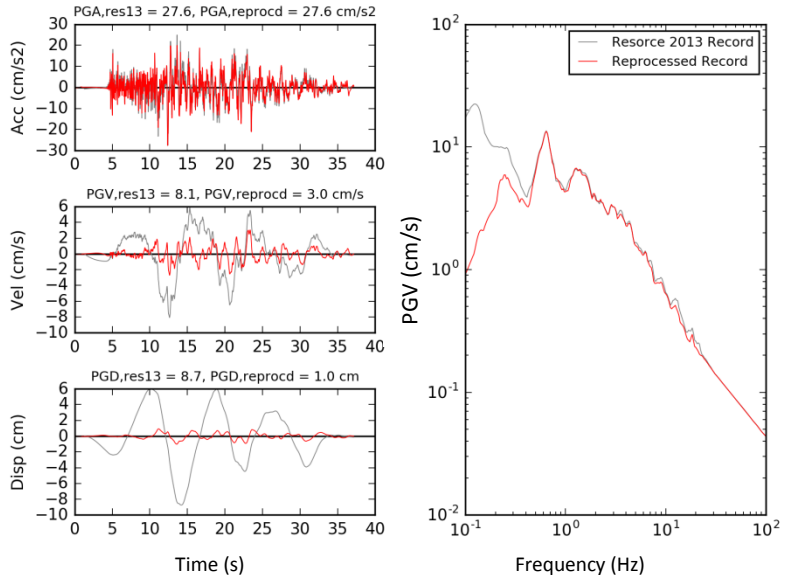

Comparison of Signal Processing:

(i) Signal processing of the record in Collection of Databases:
Removal of leading and trailing zeros and Butterworth low-pass filtering at 0.04 Hz and n_{poles} of 4.

(ii) Signal processing used in this study:
Baseline correction in acceleration, velocity and displacement time histories and Butterworth bandpass filtering between 0.15 and 45.0 Hz with n_{poles} of 2.

Conclusion:
PGD and spectra velocities on low frequency change significantly.

Figure A.2.9: Time- and frequency-domain characteristics of the differently processed records. The record is from the Duzce earthquake (station no 9900) with Mw 7.1, R_{hypo} 49 km and Vs30 455 m/s. Column (a) shows the acceleration, velocity, and displacement time-histories of the processed record in Collection of Databases in grey and the processed record in this study in red. In column (b), the comparison of the spectral shapes is shown. In column (c), the signal processing is explained.

A.2.4 List of GMs Passing the First and Second Phases

Table A.2.2: GMs passing the first phase or the second phase

(a) GMs Passing First Phase (i.e., readily available processed version is used as in the origin database)		**(b)** GMs Passing Second Phase (i.e., the signal processing in Section A.2.1 is applied)	
Database_yyyymmdd_hhmm_station_comp	**Nation**	Database_yyyymmdd_hhmm_station_comp	**Nation**
Resorce13_19801123_1834_ALT_h2.txt	Italy	Resorce13_19760517_0258_27_ h1 / h2	Uzbekistan
Resorce13_19991112_165721.4100_ 3102_ h1 / h2 3103_ h1 / h2 3104_ h1 / h2 9901_ h1 / h2 9904_ h1 / h2 9906_ h1 / h2 9907_ h1 / h2	Turkey	Resorce13_19801123_1834_ ALT_ h1 BRN_ h1 / h2 BSC_ h1 / h2 RNR_ h1 / h2 STR_ h1 / h2	Italy
		Resorce13_19830117_1241_ ARG1_ h1 / h2 2503_ h1 / h2	Greece
		Resorce13_19900620_2100_6211_ h1 / h2	Iran
Resorce13_20111023_1041_6502_ h1 / h2	Turkey	Resorce13_19971118_1307_ZAK1_ h1 / h2	Greece
		Resorce13_19991112_165721.4100 1401_ h1 / h2 9900_ h1 / h2 9902_ h1 / h2	Turkey
		Resorce13_20031226_0156_3599_ h1 / h2	Iran
		**All records from CESMD (44 of them)	

A.2.5 Effect of Different Signal Processing Approaches on Intensity Measures and Structural Responses

The signal processing approach can serve different purposes based on the project, which brings about the question of whether we should use the readily available processed records for the specific engineering applications. For example, Resorce 2013 is the database initiated mainly for the development of ground motion prediction equations, and the study herein aims at nonlinear dynamic analyses over a variety of structures with a frequency of interest between 0.50 Hz and 20.0 Hz. The methodology comparing the different signal processing approaches is sketched in Figure A.2.10. The impact on signal characteristics and structural responses are shown in Figure A.2.11. One of the most affected IMs is PGD and then PGV. The dispersion in IMs and structural responses is considerable, which is a source of uncertainty caused by signal processing. Therefore, the approach of signal processing should be characterized and/or justified based on the necessities of the engineering application to reduce such uncertainty.

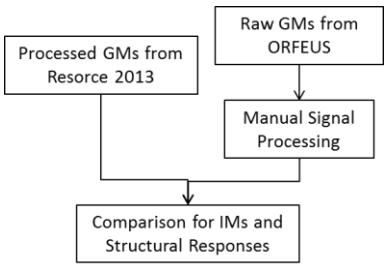

Figure A.2.10: Methodology

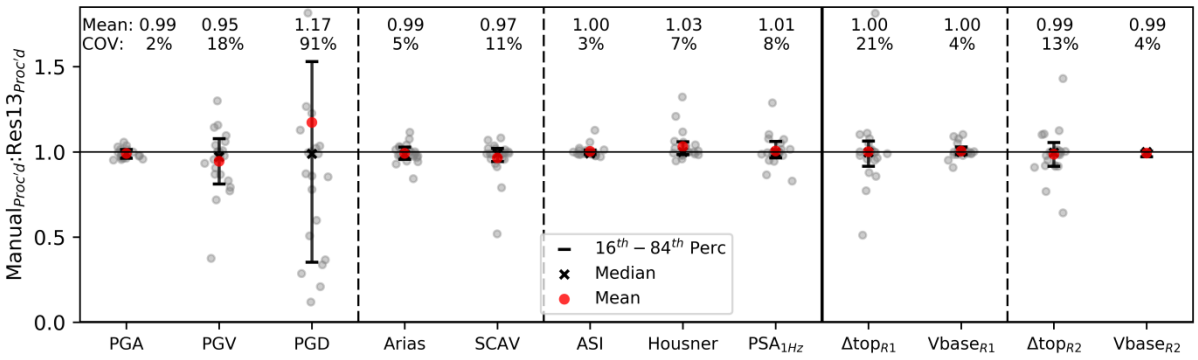

Figure A.2.11: Impact of different approaches of signal processing on signal characteristics and structural responses of the simple models. Each grey dot (23 of them) represents the ratio of value from the signal processing in this study and the processed record in Resorce 2013. Ratios lower than 1.0 signifies decrease with respect to the value from Resorce 2013 and vice-versa. Mean of the ratios is shown with the red circle. Median of the ratios is shown with the black cross marker. 16th and 84th percentiles are shown with the black horizontal bars. The mean and the coefficient of variation (COV) are noted for each value. The vertical lines categorize IMs and structural models. PGA, PGV, and PGD are amplitude-based IMs. Duration-based IMs are Arias and SCAV. Frequency-based IMs are ASI, Housner, and PSA at 1.00 Hz. Lateral displacements (Δtop) and base shear forces (Vbase) of SDOFs are shown for SDOF-R1 and SDOF-R2. I

A.3 Ground Motion Prediction Equations (GMPEs)

A.3.1 Parameters used in GMPEs

Table A.3.1: Equivalent input parameters assumed for GMPEs

(a) Rupture Properties

	Mag	Mag Type	Dip Angle the fault dip (deg)	Fault Type	Rake (deg)	Ztor (km) depth to top of rupture	W (km) down-dip rupture width	Zhypo hypocentral depth (km)
M7.0R40 Vs450 Normal Fault	7.0	Moment	50.0	Normal	-90.0	5.62	20.42	15.0

(b) Distance Properties (Azimuth = 90 deg)

Rhypo (km)	**Rjb (km)**	**FHW**	**Rx (km)**	**Rrup (km)**
source-to-hypocentral distance	*horizontal distance to the surface projection of the rupture*	*Hanging-wall flag*	*horizontal distance to the surface projection of the top edge of the rupture measured perpendicular to the fault strike*	*slant distance to the closest point on the rupture plane*
40.0	31.83	1	44.96	38.28

(c) Site Properties

Vs_{30} (m/s)	**Z1.0 (km)**		**Z2.5 (km)**	**Vs_{30} Measured?**
avg shear-wave velocity of top 30 m	*depth where Vs= 1.0 km/s*		*depth where Vs= 2.5 km/s*	
	AB2014	*CY2014*		
450	0.25	0.16	1.41	No

***Table A.3.2: Equivalent input parameters used for* (1) AB2014** (AbrahamsonEtAl2014)

EQ Scenario	**Mag**	**Mag Type**	**Dist (km)**	**Dist Type**	**Dist 2= Rrup**	**Dist 3= Rx**	**Dist 4= Ry0**
mag7.0_dist40_Vs450	7.0	Moment	31.83	Rjb	38.28	44.96	0.00

Fault Type	**DIP_Angle**	**Ztor**	**Z2.5 (m)**	**W (km)**	**Vs_{30} Meas?**	**Vs_{30} (m/s)**	**Z1.0 (km)**
Normal-F	50.0	5.62	1 410	20.42	No	450	0.25

***Table A.3.3: Equivalent input parameters used for* (2) AK2014** (AkkarEtAlRhyp2014)

EQ Scenario	**Mag**	**Mag Type**	**Dist (km)**	**Dist Type**	**Vs_{30} (m/s)**	**Fault Type**
mag7.0_dist40_Vs450	7.0	Moment	40.0	R_{hypo}	450	Normal-F

***Table A.3.4: Equivalent input parameters used for (3)* BA2008/11** (BooreAtkinson2011, same results with BooreAtkinson2008)

EQ Scenario	**Mag**	**Mag Type**	**Dist (km)**	**Dist Type**	**Vs_{30} (m/s)**	**Fault Type**
mag7.0_dist40_Vs450	7	Moment	31.83	Rjb	450	Normal-F

***Table A.3.5: Equivalent input parameters used for (4)* BT2003** (BergeThierryEtAl2003SIGMA):

EQ Scenario	**Mag**	**Mag Type**	**Dist (km)**	**Dist Type**	**Soil Type**
mag7.0_dist40_Vs450	6.99	Surface	40.0	D_{hypo}	SOIL

***Table A.3.6: Equivalent input parameters used for (5)* BD2014** (BindiEtAl2014Rhyp)

EQ Scenario	**Mag**	**Mag Type**	**Dist (km)**	**Dist Type**	**Vs_{30} (m/s)**	**Fault Type**
mag7.0_dist40_Vs450	7.0	Moment	40.0	R_{hypo}	450	Normal-F

Table A.3.7: Equivalent input parameters used for (6) CB2014 (CampbellBozorgnia2014)

EQ Scenario	Mag	Mag Type	Dist (km)	Dist Type	Dist 2= Rrup	Dist 2= Rx	Vs_{30} (m/s)
mag7.0_dist40_Vs450	7.0	Moment	31.83	Rjb	38.28	44.96	450

Fault Type	DIP_Angle	Ztor	W (km)	Zhypo (km)	Ztor	Z2.5 (m)
Normal-F	50.0	5.62	20.42	15.00	5.62	1 410

Table A.3.8: Equivalent input parameters used for (7) **CY2014** (ChiouYoungs2014)

EQ Scenario	Mag	Mag Type	Dist (km)	Dist Type	Dist 2= Rrup	Dist 3= Rx
mag7.0_dist40_Vs450	7.0	Moment	31.83	Rjb	38.28	44.96

DIP_Angle	Fault Type	Ztor	Vs_{30} (m/s)	Z1.0 (m)	FM
50.0	Normal-F	5.62	450	160	1

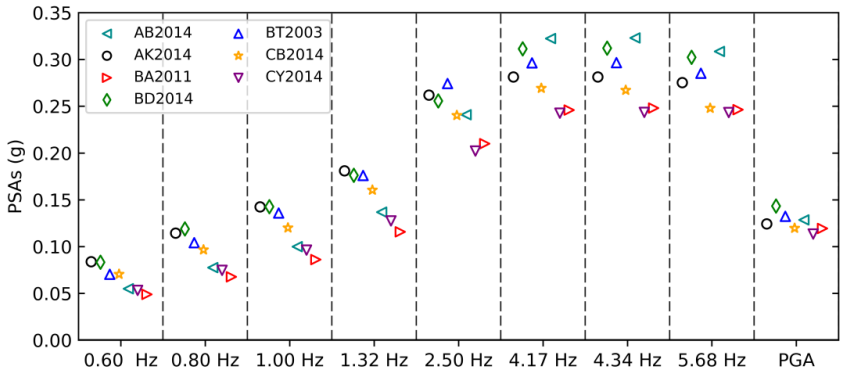

Figure A.3.1: Target PSAs at the fundamental frequency of structural models and at PGA

A.3.2 Test of Input Parameters

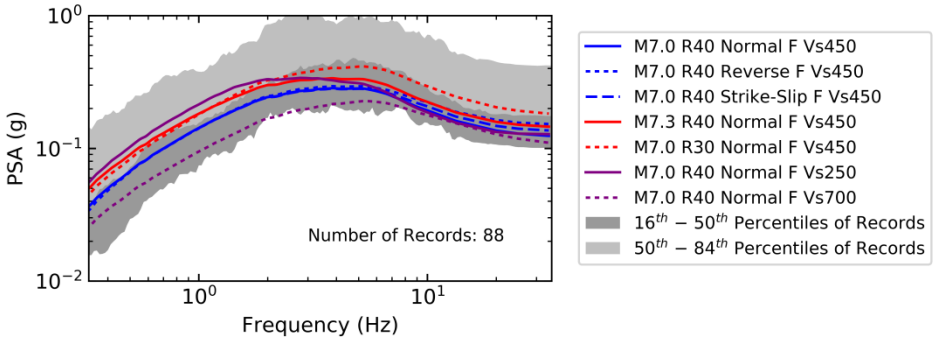

Figure A.3.2: Spectral distribution of selected EQ records and median spectra of AK2014. The x-axis shows the frequencies, and the y-axis shows pseudo-spectral accelerations (PSAs). The 16th percentile to the median of the EQ records is shown with the darker grey area. The median to the 84th percentile of the EQ records is highlighted with the lighter grey area. The median spectra of AK2014 are plotted with a unique color and style according to the set of parameters in the legend box. The parameters correspond to the assumed scenario and metadata of the EQ records, i.e., style-of-faulting (normal, reverse, and strike-slip), the moment magnitudes (M7.0 and M7.3), the hypocentral distances (R30 and R40), and the site conditions (Vs30 of 250, 450, and 700 m/s). The solid blue line represents the hypothetical scenario.

Median PGA is 0.18 g for the EQ records and 0.11 g for the hypothetical scenario. At 1.00 Hz, median PSA is 0.11 g for both cases. The scenario has a similar median spectral shape with the EQ records at low frequencies. After 1.5 Hz, the median spectrum of the EQ records locates mostly above the scenario.

The target spectrum translates above when the hypocentral distance is decreased or the moment magnitude is increased. Target spectra with softer and stiffer soils exhibit large spectral difference up to 10.0 Hz, and the difference reduces at higher frequencies. Changes in hypocentral distance and magnitude translate the median shape. With respect to the selected scenario's shape, high-frequency spectral amplitudes are affected by focal mechanism; low-frequency spectral amplitudes are affected by soil conditions. The median spectrum is sensitive to input parameters.

A.4 Record-to-Record Variability in Bins

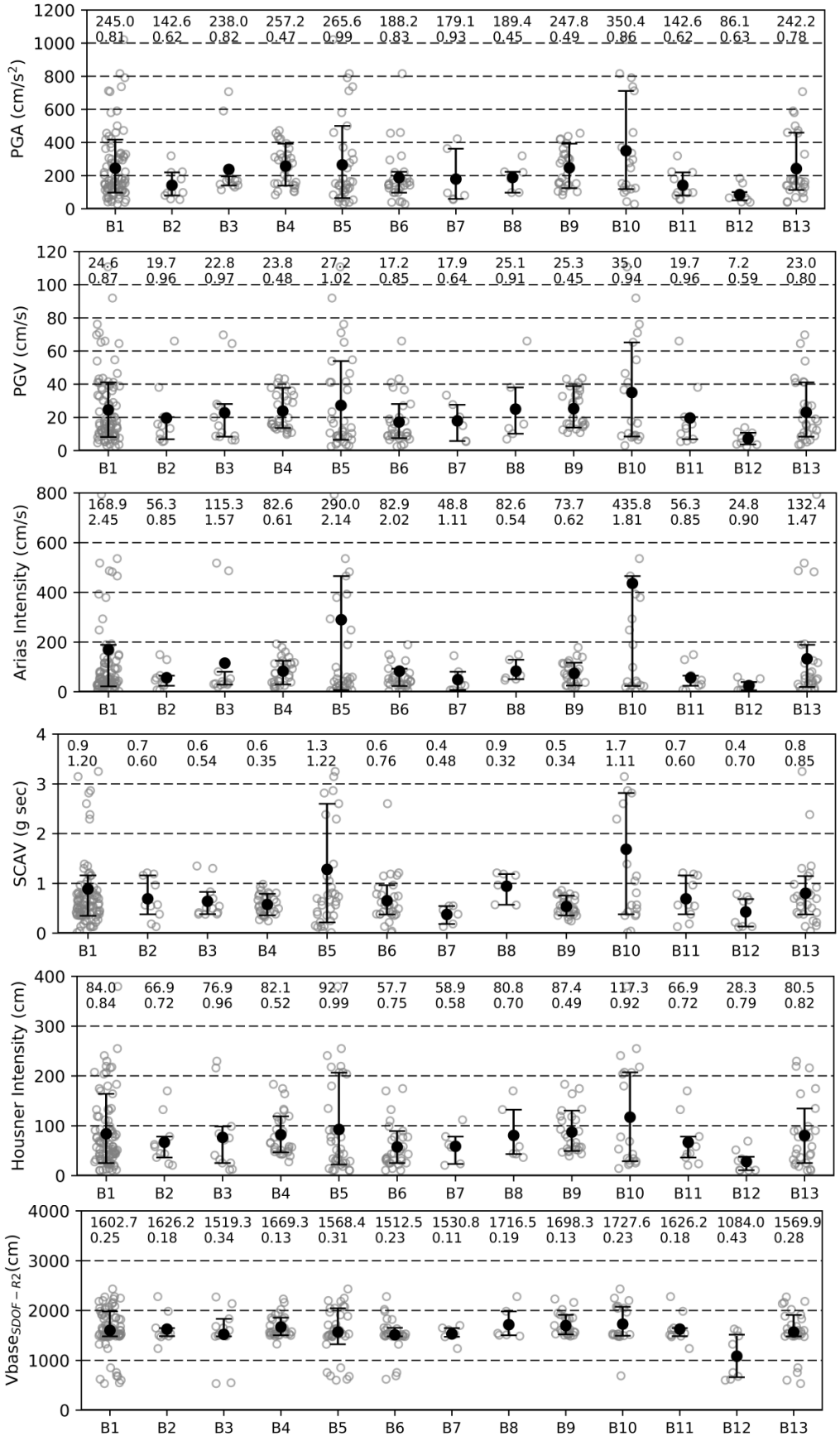

Figure A.4.1: Record-to-record variability with the bins formed with the site-specific settings and event dominancy

The value of each GM is shown with unfilled grey circles. The average is shown with the black filled circle. The 16th and 84th percentiles are shown with the horizontal bars. The mean and the coefficient of variation (COV) are noted for each bin. There are 13 record bins from B1 to B13 (with the number of records in each):

B1: All (88)
B2: Normal Fault (10)
B3: Reverse Fault (12)
B4: Oblique Fault (30)
B5: Strike-Slip F. (36)
B6: Vs450 (30)
B7: Vs800+ (6)
B8: Normal+Vs450 (6)
B9: Loma Prieta (26)
B10: Duzce Event (20)
B11: Irpina Event (10)
B12 Landers Event (8)
B13: Homogenous (28)

All bin represents the magnitude-distance bin. The Normal Fault (NF) bin selects the records with normal fault from the All bin and so on. The Vs450 bin selects the records with Vs30 between 350 and 550 m/s from the All bin. The NF and Vs450 bin represent the intersection of the two bins. The Homogenous bin includes two GMs per EQ event.

A.5 Spectrum Compatible GM Selection

A.5.1 Effect on Frequency Range

This part is adapted from Isbiliroglu (2016). In spectrum compatible selection, the effect of different frequency ranges is compared for the elastic PSAs in Figure A.4.1 and the inelastic PSAs (i.e., the response of SDOF models) in Figure A.4.2. For the shown frequencies and the elastic and inelastic PSAs, the effect of the frequency range remains insignificant.

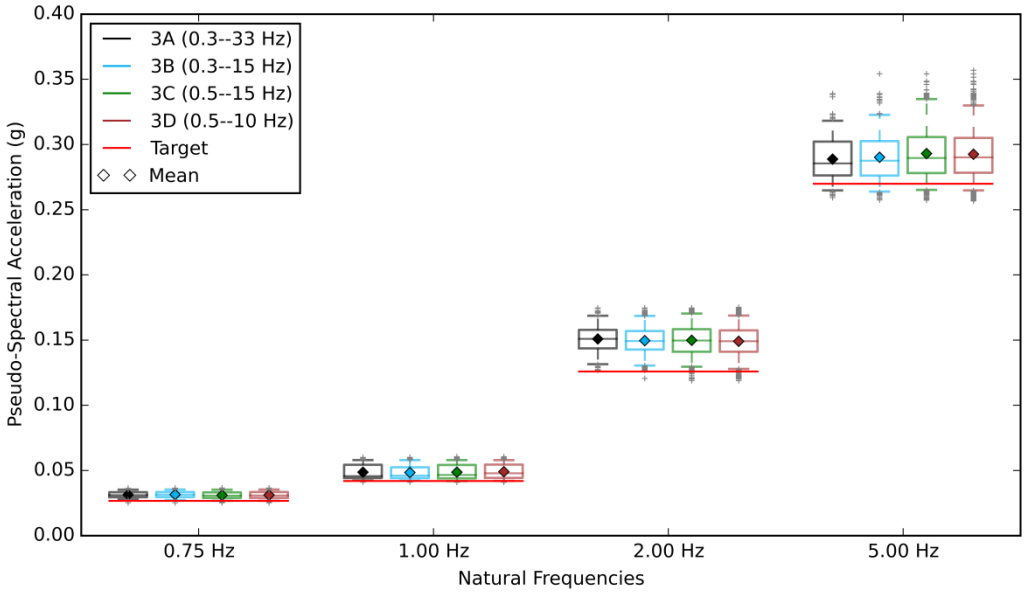

Figure A.5.1: Distribution of elastic PSAs at four fundamental frequencies. The frequencies of 0.75, 1.00, 2.00, and 5.00 Hz are shown in the x-axis. Mean values are shown with the diamond markers. The boxes comprise 25th and 75th percentiles. The median is shown with a horizontal line within each box. The whiskers represent the 5th, and 95th percentiles and the probable outliers are shown with grey markers. The damping ratio is 5%. The target PSA is shown with the horizontal red line. The target is BT2003 for Mw 5.35 and R = 10 km. The upper and lower amplitude ratios are 0.95 and 1.40. All GM sets are collected with the given frequency range in the legend. The 75% of the GM sets are above the target at these fundamental frequencies. The mean values are very close to each other for the cases with different frequency ranges.

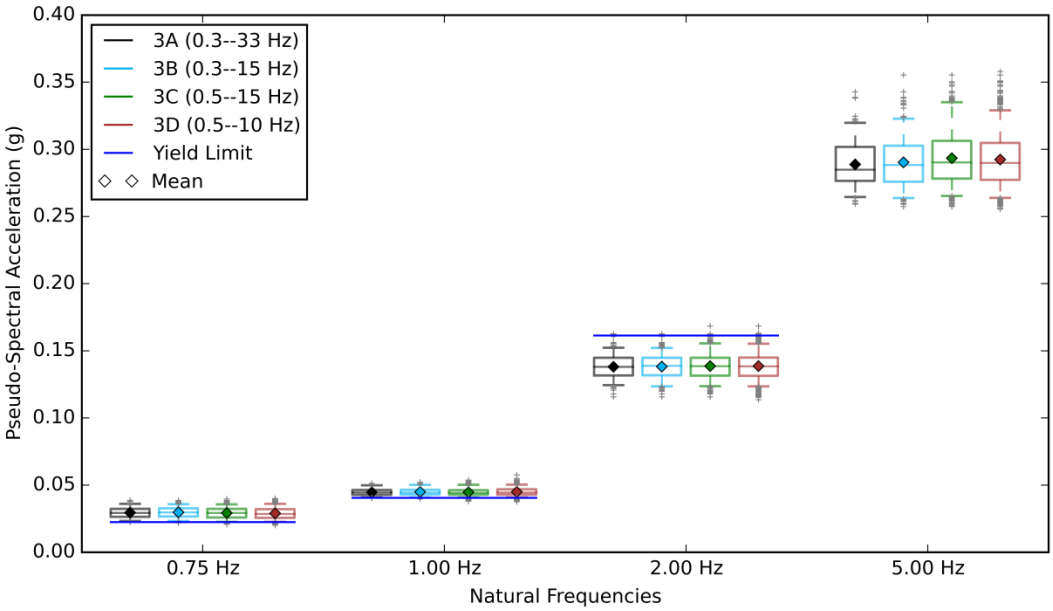

Figure A.5.2: Distribution of inelastic PSAs at four fundamental frequencies. Similar graphical elements are used with A.4.1. The horizontal blue line represents the yielding limit. The elastoplastic material is defined to deform irrecoverably (no degradation properties are included). The SDOF oscillators with fundamental frequencies of 0.75 and 1.00 Hz are mostly yielded. The SDOF at 5.00 Hz remains in the elastic limit.

A.5.2 Use of Site-Specific or Event-Dominant Record Bin

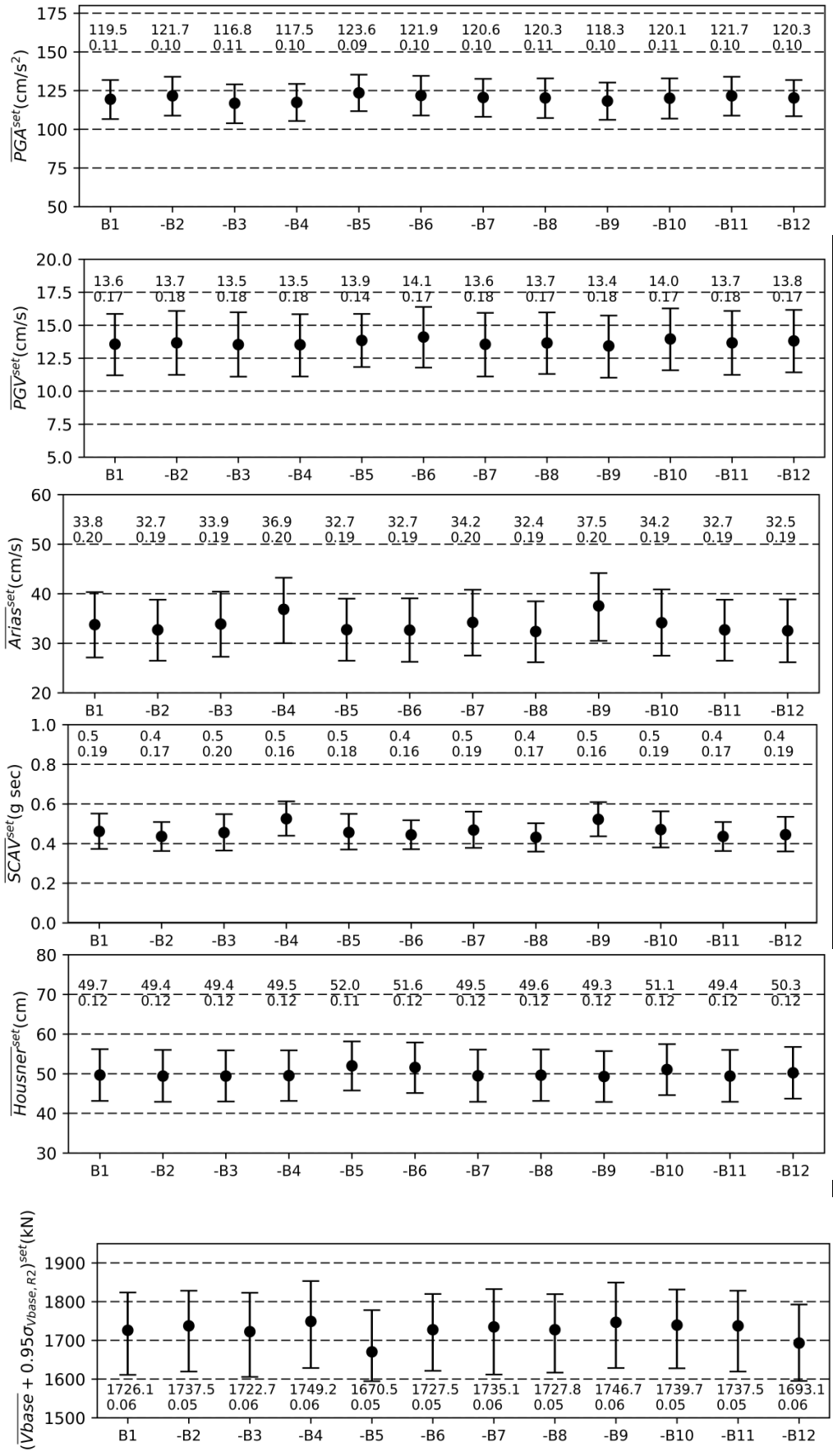

Figure A.5.3: Effect of removing site-specific and even dominant records in spectrum compatible selection. The GM selection is performed with the median of AK2014 for the scenario of M7.0R40, Vs30 450 m/s, and normal fault. The amplitude tolerance is 0.5σ-around the target. 5 GM per set is used. Intraset approaches (such as an average of 5 GMs, average plus 95% standard deviation of 5 GMs) are used in the y-axis as explained in Section 1.2.2. The mean and COV of the values from all GM sets are shown in the figures.B1 in the x-axis represents all eligible GM sets with magnitude-distance bin. The next rows represent the remaining mean and its COV when the records in B2 to B12 are removed from all GM set:
B1: All (88)
B2: Normal Fault (10)
B3: Reverse Fault (12)
B4: Oblique Fault (30)
B5: Strike-Slip F. (36)
B6: Vs450 (30)
B7: Vs800+ (6)
B8: Normal+Vs450 (6)
B9: Loma Prieta (26)
B10: Duzce Event (20)
B11: Irpina Event (10)
B12 Landers Event (8)

For example, The -Normal Fault (NF) bin removes the records with normal fault from the GM sets. The -Vs450 bin removes the records with Vs30 between 350 and 550 m/s. The -Vs800+ bin removes the records with Vs30 greater than 800 m/s.

Table A.5.1: Effect of removing site-specific and even dominant records in spectrum compatible selection. The GM selection is performed with the median of AK2014 for the scenario of M7.0R40, Vs30 450 m/s, and normal fault as shown in Figure 1.8.2. For PSAs at 1.00 Hz and Δtop of SDOF-R2, different intraset approaches (such as an average of 5 GMs, the standard deviation of 5 GMs, and average plus 95% standard deviation of 5 GMs) are considered as explained in Section 1.2.2. The All bin represents all eligible GM sets with magnitude-distance bin. The mean and COV of the values from all GM sets are shown in the first row. The next rows represent the remaining mean and its COV when the records in the bin are removed from all GM sets. The percentage change of mean with respect to the All bin is also noted. The percentages changes above and beyond ±9% are highlighted with bold font.

For example, The –Normal Fault (NF) bin removes the records with normal fault from the GM sets. It is valid for other style-of-faulting. The –Vs450 bin removes the records with Vs30 between 350 and 550 m/s. The –Vs800+ bin removes the records with Vs30 greater than 800 m/s. The -NF+Vs450 bin removes the intersection of the two bins. The rest of the bins remove the records of the specific event.

The cases revealing significant changes are highlighted with bold font style. Strike-slip records occur in the majority of the GM sets, and their removal eliminates about 96% of all sets. The GM sets without oblique fault result in 17% increase in the mean of all $\sigma_{\Delta\text{top}}^{\text{set}}$ and about 10% increase in the mean of all $(\overline{\Delta\text{top}}+0.95\sigma_{\Delta\text{top}})^{\text{set}}$. The GM sets without strike-slip result in 14% decrease in the mean of all $\sigma_{PSA,fo}^{\text{set}}$, 24% decrease in mean the of all $\sigma_{\Delta\text{top}}^{\text{set}}$, and 9% decrease in mean the of all $(\overline{\Delta\text{top}}+0.95\sigma_{\Delta\text{top}})^{\text{set}}$. The GM sets without the Loma Prieta event causes 15% increase in mean the of all $\sigma_{\Delta\text{top}}^{\text{set}}$ and 8% increase in mean the of all $(\overline{\Delta\text{top}}+0.95\sigma_{\Delta\text{top}})^{\text{set}}$. Other cases slightly change the final results.

Record Bins	# Sets	PSA at 1.00 Hz (cm/s^2)				Δtop of SDOF-R2 at 1.00 Hz (cm)			
		$\overline{\text{PSA}_{\text{fo}}}^{\text{set}}$		$\sigma_{PSA.fo}^{set}$		$\overline{\Delta top}^{set}$		$(\overline{\Delta top}+0.95\sigma_{\Delta top})^{set}$	
		Mean	COV	Mean	COV	Mean	COV	Mean	COV
All	982 535	135	0.16	78	0.34	3.3	0.20	5.3	0.30
–Normal F	404 045	135 (0%)	0.16	79 (2%)	0.35	3.3 (0%)	0.20	5.3 (0%)	0.28
–Reverse F	432 665	136 (0%)	0.16	80 (3%)	0.35	3.2 (-1%)	0.21	5.3 (-1%)	0.33
–Oblique F	152 012	133 (-1%)	0.14	79 (1%)	0.38	3.5 (5%)	0.20	5.8 **(10%)**	0.30
–Strike-Slip	38 670	140 (3%)	0.15	67 **(-14%)**	0.34	3.3 (-1%)	0.16	4.8 **(-9%)**	0.23
–Vs450	180 590	139 (3%)	0.16	78 (0%)	0.28	3.3 (2%)	0.19	5.2 (-1%)	0.25
–Vs800+	578 183	134 (-1%)	0.15	77 (-1%)	0.36	3.3 (0%)	0.20	5.3 (0%)	0.31
–NF+Vs450	698 639	136 (1%)	0.16	80 (3%)	0.34	3.3 (0%)	0.19	5.3 (0%)	0.27
–Loma P	171 522	133 (-2%)	0.14	79 (1%)	0.37	3.4 (4%)	0.20	5.7 **(8%)**	0.30
–Duzce	360 818	137 (1%)	0.16	81 (4%)	0.29	3.3 (0%)	0.20	5.3 (1%)	0.29
–Irpina	404 045	135 (0%)	0.16	79 (2%)	0.35	3.3 (0%)	0.20	5.3 (0%)	0.28

Table A.5.2: Effect of removing site-specific and even dominant records in spectrum compatible selection. The GM selection is performed with the median of ***BA2011*** for the scenario of M7.0R40, Vs30 450 m/s, and normal fault. Further information can be found in the caption of Table A.5.1.

Record Bins	# Sets	PSA at 1.00 Hz (cm/s^2)				Δtop of SDOF-R2 (cm)					
		$\overline{PSA_{fo}}^{set}$		$\sigma_{PSA.fo}^{set}$		$\overline{\Delta top}^{set}$		$\sigma_{\Delta top}^{set}$		$(\overline{\Delta top}+0.95\sigma_{\Delta top})^{set}$	
		Mean	COV	Mean	COV	Mean	COV	Mean	COV	Mean	COV
All	30 972	88	0.14	61	0.33	2.0	0.14	1.2	0.41	3.2	0.22
–Normal F	13 192	88 (0%)	0.14	64 (4%)	0.31	2.0 (1%)	0.15	1.3 (7%)	0.41	3.3 (3%)	0.23
–Reverse F	16 008	87 (-1%)	0.15	60 (-2%)	0.34	2.0 (-1%)	0.15	1.2 (-3%)	0.42	3.1 (-2%)	0.22
–Oblique F	11 137	88 (0%)	0.14	64 (4%)	0.28	2.0 (2%)	0.15	1.4 **(10%)**	0.46	3.3 (5%)	0.26
–Strike-Slip	51	90 (3%)	0.13	54 **(-12%)**	0.34	2.1 (4%)	0.09	1.0 **(-15%)**	0.32	3.1 (-3%)	0.15
–Vs450	2 075	88 (0%)	0.15	67 (9%)	0.32	2.0 (1%)	0.13	1.3 (7%)	0.33	3.3 (3%)	0.18
–Vs800+	17 523	88 (0%)	0.14	62 (0%)	0.31	2.0 (0%)	0.15	1.3 (2%)	0.41	3.2 (1%)	0.22
–NF+Vs450	23 594	88 (0%)	0.15	64 (4%)	0.32	2.0 (1%)	0.15	1.3 (5%)	0.41	3.2 (3%)	0.22
–Loma P.	11 596	88 (0%)	0.14	65 (5%)	0.28	2.0 (1%)	0.16	1.4 **(10%)**	0.45	3.3 (5%)	0.25
–Duzce	5 690	85 (-3%)	0.15	68 **(10%)**	0.30	1.9 (-3%)	0.13	1.4 **(9%)**	0.33	3.2 (1%)	0.19
–Irpina	13 192	88 (0%)	0.14	64 (4%)	0.31	2.0 (1%)	0.15	1.3 (7%)	0.41	3.3 (3%)	0.23

Table A.5.3: Effect of removing site-specific and even dominant records in spectrum compatible selection. The GM selection is performed with the median of ***BT2003*** for the scenario of M7.0R40 and soil conditions. Further information can be found in the caption of Table A.5.1.

Record Bins	# Sets	PSA at 1.00 Hz (cm/s^2)				Δtop of SDOF-R2 (cm)					
		$\overline{PSA_{fo}}^{set}$		$\sigma^{set}_{PSA.fo}$		$\overline{\Delta top}^{set}$		$\sigma^{set}_{\Delta top}$		$(\overline{\Delta top} + 0.95\sigma_{\Delta top})^{set}$	
		Mean	COV	Mean	COV	Mean	COV	Mean	COV	Mean	COV
All	924 767	127	0.16	75	0.34	3.0	0.19	1.9	0.53	4.8	0.30
–Normal F	413 166	127 (0%)	0.16	77 (2%)	0.34	3.0 (0%)	0.19	1.9 (2%)	0.50	4.8 (1%)	0.29
–Reverse F	408 193	127 (0%)	0.17	77 (2%)	0.35	2.9 (-1%)	0.20	1.9 (-1%)	0.58	4.7 (-1%)	0.32
–Oblique F	139 667	124 (-2%)	0.15	76 (1%)	0.40	3.1 (4%)	0.20	2.3 **(18%)**	0.51	5.3 **(10%)**	0.31
–Strike-Slip	30 903	133 (5%)	0.16	67 **(-11%)**	0.34	3.0 (1%)	0.14	1.5 **(-22%)**	0.44	4.4 **(-8%)**	0.21
–Vs450	137 757	131 (3%)	0.17	79 (4%)	0.28	3.1 (2%)	0.18	1.9 (-1%)	0.45	4.9 (1%)	0.26
–Vs800+	582 403	126 (0%)	0.16	74 (-1%)	0.35	3.0 (0%)	0.20	1.9 (0%)	0.55	4.8 (0%)	0.31
–NF+Vs450	660 133	128 (1%)	0.17	78 (3%)	0.33	3.0 (1%)	0.19	1.9 (1%)	0.49	4.8 (1%)	0.28
–Loma P.	164 950	124 (-2%)	0.15	77 (2%)	0.37	3.1 (3%)	0.20	2.2 **(15%)**	0.51	5.2 (7%)	0.31
–Duzce	285 983	128 (1%)	0.17	81 (7%)	0.28	3.0 (0%)	0.18	2.0 (3%)	0.49	4.8 (1%)	0.28
–Irpina	413 166	127 (0%)	0.16	77 (2%)	0.34	3.0 (0%)	0.19	1.9 (2%)	0.50	4.8 (1%)	0.29

A.5.3 GM Sets with and without Same-Event or Same-Station Records

Table A.5.4: ***Effect of the interdependence of GMs in a set.*** The All bin refers to the sets without same-event same-station (i.e., sets with x and y components) records. The case (i) includes the sets that do not consist of any same event records. Then, the case (ii) includes the sets with x and y components. Two spectrum compatible GM selections are performed: one with the median of AK2014 and another with the median of BT2003 for the scenario of M7.0R40, Vs30 450, and normal fault. The amplitude tolerance is 0.5σ around the target. 5 GM per set is used. For PSAs at 1.00 Hz and Δtop of SDOF-R2, different intraset approaches (such as an average of 5 GMs, the standard deviation of 5 GMs, and average plus 95% standard deviation of 5 GMs) are considered as explained in Section 1.2.2.

GMPE	GM Sets	Number of GM Sets	PSA at 1.00 Hz (cm/s^2)				Δtop of SDOF-R2 (cm)					
			$\overline{PSA_{fo}}^{set}$		$\sigma^{set}_{PSA.fo}$		$\overline{\Delta top}^{set}$		$\sigma^{set}_{\Delta top}$		$(\overline{\Delta top} + 0.95\sigma_{\Delta top})^{set}$	
			Mean	COV	Mean	COV	Mean	COV	Mean	COV	Mean	COV
AK2014	All	982 535	135	0.16	78	0.34	3.3	0.20	2.1	0.52	5.3	0.30
	(i) *	110 428	134	0.15	75	0.27	3.4	0.20	2.1	0.42	5.6	0.27
	(ii)*	73 152	134	0.15	76	0.36	3.3	0.20	2.3	0.53	5.3	0.30
BT2003	All	924 767	127	0.16	75	0.34	3.0	0.19	1.9	0.53	4.8	0.30
	(i)*	94 777	125	0.15	73	0.27	3.1	0.20	2.1	0.46	5.1	0.28
	(ii)*	69 626	125	0.15	71	0.36	3.0	0.20	1.8	0.58	4.7	0.31

* All sets are refined to exclude (i) same earthquake event and to include (ii) same-event same-station GMs

A.5.4 Selected and Unselected GMs in Spectrum Compatibility

Table A.5.5: List of earthquake records that do not occur in GM sets. The GM selection is performed with the median of ***AK2014*** for the scenario of M7.0R40, Vs30 450 m/s, and normal fault. The amplitude tolerance is 0.5σ around the target. 5 GM per set is used. Same 15 GMs are identified in Section 1.7.2.

Database	Event Date (yyyymmdd_hhmm)	Event Name	Fault Type	Mw	Unselected Stations	# of Unselected GMs
CESMD	19891017_1704	Loma Prieta	Oblique	6.9	47379[34, 1428], 47381[36, 278]	2
CESMD	20061015_0707	Hawaii	Strike-slip	7.1	02849[46, N/A]	2
Resorce 2013	19760517_0258	NW Uzbekistan	Reverse	6.8	27[32, 121]	2
Resorce 2013	19900620_2100	Western Iran	Strike-slip	7.3	6211[41, **621**]	2
Resorce 2013	19991112_165721	Duzce	Strike-slip	7.1	1401[37, 294], 3102[30, N/A], 3103[31, N/A], 3104[30, N/A], 9901[31, 481]	7

Table A.5.6: Record-to-record variability of the identified GMs to be refined and to be discarded.

	# GMs	PGA (g)		PGV (cm/s)		Arias (cm/s)		SCAV (g sec)		$\Delta top_{SDOF\text{-}R2}$ (cm)		$Vbase_{SDOF\text{-}R2}$ (kN)	
		Mean	COV	Mean	COV	Mean	COV	Mean	COV	Mean	COV	Mean	COV
Refined*	73	0.179	0.59	19.0	0.81	61	1.12	0.59	0.76	4.7	0.95	1 535	0.25
Discarded*	15	0.594	0.36	52.0	0.50	694	1.20	2.31	0.80	11.0	0.50	1 931	0.15

*The GMs that are identified in the caption of Figure 1.7.2 (***AK2014***) are discarded. For the refined and discarded GMs, the comparison of the mean and COV IMs is given. It is noted that Arias intensity of the discarded records is significantly larger than the refined GMs. There is a large Δtop demand by the discarded GMs.

Table A.5.7: List of earthquake records that do not occur in GM sets. The GM selection is performed with the median of ***BT2003*** for the scenario of M7.0R40 and soil site. The amplitude tolerance is 0.5σ around the target. 5 GM per set is used.

Database	Event Date (yyyymmdd_hhmm)	Event Name	Fault Type	Mw	Unselected Stations	# of Unselected GMs
CESMD	19891017_1704	Loma Prieta	Oblique	6.9	47379[34, 1428], 47380[35, 271], 47381[36, 278]	4
CESMD	20061015_0707	Hawaii	Strike-slip	7.1	02849[46, N/A]	2
Resorce 2013	19760517_0258	NW Uzbekistan	Reverse	6.8	27[32, 121]	2
Resorce 2013	19900620_2100	Western Iran	Strike-slip	7.3	6211[41, **621**]	2
Resorce 2013	19991112_165721	Duzce	Strike-slip	7.1	1401[37, 294], 3102[30, N/A], 3103[31, N/A], 3104[30, N/A], 9901[31, 481]	8

Table A.5.8: List of earthquake records that do not occur in GM sets. The GM selection is performed with the median of ***BA2011*** for the scenario of M7.0R40, Vs30 450 m/s, and normal fault. The amplitude tolerance is 0.5σ around the target. 5 GM per set is used.

Database	Event Date (yyyymmdd_hhmm)	Event Name	Fault Type	Mw	Unselected Stations	# of Unselected GMs
CESMD	19891017_1704	Loma Prieta	Oblique	6.9	47379[34, 1428], 47380[35, 271], 47381[36, 278], 57217[35, 597], 57382[37, 222], 57425[44, 334], 58065[33, 381]	12
CESMD	20061015_0707	Hawaii	Strike-slip	7.1	02849[46, N/A]	2
Resorce 2013	19760517_0258	NW Uzbekistan	Reverse	6.8	27[32, 121]	2
Resorce 2013	19801123_1834	Irpinia	Normal	7.3	STR[36, 1122]	2
Resorce 2013	19900620_2100	Western Iran	Strike-slip	7.3	6211[41, **621**]	2
Resorce 2013	19991112_165721	Duzce	Strike-slip	7.1	1401[37, 294], 3102[30, N/A], 3103[31, N/A], 3104[30, N/A], 9901[31, 481]	10

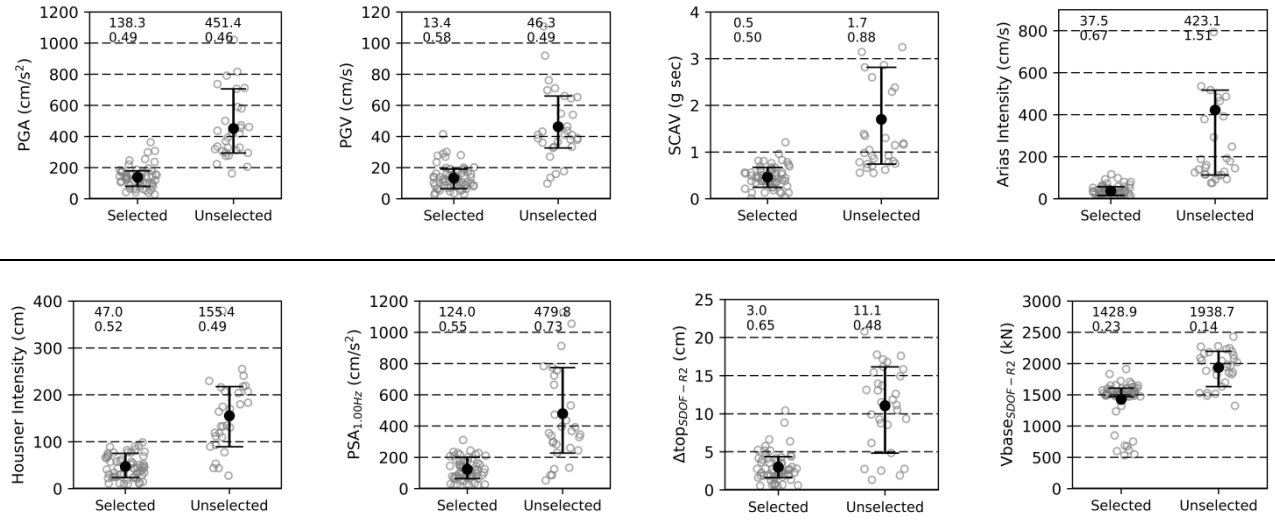

Figure A.5.4: Record-to-record variability of selected and unselected GMs after the spectrum compatibility. The GM selection is performed with the median of ***BA2011*** for the scenario of M7.0R40, Vs30 450 m/s, and normal fault. The amplitude tolerance is 0.5σ around the target. 5 GM per set is used. The value of each GM is shown with unfilled grey circles. The average is shown with the black filled circle. The 16th and 84th percentiles are shown with the horizontal bars. The mean and the coefficient of variation (COV) are noted for each bin.

A.6 GMPEs and Upper and Lower Amplitude Tolerances

Table A.6.1: Impact of GMPEs used as target spectra on the distribution of intensity measures. In the spectrum compatible selection, the upper and lower amplitude tolerances are defined with the 0.5σ of the GMPE around its median spectra. The frequency tolerance is from 0.50 Hz to 20.0 Hz. Five GMs per set are used. The given amounts of GM sets are collected for the GMPEs. AK2014, BD2014, and BT2003 reveal the largest amount of GM sets due to the sigma and the closeness to the median of the magnitude-distance bin (Figure 1.8.1). The mean and COV of IMs are then obtained as the average of 5 GMs, i.e., $\overline{\mathrm{Val}}^{\mathrm{set}}$ by including all GM sets. The dispersions in the distribution of all $\overline{\mathrm{IM}}^{\mathrm{set}}$ exist for each GMPE. COVs of all $\overline{\mathrm{PGV}}^{\mathrm{set}}$, $\overline{\mathrm{Arias}}^{\mathrm{set}}$, and $\overline{\mathrm{SCAV}}^{\mathrm{set}}$ are always above 0.20, which is also greater than COVs of the rest.

GMPE	Amount of GM Sets	$\overline{\mathrm{PGA}}^{\mathrm{set}}$ (g)		$\overline{\mathrm{PGV}}^{\mathrm{set}}$ (cm/s)		$\overline{\mathrm{Arias}}^{\mathrm{set}}$ (cm/s)		$\overline{\mathrm{SCAV}}^{\mathrm{set}}$ (g sec)		$\overline{\mathrm{ASI}}^{\mathrm{set}}$ (cm/s)		$\overline{\mathrm{Housner}}^{\mathrm{set}}$ (cm)	
		Mean	COV	Mean	COV	Mean	COV	Mean	COV	Mean	COV	Mean	COV
AB2014	134 822	0.17	0.14	14.7	0.24	49.1	0.23	0.63	0.20	160	0.14	53.6	0.13
AK2014	982 535	0.17	0.18	20.6	0.26	54.2	0.28	0.68	0.21	160	0.17	73.5	0.16
BA2011	**30 972**	**0.14**	**0.11**	**12.7**	**0.23**	**40.1**	**0.23**	**0.58**	**0.23**	**136**	**0.11**	**48.0**	**0.14**
BD2014	**1 117 583**	**0.18**	**0.18**	**21.1**	**0.29**	**58.4**	**0.30**	**0.70**	**0.22**	**170**	**0.17**	**73.5**	**0.18**
BT2003	924 767	0.17	0.18	19.1	0.26	53.9	0.27	0.66	0.21	165	0.18	68.3	0.15
CB2014	210 372	0.15	0.12	17.5	0.25	47.3	0.24	0.65	0.21	145	0.13	64.4	0.13
CY2014	33 860	0.15	0.11	13.6	0.26	43.3	0.22	0.62	0.22	137	0.10	52.0	0.14

Table A.6.2: Effect of GMPEs used as target spectra in spectrum compatible selection with* the tolerances of ±0.5σ of the target.** The GM selection is performed with the median of ***GMPEs for the scenario of M7.0R40, Vs30 450 m/s, and normal fault. 5 GM per set is used. For PSAs at 1.00 Hz, Δtop, and Vbase of SDOF-R2, different intraset approaches (such as an average of 5 GMs and average plus 95% standard deviation of 5 GMs) are considered as explained in Section 1.2.2.

GMPEs	Amount of GM Sets	PSA at 1.00 Hz (cm/s^2)				Δtop of SDOF-R2 (cm)				Vbase of SDOF-R2 (kN)			
		$\overline{\mathrm{PSA_{fo}}}^{\mathrm{set}}$		$(\overline{\mathrm{PSA_{fo}}} + 0.95\sigma_{PSA,fo})^{set}$		$\overline{\Delta\mathrm{top}}^{\mathrm{set}}$		$(\overline{\Delta top} + 0.95\sigma_{\Delta top})^{set}$		$\overline{\mathrm{Vbase}}^{\mathrm{set}}$		$(\overline{Vbase} + 0.95\sigma_{Vbase})^{set}$	
		Mean	COV	Mean	COV	Mean	COV	Mean	COV	Mean	COV	Mean	COV
AB2014	134 822	100	0.15	161	0.19	2.2	0.15	3.5	0.24	1330	0.08	1665	0.04
AK2014	982 535	135	0.16	209	0.18	3.3	0.20	5.3	0.30	1447	0.07	1726	0.06
BA2011	30 972	88	0.14	146	0.19	2.0	0.14	3.2	0.22	1262	0.08	1639	0.04
BD2014	1 117 583	132	0.17	206	0.20	3.3	0.22	5.4	0.34	1449	0.07	1726	0.06
BT2003	924 767	127	0.16	199	0.19	3.0	0.19	4.8	0.30	1421	0.08	1708	0.05
CB2014	210 372	120	0.15	189	0.17	2.8	0.18	4.4	0.27	1393	0.07	1702	0.05
CY2014	33 860	94	0.15	157	0.20	2.2	0.17	3.5	0.26	1289	0.08	1658	0.04

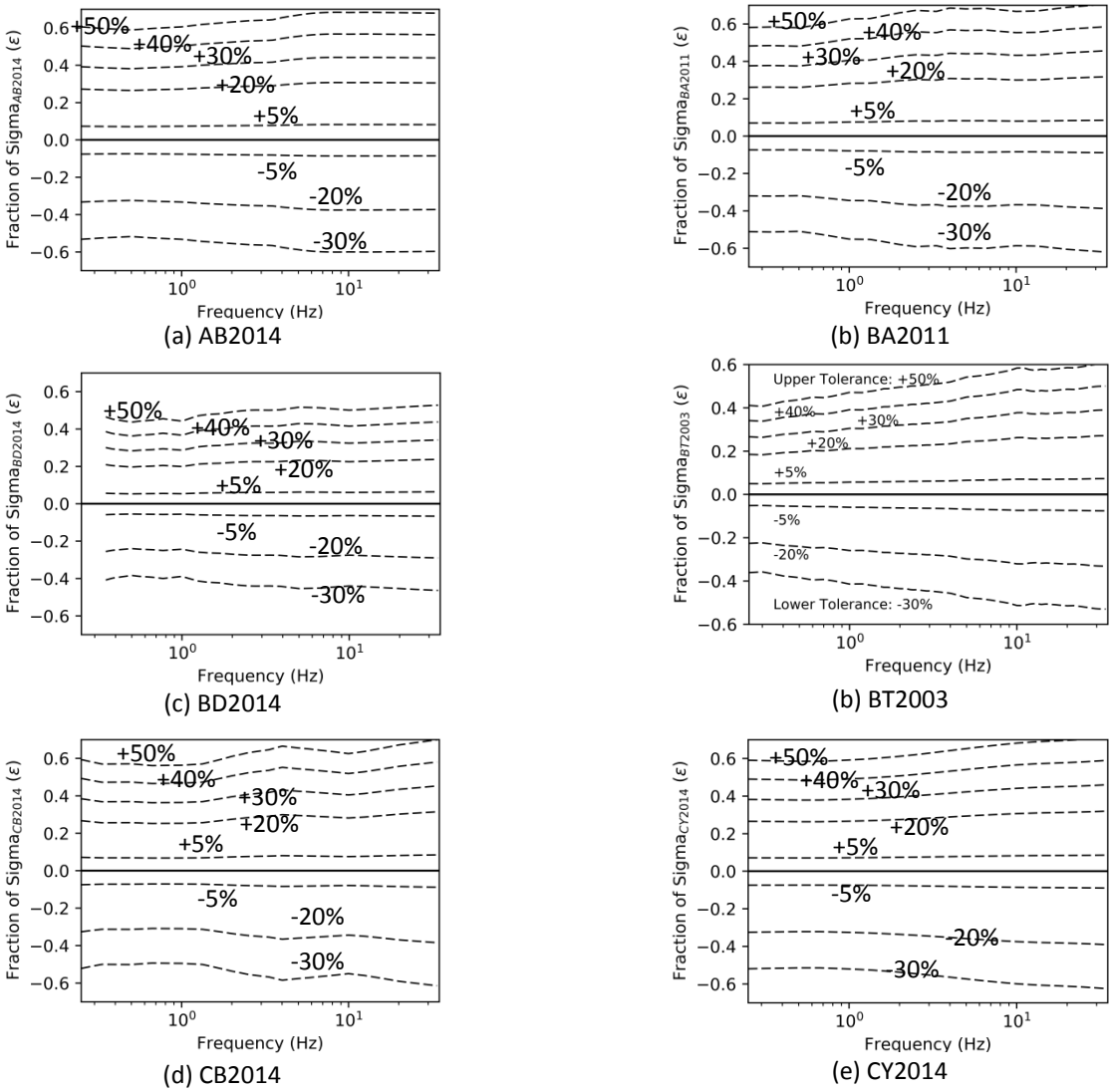

Figure A.6.1: Equivalent epsilons of linear tolerances (in the natural logarithmic base). The equivalent fraction of sigma (ε) is calculated with the ratio of linear tolerances in natural logarithm and sigma of GMPE. The dashed lines represent the given linear tolerances. For example, in BT2003, linear +50% has equivalent ε ranging between 0.4 and 0.6.

Table A.6.3: Amount of GM sets under different upper and lower amplitude tolerance. The upper and lower amplitude tolerances are defined with the sigma-based tolerances, linear symmetric tolerances, and asymmetric tolerances. The frequency tolerance is from 0.50 Hz to 20.0 Hz. Five GMs per set are used. All GM sets are collected.

Tolerance Types		AB2014	AK2014	BA2011	BT2003	BD2014	CB2014	CY2014
Sigma-Based Tolerances	±0.5 Eps	134 822	982 535	30 972	1 117 583	924 767	210 372	33 860
	±0.4 Eps	22 530	324 238	4 533	381 797	251 491	37 880	2 946
	±0.3 Eps	776	40 622	122	24 751	20 096	1 408	39
Symmetric Tolerances	±30%	78 212	203 534	17 853	189 157	141 726	95 228	18 071
	±25%	18 724	56 653	4 122	31 849	31 725	21 255	2 599
	±20%	1 541	6 532	334	1 524	2 456	1 552	96
Asymmetric Tolerances	-5% +50%	17 232	34 174	5 472	8 743	17 882	17 230	1 073
	-5% +40%	1 903	5 468	420	669	1 971	1 872	37
	-5% +30%	51	227	11	10	53	37	1

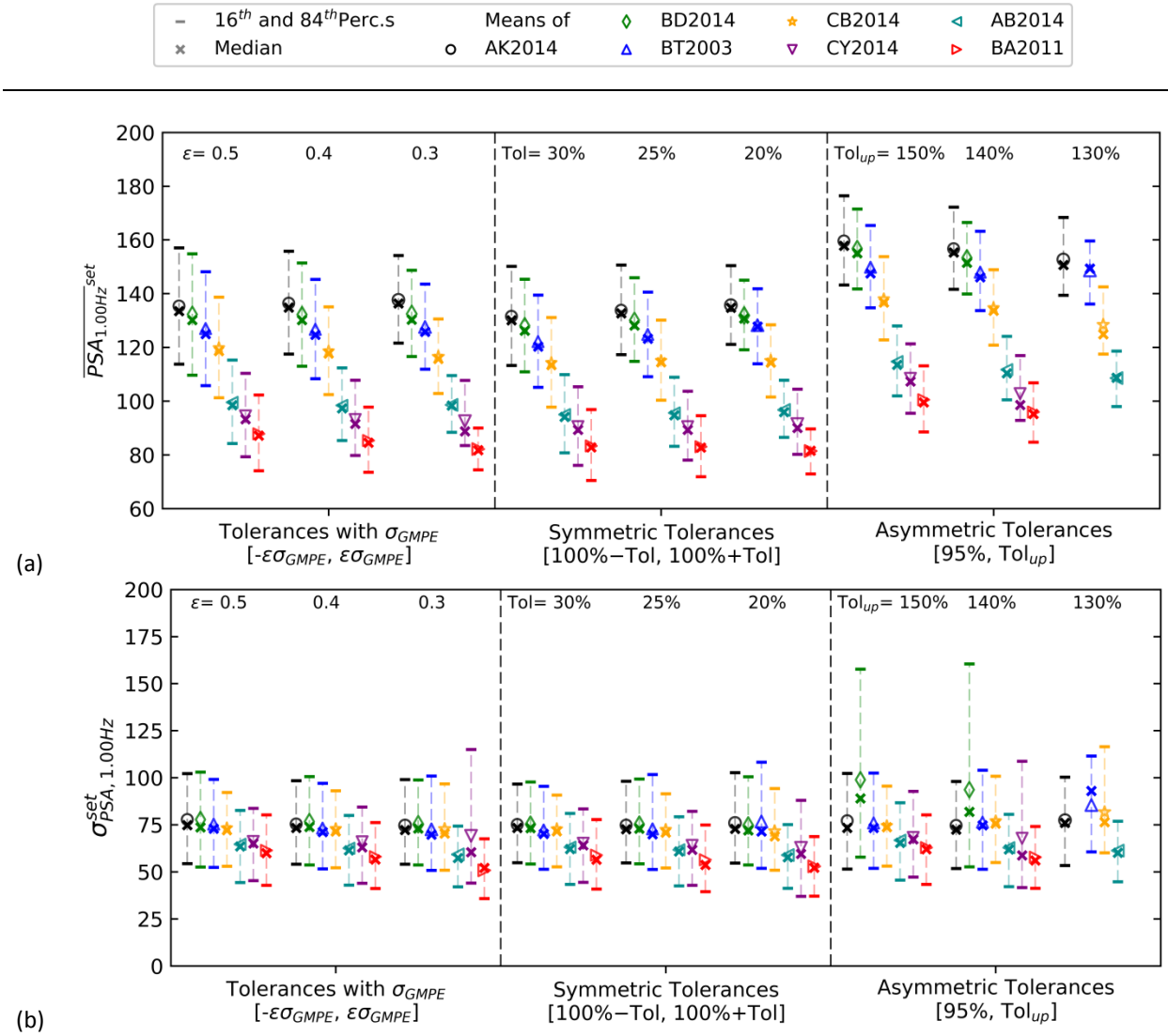

Figure A.6.2: Distribution of PSAs at 1.00 Hz (cm/s^2) with different upper and lower amplitude tolerances. Selection of GM sets is made as explained in the caption of Table A.6.2. Results with the intraset approach of (a) average of 5 GMs and (b) standard deviation of a set are shown. Means are demonstrated with the markers and colors in the legend box for GMPEs. Medians are shown with the cross markers. The 16th and 84th percentiles are plotted with the horizontal bars.

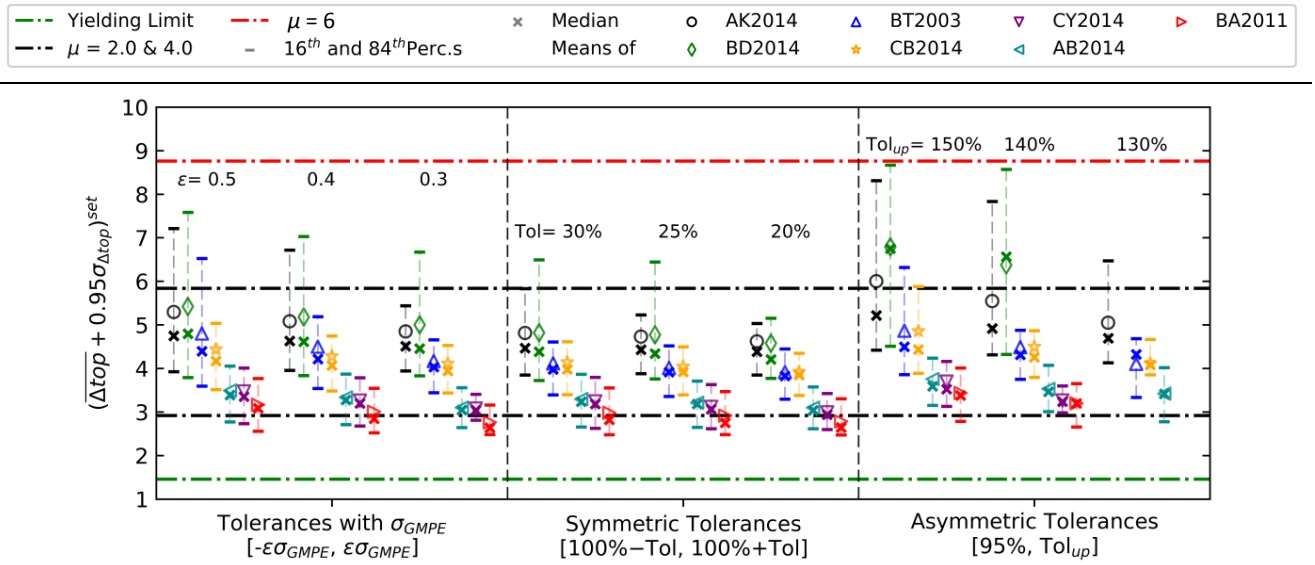

Figure A.6.3: Distribution of Δtop (cm) of SDOF-R2 at 1.00 Hz with different upper and lower amplitude tolerances. Selection of GM sets is made as explained in Table A.6.3. Results with the intraset approach of the average of 5 GMs are shown. Means are demonstrated with the markers and colors in the legend box for corresponded GMPEs. Medians are shown with the cross markers. The 16th and 84th percentiles are plotted with the horizontal bars. The horizontal dashed lines correspond to the yielding limit and different ductility demands (μ).

Table A.6.4: Impact of upper and lower amplitude tolerances on PSAs at 1.00 Hz and Δtop of SDOF-R2 at 1.00 Hz. The GM selection is performed with the median of AK2014 for the scenario of M7.0R40, Vs30 450 m/s, and normal fault. For PSAs at 1.00 Hz and Δtop of SDOF-R2, different intraset approaches (such as an average of 5 GMs, the standard deviation of 5 GMs, and average plus 95% standard deviation of 5 GMs) are considered as explained in Section 1.2.2. The results of the most flexible tolerances (shaded columns) are used as a benchmark for the differences in mean in the parenthesis. The differences more than ±10% are highlighted with the bold font.

Tolerance Types		Amount of GM Sets	PSA at 1.00 Hz (cm/s^2)				Δtop of SDOF-R2 at 1.00 Hz (cm)			
			$\overline{PSA_{fo}}^{set}$		$\sigma^{set}_{PSA.fo}$		$\overline{\Delta top}^{set}$		$(\overline{\Delta top} + 0.95\sigma_{\Delta top})^{set}$	
			Mean	COV	Mean	COV	Mean	COV	Mean	COV
Sigma Based Tolerances	±0.5ε	982 535	135	0.16	78	0.34	3.3	0.20	5.3	0.30
	±0.4ε	324 238	136 (1%)	0.13	75 (-3%)	0.30	3.2 (-2%)	0.17	5.1 (-4%)	0.27
	±0.3ε	40 622	138 (2%)	0.11	75 (-4%)	0.29	3.2 (-4%)	0.15	4.8 (-8%)	0.25
Symmetric Tolerance	±30%	203 534	132	0.13	75	0.28	3.1	0.16	4.8	0.26
	±25%	56 653	134 (2%)	0.12	75 (0%)	0.28	3.1 (0%)	0.15	4.7 (-2%)	0.25
	±20%	6 532	136 (3%)	0.10	76 (1%)	0.29	3.0 (1%)	0.13	4.6 (-4%)	0.23
Asymmetric Tolerances	-5% +50%	34 174	160	0.10	77	0.39	3.8	0.16	6.0	0.29
	-5% +40%	5 468	157 (-2%)	0.09	75 (-3%)	0.31	3.6 (-6%)	0.15	5.5 (-9%)	0.27
	-5% +30%	227	153 (-5%)	0.08	77 (0%)	0.28	3.4 (**-13%**)	0.12	5.0 (**-18%**)	0.25

A.7 Sufficient Amount of Sets

A.7.1 Testing GM Sets

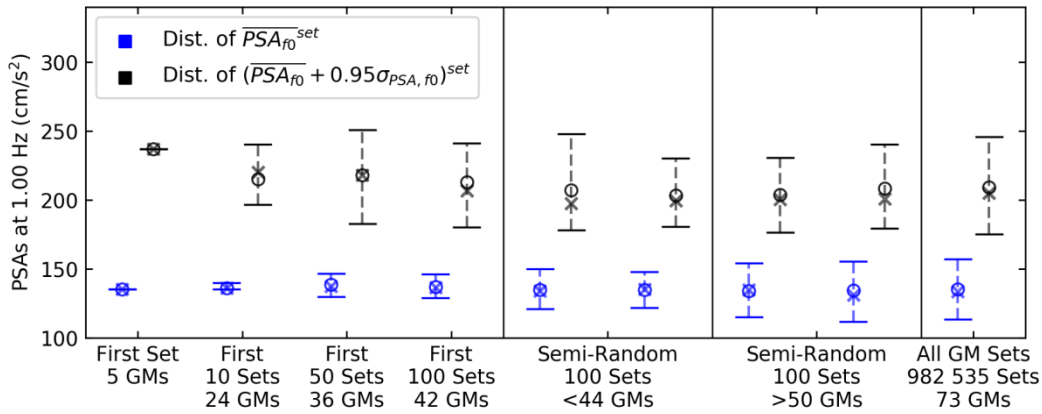

Figure A.7.1: Distribution of PSAs at 1.00 Hz with the inclusion of the various amount of GM sets. First set, first 10 sets, first 50 sets, and first 100 sets are taken from the previous graph and are included for comparison. They are the sets that are commonly selected in the current practice. They have 5 GMs, 24 GMs, 36 GMs, and 42 GMs, respectively. All GM sets have 982 535 GM sets and use 73 GMs. There is a difference in the amount of GMs and the distribution of GM sets. As a result, two different approaches are used to retrieve four semi-random 100 GM sets. The first approach is to select two semi-random 100 sets having less than 44 GMs, which cover 60% of all GMs. The second approach is to select two semi-random 100 sets with at least 50 GMs, which cover 75% of all GMs.

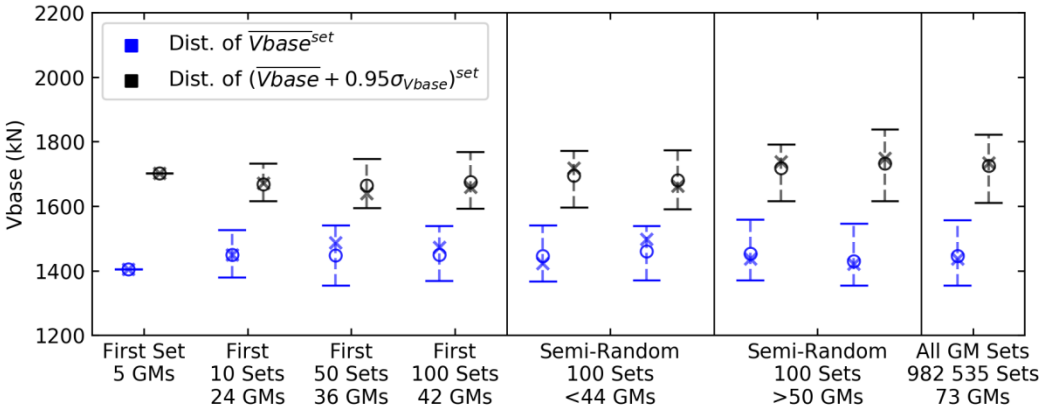

Figure A.7.2: Distribution of Vbase of SDOF's (R2) displacements (Δtop) with the inclusion of the various amount of GM sets. First set, first 10 sets, first 50 sets, and first 100 sets are taken from the previous graph and are included for comparison. They are the sets that are commonly selected in the current practice. They have 5 GMs, 24 GMs, 36 GMs, and 42 GMs, respectively. All GM sets have 982 535 GM sets and use 73 GMs. There is a difference in the amount of GMs and the distribution of GM sets. As a result, two different approaches are used to retrieve four semi-random 100 GM sets. The first approach is to select two semi-random 100 sets having less than 44 GMs, which cover 60% of all GMs. The second approach is to select two semi-random 100 sets with at least 50 GMs, which cover 75% of all GMs.

A.7.2 Approach to Avoid GM Dominancy with Partial GM Sets: The Cycle-and-Shift Algorithm

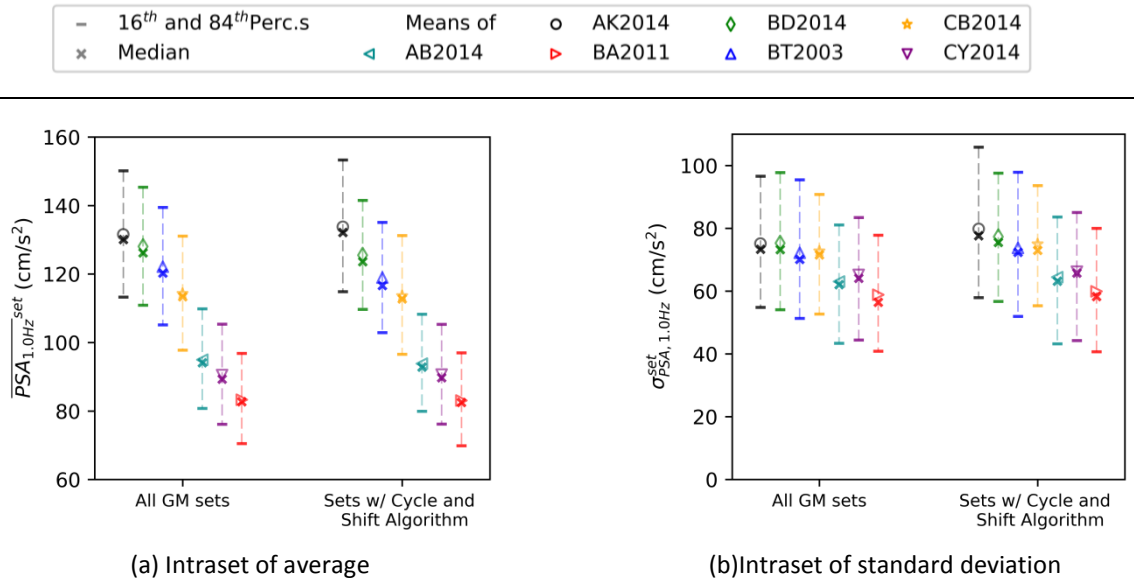

(a) Intraset of average

(b)Intraset of standard deviation

Figure A.7.3: Comparison of the distribution of PSAs at 1.00 Hz with all GM sets and sets obtained with the cycle-and-shift algorithm. The upper and lower amplitude tolerances are defined with ±30% of its median spectra. The frequency tolerance is from 0.50 Hz to 20.0 Hz. Five GMs per set are used. 16th and 84th percentiles are plotted with horizontal line markers. Medians are shown with cross markers. Means are demonstrated with the markers and colors in the legend box for corresponded GMPEs. The average from 5 GMs per set (a) is shown. The average with 95% of standard deviation per set (b) is also shown.

With the cycle-and-shift algorithm, the amounts of GM sets are 15 781 in AB2014, 20 095 in AK2014, 8 284 in BA2011, 22 831 in BT2003, 20 564 in BD2014, 18 205 in CB2014, and 9 391 in CY2014. The amounts of all GM sets are given in Table A.6.3.

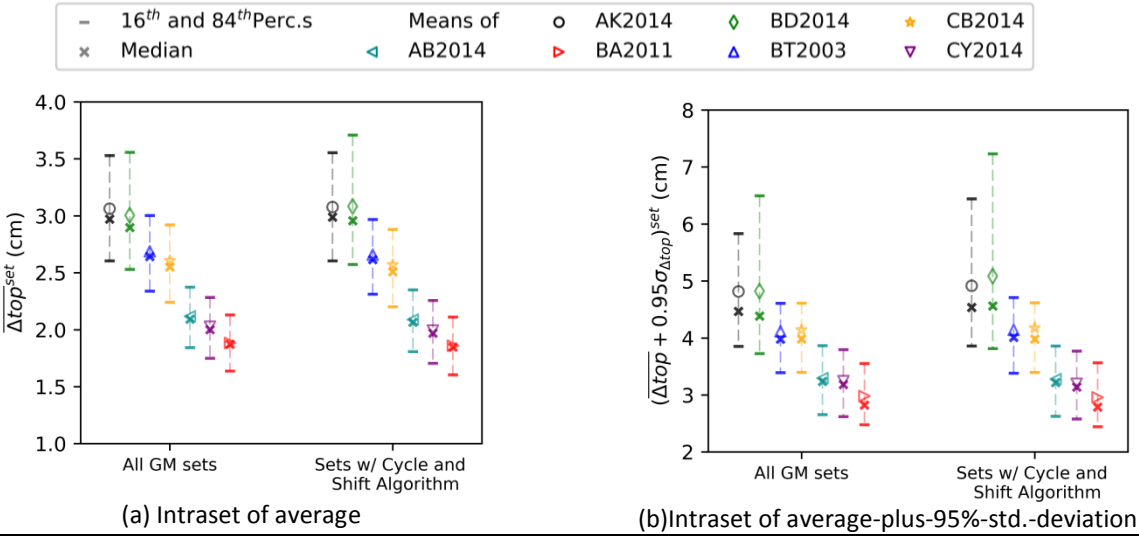

(a) Intraset of average

(b)Intraset of average-plus-95%-std.-deviation

Figure A.7.4: Comparison of the distribution of lateral displacements (Δtop) with all GM sets and sets obtained with cycle-and-shift algorithm. The same graphical elements in Figure A.7.3 are valid here. The average from 5 GMs per set (a) is shown. The average with 95% of standard deviation per set (b) is also shown. The structural responses are obtained from SDOF-R2 at 1.00 Hz.

The amount of sets is about 20 000 with the cycle-and-shift algorithm, where it is about 1 000 000 with all sets (the procedure in Section 1.2.1) in AK2014. The sets obtained by the cycle-and-shift algorithm can represent the whole set distribution with an exception in the AK2014's and BD2014's 84th percentiles from all $(\overline{\Delta\text{top}} + 0.95\sigma_{\Delta\text{top}})^{\text{set}}$. It may be enhanced by the different combination of r_{shift}, N_{set}, and $t_{max.}$

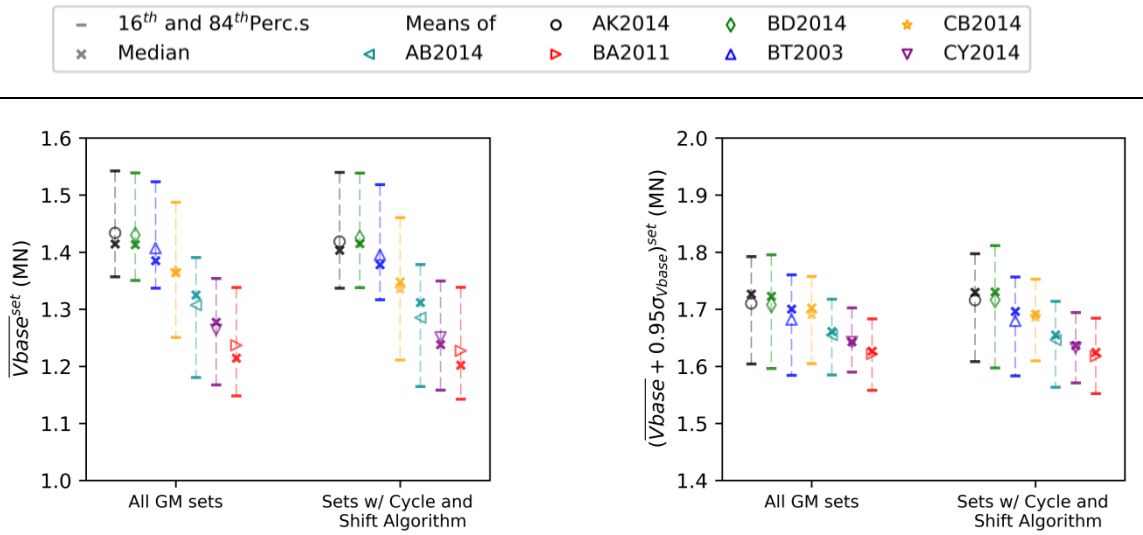

(a) Intraset of average

(b) Intraset of average-plus-95%-std.-deviation

Figure A.7.5: Comparison of the distribution of base shear forces (Vbase) all GM sets and sets obtained with the cycle-and-shift algorithm. The upper and lower amplitude tolerances are defined with ±30% of its median spectra. The frequency tolerance is from 0.50 Hz to 20.0 Hz. Five GMs per set are used. 16th and 84th percentiles are plotted with horizontal line markers. Medians are shown with cross markers. Means are demonstrated with the markers and colors in the legend box for corresponded GMPEs. The average from 5 GMs per set (a) is shown. The average with 95% of standard deviation per set (b) is also shown. The structural responses of SDOF-R2 at 1.00 Hz are shown.

A.8 Amount of GMs per set

***Table A.8.1: Change of mean estimates with respect to the values obtained for* BT2003, ±30%, 5 GMs/set, and cycle-and-shift algorithm** The results of five GMs per set are used as a reference. They are obtained with the cycle-and-shift algorithm and are selected with a target spectrum of BT2003 and ±30% symmetric tolerances. Intraset variability is included.

In order to quantify the impact of using various amounts of GMs per set, statistical analysis is performed, and changes in PSAs, Δtop, and Vbase estimates are given in Table 1.11.1. Mean PSAs, Δtop, and Vbase estimates experience a maximum decrease of 17%, 8%, and 8%, respectively. COV estimates usually decrease as a function of the number of GMs per set. Overall, using more GMs per set decreases the mean estimates slightly as much as 8% and the COV estimates as much as 60% when intraset variability is used.

GMs per set	λ	Amount of GM Sets	PSA at 1.00 Hz (cm/s²)						Δtop of SDOF-R2 (cm)					
			$\overline{PSA_{fo}}^{set}$			$\sigma^{set}_{PSA.fo}$			$\overline{\Delta top}^{set}$			$(\overline{\Delta top} + \lambda\sigma_{\Delta top})^{set}$		
			Mean		COV	Mean		COV	Mean		COV	Mean		COV
5	0.95	21 942	119		0.13	73		0.31	2.7		0.14	4.1		0.22
7	0.73	31 431	119	(0%)	0.12	79	(8%)	0.41	2.8	(4%)	0.14	4.1	(0%)	0.24
11	0.55	31 382	119	(0%)	0.10	77	(4%)	0.41	2.8	(6%)	0.12	3.8	(-8%)	0.20
13	0.49	31 911	120	(1%)	0.10	78	(6%)	0.40	2.8	(7%)	0.11	3.8	(-8%)	0.18
19	0.38	27 501	122	(3%)	0.09	76	(3%)	0.27	2.9	(10%)	0.09	3.7	(-11%)	0.14
23	0.34	25 000	125	(5%)	0.08	77	(5%)	0.25	3.0	(12%)	0.08	3.7	(-11%)	0.11
29	0.34	20 009	127	(7%)	0.07	78	(6%)	0.22	3.0	(15%)	0.06	3.7	(-9%)	0.08

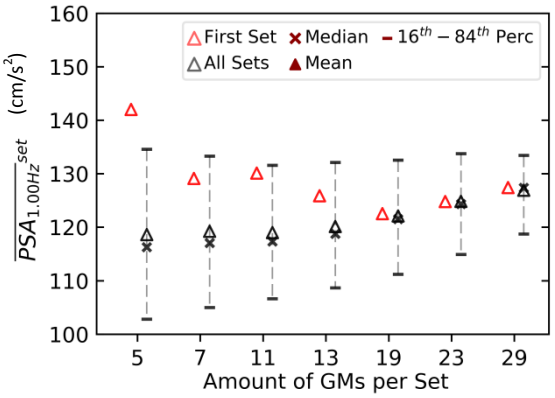

Figure A.8.1: Δtop estimates of SDOF-R2 at 1.00 Hz when different amount of GMs per set is used. Same-event and same-station records in a set are allowed because there are not any available sets for 11 GMs per set and more.

Mean Δtop estimates of the first set are shown in red color and distribution of Δtop estimates of all sets are shown in black color for a different amount of GMs per set. Estimates without and with intraset variability are given. Medians are shown with a cross marker. Means are shown with triangle markers. 16th and 84th percentiles are marked with a horizontal line.

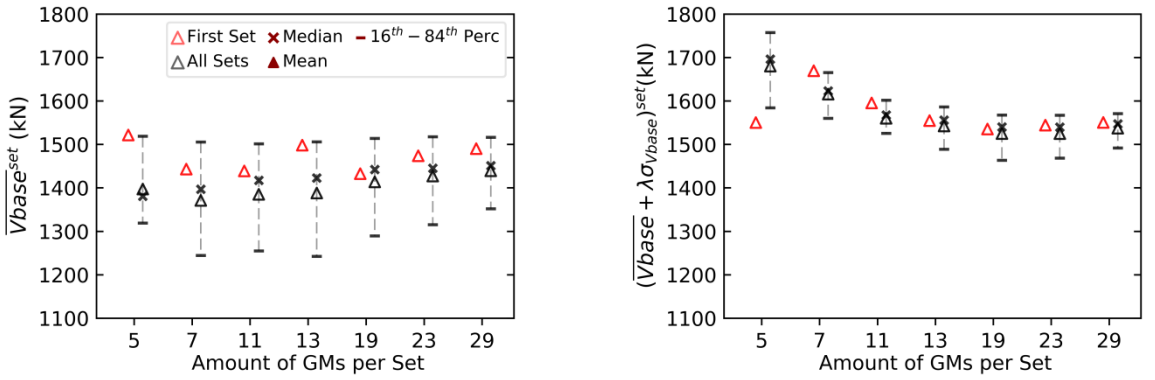

(a)Intraset of average

(b)Intraset of average plus percentile of std. deviation

Figure A.8.2: Δtop estimates of SDOF-R2 at 1.00 Hz when different amount of GMs per set is used.
Same-event and same-station records in a set are allowed because there are not any available sets for 11 GMs per set and more. Intraset variability is determined as stated in ASN/2/01 (2006) such as average plus λ of standard deviation, where λ is calculated according to Fisher's student method. λ is 95%, 73%, 55%, 49%, 38%, 34%, and 34% for 5, 7, 11, 13, 19, 23, and 29 GMs per set, respectively.

Mean Δtop estimates of the first set are shown in red color and distribution of Δtop estimates of all sets are shown in black color for a different amount of GMs per set. Estimates without and with intraset variability are given. Medians are shown with a cross marker. Means are shown with triangle markers. 16th and 84th percentiles are marked with a horizontal line.

APPENDIX B

ADDITIONAL ELEMENTS FOR PART 2

B.1 Refinement of Spectrum-Matched Ground Motions (Methods C and D)

(a) Time-Histories | (b) Response Spectra | (c) Modification Process

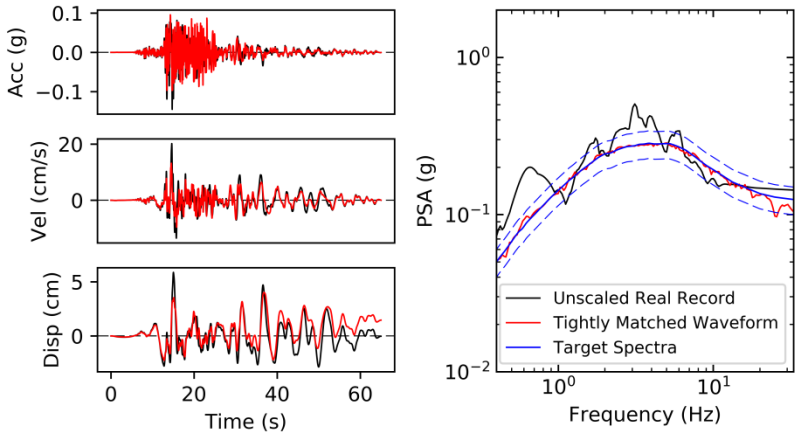

The goal is to match the unscaled real record within ±20% of the target spectrum from 0.30 Hz to 33.00 Hz. RSPMatch09 is used with a convergence damping factor of 1.0, a group size of 60, and a linear PGA scaling.

After the spectrum matching:

(i) The maximum reported misfit is 14% by the software, and the apparent misfit is above the limit around 22.0 Hz, which is tolerated.

(ii) Residual displacement of 1.5 cm is observed.

Conclusion: The generated waveform is not eligible.

Figure B.1.1: Time- and frequency-domain characteristics of the unscaled earthquake record and the tightly spectrum-matched GM with the residual displacement in Method D. The record is from the Petrolia earthquake (89509 station) in California with Mw 7.0, R_{hypo} 39 km, and Vs30 519 m/s. Method D (RSPMatch09) modifies the GMs with respect to the target, which is the median of AK2014 for the scenario of M7.0R40 and Vs450. Column (a) shows the acceleration, velocity, and displacement time-histories of the unscaled record in black and the spectrum-matched waveform in red. In column (b), the manipulation of the spectral shape is shown.

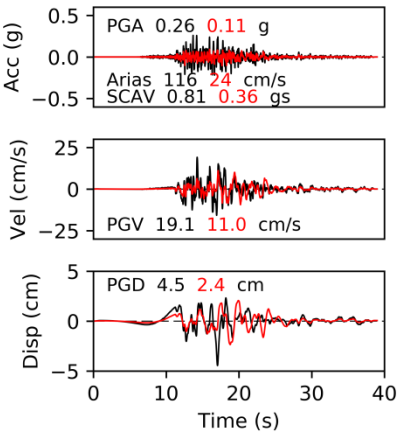

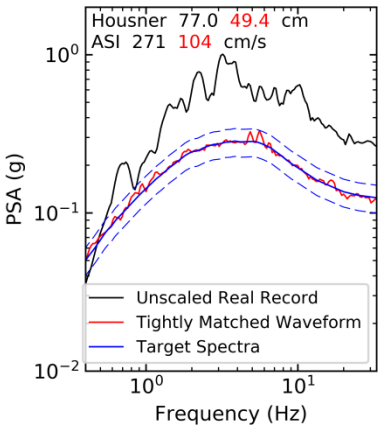

The goal is to match the unscaled real record within ±20% of the target spectrum from 0.30 Hz to 33.00 Hz. RSPMatch09 is used with a convergence damping factor of 1.0, a group size of 60, and a linear PGA scaling.

After the spectrum matching:

(i) The maximum misfit is 19%, less than 20%.

(ii) The time-histories have zero units at its both ends.

(iii) The change in Arias is 0.21, below the permitted lower limit, 0.30.

(iv) The IMs are within the observed range.

Conclusion: The generated waveform is not selected due to the extreme decrease in Arias intensity.

Figure B.1.2: Time- and frequency-domain characteristics of the unscaled earthquake record and the uneligible tightly spectrum-matched GM in Method D. The record is from the Hawaii earthquake (20061510_0707, station 02810) with Mw 6.7, and R_{hypo} 35 km. Method D modifies the GMs with respect to the target, which is the median of AK2014 for the scenario of M7.0R40 and Vs450. Column (a) shows the acceleration, velocity, and displacement time-histories of the unscaled record in black and the spectrum-matched waveform in red. In column (b), the manipulation of the spectral shape is shown. The added wavelets (by the software) result in the significant change in the acceleration and the velocity histories. The reason why the displacement history is slightly affected is the frequency content of the displacement history (0.10—0.20 Hz) being below the lower limit. In column (c), the modification process is explained along with the justification.

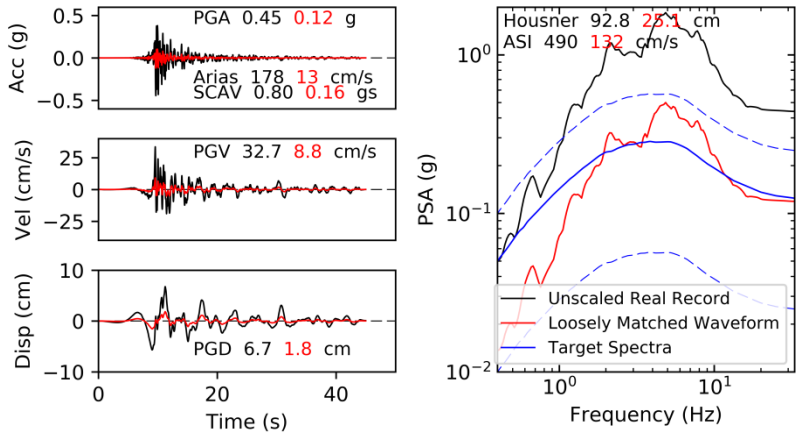

The goal is to match the unscaled real record between 20% and 200% of the target from 0.30 Hz to 33.00 Hz. RSPMatch09 is used with a convergence damping factor of 0.15, a group size of 60, and a linear PGA scaling.

After the spectrum matching:

(i) The spectrum is within the allowed PSAs highlighted with the blue dashed lines.

(ii) There is no residual in the time-histories.

(iii) Change in Arias intensity is 0.07, less than the lower limit of 0.30.

(iv) The IMs are within the observed range.

Conclusion: The generated waveform is not selected due to the extreme decrease in Arias intensity.

Figure B.1.3: Time- and frequency-domain characteristics of the unscaled earthquake record and the uneligible loosely spectrum-matched GM in Method C. The record is from the Loma Prieta earthquake (station 47381) with Mw 6.9, R_{hypo} 36 km, and Vs30 278 m/s. Methods C modifies the GMs with respect to the target, which is the median of AK2014 for the scenario of M7.0R40 and Vs450. The allowed PSAs are plotted with the blue dashed lines. Column (a) shows the acceleration, velocity, and displacement time-histories of the unscaled record in black and the spectrum-matched waveform in red. In column (b), the spectral shapes are compared. The changes in spectra and time-histories are extreme; in other words, the characteristics of the unmodified GM are not conserved. In column (c), the modification process is explained.

B.2 Parameters used in RSPmatch09

The explanation of the technical parameter required by spectrum matching is provided in the user manual of RSPMatch09 (Al Atik and Abrahamson, 2010). The folders and files are organized in a certain way to launch the spectrum matching. The main folder includes a target spectrum (in a compatible format with an extension of ".tgt"), an unscaled earthquake record (in a compatible format with an extension of ".acc"), and the main code to call RSPMatch09 (labeled as "All_Files.inp"). Also, two folders named as "Inp" (including four ".inp" codes to be loaded at each pass) and "Out" (saving the spectrum matched waveforms at each pass) are created. In Methods C and D, the following parameters are used:

- improved tapered cosine function (method 7),
- PGA scaling only at the first phase,
- group size of 30,
- spectral matching between 0.30 and 33.00 Hz,
- convergence damping factor of 0.15 and convergence tolerance of 100% for Method C, and
- convergence damping factor of 1.00 and convergence tolerance of 20% for Method D.

Two parameters cause the differences between Methods C and D: the convergence damping factor and the convergence tolerance. In Figures B.2.1, B.2.2, B.2.3, B.2.4 and B.2.5, an example of Method C with the main code loading four sub-codes at each pass are provided. Target spectrum is obtained by BT2003 for M7.0R40 and Vs30 450 m/s. It is labeled as "BT2003_mag7.0_dist40_Vs450.tgt". "CESMD___20061510_0707__02810__Chan01_360.acc" is the unscaled earthquake record.

```
4                    ! Total number of passes
Inp/RUN1.inp
Inp/RUN2.inp
Inp/RUN3.inp
Inp/RUN4.inp
```

Figure B.2.1: The script in All_Files.inp

```
20              \Maximum no. of iterations
1.0             \Tolerance for maximum mismatch (in fraction of target)
0.15              \Convergence damping
7                     \Model (1, 6 or 7)
1.25 0.25 1.0 4.0     \Alpha model, a1, a2, f1, f2 (not used for models 1 or 7)
2  0.           \Scale flag, scale period to PGA  (=0 no, =1 yes, =2 yes but once)
1               \Interpolate to 1/dtFlag of the input time step
1.0e-04           \Minimum eigenvalue
60              \Group size
34.             \Max freq
0.0 0.0 4         \FBand, nPole (deactivated for model 7
0               \Mod PGA (1=yes) (deactivated for model 7
0  0.0            \Randomize target? (iSeed, ranFactor)
1.0  33                       \FreqMatch
0                               \Baseline cor flag (1=yes) (deactivated for model 7)
1.0                           \Scale factor
BT2003_mag7.0_dist40_Vs450.tgt
CESMD___20061510_0707__02810__Chan01_360.acc
Out/Run1.acc
Out/Run1.rsp
Out/Run1.unm
```

Figure B.2.2: The script in Inp/Run1.inp

```
20                  \Maximum no. of iterations
1.0                 \Tolerance for maximum mismatch (in fraction of target)
0.15                \Convergence damping
7                   \Model (1, 6 or 7)
1.25 0.25 1.0 4.0   \Alpha model, a1, a2, f1, f2 (not used for models 1 or 7)
0  0.               \Scale flag, scale period to PGA  (=0 no, =1 yes, =2 yes but once)
1                   \Interpolate to 1/dtFlag of the input time step
1.0e-04             \Minimum eigenvalue
60                  \Group size
34.                 \Max freq
0.0 0.0 4           \FBand, nPole (deactivated for model 7
0                   \Mod PGA (1=yes) (deactivated for model 7
0  0.0              \Randomize target? (iSeed, ranFactor)
0.75  33            \FreqMatch
0                   \Baseline cor flag (1=yes) (deactivated for model 7)
1.0                 \Scale factor
BT2003_mag7.0_dist40_Vs450.tgt
Out/Run1.acc
Out/Run2.acc
Out/Run2.rsp
Out/Run2.unm
```

Figure B.2.3: The script in Inp/Run2.inp

```
20                  \Maximum no. of iterations
1.0                 \Tolerance for maximum mismatch (in fraction of target)
0.15                \Convergence damping
7                   \Model (1, 6 or 7)
1.25 0.25 1.0 4.0   \Alpha model, a1, a2, f1, f2 (not used for models 1 or 7)
0  0.               \Scale flag, scale period to PGA  (=0 no, =1 yes, =2 yes but once)
1                   \Interpolate to 1/dtFlag of the input time step
1.0e-04             \Minimum eigenvalue
60                  \Group size
34.                 \Max freq
0.0 0.0 4           \FBand, nPole (deactivated for model 7
0                   \Mod PGA (1=yes) (deactivated for model 7
0  0.0              \Randomize target? (iSeed, ranFactor)
0.5  33             \FreqMatch
0                   \Baseline cor flag (1=yes) (deactivated for model 7)
1.0                 \Scale factor
BT2003_mag7.0_dist40_Vs450.tgt
Out/Run2.acc
Out/Run3.acc
Out/Run3.rsp
Out/Run3.unm
```

Figure B.2.4: The script in Inp/Run3.inp

```
20                  \Maximum no. of iterations
1.0                 \Tolerance for maximum mismatch (in fraction of target)
0.15                  \Convergence damping
7                         \Model (1, 6 or 7)
1.25 0.25 1.0 4.0       \Alpha model, a1, a2, f1, f2 (not used for models 1 or 7)
0  0.               \Scale flag, scale period to PGA  (=0 no, =1 yes, =2 yes but once)
1                   \Interpolate to 1/dtFlag of the input time step
1.0e-04               \Minimum eigenvalue
60                  \Group size
34.                 \Max freq
0.0 0.0 4             \FBand, nPole (deactivated for model 7
0                   \Mod PGA (1=yes) (deactivated for model 7
0  0.0              \Randomize target? (iSeed, ranFactor)
0.3  33                             \FreqMatch
0                                     \Baseline cor flag (1=yes) (deactivated for model 7)
1.0                                 \Scale factor
BT2003_mag7.0_dist40_Vs450.tgt
Out/Run3.acc
Out/Run4.acc                                  \End result: Spectrum matched waveform
Out/Run4.rsp
Out/Run4.unm
```

Figure B.2.5: The script in Inp/Run4.inp

B.3 Impact of Ground Motion Modification in Intensity Measures

Table B.3.1: Intensity measures in Methods A, B, C, and D.

Intensity Measure	Method A (73 Records)		Method B at 1.00 Hz (52 GMs)		Method B at 2.50 Hz (45 GMs)		Method C (24 GMs)		Method D (14 GMs)	
	Mean	COV	Mean	COV	Mean	COV	Mean	COV	Mean	COV
PGA (g)	0.18	0.58	0.21	0.79	0.13	0.43	0.12	0.08	0.11	0.09
PGV (cm/s)	19.0	0.81	16.7	0.41	13.5	0.52	10.5	0.34	11.7	0.14
PGD (cm)	8.1	1.71	5.8	0.59	5.8	0.82	3.5	0.43	4.3	0.32
Arias (cm/s)	61.0	1.11	89.6	1.73	37.6	0.93	30.9	0.46	29.0	0.15
SCAV (gs)	0.59	0.76	0.66	0.70	0.50	0.57	0.48	0.54	0.45	0.20
ASI (cm/s)	161	0.56	195	0.74	118	0.29	119	0.12	104	0.01
Housner (cm)	64.9	0.71	56.0	0.26	48.9	0.48	42.3	0.34	48.0	0.01
PSA at 1.0 Hz (g)	0.18	0.81	0.14	0.00	0.14	0.57	0.13	0.45	0.14	0.04
PSA at 2.5 Hz (g)	0.41	0.68	0.49	0.99	0.26	0.00	0.30	0.24	0.27	0.05

Method B at 1.0 Hz is scaled to the target PSA at 1.0 Hz. Method B at 2.5 Hz is scaled to the target PSA at 2.5 Hz. The target is the median of AK2014 for the scenario of M7.0R40, Vs450, and normal fault. Amount of ground motions is noted for each method.

The observed IMs in MA have a considerable variability: the largest for PGD with a COV of 1.71 and the least for ASI with a COV of 0.56. MB and MC reveal comparable variability with MA except for PSAs at the scaling frequency (at 1.00 Hz and 2.50 Hz) in MB and PGA in MC. (e.g., the COVs range between 0.09 and 0.32).

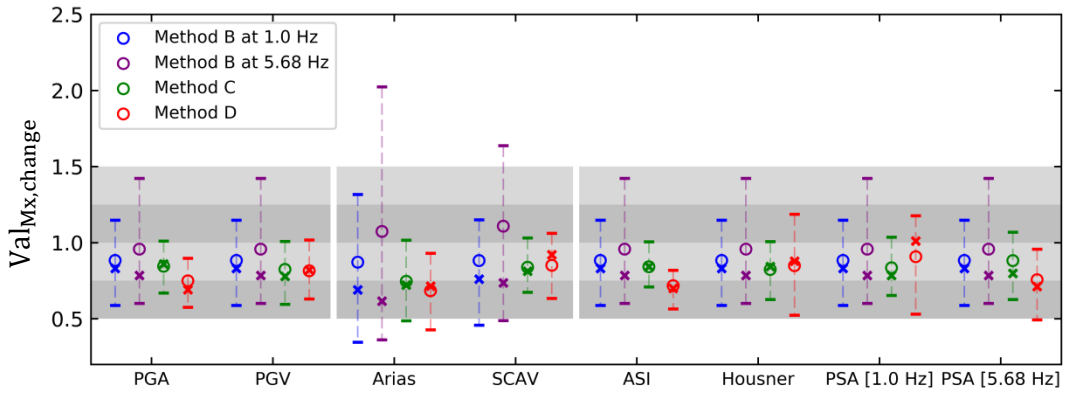

Figure B.3.1: The change of intensity measures (IMs) of ground motions (GMs) in Methods B, C, and D with respect to Method A. The change is defined as a ratio of IMs of the modified ground motion (GM) and the unmodified GM. Values greater than 1.0 represents an increase in IM with respect to the unscaled real record in Method A and vice versa. The 16th and 84th percentiles of the distribution are shown with the horizontal bars. The median and the mean of the distribution are shown with the cross marker and the unfilled circle. The modifications in Methods B, C, and D are applied according to the median of **BA2011** for the scenario of M7.0R40, Vs450, and normal fault. Method B at 1.0 Hz is scaled to the target PSA at 1.0 Hz. Method B at 2.5 Hz is scaled to the target PSA at 2.5 Hz.

For Method B, the refinement is applied with a scaling factor limit between 0.5 and 2.0. For Methods C and D, the refinement is applied with a change limit of Arias intensity between 0.3 and 1.7. The mean change of IMs is between 0.70 and 1.10. The duration-based IMs such as Arias and SCAV are amplified the most by MB at 5.68 Hz. On average, the change of the IMs is the least with MB at 5.68 Hz. MC has the most consistent dispersion in the changes in the IMs.

B.4 Complex Structural Models

B.4.1 S1 Model: 8-Story RC Structure

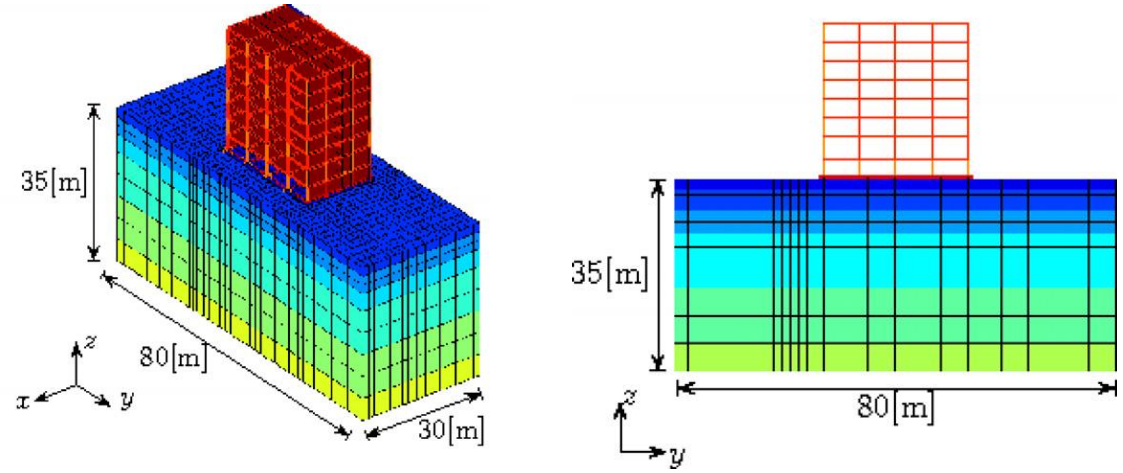

(a) 3D Approach (b) 2D Simplified Approach

Figure B.4.1: The finite model of the S1 model (Saez et al., 2011). 2D simplified approach (with the moment resisting frame and the elastic fixed-base) is used in this study.

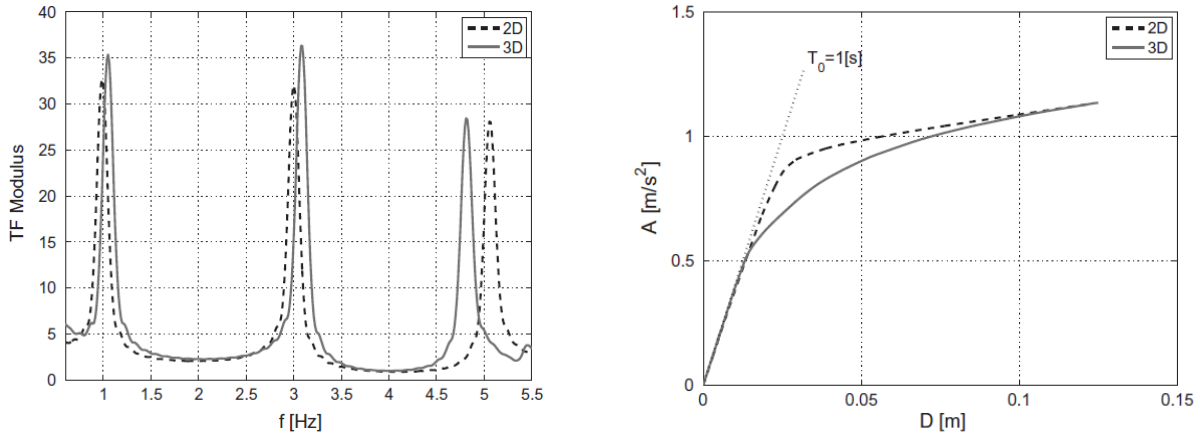

(a) Elastic fixed-base transfer function modulus (b) Capacity curve

Figure B.4.2: Verification of a 2D equivalent model of S1 (Saez et al., 2011). 2D approach (with the moment resisting frame) is used in this study. The oscillation frequencies at the first and second modes are 1.00 Hz and 3.00 Hz, respectively.

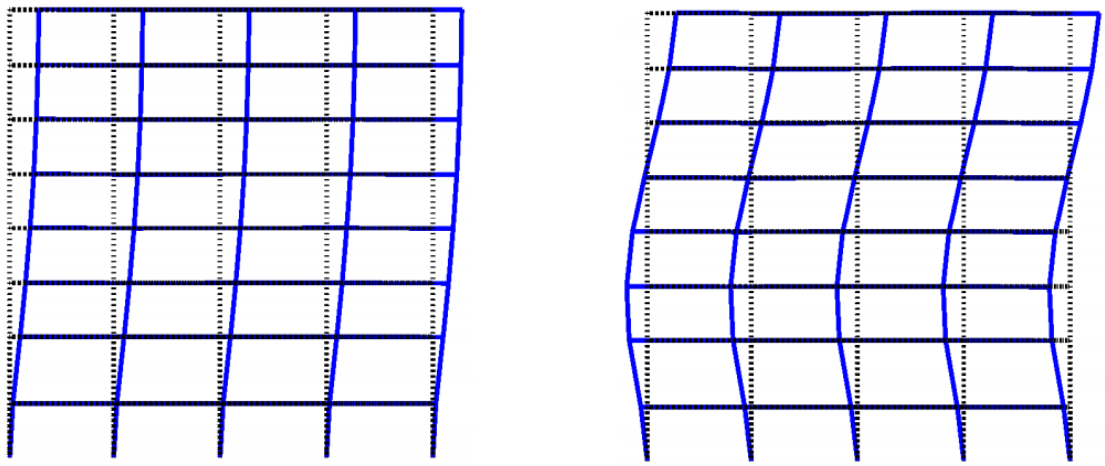

(a) First Modal Shape at f0= 1.00 Hz (b) Second Modal Shape at f1= 3.00 Hz

Figure B.4.3: First two modal shapes of the S1 model

B.4.2 S2 Model: 7-Story RC Structure

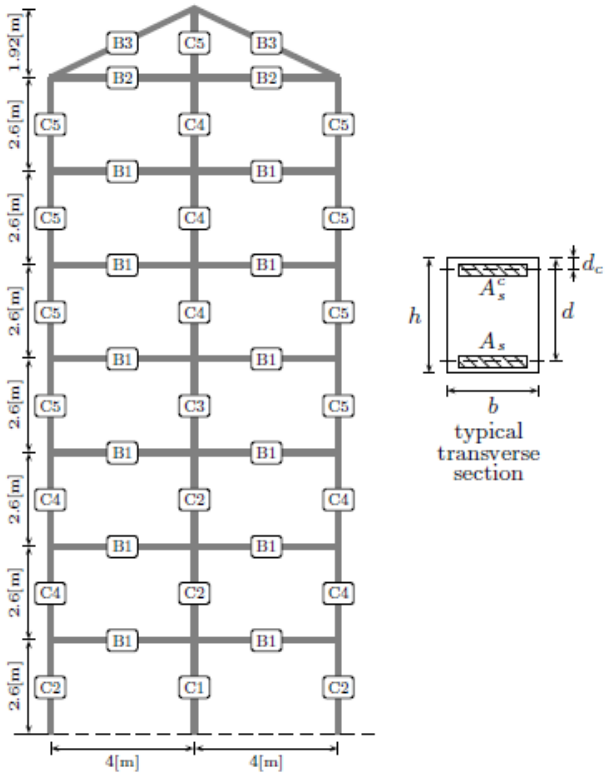

(a) Geometry

Label	h[m]	b_s[m]	d_c[m]	d_s[m]	A_s[cm2]	A_s^c[cm2]	ρ[kg/m3]
B1	0.6	0.3	0.04	0.56	25.34	25.34	34900
B2	0.7	0.3	0.04	0.66	11.40	11.40	30285
B3	0.3	0.2	0.04	0.26	8.55	8.55	70500
C1	0.6	0.5	0.04	0.56	40.54	40.54	-
C2	0.6	0.5	0.04	0.56	30.95	30.95	-
C3	0.6	0.4	0.04	0.56	40.54	40.54	-
C4	0.6	0.4	0.04	0.56	30.95	30.95	-
C5	0.6	0.4	0.04	0.56	14.41	14.41	-

(b) Traverse section properties

Mechanical property	Symbol	Value
Resistance to compressive stresses	f_c	25[MPa]
Yield stress of steel	f_y	440[MPa]
Ultimate stress of steel	f_{s_u}	596[MPa]
Elastic modulus of steel	E_s	200[GPa]
Elastic modulus of concrete	E_c	25.5[GPa]
Crushing strain of concrete	ε_c	0.003

(c) Mechanical properties

Figure B.4.4: Description of the S2 model (Adapted from Saez, 2009)

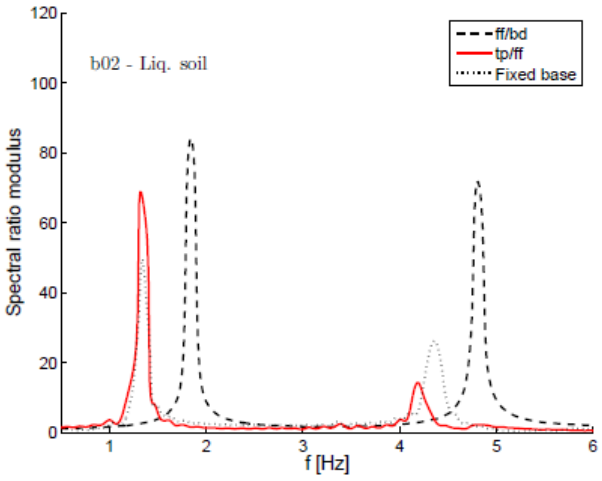

Figure B.4.5: Obtained spectral ratios for the S2 model on elastic fixed-base (Adapted from Saez, 2009). Elastic fixed-base shown in the grey dashed lines is the concern of this study. The oscillation frequencies at the first and second modes are 1.32 Hz and 4.35 Hz, respectively.

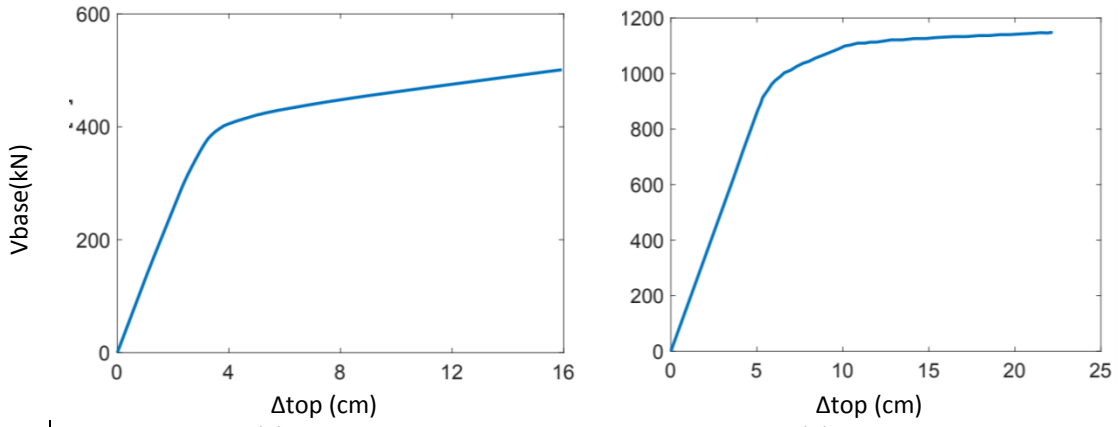

(a) S1 Model (b) S2 Model

Figure B.4.6: Push-over curves for the S1model in (a) and the S2 model in (b).

B.4.3 S3 Model: 2-Story RC Structure

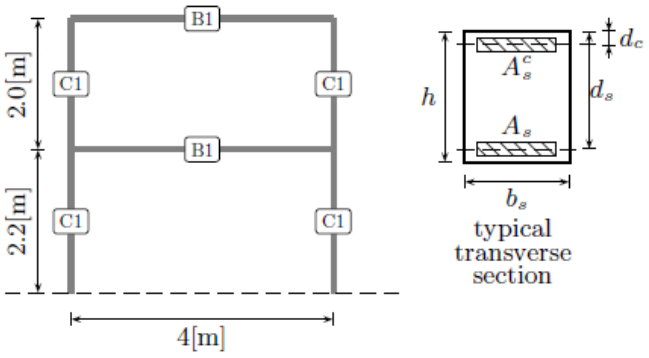

(a) Geometry

Label	h[m]	b_s[m]	d_c[m]	d_s[m]	A_s[cm2]	A_s^c[cm2]	ρ[kg/m3]
B1	0.4	0.3	0.03	0.37	11.4	11.4	42473
C1	0.4	0.4	0.02	0.38	11.4	11.4	-

(b) Traverse section properties

Mechanical property	Symbol	Value
Resistance to compressive stresses	f_c	30[MPa]
Yield stress of steel	f_y	418[MPa]
Ultimate stress of steel	f_{s_u}	596[MPa]
Elastic modulus of steel	E_s	210[GPa]
Elastic modulus of concrete	E_c	26.5[GPa]
Crushing strain of concrete	ε_c	0.0034

(c) Mechanical properties

Figure B.4.7: Description of the S3 model (Adapted from Saez, 2009)

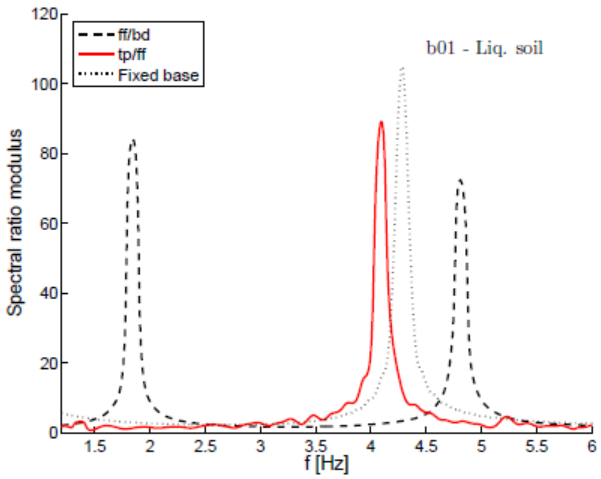

Figure B.4.8: Obtained spectral ratios for the S3 model with the elastic-fixed base (Saez, 2009). Elastic fixed-base shown in grey dashed lines is the concern of this study. The oscillation frequency at the first mode is 4.17 Hz.

B.4.4 S4 Model: 2-Story Masonry Structure

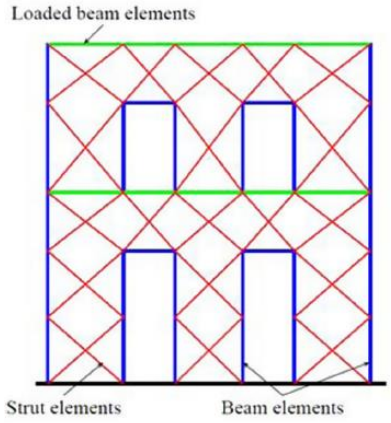

Figure B.4.9: Geometry and modeled elements of the S4 model (Lopez-Caballero et al., 2011).

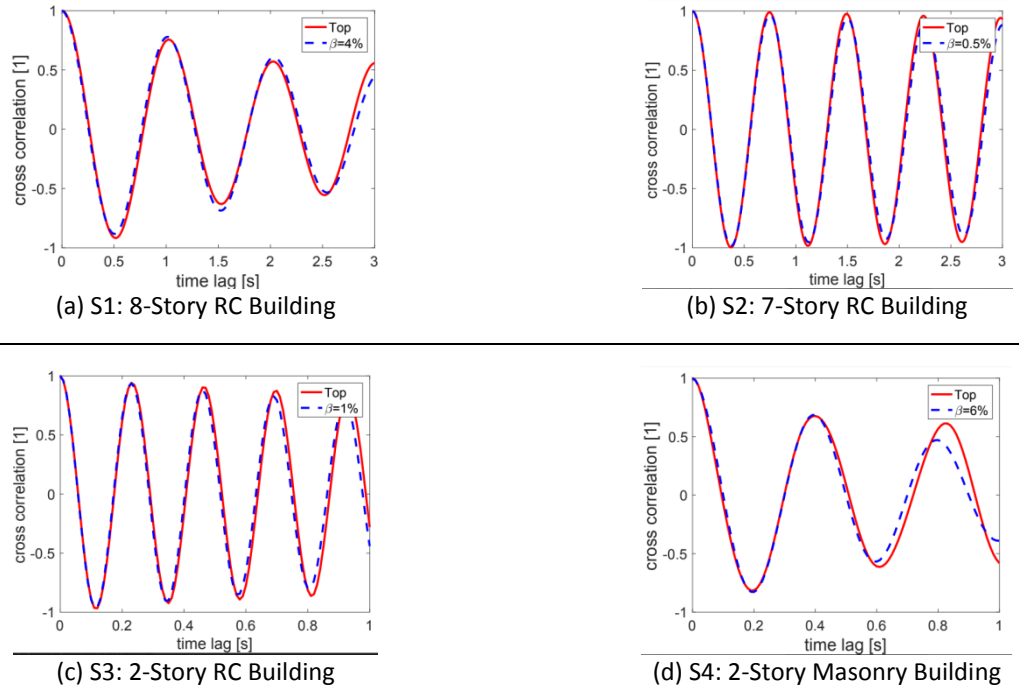

(a) S1: 8-Story RC Building

(b) S2: 7-Story RC Building

(c) S3: 2-Story RC Building

(d) S4: 2-Story Masonry Building

Figure B.4.10: Evaluation of damping ratios under an unscaled earthquake record. The x-axis represents the time lag in seconds. The y-axis is the cross-correlation. The red curve represents the cross-correlation of roof displacement (Δtop). The blue dashed curve represents the fitted damping ratio (β). The record is the Loma Prieta Earthquake (station of 47006) with Mw 7.1, Rhypo 34 km, and Vs30 730 m/s. For the given record, the damping ratios are 4%, 0.5%, 1%, and 6% for the S1, S2, S3, and S4 models, respectively.

B.4.5 S5 Model: 1-Story RC Structure

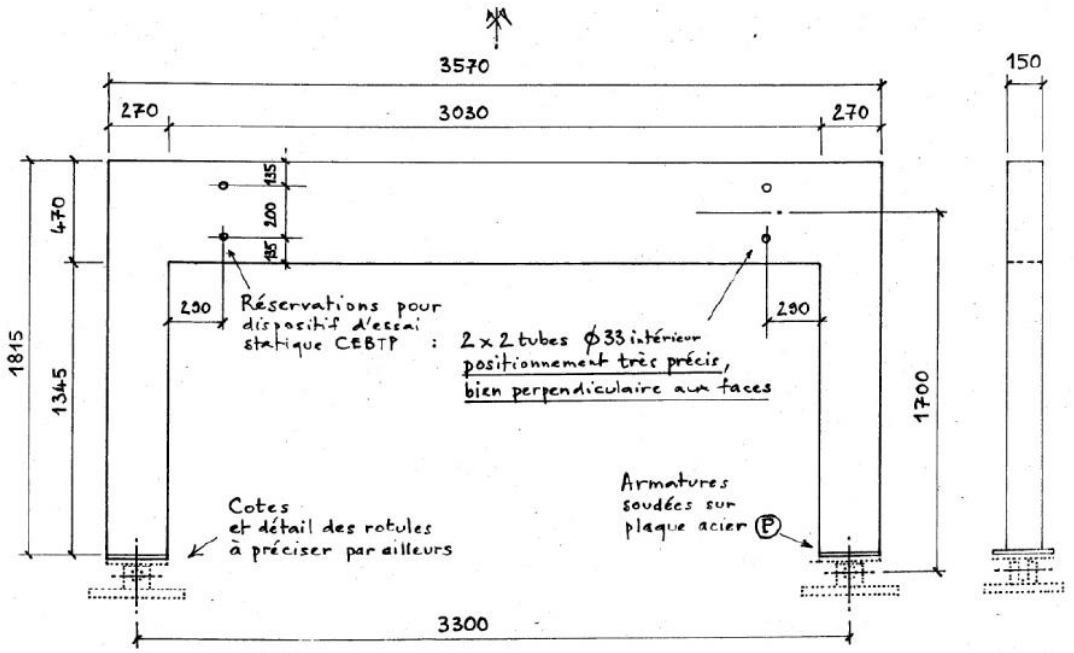

Figure B.4.11: Geometry of the model (CEA Report 2007). Units are in mm. Compression strength of the concrete is 30 MPa. Splitting tensile strength is 2.65 MPa. Young's modulus is 28 500 MPa. The reinforcement details are given in the reference.

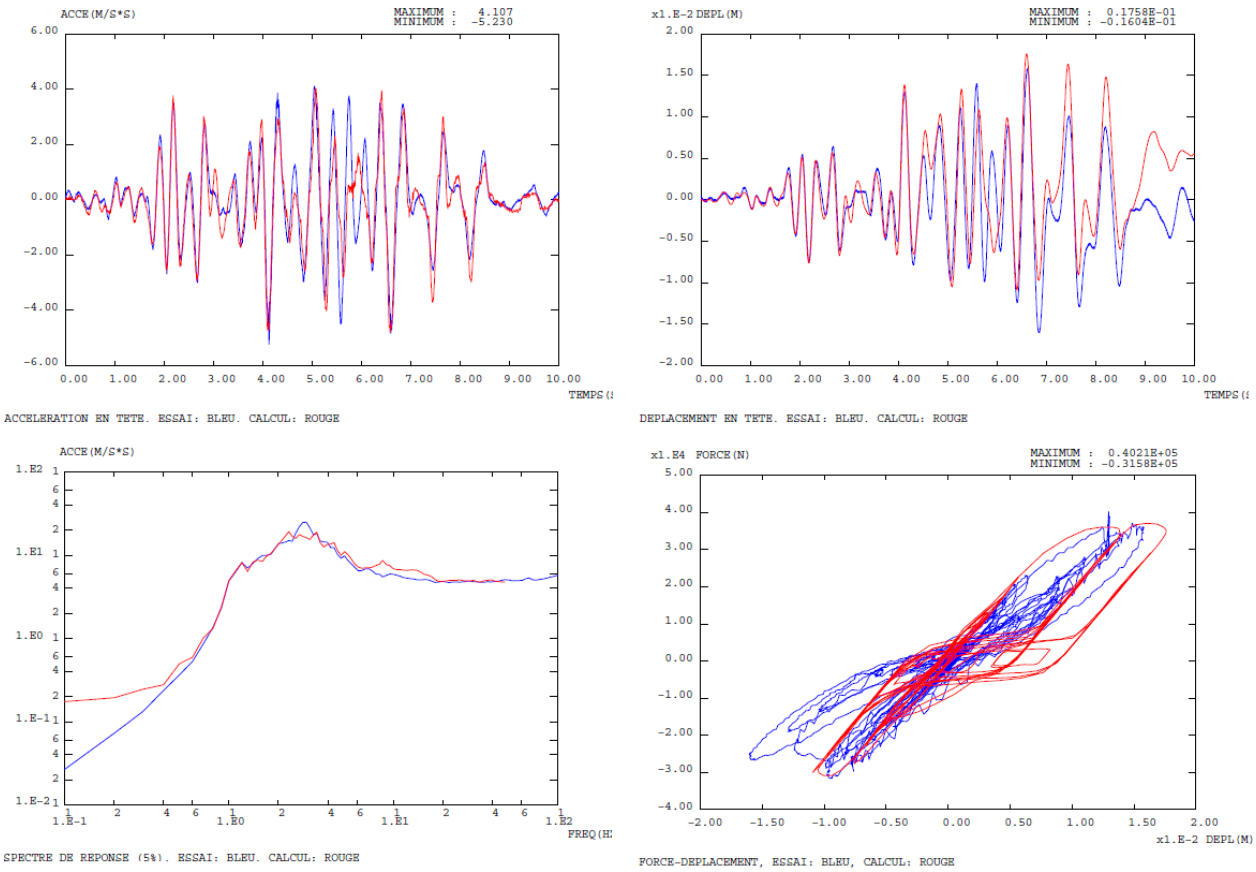

Figure B.4.12: Comparison of the experimental results in blue and the numerical modeling results in red (CEA Report 2007).

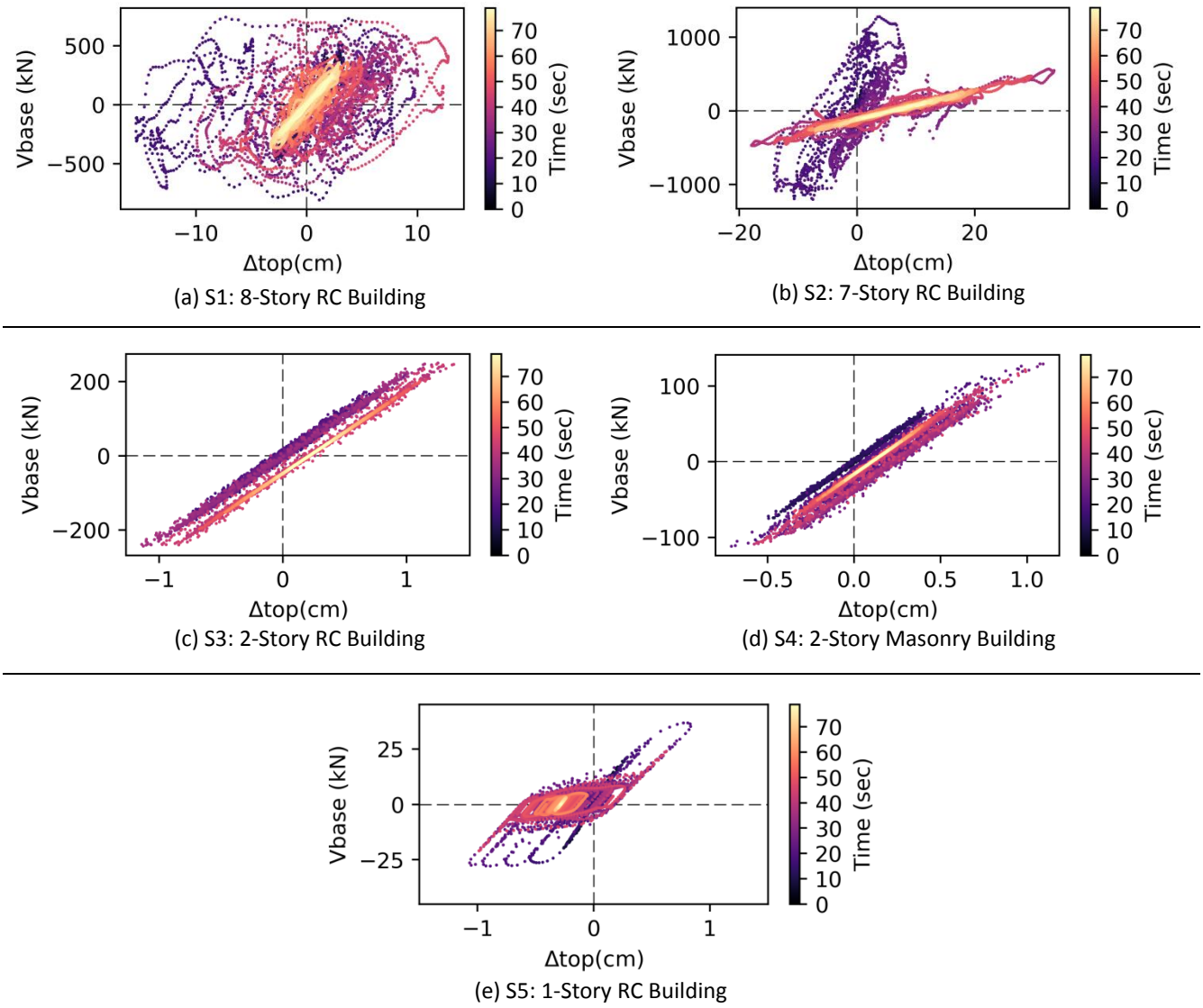

Figure B.4.13: Response histories of the complex model under an unscaled earthquake record. The x-axis represents the roof displacements relative to the ground (Δtop). The y-axis is the sum of base shear forces (Vbase). The color of the curve relates to the period of time given in the legend: the darker colors represent the initial part, and the lighter colors represent the final part. Positive and negative values signify the direction of the movement. The record is the Duzce Earthquake (station of 4100_3104) with Mw 7.1 and Rhypo 34 km.

B.5 Structural Responses of Simple Structural Models

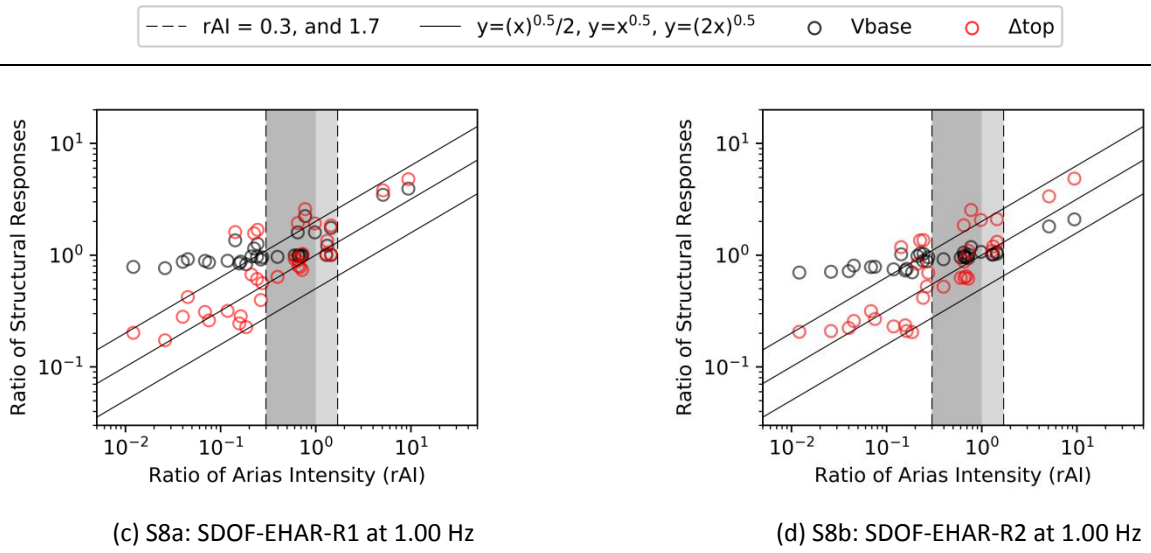

(c) S8a: SDOF-EHAR-R1 at 1.00 Hz

(d) S8b: SDOF-EHAR-R2 at 1.00 Hz

Figure B.5.1: Comparison of the ratio of Arias intensity (rAI) in Method D and the corresponding change in structural responses of the simple models. The x- and y-axes are in logarithmic scale. The change in Vbase at the corresponding rAI is plotted with the black circles. The change in Δtop at the corresponding rAI is plotted with green circles. The change is defined according to Equation 2.3.1, the ratio between a structural response in Method D and the corresponding response in Method A. rAI greater than the unity implies an amplification of Arias intensity and vice versa. The ratio of the response greater than the unity implies an increase in the structural response and vice versa. Each data represents a tightly spectrum-matched GM according to the target, the median of AK2014 for the scenario of M7.0R40, Vs450, and normal fault. The permitted level of rAI is between 0.3 and 1.7. The S8a model is designed to resist the lateral design forces linearly. The S8b model is designed for half of the lateral design forces and exhibits an inelastic behavior at the lateral design forces.

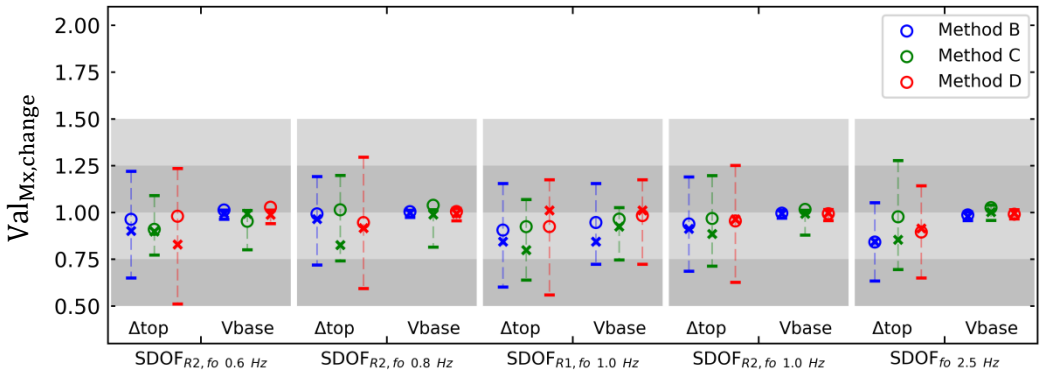

Figure B.5.2: The change in structural responses of simple models in Methods B, C, and D with respect to Method A. The change is defined as a ratio of the structural response of the modified ground motion (GM) and the unmodified GM in Method A. Values greater than 1.0 represents an increase in structural response with respect to Method A and vice versa. The 16th and 84th percentiles of the distribution are shown with the horizontal bars. The median and the mean of the distribution are shown with the cross marker and the unfilled circle. The target is the median of **BA2011** for the scenario of M7.0R40, Vs450, and normal fault. The changes in maximum absolute of the base shear forces (Vbase) and the maximum absolute of the roof displacements (Δtop) are shown. There are about 50 GMs in Method B, 24 GMs in Method C, and 14 GMs in Method D.

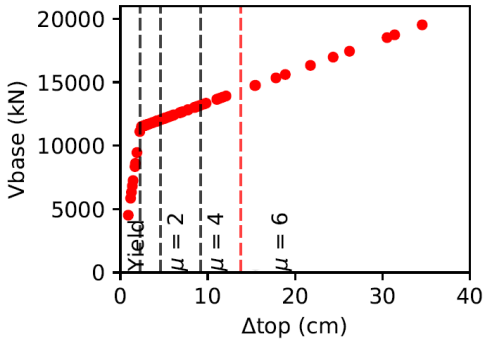

(a) S6: SDOF-R2 at 0.60 Hz

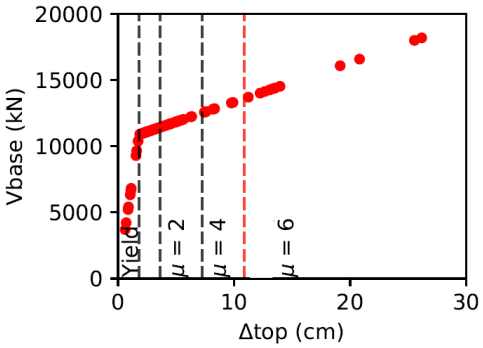

(b) S7: SDOF- R2 at 0.80 Hz

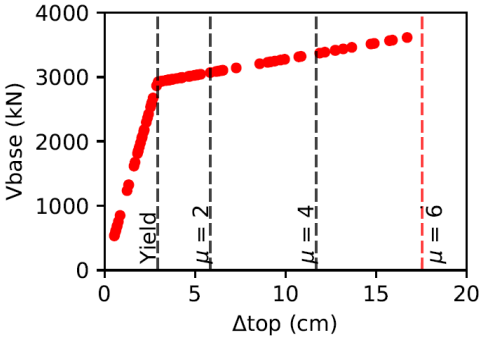

(c) S8a: SDOF-R1 at 1.00 Hz

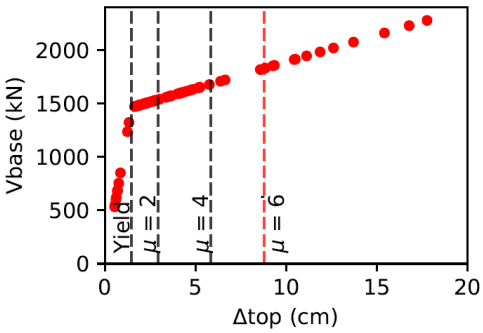

(d) S8b: SDOF-R2 at 1.00 Hz

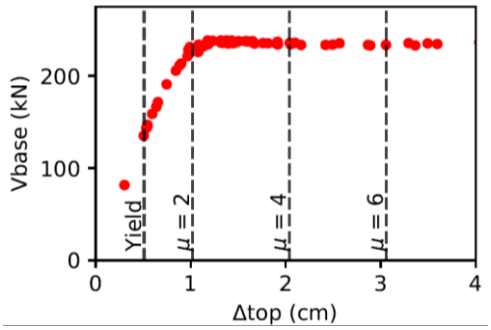

(e) S9: SDOF-R2 at 2.50 Hz

Figure B.5.3: Structural responses of the simple models under unscaled earthquake records (Method A). The structural responses are shown with red circles. The x-axis shows the maximum absolute of the lateral structural displacements (Δtop). The y-axis shows the maximum absolute of the base shear forces (Vbase). The amount of GMs is given in the legend box. The yielding limit and displacement ductility levels, μ, at 2, 4, and 6 are plotted with the vertical dashed lines.

B.6 Structural Responses of Complex Structural Models

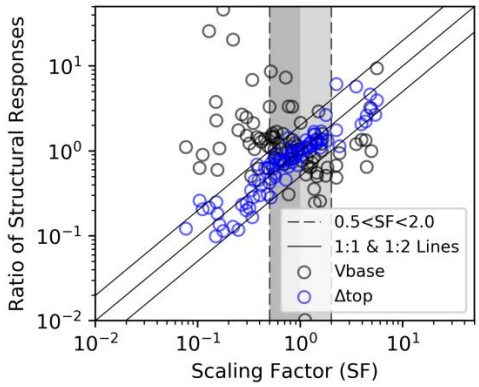

(a) S1: 8-Story RC Model

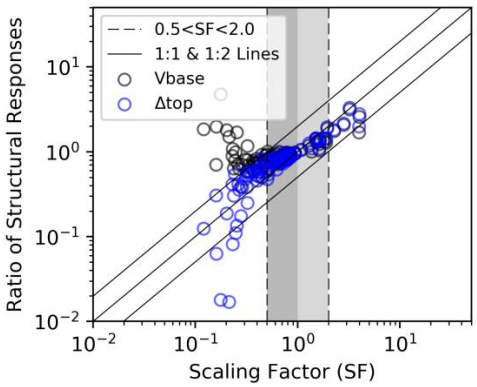

(b) S4: 2-Story Masonry Model

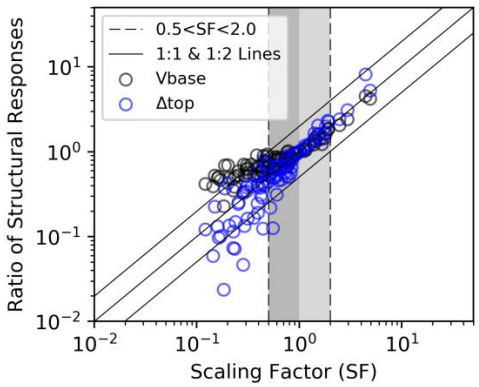

(c) S5: 1-Story RC Model

Figure B.6.1: The comparison of scaling factor (SF) in Method B and the corresponding changes in structural responses of the complex models. The x- and y-axes are in logarithmic scale. The change in Vbase at the corresponding SF is plotted with the black circles. The change in Δtop at the corresponding SF is plotted with blue circles. The 1:1, 1:2, and 2:1 lines are shown with the solid black lines. Each data represents GM scaled to the target PSA at f0. The SF greater than the unity imply an amplification of the signal characteristics and vice versa. The ratio of the response greater than the unity implies an increase in the structural response and vice versa. The base shear forces (Vbase) are obtained at the time of maximum absolute of the roof displacements (Δtop). The change is defined according to Equation 2.3.1, the ratio between a structural response in Method B and the corresponding response in Method A. The target is the median of AK2014 for the scenario of M7.0R40, Vs450, and normal fault. The permitted level of SF is between 0.5 and 2.0 as shown with the vertical dashed lines. The models (described in Section 2.4.2) have f0 of 1.00 Hz in (a), 4.17 Hz in (b) and 5.68 Hz in (c).

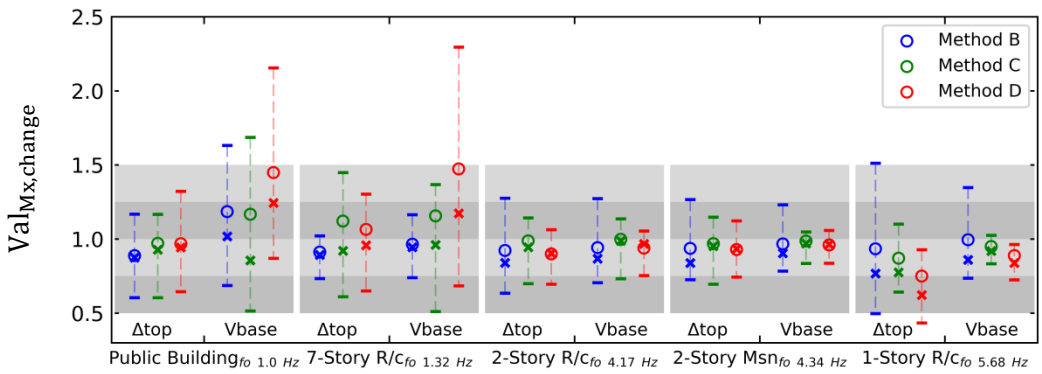

Figure B.6.2: The change in structural responses of complex models in Methods B, C, and D with respect to Method A. The change is defined as a ratio of the structural response of the modified GM and the unmodified GM in Method A. (Continued)

Values greater than 1.0 represents an increase in structural response with respect to Method A and vice versa. The 16th and 84th percentiles of the distribution are shown with the horizontal bars. The median and the mean of the distribution are shown with the cross marker and the unfilled circle. The target is the median of BA2011 for the scenario of M7.0R40, Vs450, and normal fault. The changes in the base shear forces (Vbase) are obtained at the time of the maximum absolute of the roof displacements (Δtop). There are about 50 GMs in Method B, 24 GMs in Method C, and 14 GMs in Method D. The 8-story RC model is labeled as Public Building.

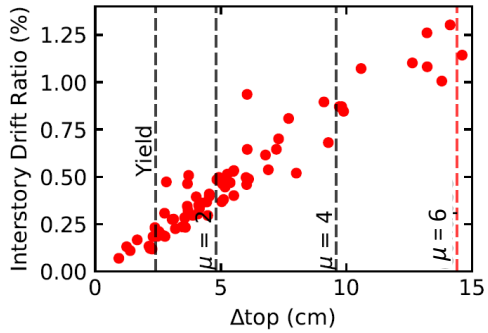

(a) S1: 8-Story RC Building

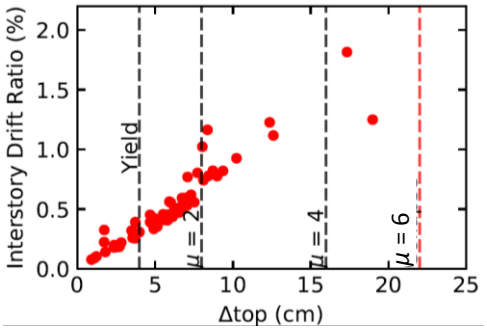

(b) S2: 7-Story RC Building

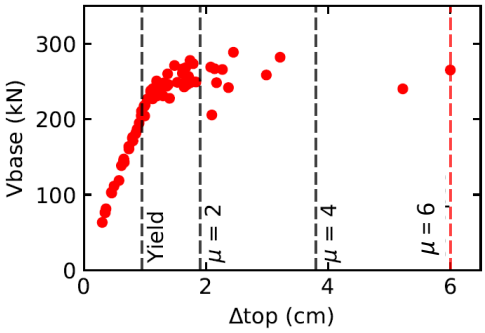

(c) S3: 2-Story RC Building

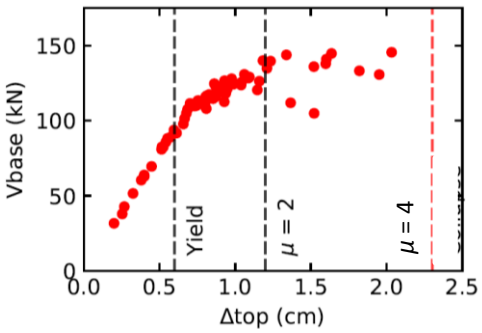

(d) S4: 2-Story Masonry Building

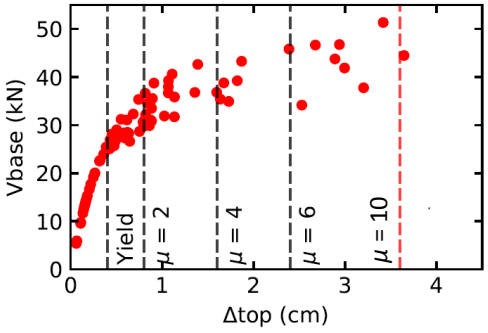

(e) S5: 1-Story RC Building

Figure B.6.3: Structural responses of the complex models under unscaled earthquake records (Method A). The structural responses are shown with red circles. The x-axis shows the maximum absolute of the lateral structural displacements (Δtop). The y-axis shows the maximum absolute of the base shear forces (Vbase). The amount of GMs is given in the legend box. The yielding limit and displacement ductility levels, μ, at 2, 4, 6, and 10 are plotted with the vertical dashed lines.

B.7 Impact of Ground Motion Prediction Equation on Variability

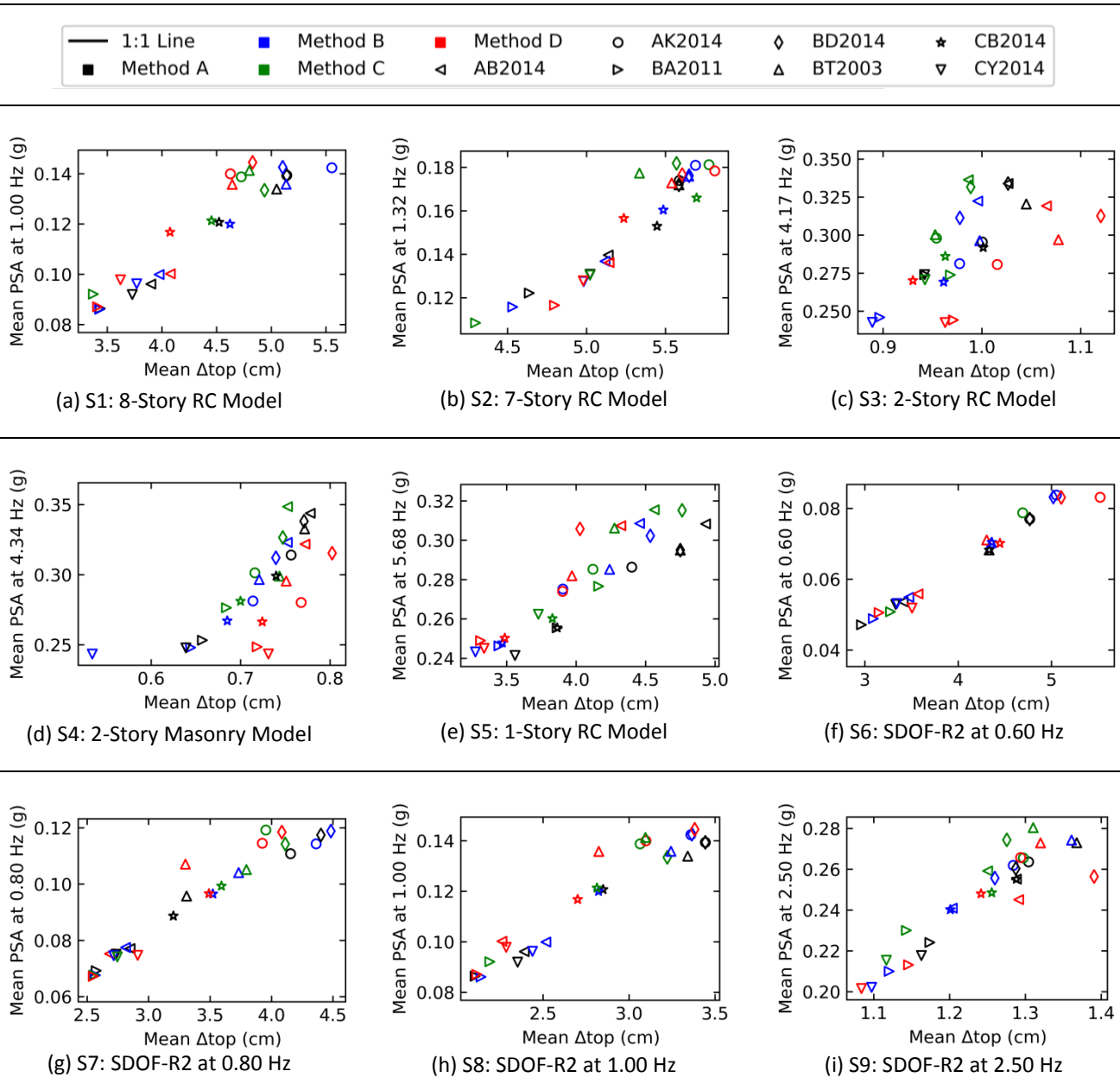

Figure B.7.1: The mean of input PSAs at f0 versus the mean of output lateral structural displacements (Δtop) in Methods A, B, C, and D for seven GMPEs. The x-axis illustrates the coefficient of variance (COV) of maximum absolutes of roof displacements (Δtop). The y-axis illustrates COV of input PSAs at f0. The solid black line is the equality line. The earthquake scenario is M7.0R40, Vs450, and normal fault. GMPEs such as AB2014, AK2014, BA2011, BD2014, BT2003, CB2014, and CY2014 are drawn as in the legend. Methods A, B, C, and D are represented with black, blue, green, and red.GMs in MA and MC are selected if they are within **±30%** of the target PSA at f0 (horizontal dashed line). GMs in MB are refined to have a scaling factor between **0.7 and 1.3**. GMs in MD have PSAs at f0 between ±20% of the target PSA at f0. Mean is shown if there are at least 9 data.

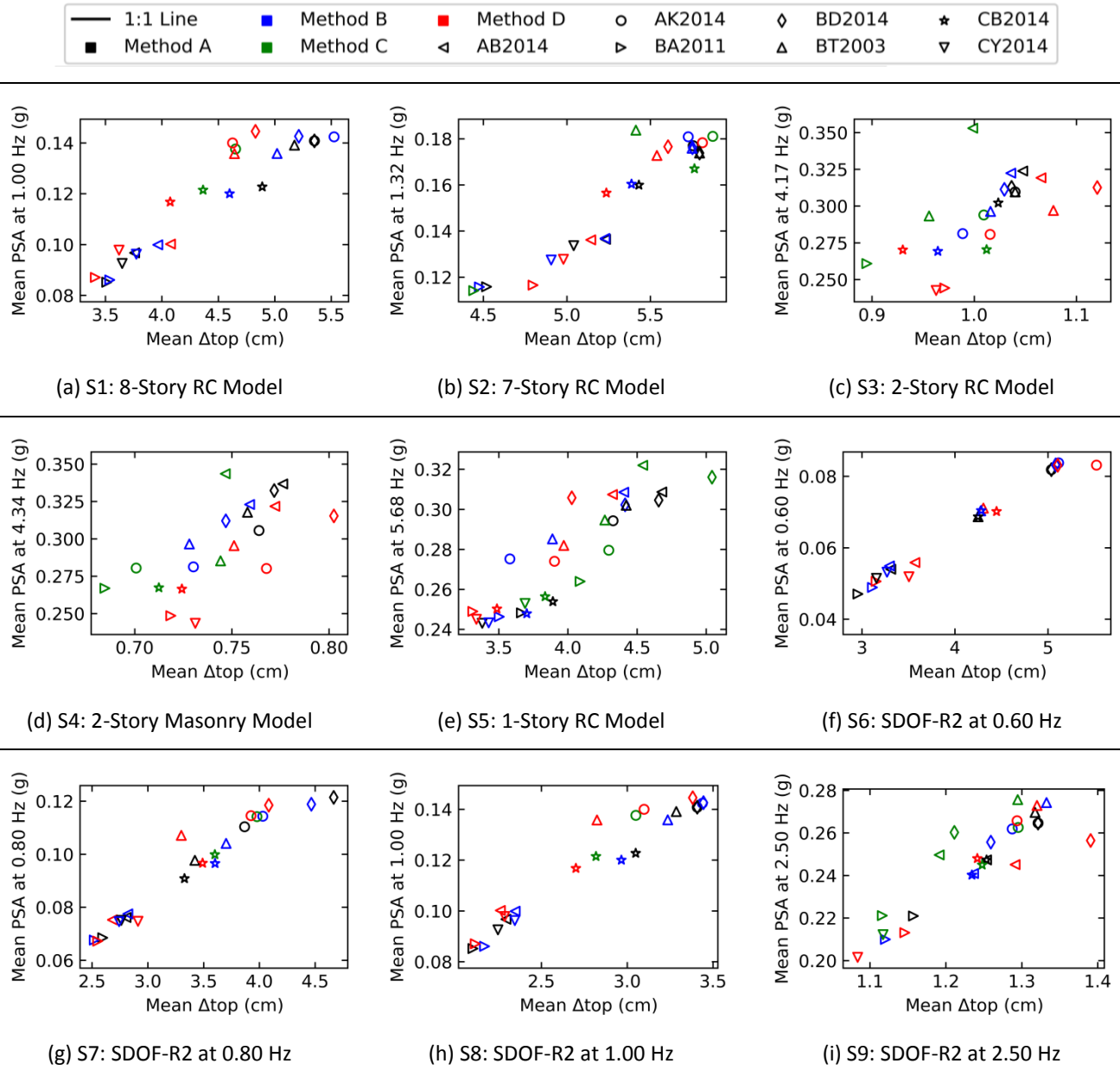

(a) S1: 8-Story RC Model

(b) S2: 7-Story RC Model

(c) S3: 2-Story RC Model

(d) S4: 2-Story Masonry Model

(e) S5: 1-Story RC Model

(f) S6: SDOF-R2 at 0.60 Hz

(g) S7: SDOF-R2 at 0.80 Hz

(h) S8: SDOF-R2 at 1.00 Hz

(i) S9: SDOF-R2 at 2.50 Hz

Figure B.7.2: The mean of input PSAs at f0 versus the mean of output lateral structural displacements (Δtop) in Methods A, B, C, and D for seven GMPEs. The x-axis illustrates the coefficient of variance (COV) of maximum absolutes of roof displacements (Δtop). The y-axis illustrates COV of input PSAs at f0. The solid black line is the equality line. The earthquake scenario is M7.0R40, Vs450, and normal fault. GMPEs such as AB2014, AK2014, BA2011, BD2014, BT2003, CB2014, and CY2014 are drawn as in the legend. Methods A, B, C, and D are represented with black, blue, green, and red.GMs in MA and MC are selected if they are within **±20%** of the target PSA at f0 (horizontal dashed line). GMs in MB are refined to have a scaling factor between **0.8 and 1.2**. GMs in MD have PSAs at f0 between **±20%** of the target PSA at f0. Mean is shown if there are at least 9 data.

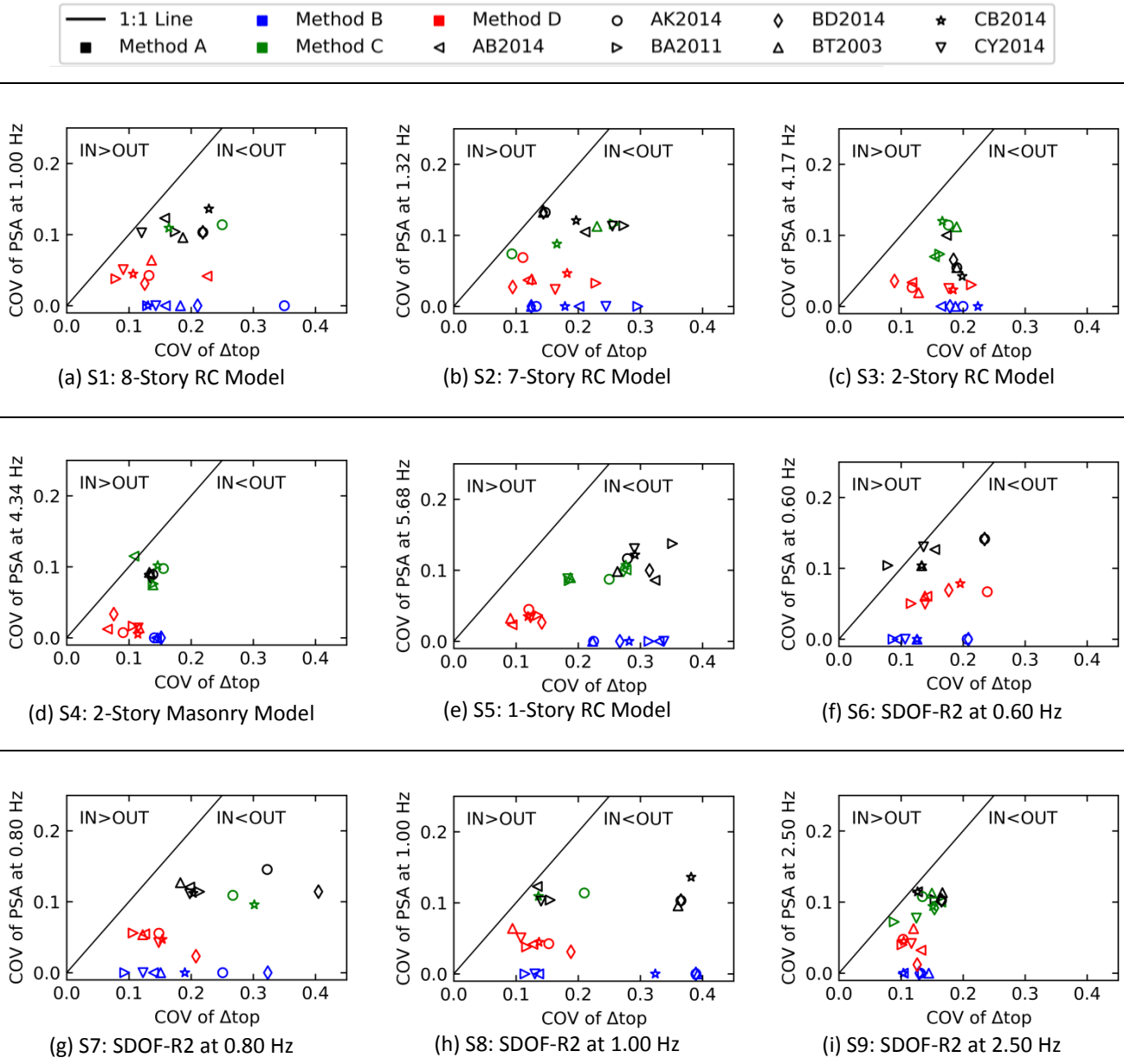

(a) S1: 8-Story RC Model (b) S2: 7-Story RC Model (c) S3: 2-Story RC Model

(d) S4: 2-Story Masonry Model (e) S5: 1-Story RC Model (f) S6: SDOF-R2 at 0.60 Hz

(g) S7: SDOF-R2 at 0.80 Hz (h) S8: SDOF-R2 at 1.00 Hz (i) S9: SDOF-R2 at 2.50 Hz

Figure B.7.3: COV of input PSAs at f0 versus COV of output lateral structural displacements (Δtop) in Methods A, B, C, and D for seven GMPEs. The x-axis illustrates the coefficient of variance (COV) of maximum absolutes of roof displacements (Δtop). The y-axis illustrates COV of input PSAs at f0. The solid black line is the equality line. The earthquake scenario is M7.0R40, Vs450, and normal fault. GMPEs such as AB2014, AK2014, BA2011, BD2014, BT2003, CB2014, and CY2014 are drawn as in the legend. Methods A, B, C, and D are represented with black, blue, green, and red.GMs in MA and MC are selected if they are within **±20%** of the target PSA at f0 (horizontal dashed line). GMs in MB are refined to have a scaling factor between **0.8 and 1.2**. GMs in MD have PSAs at f0 between **±20%** of the target PSA at f0. COV is shown if there are at least 9 data.

B.8 Alternatives to Methods B, C, and D

B.8.1 Alternatives of Linear Scaling (Method B)

The linear amplitude scaling to the target PSA at the natural frequency of a structure, f0, (Method B) may not be advantageous due to the higher mode effect, the elongation of the period, and the analysis of the components in a structure. Therefore, two alternatives of the linear scaling are tested: (1) scaling to the peak ground acceleration (PGA), Method B (MB) at PGA, and (2) the two-point scaling, MB at 2PT, the average of scaling factors at 0.50 Hz and at 20.0 Hz (frequency limits). The GM modification criteria in Section 2.2.1 (i.e., 0.50<scaling factor<2.00) are exactly applied.

The spectral distributions of GMs are shown in Figure B.8.1. In MB at PGA, the spectral variability is not homogenous, i.e., reduced variability at high frequencies and wide variability in the low frequencies. In MB at 2PT, the spectral variability is relatively more homogenous and comparable with the PSA dispersion observed in unscaled earthquake records (shown in Figure 2.3.1.a).

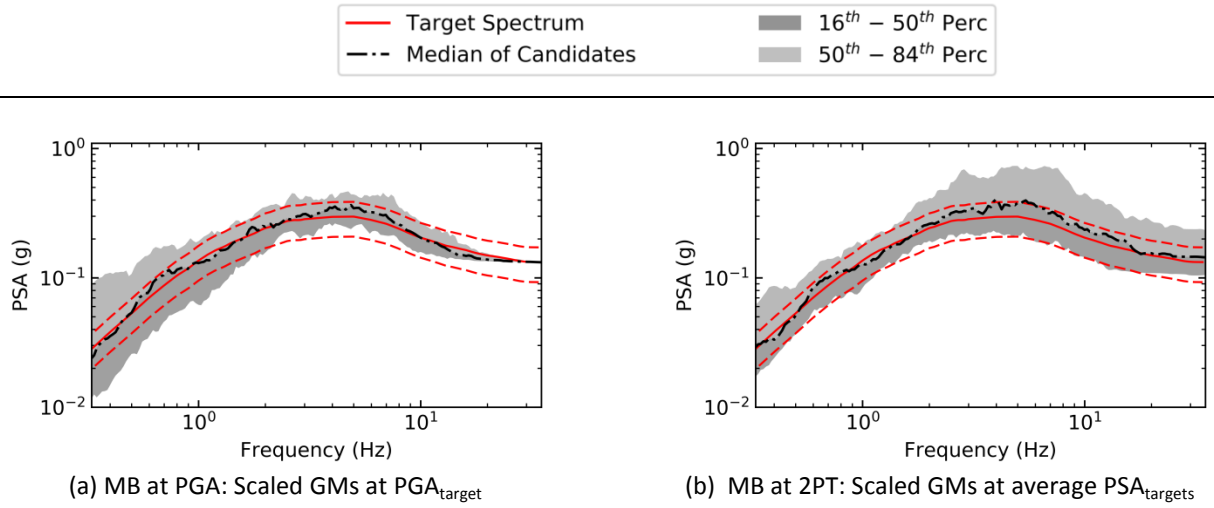

(a) MB at PGA: Scaled GMs at PGA_{target} (b) MB at 2PT: Scaled GMs at average $PSA_{targets}$

Figure B.8.1: Distribution of spectra of structure-independent alternatives of MB. The modifications are applied according to the target, which is the median of BT2003 for the earthquake scenario of M7.0R40 and soil site. The red dashed lines show ±30% around the median of BT2003. MB at PGA scales the GMs to the target PGA in (a). MB at 2PT scales the GMs to the average of scaling factors at 0.50 Hz and 20.0 Hz. There are 50 GMs in MB at PGA, and there are 56 GMs in MB at 2PT.

As illustrated in Figure B.8.2, MB at 2PT (in purple) reveals consistent dispersions for the shown intensity measures (IMs), which are relatively less than MB at 1.00 Hz (in blue) except for the scaling point (PSA at 1.00 Hz). MB at PGA (in dark gold) demonstrates a comparable level of dispersion with MB at 2PT with the exception of the scaling point.

Overall, MB at PGA and MB at 2PT preserve the spectral variability around the interest of the structure and the variability in IMs, which has the indication that they can replicate structural response dispersions obtained by the unscaled earthquake records better than MB at f0.

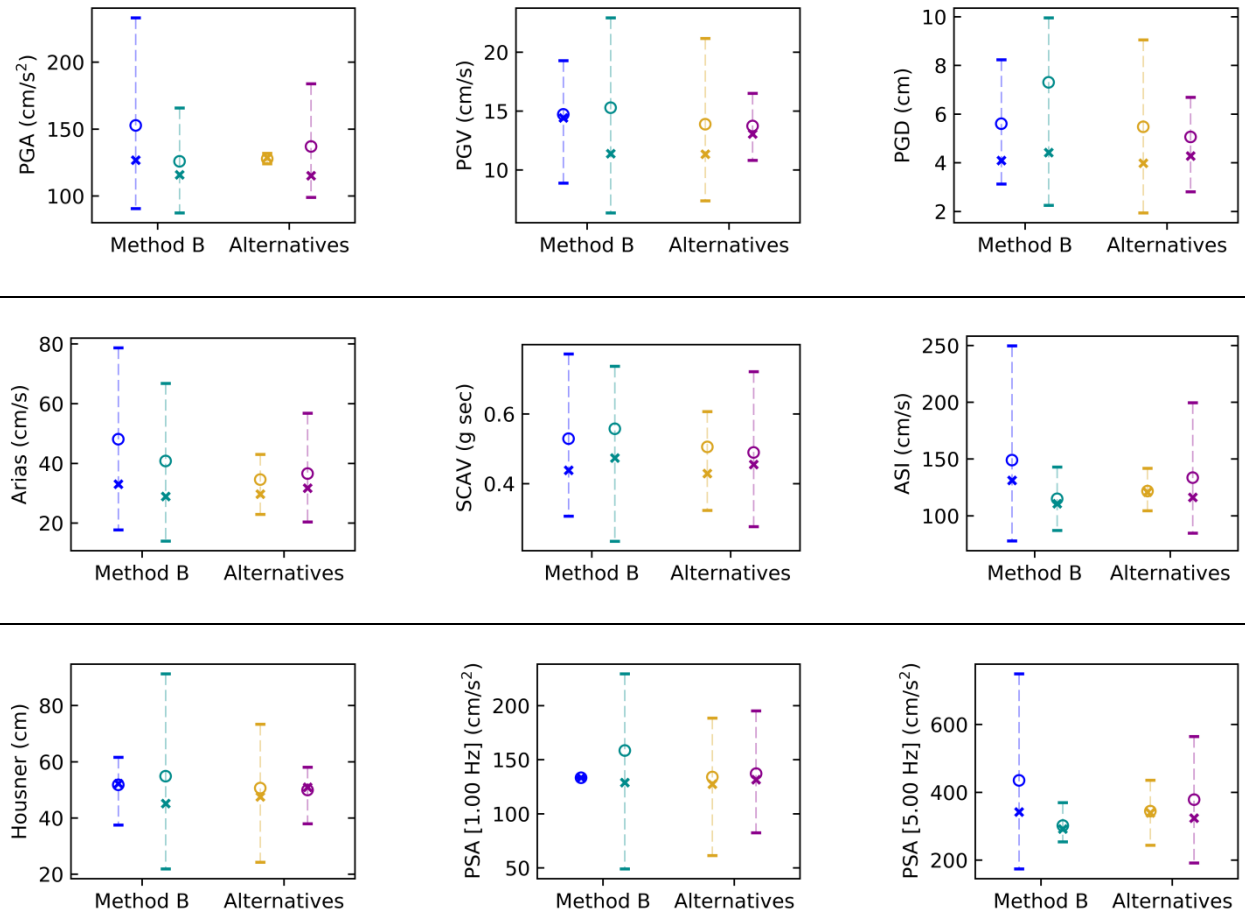

Figure B.8.2: Intensity measures obtained by Method B at 1.00 Hz in blue color, Method B at 5.68 Hz in turquoise color, Method B at PGA in dark golden color, and Method B at 2PT in purple color. The y-axes plot intensity measures (IMs). The x-axes the linear scaling methods. The 16th and 84th percentiles of the distributions are shown with the horizontal bars. The mean of the distribution is shown with the unfilled circle. The median is plotted with the cross marker. The target is the median of BT2003 for the scenario of M7.0R40 and Vs450. The linear scaling is limited with scaling factors between 0.50 and 2.00.

B.8.2 Alternatives of Spectrum Matched Waveforms (Methods C and D)

Spectrum matched waveforms are obtained with the PGA scaling prior to the spectrum matching, which is a common practice. In order to partially test the effect of PGA scaling, the spectrum matching is performed as explained in Section 2.2.2. The criteria on whether or not reject spectrum matched waveforms in Section 2.2.2 are applied. The PGA scaling in spectrum matching affects the spectral variability at a higher frequency in MC and insignificantly in MD as shown in Figure 2.8.1. There are more GMs retrieved if PGA scaling is not applied.

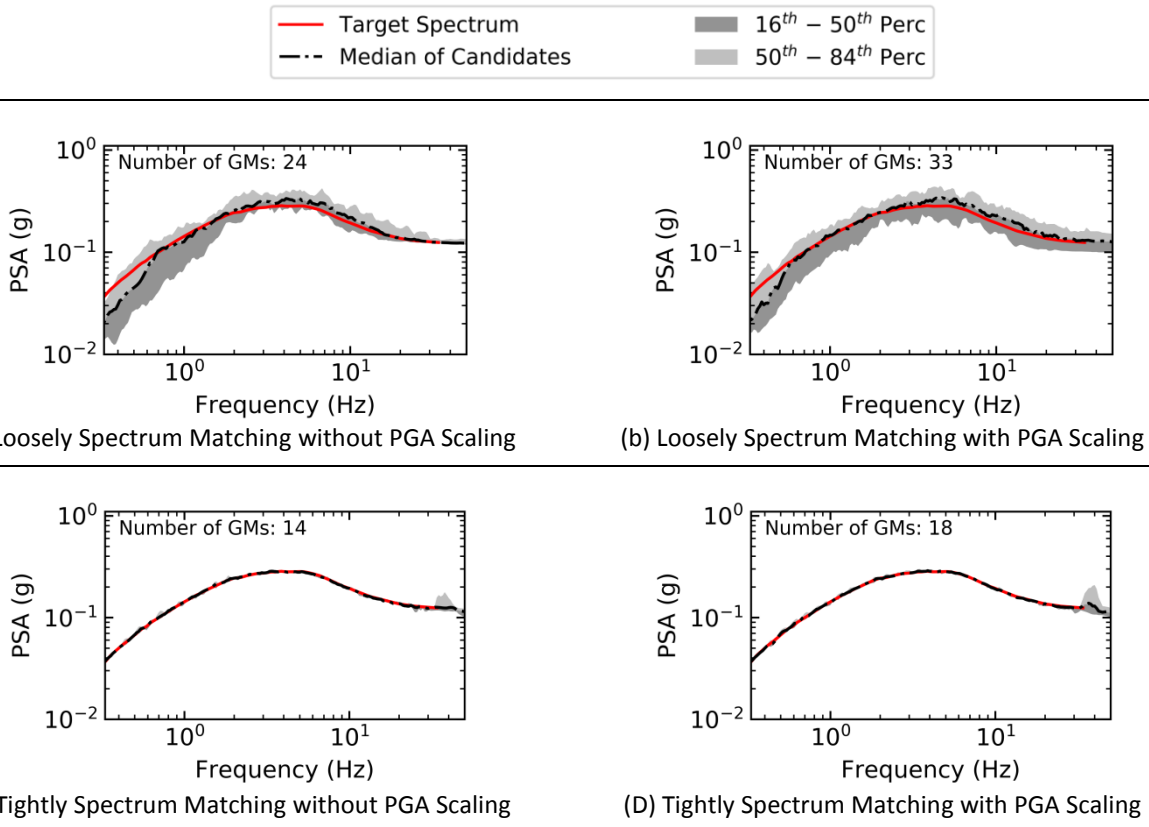

(a) Loosely Spectrum Matching without PGA Scaling

(b) Loosely Spectrum Matching with PGA Scaling

(c) Tightly Spectrum Matching without PGA Scaling

(D) Tightly Spectrum Matching with PGA Scaling

Figure B.8.3: Distribution of spectra of alternatives of Methods C and D with and without PGA scaling. The modifications are applied according to the target, which is the median of AK2014 for the earthquake scenario of M7.0R40, Vs450, and normal fault. The loosely spectrum matching and tightly spectrum matching are applied with and without PGA scaling. The amount of GMs is noted on each subfigure.

The tests are extended to certain IMs in Figure B.8.4. The IM dispersions in Method C are all affected by the PGA scaling, and PGA, PGV, PGD, Arias, SCAV, and ASI and PSAs at higher frequencies show larger dispersion, which can indicate that the structural response dispersions will be better replicated for the structures with a natural frequency higher than 2.00 Hz. For Method D, PGA scaling affects the results slightly. Dispersion of Arias and SCAV increase slightly.

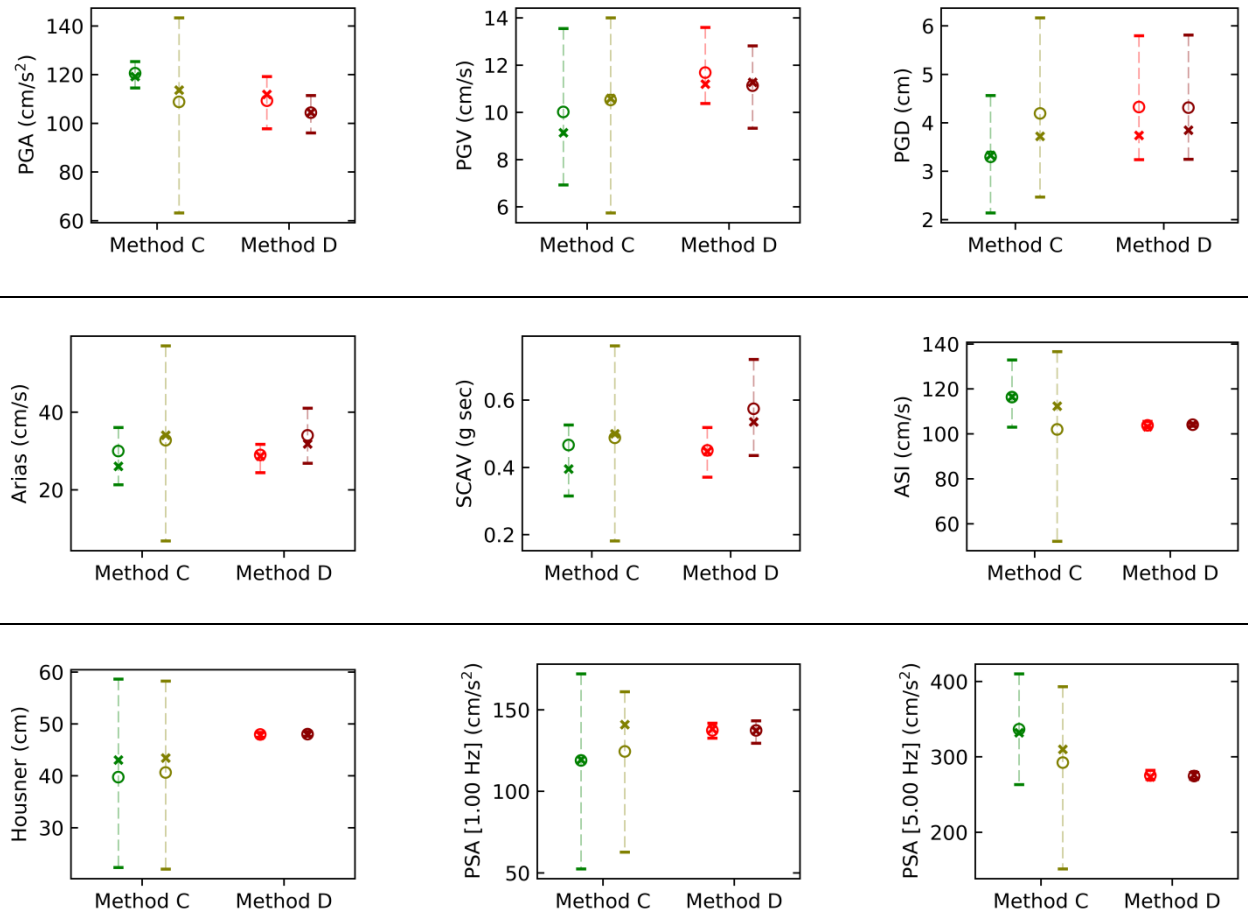

Figure B.8.4: Intensity measures obtained by Method C with PGA scaling (in green color), Method C without PGA scaling (in green olive color), Method D with PGA scaling (in red color), and Method D without PGA scaling (in dark red color). The y-axes plot intensity measures (IMs). The x-axes the linear scaling methods. The 16th and 84th percentiles of the distributions are shown with the horizontal bars. The mean of the distribution is shown with the unfilled circle. The median is plotted with the cross marker. The target is the median of AK2014 for the scenario of M7.0R40 and Vs450.

APPENDIX C

ADDITIONAL ELEMENTS FOR PART 3

C.1 Symmetric Tolerances: GMSM Methods Considering Interset and Intraset Variability

C.1.1 Impact on Input PSAs at f0

(a) Distribution of Each Set's Average (of 5 GMs) (b) Distribution of Each Set's Standard Deviation

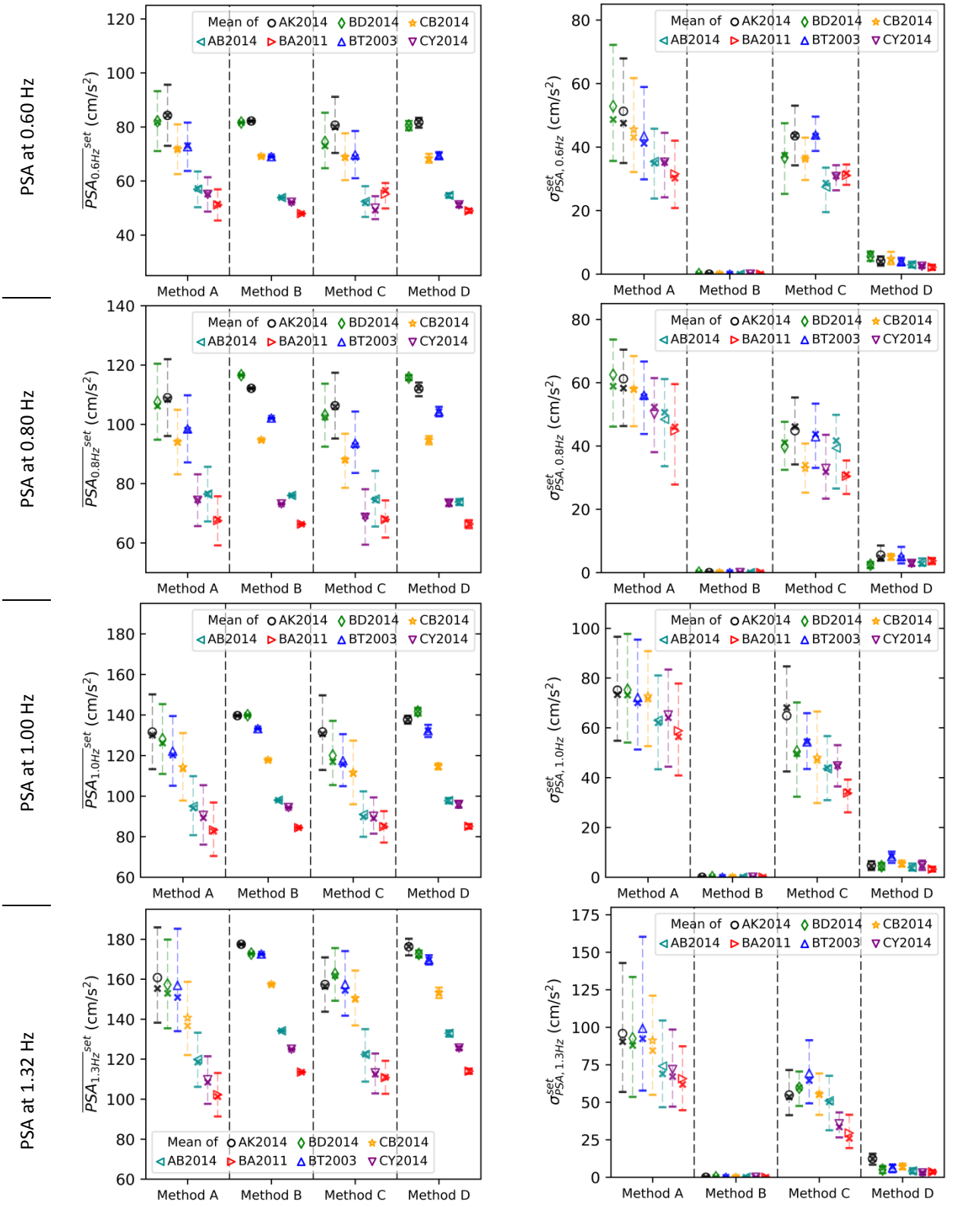

➔ Figure C.1.1, Continued, 1/2

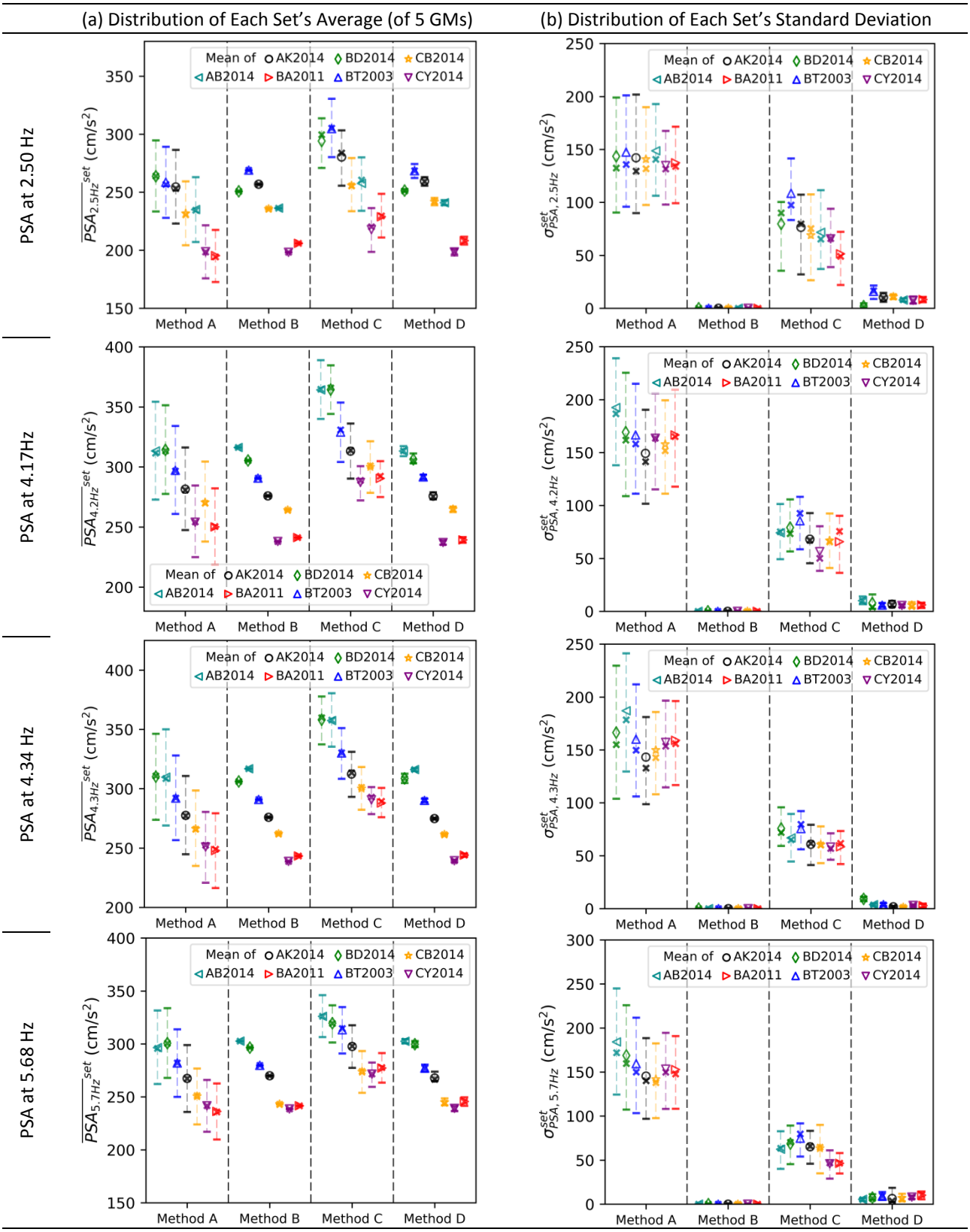

Figure C.1.1: Distribution of pseudo-spectral accelerations (PSA) at f0 (in row-wise) with all GM sets considering each set's average in column (a) and each set's standard deviation in column (b) with the <u>symmetric</u> tolerances. Each set includes five ground motions. The upper and lower amplitude tolerances are -30% and +30% of the target for Methods A, B, and C, and between-5% and +5% of the target for Method D. The frequency range is from 0.50 Hz and 20.0 Hz. The target is obtained for the scenario of M7.0R40, Vs450, and normal fault as explained in Section 1.4. Means are demonstrated with the markers and colors in the legend box for corresponded GMPEs. Medians are shown with the cross markers. The 16th and 84th percentiles are plotted with the horizontal bars.

C.1.2 Impact on Roof (or Lateral) Displacements (Δtop)

(a) Distribution of Each Set's Average (of 5 GMs) (b) Distribution of Each Set's Average-Plus-95%-Sigma

S1: 8-Story RC Building (f0 =1.00Hz)

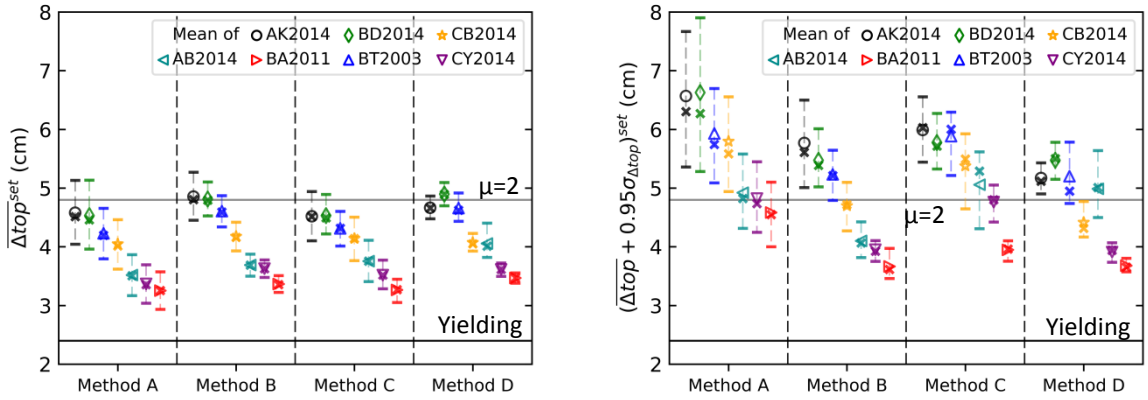

S2: 7-Story RC Building (f0 =1.32Hz)

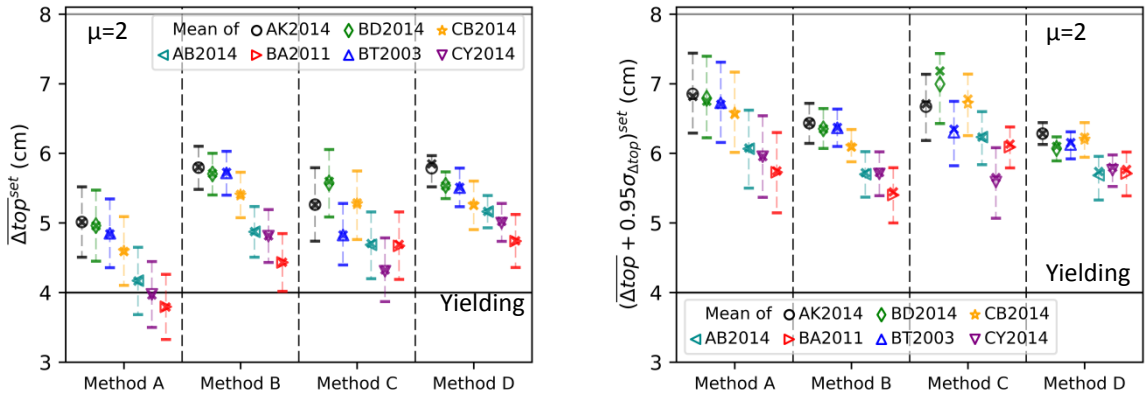

S3: 2-Story RC Building (f0 =4.17Hz)

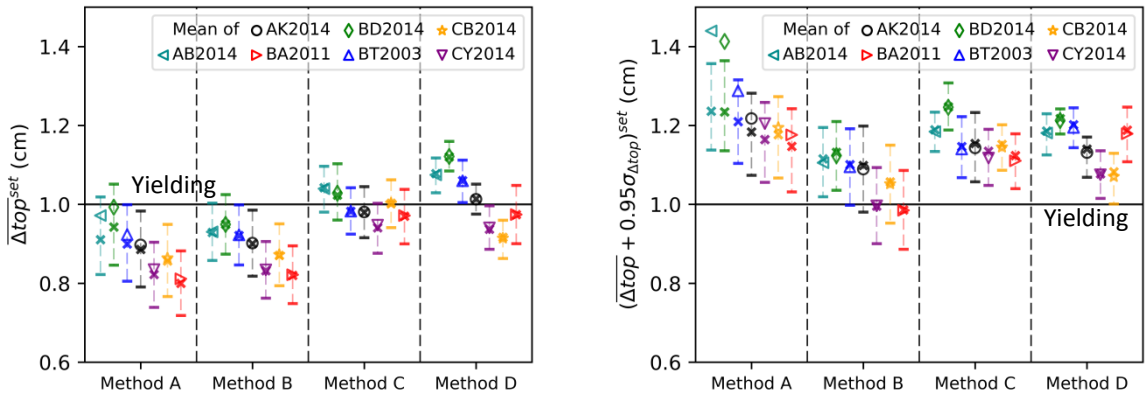

S4: 2-Story Masonry Building (f0=4.34Hz)

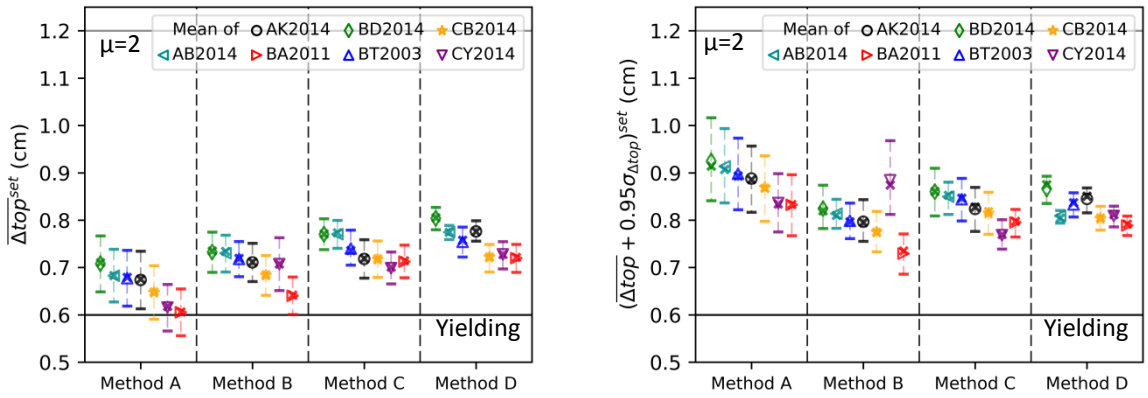

➔ Figure C.1.2, Continued, 1/3

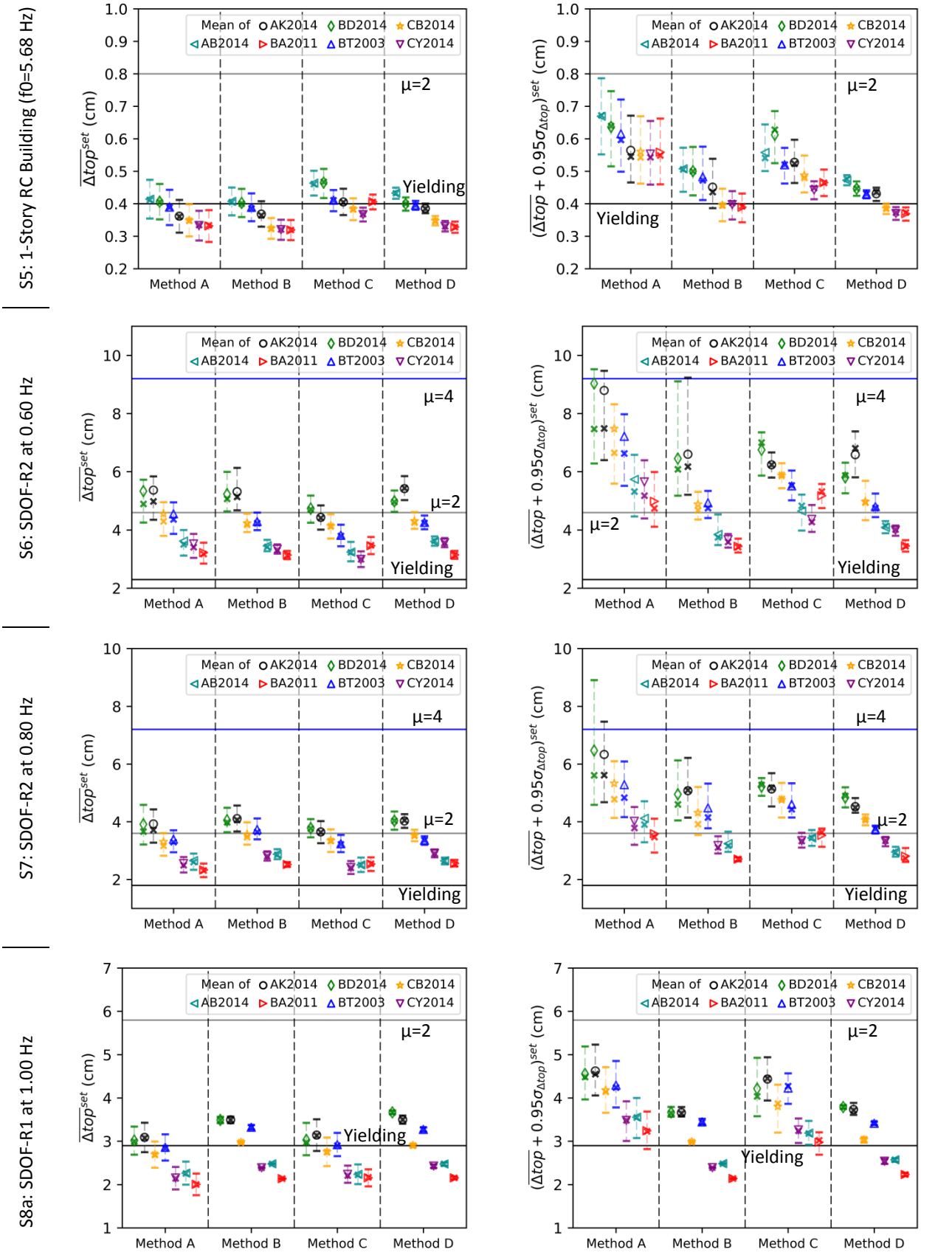

➔ Figure C.1.2, Continued, 2/3

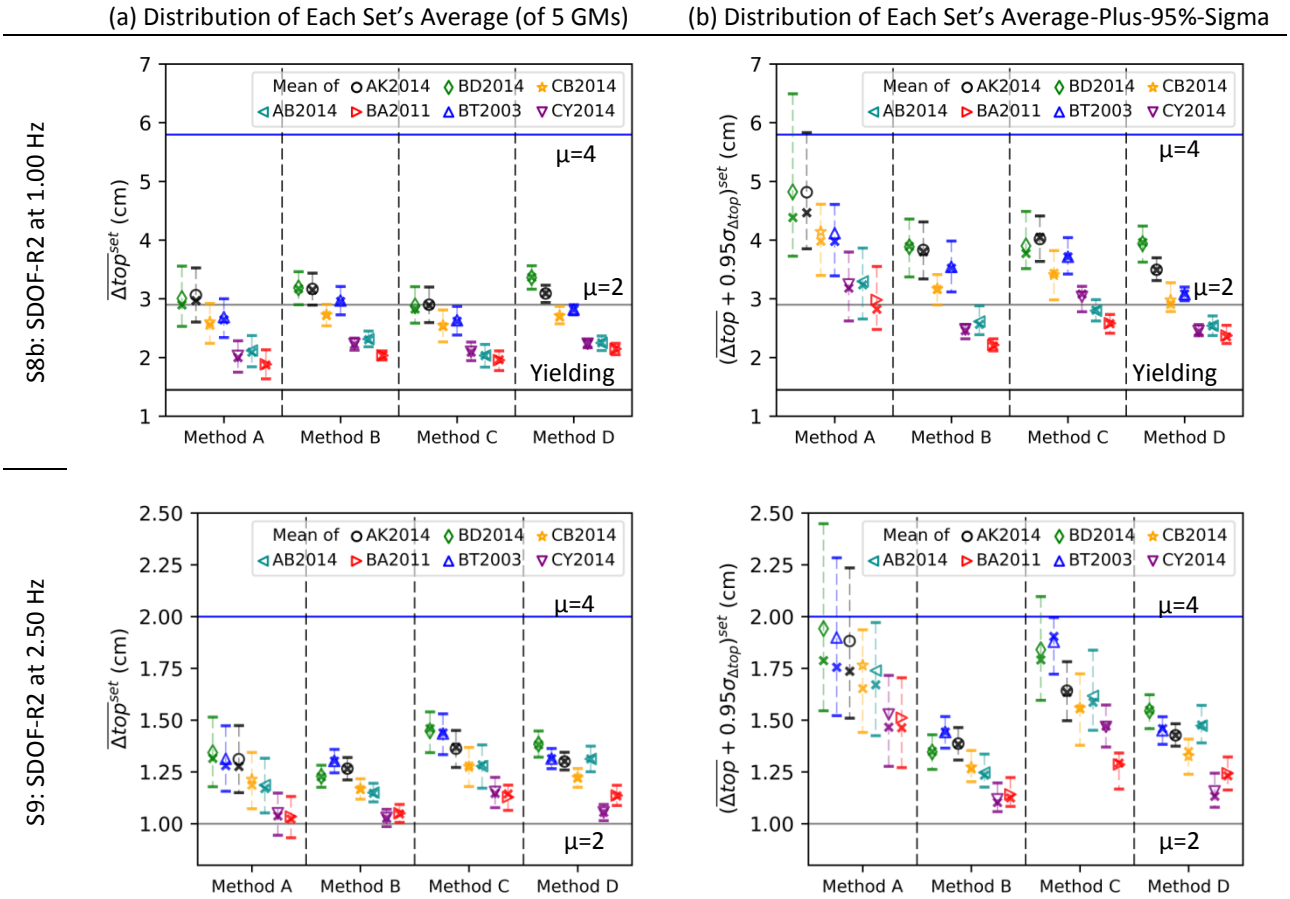

Figure C.1.2: Distribution of roof (or lateral) displacements (Δtop) with all GM sets considering intraset variability with the symmetric tolerances. Each set includes five ground motions. The upper and lower amplitude tolerances are -30% and +30% of the target for Methods A, B, and C, and between-5% and +5% of the target for Method D. The frequency range is from 0.50 Hz and 20.0 Hz. The target is obtained for the scenario of M7.0R40, Vs450, and normal fault as explained in Section 1.4. In column-wise, distributions of each set's average are shown in (a), and the distributions of each set's average-plus-95%-standard-deviation are shown in (b). In row-wise, the responses of structural models are listed. Means are demonstrated with the markers and colors in the legend box for the corresponded GMPEs. Medians are shown with the cross markers. The 16th and 84th percentiles are plotted with the horizontal bars. The yielding limits and ductility demands (μ) of 2 and 4 are shown with horizontal solid lines of black, grey, and blue, respectively.

C.1.3 Impact on Base Shear Forces (Vbase)

(a) Distribution of Each Set's Average (of 5 GMs) (b) Distribution of Each Set's Average-Plus-95%-Sigma

S1: 8-Story RC Building (f0 =1.00Hz)

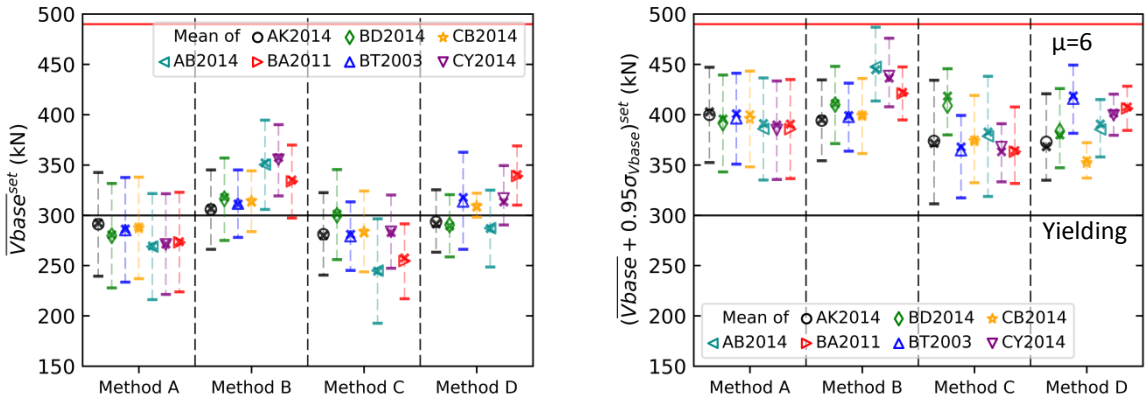

S2: 7-Story RC Building (f0 =1.32Hz)

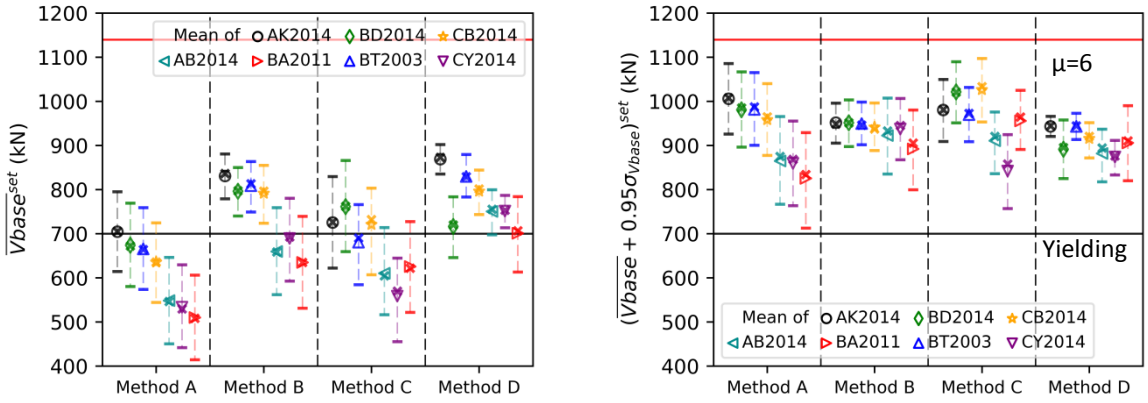

S3: 2-Story RC Building (f0 =4.17Hz)

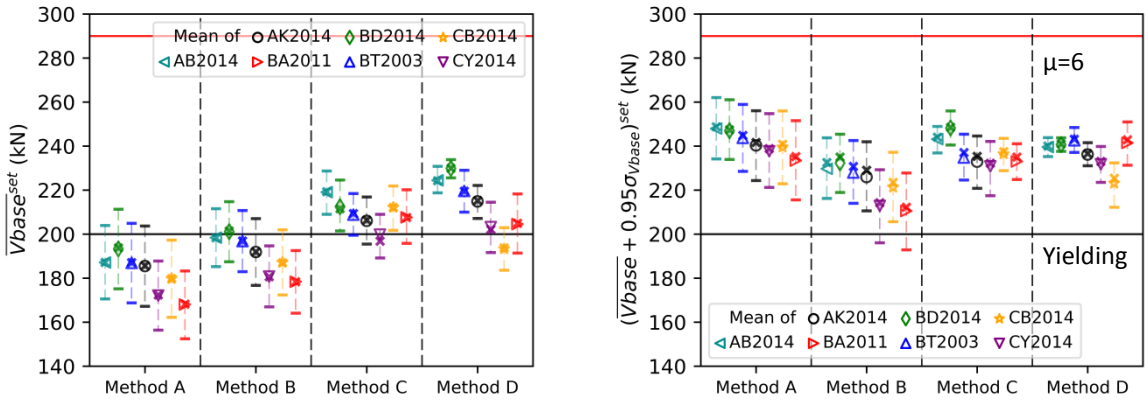

S4: 2-Story Masonry Building (f0=4.34Hz)

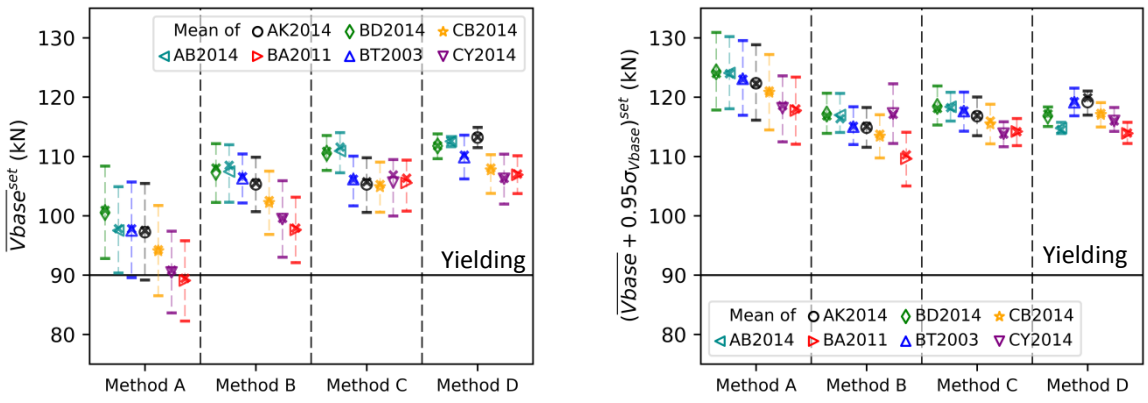

➔ Figure C.1.3, Continued, 1/3

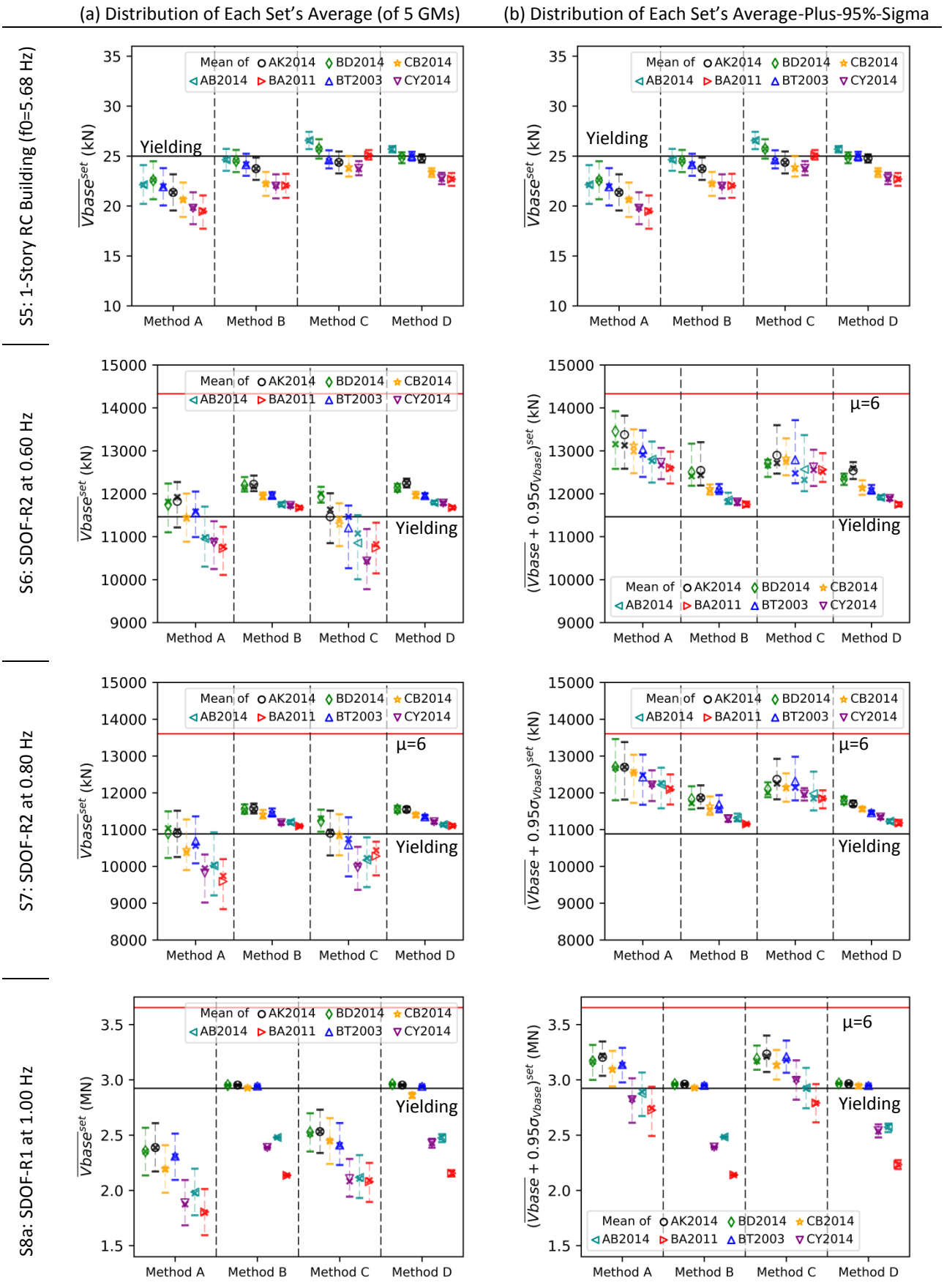

➔ Figure C.1.3, Continued, 2/3

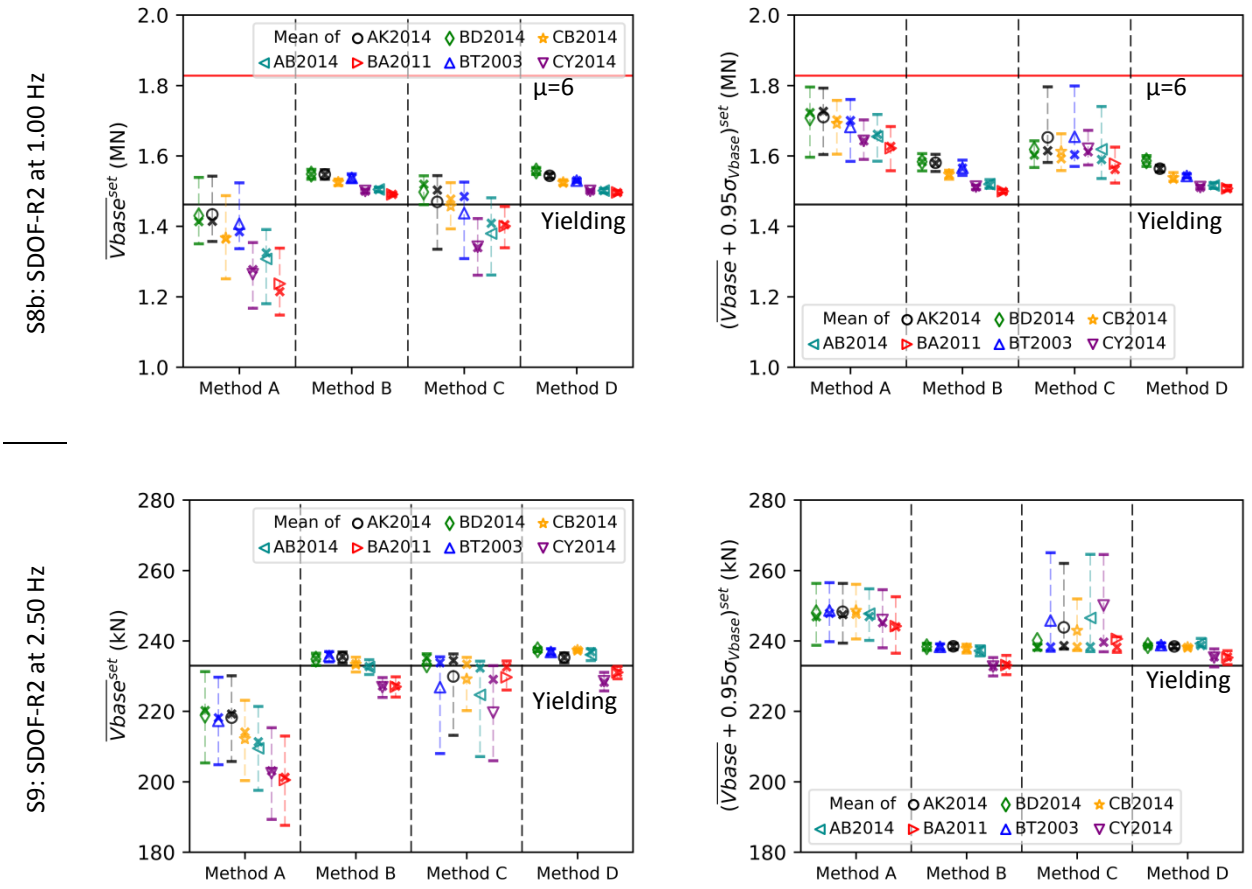

Figure C.1.3: Distribution of base shear forces (Vbase) with all GM sets considering intraset variability with the symmetric tolerances. Each set includes five ground motions. The upper and lower amplitude tolerances are -30% and +30% of the target for Methods A, B, and C, and between-5% and +5% of the target for Method D. The frequency range is from 0.50 Hz and 20.0 Hz. The target is obtained for the scenario of M7.0R40, Vs450, and normal fault as explained in Section 1.4. In column-wise, distributions of each set's average are shown in (a), and the distributions of each set's average-plus-95%-standard-deviation are shown in (b). In row-wise, the responses of structural models are listed. Means are demonstrated with the markers and colors in the legend box for the corresponded GMPEs. Medians are shown with the cross markers. The 16^{th} and 84^{th} percentiles are plotted with the horizontal bars. The yielding limit and the ductility demands, μ, are shown with a horizontal solid line of black and red, respectively. Vbase is obtained at the response time when the absolute maximum of Δtop is obtained.

C.1.4 Impact on Intensity Drift Ratio (IDR)

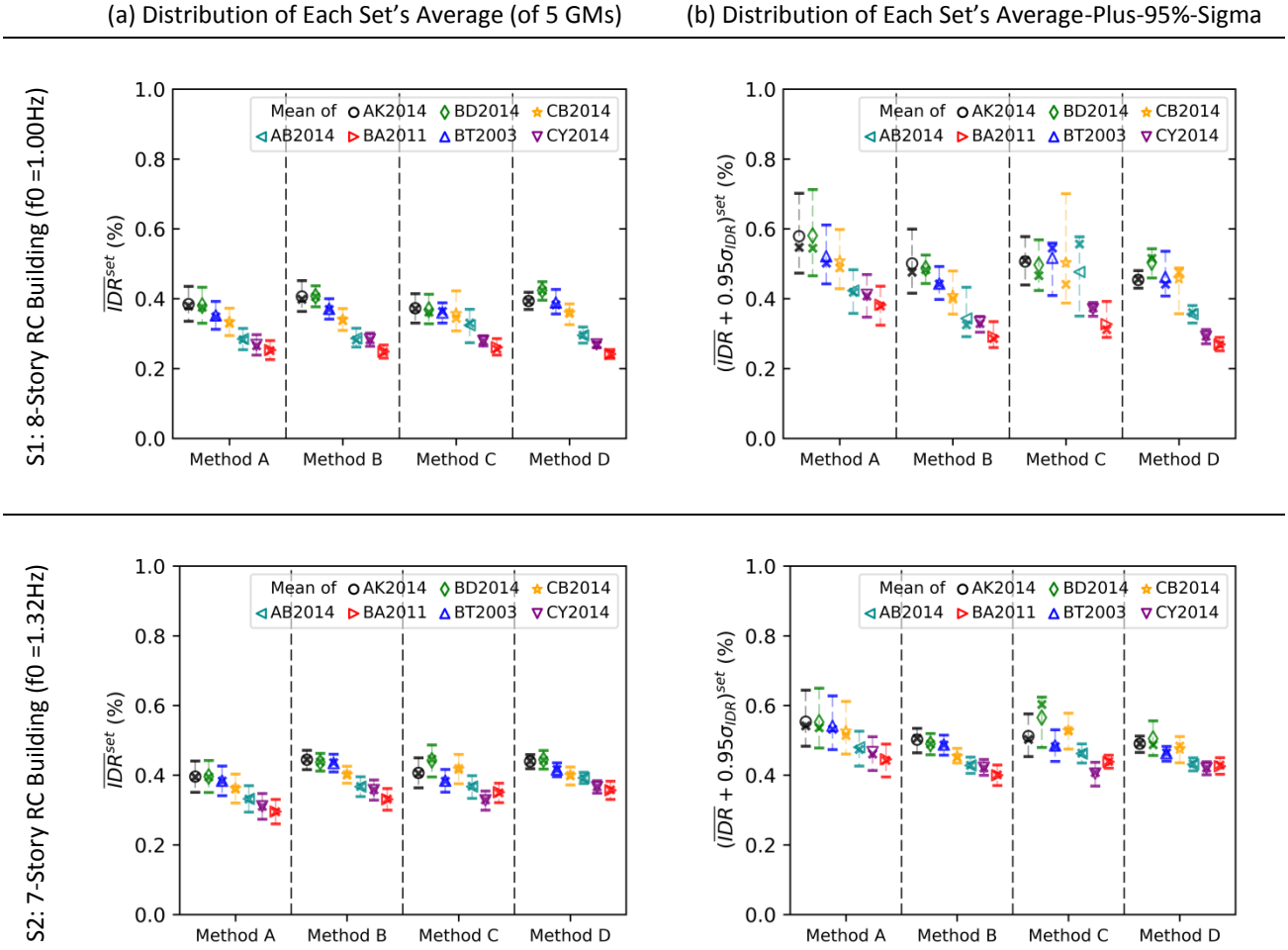

Figure C.1.4: Distribution of interstory drift ratio (IDR) with all GM sets considering intraset variability with the symmetric tolerances. Each set includes five ground motions. The upper and lower amplitude tolerances are -30% and +30% of the target for Methods A, B, and C, and between-5% and +5% of the target for Method D. The frequency range is from 0.50 Hz and 20.0 Hz. The target is obtained for the scenario of M7.0R40, Vs450, and normal fault as explained in Section 1.4. In column-wise, distributions of each set's average are shown in (a), and the distributions of each set's average-plus-95%-standard-deviation are shown in (b). In row-wise, the responses of structural models are listed. Means are demonstrated with the markers and colors in the legend box for the corresponded GMPEs. Medians are shown with the cross markers. The 16th and 84th percentiles are plotted with the horizontal bars. IDR is obtained at the response time when the absolute maximum of Δtop is obtained.

C.1.5 Impact on Global Damage Index (DI)

(a) Distribution of Each Set's Average (of 5 GMs) (b) Distribution of Each Set's Average-Plus-95%-Sigma

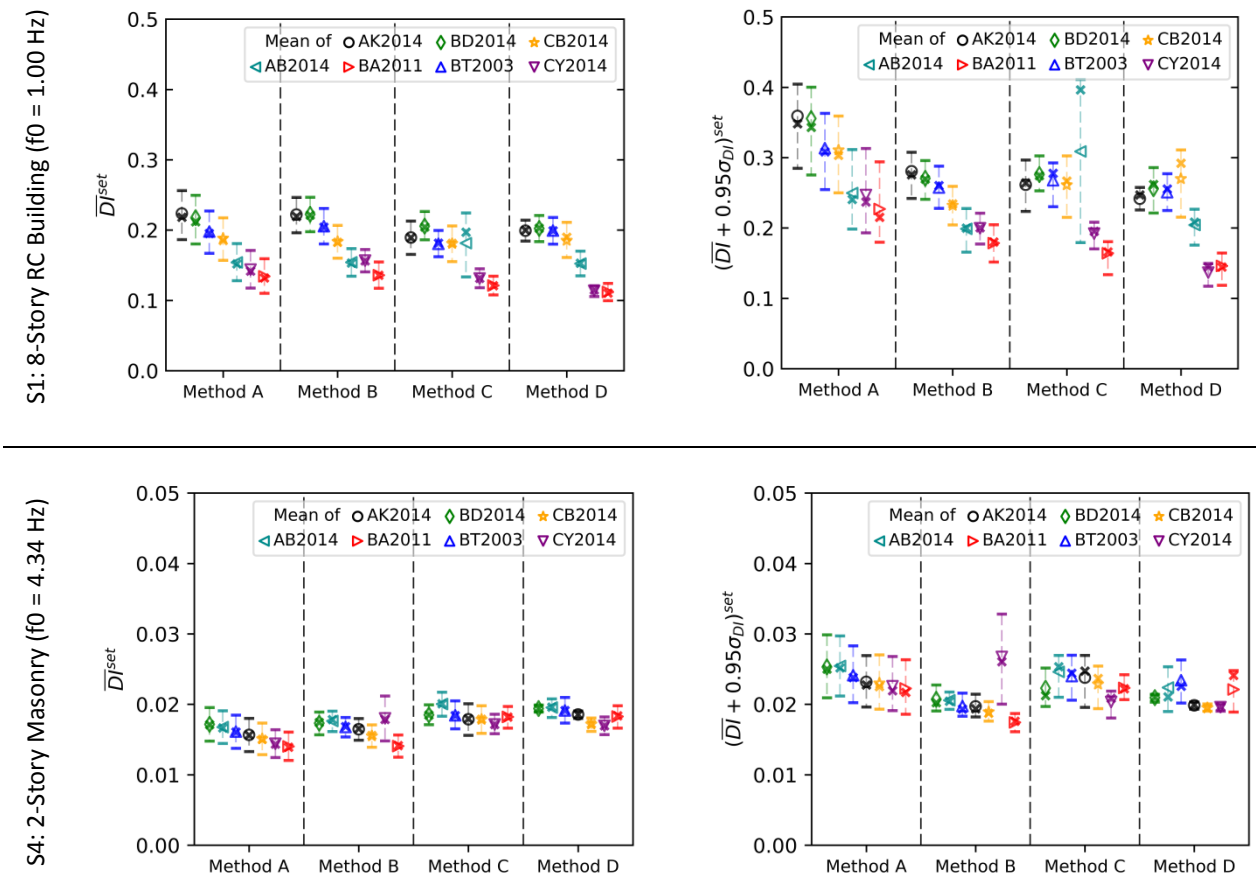

Figure C.1.5: Distribution of global damage index (DI) with all GM sets considering intraset variability with the symmetric tolerances. Each set includes five ground motions. The upper and lower amplitude tolerances are -30% and +30% of the target for Methods A, B, and C, and between-5% and +5% of the target for Method D. The frequency range is from 0.50 Hz and 20.0 Hz. The target is obtained for the scenario of M7.0R40, Vs450, and normal fault as explained in Section 1.4. In column-wise, distributions of each set's average are shown in (a), and the distributions of each set's average-plus-95%-standard-deviation are shown in (b). In row-wise, the responses of structural models are listed. Means are demonstrated with the markers and colors in the legend box for the corresponded GMPEs. Medians are shown with the cross markers. The 16th and 84th percentiles are plotted with the horizontal bars. Global DI is obtained at the response time when the absolute maximum of Δtop is obtained.

C.1.6 Comparison of Mean of Output Distributions with Mean of Input Distributions

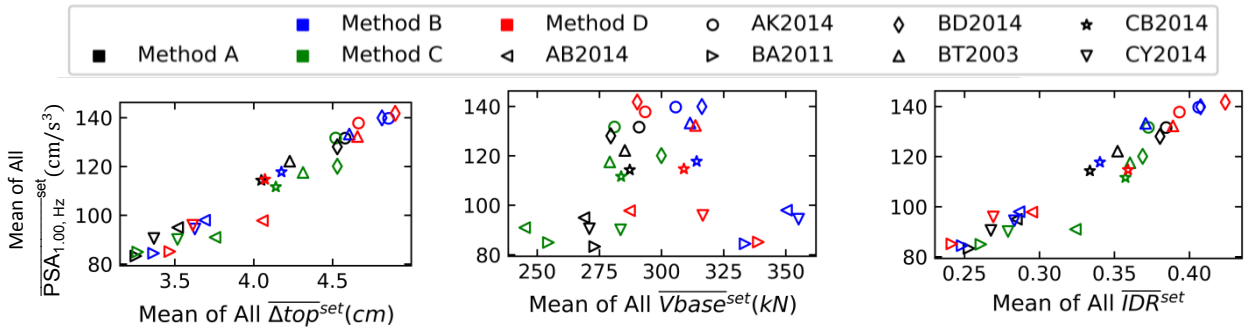

Figure C.1.6: Mean of PSA distributions at f0 (y-axis) versus mean of structural response distributions (x-axis) such as Δtop, Vbase, and IDR for the S1 model (8-Story RC). The means of all set distribution are obtained from Figures C.1.1, C.1.2, C.1.3, and C.1.4. Each point represents the mean Δtop estimate from a GMPE used as a target given in the legend box. Methods B, C, and D are plotted with blue, red, and red, respectively.

C.1.7 Comparison of Dispersion in Input and Output Distributions

1: 8-Story RC f0 = 1.00 Hz	**2**: 7-Story RC f0 = 1.32 Hz	**3**: 2-Story RC f0 = 4.17 Hz	**4**: 2-Story Masonry f0 = 4.34 Hz	**5**: 1-Story RC f0 = 5.68 Hz

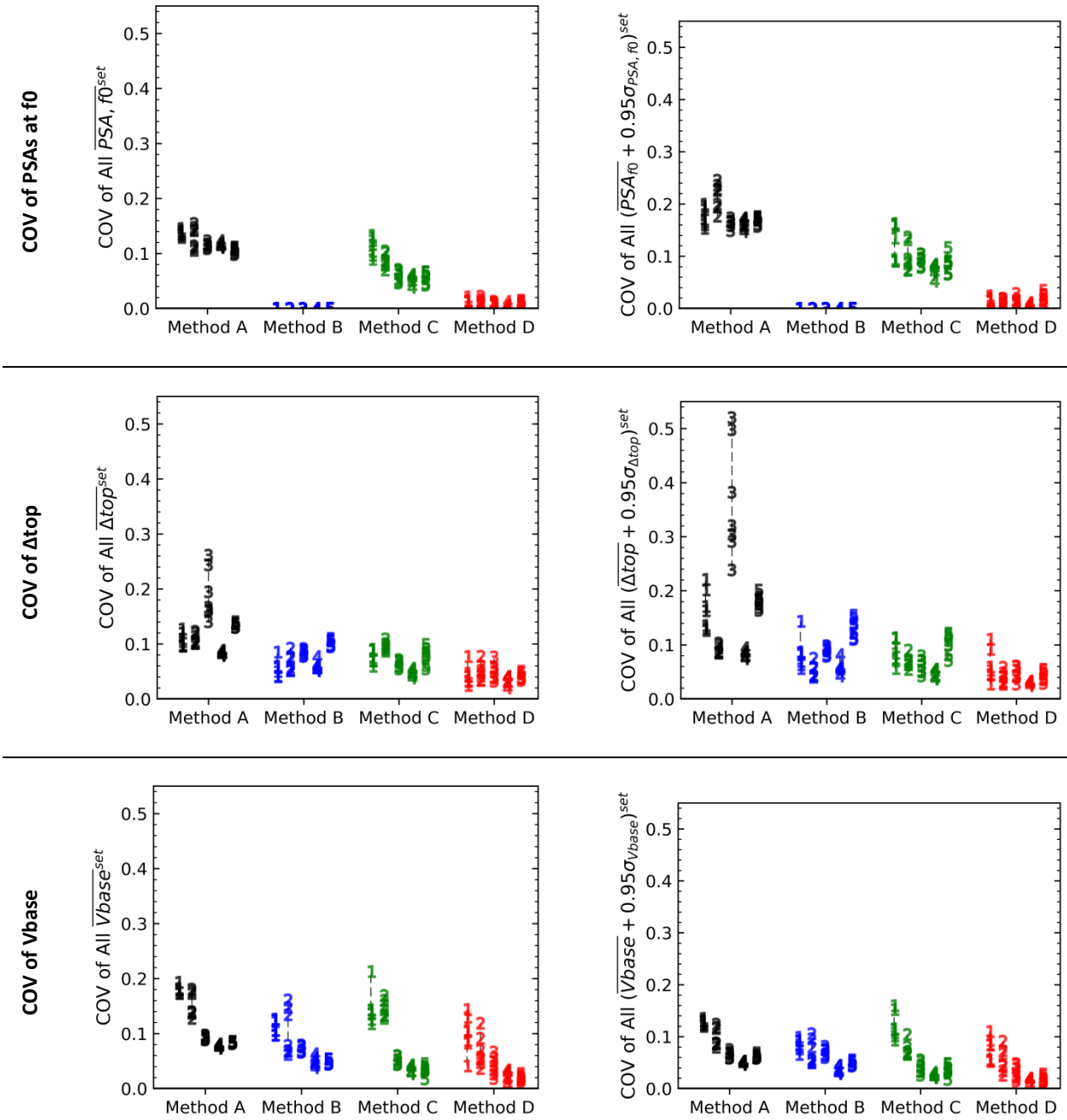

(a) Distribution of Each Set's Average (of 5 GMs) (b) Distribution of Each Set's Average-Plus-95%-Sigma

Figure C.1.7: Comparison of interset variability for complex structural models with each set's average in column (a) and each set's average-plus-95%-sigma in column (b). In row-wise, PSAs at f0, Δtop, and Vbase are shown. Each data point is the COV of all set distribution illustrated in Figures C.1.1, C.1.2, and C.1.3. Each GMPE (7 of them) is plotted for the structural models. The markers are shown with the ID of the structural model given in the box above the figure. Methods A, B, C, and D are shown with black, blue, green, and red, respectively.

6: SDOF-R2 f0 = 0.60 Hz	**7**: SDOF=R2 f0 = 0.80 Hz	**8**(a): SDOF-R1 f0 = 1.00 Hz	(8)**b**: SDOF-R2 f0 = 1.00 Hz	**9**: SDOF-R2 f0 = 2.50 Hz

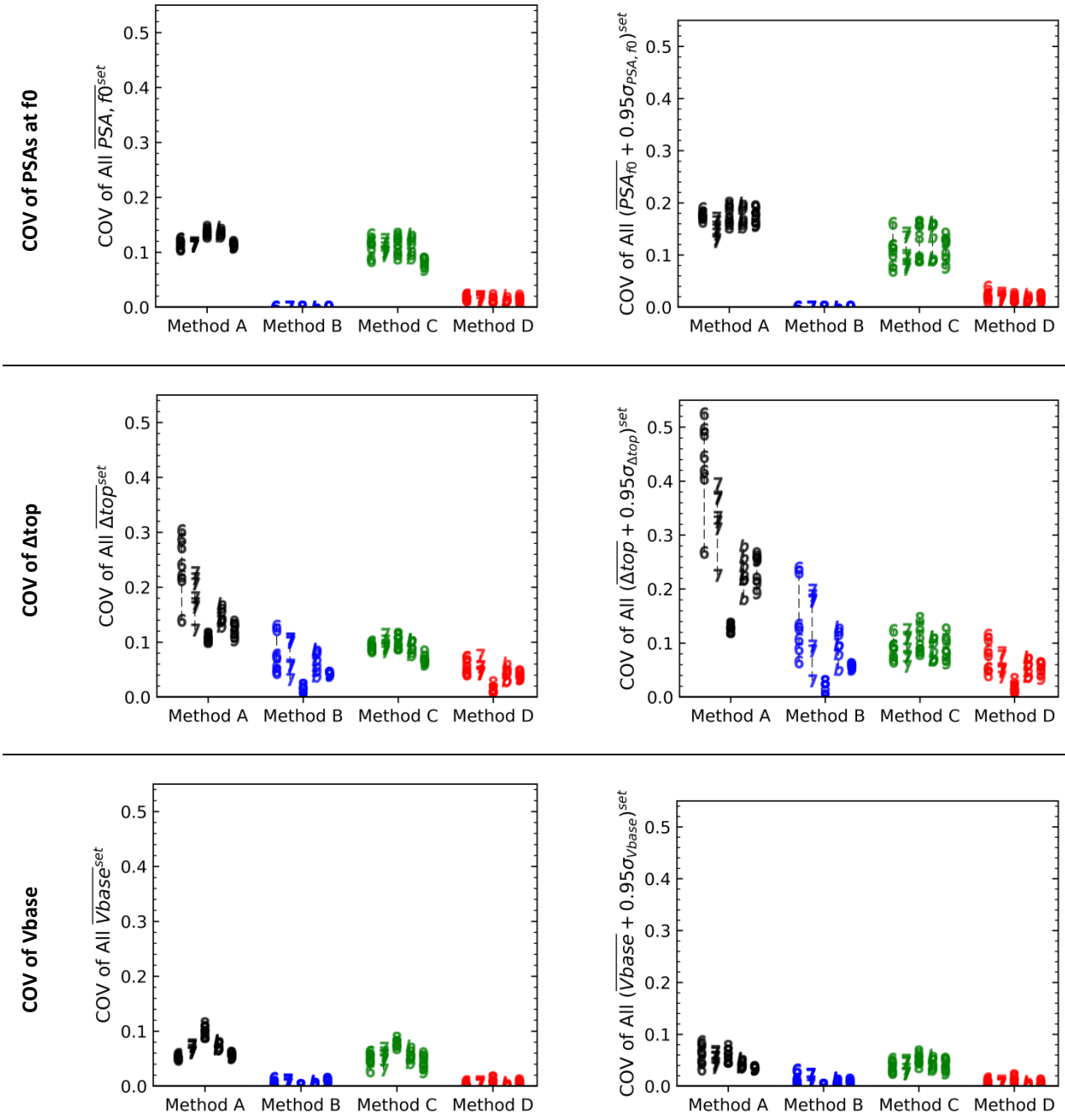

(a) Distribution of Each Set's Average (of 5 GMs) (b) Distribution of Each Set's Average-Plus-95%-Sigma

Figure C.1.8: Comparison of interset variability for simple structural models with each set's average in column (a) and each set's average-plus-95%-sigma in column (b). In row-wise, PSAs at f0, Δtop, and Vbase are shown. Each data point is the COV of all set distribution illustrated in Figures C.1.1, C.1.2, and C.1.3. Each GMPE (7 of them) is plotted for the structural models. The markers are shown with the ID of the structural model in the box above the figure. Methods A, B, C, and D are shown with black, blue, green, and red, respectively.

C.1.8 Quantification of Impact due to the Intraset and Interset Variability

1: 8-Story RC f0 = 1.00 Hz	**2**: 7-Story RC f0 = 1.32 Hz	**3**: 2-Story RC f0 = 4.17 Hz	**4**: 2-Story Masonry f0 = 4.34 Hz	**5**: 1-Story RC f0 = 5.68 Hz

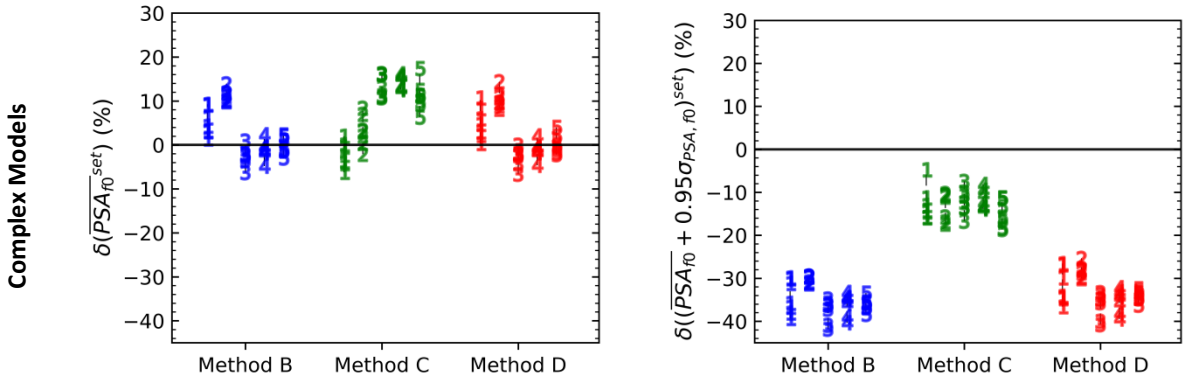

6: SDOF-R2 f0 = 0.60 Hz	**7**: SDOF=R2 f0 = 0.80 Hz	**8**(a): SDOF-R1 f0 = 1.00 Hz	(8)**b**: SDOF-R2 f0 = 1.00 Hz	**9**: SDOF-R2 f0 = 2.50 Hz

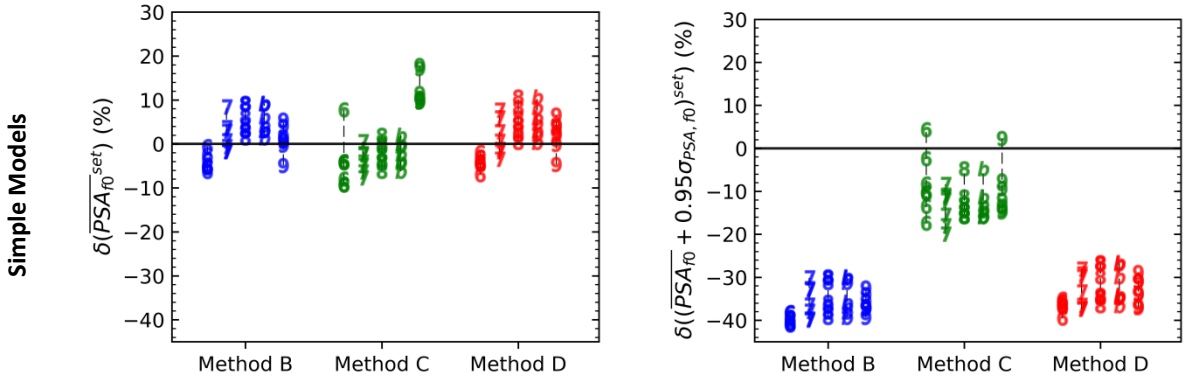

Figure C.1.9: Change in mean PSAs at f0 for seven GMPEs when Methods B, C, and D are used instead of Method A. The spectrum compatible selection is made with each set including five ground motions. The upper and lower amplitude tolerances are -30% and +30% of the target for Methods A, B, and C, and between-5% and +5% of the target for Method D. The frequency range is from 0.50 Hz and 20.0 Hz. The target is obtained for the scenario of M7.0R40, Vs450, and normal fault as explained in Section 1.4. In column-wise, distributions of each set's average are shown on the left column, and the distributions of each set's average-plus-95%-standard-deviation are shown on right column. In row-wise, the responses of structural models are listed. Each GMPE (7 of them) is plotted for the structural models. The markers are shown with the ID of the structural model given in the box above the figure. Methods B, C, and D are shown with blue, green, and red colors, respectively. The negative values represent the underprediction relative to Method A and vice versa.

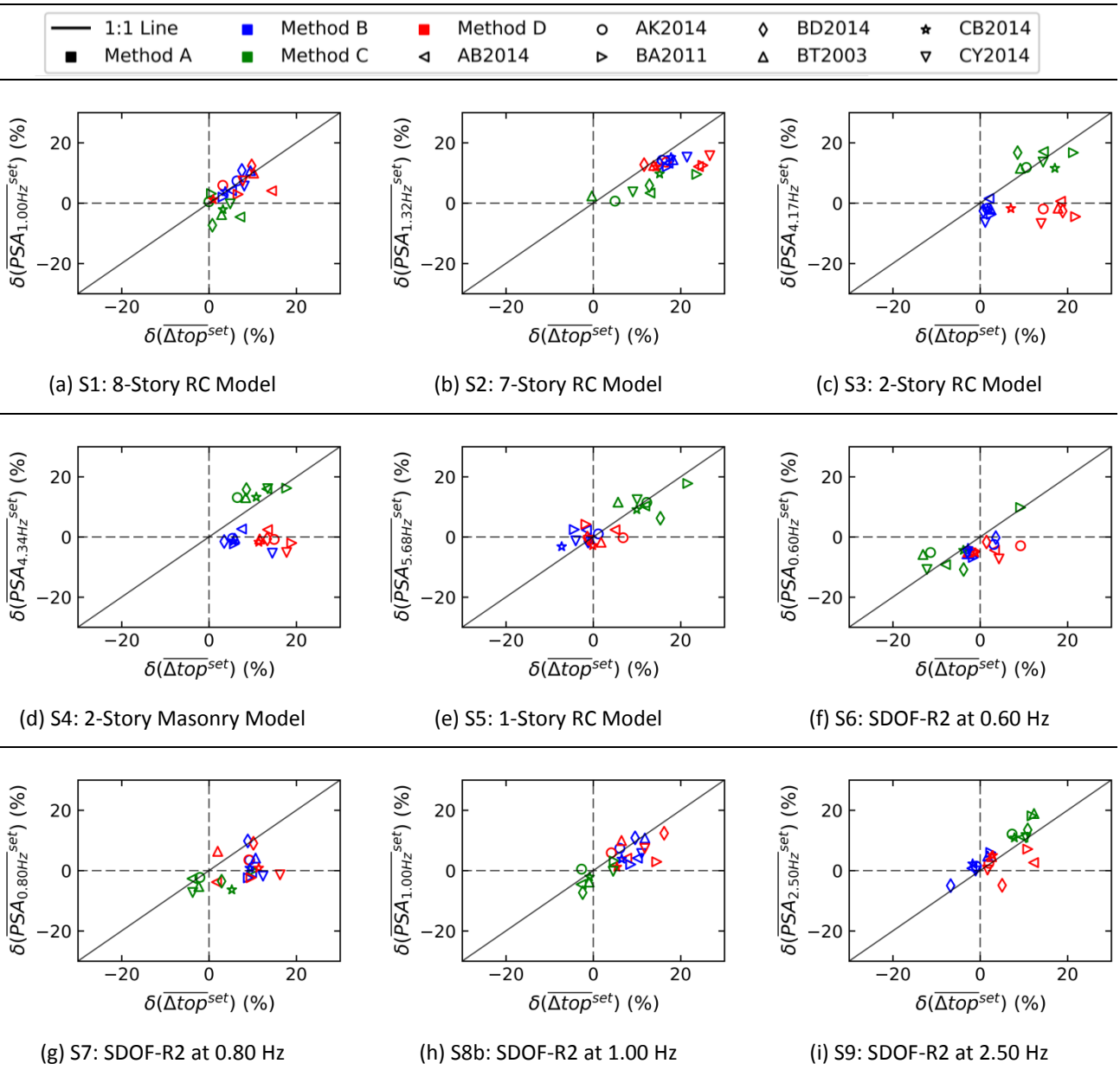

(a) S1: 8-Story RC Model

(b) S2: 7-Story RC Model

(c) S3: 2-Story RC Model

(d) S4: 2-Story Masonry Model

(e) S5: 1-Story RC Model

(f) S6: SDOF-R2 at 0.60 Hz

(g) S7: SDOF-R2 at 0.80 Hz

(h) S8b: SDOF-R2 at 1.00 Hz

(i) S9: SDOF-R2 at 2.50 Hz

Figure C.1.10: The difference in the median of input PSAs at f0 versus the difference in the median of output lateral structural displacements (Δtop) with respect to Method A for seven GMPEs. The x-axis illustrates the difference in the mean of Δtop distributions. The y-axis illustrates the differences in the mean of input PSAs at f0. The solid black line is the equality line. The earthquake scenario is M7.0R40, Vs450, and normal fault. GMPEs such as AB2014, AK2014, BA2011, BD2014, BT2003, CB2014, and CY2014 are shown with the marker in the legend. Methods B, C, and D are represented with blue, green, and red, respectively. The spectrum selection is made with each set including five ground motions. The upper and lower amplitude tolerances are -30% and +30% of the target for Methods A, B, and C, and between-5% and +5% of the target for Method D. The frequency range is from 0.50 Hz and 20.0 Hz. The negative values represent the underprediction relative to Method A and vice versa.

C.1.9 Quantification with Logic Tree

S1: 8-Story RC	**S2**: 7-Story RC	**S3**: 2-Story RC	**S4**: 2-Story Masonry	**S5**: 1-Story RC
f0 = 1.00 Hz	f0 = 1.32 Hz	f0 = 4.17 Hz	f0 = 4.34 Hz	f0 = 5.68 Hz

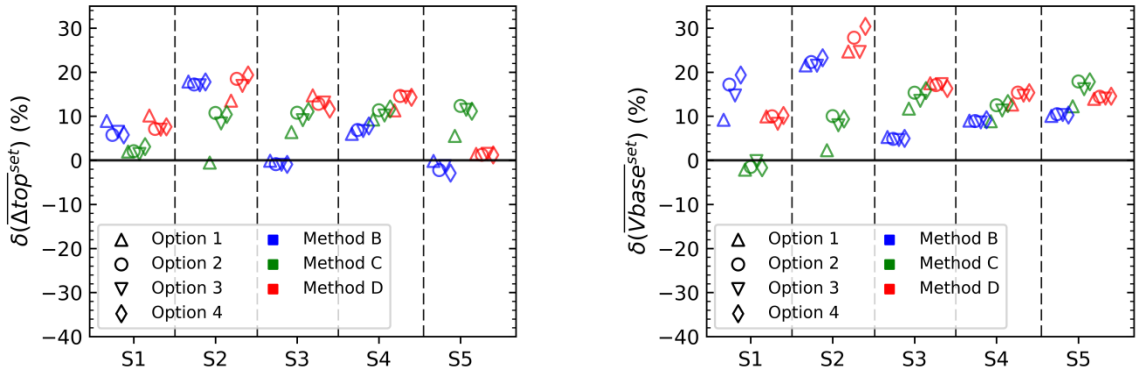

(a) Differences in Roof Displacements (Δtop) (b) Differences in Base Shear Forces (Vbase)

Figure C.1.11: The difference in structural response distributions with the logic tree approach for each set's average. The spectrum compatible selection is made as explained in the caption of Figure 3.4.2. The differences are quantified according to Equations 3.4.1. The labels in y-axis show the ID of the structural model given in the legend above the subfigure. Methods B, C, and D are shown with blue, green, and red colors, respectively. The negative values represent the underprediction relative to Method A and vice versa. The GMPE weight options are provided in Table 3.4.1.

S6: SDOF-R2	**S7**: SDOF=R2	**S8**a: SDOF-R1	S8**b**: SDOF-R2	**S9**: SDOF-R2
f0 = 0.60 Hz	f0 = 0.80 Hz	f0 = 1.00 Hz	f0 = 1.00 Hz	f0 = 2.50 Hz

Complex Models

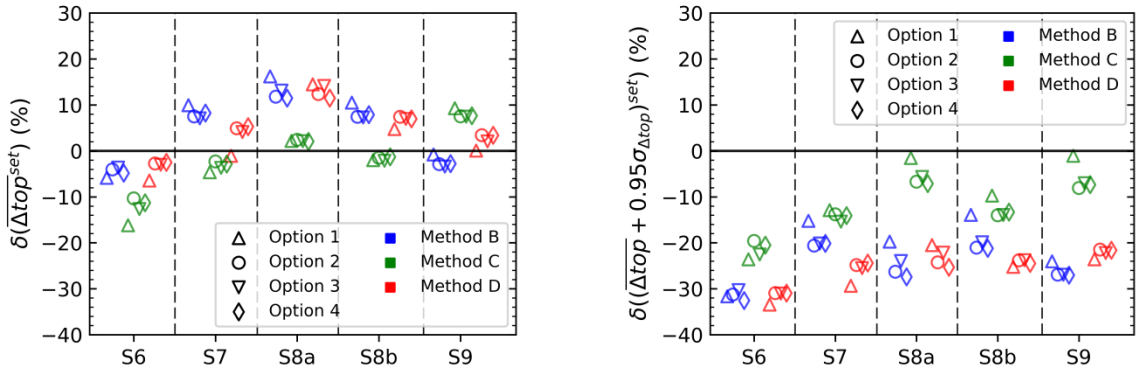

Simple Models

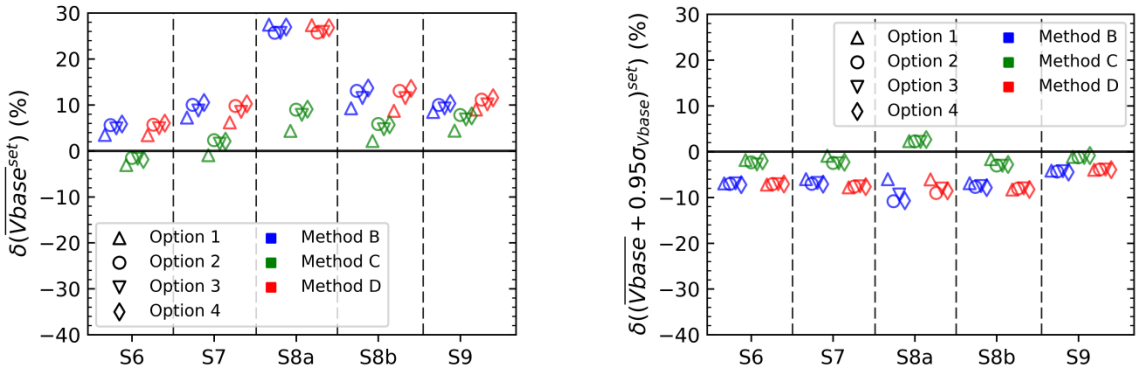

(a) Differences in Roof Displacements (Δtop) (b) Differences in Base Shear Forces (Vbase)

Figure C.1.12: The difference in structural response distributions with the logic tree approach for simple structural models. The similar graphical elements are used with the previous figure.

C.2 Asymmetric Tolerances: GMSM Methods Considering Inter- and Intraset Variability

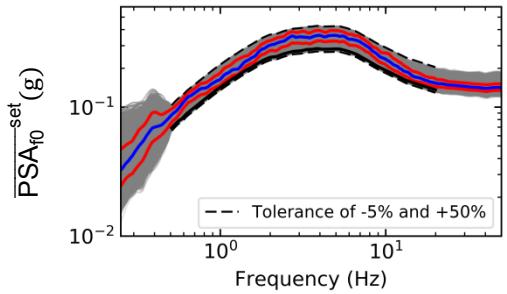

Method A: Unscaled Earthquake Records

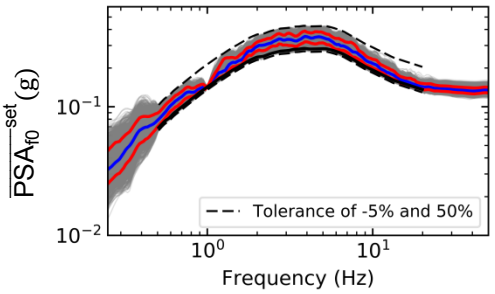

Method B: Linearly Scaled Records to PSA at 1.0 Hz

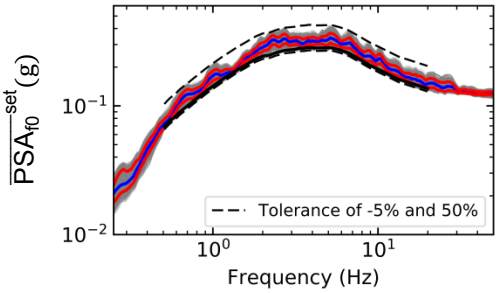

Method C: Loosely Matched Waveforms

Figure C.2.1: Average spectra of all eligible GM sets with the asymmetric tolerances. The target is shown with solid black line and is the median of AK2014 for the scenario of M7.0R40, Vs450, and normal fault. Each set includes five ground motions. The upper and lower amplitude tolerances are shown with dashed black lines: -5% and +50% of the target for Methods A, B, and C. The frequency range is from 0.50 Hz and 20.0 Hz. Grey lines represent the average spectra of the GM sets, $\overline{PSA_{f0}}^{set}$. The 16th and 84th percentiles of eligible GM spectra, $\overline{PSA_{f0}}^{set}$, are shown with solid red lines. The median of all $\overline{PSA_{f0}}^{set}$ is shown with the solid blue line. For Methods A, B, and C, there are 34 174, 8 647, and 948 GM sets, respectively.

C.2.1 Impact on Input PSAs at f0

(a) Distribution of Each Set's Average (of 5 GMs) | (b) Distribution of Each Set's Standard Deviation

PSA at 0.60 Hz

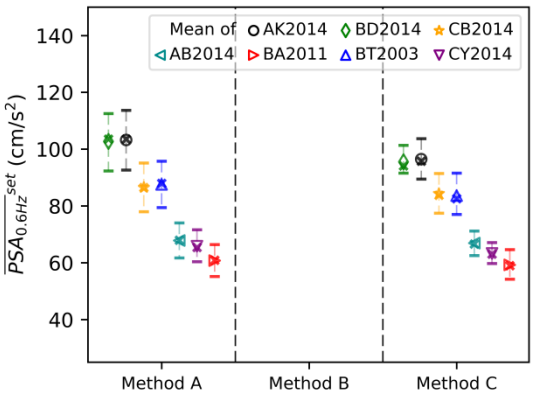

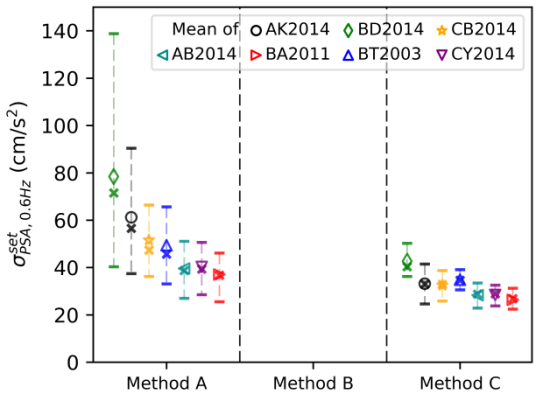

PSA at 0.80 Hz

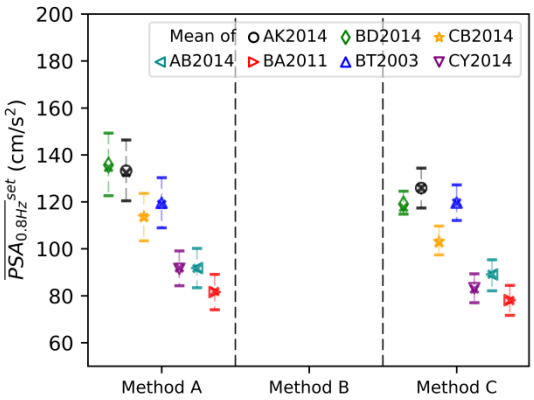

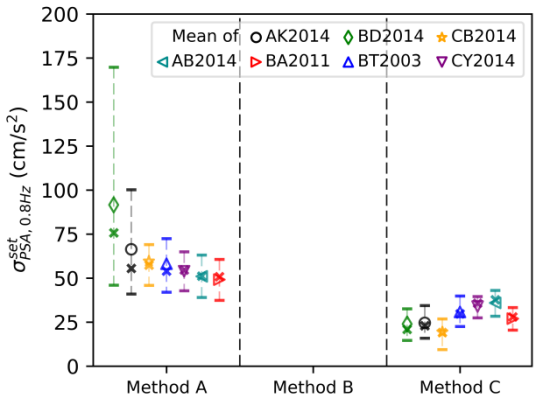

PSA at 1.00 Hz

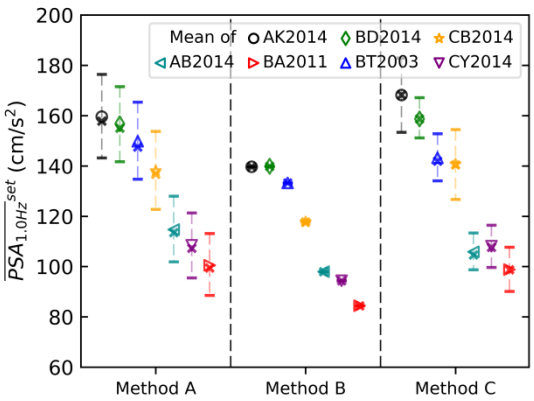

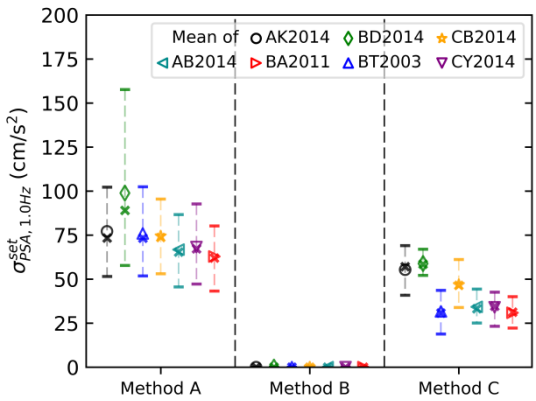

PSA at 1.32 Hz

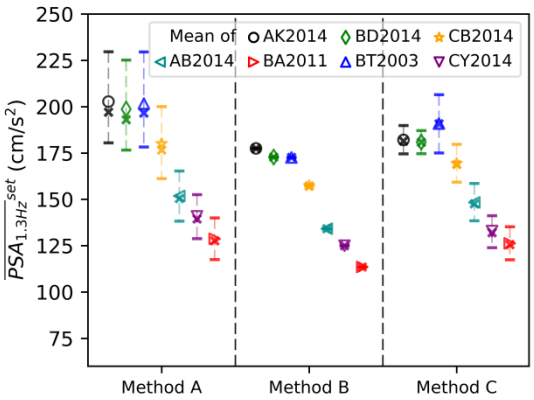

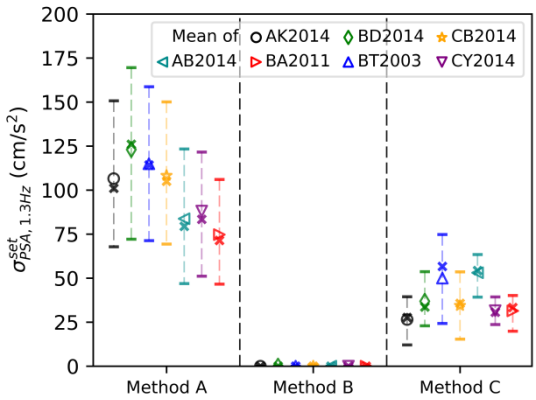

➔ Figure C.2.2, Continued, 1/2

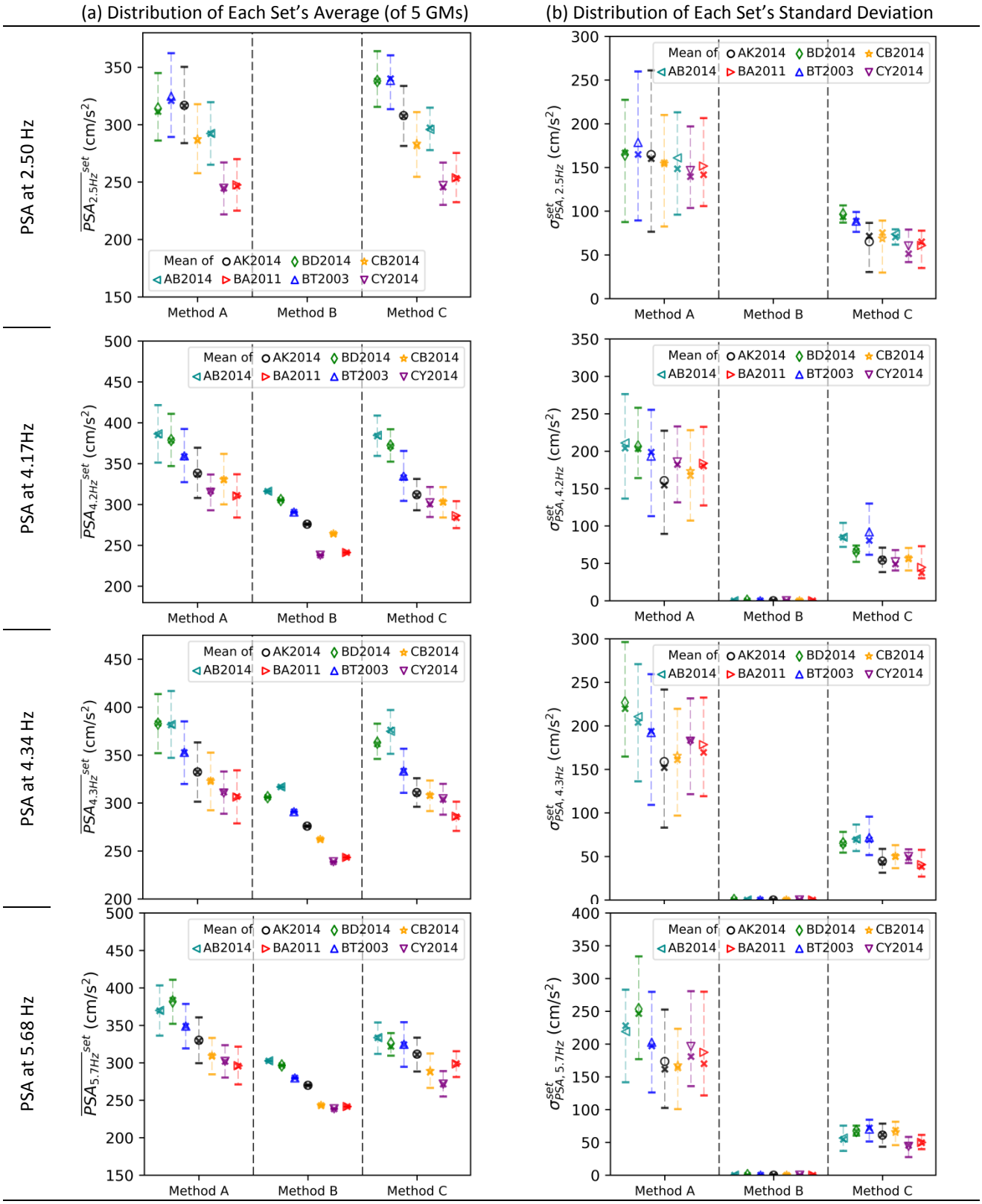

Figure C.2.2: Distribution of pseudo-spectral accelerations (PSA) at f0 (in row-wise) with all GM sets considering each set's average in column (a) and each set's standard deviation in column (b) with the asymmetric tolerances. Each set includes five ground motions. The upper and lower amplitude tolerances are -5% and +50% of the target for Methods A, B, and C. The frequency range is from 0.50 Hz and 20.0 Hz. The target is obtained for the scenario of M7.0R40, Vs450, and normal fault as explained in Section 1.4. Means are demonstrated with the markers and colors in the legend box for corresponded GMPEs. Medians are shown with the cross markers. The 16th and 84th percentiles are plotted with the horizontal bars. MB is not available for PSAs at 0.60, 0.80, and 2.50 Hz.

C.2.2 Impact on Roof (or Lateral) Displacements (Δtop)

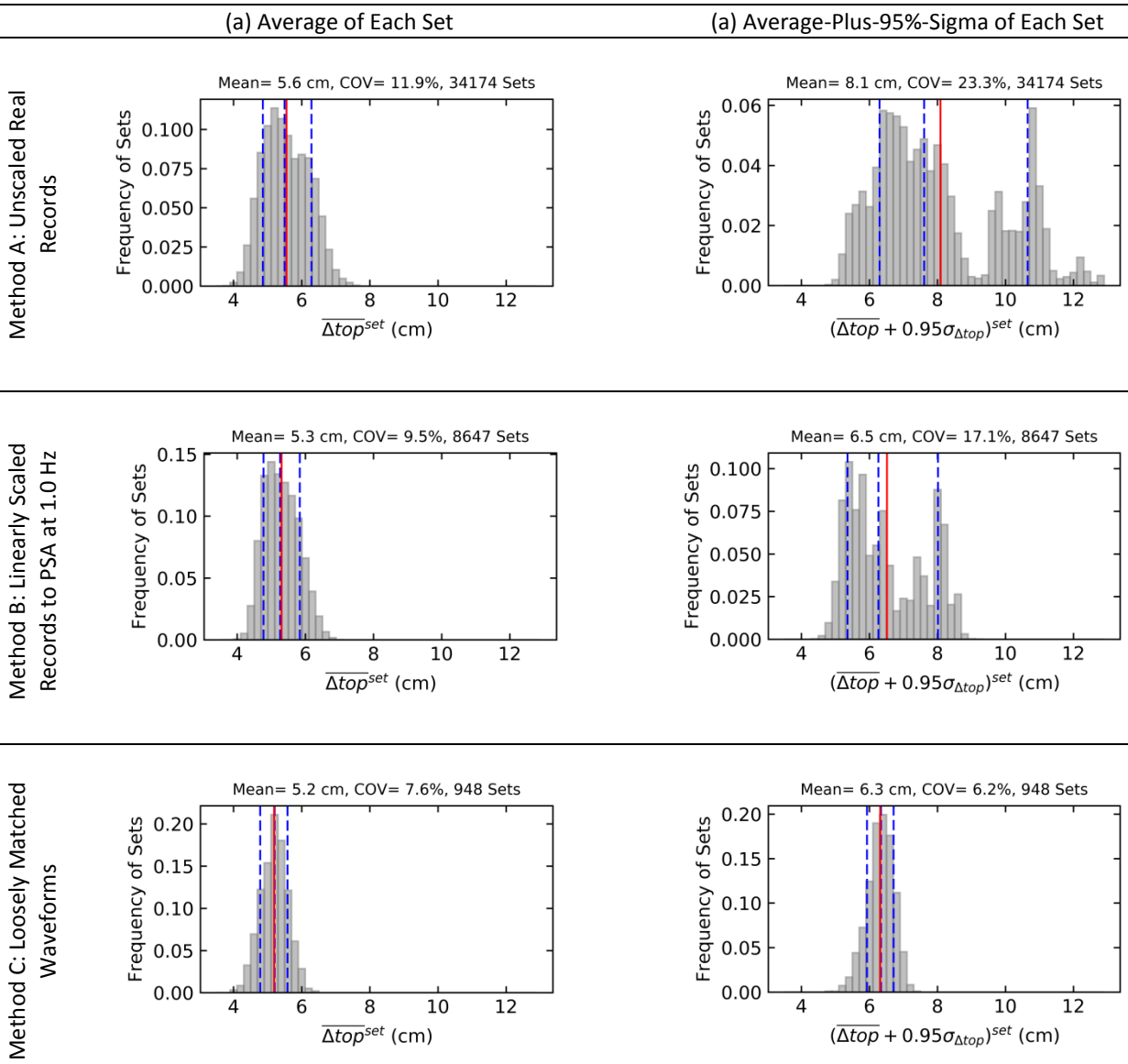

Figure C.2.3: All-eligible-set distribution of PSAs at 1.0 Hz versus the roof displacements of the S1 model (8-Story RC) with the asymmetric tolerance. The target is the median of AK2014 for the scenario of M7.0R40, Vs450, and normal fault. The spectrum compatible selection is performed with a tolerance from-5% to +50% of the target. The nonlinear dynamic analyses are performed to collect the maximum absolute roof displacements of 8-Story RC, the 8-story reinforced concrete model. The average values of five ground motions in a set are shown in the distribution. The mean and the coefficient of variance (COV) of the all-eligible-set distributions are printed over the subfigures. 16th, 50th, and 84th percentiles and median of average values are plotted. The frequency of sets is normalized to 1.0. a tail-like distribution can be observed for $(\overline{\Delta \text{top}} + 0.95\sigma_{\Delta \text{top}})^{\text{set}}$ determined by MA and MB. It suggests that there are not sufficient GM sets revealing structural responses in this range.

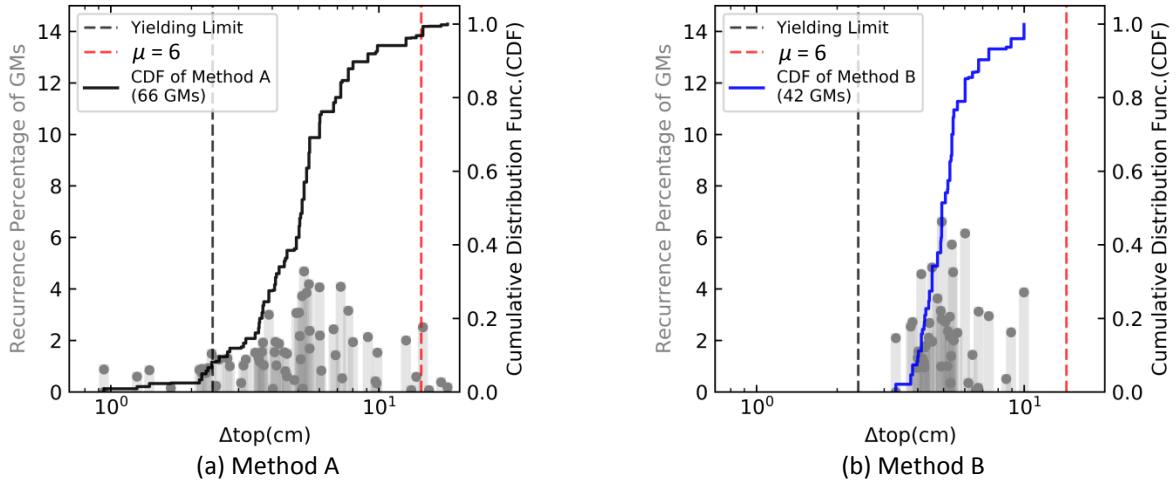

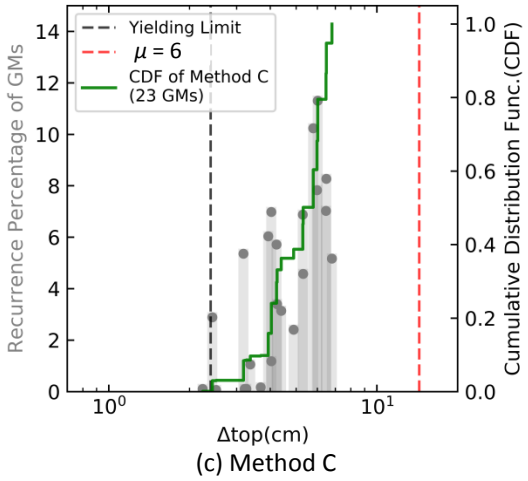

Figure C.2.4: Comparison of recurrence percentages of GMs and cumulative distribution functions (CDF) for roof displacements (Δtop) of the S1 model, 8-story RC model. The spectrum compatible selection is performed as explained in the caption of Figure C.2.3. The x-axis represents the roof displacements (Δtop) from each GM. Along the left-side y-axis, the reoccurrence percentages of GMs are shown, i.e., the frequency of GMs that are repeated among all GM sets. The vertical grey bars are related to the left-side y-axis. Along the right-side y-axis, cumulative distribution function (CDF) is shown. CDF is the summation of reoccurrence frequencies. The solid lines in black (Method A in a), in blue (Method B in b), in green (Method C in c), and in red (Method D in d) relate to the right-side y-axis. The yielding limit of the S1 model is shown with the vertical black dashed lines. The ductility demand, μ, of 6 is shown with the vertical red dashed lines. The amount of GMs is noted in the legend box.

The GMs causing more substantial structural damage (in terms of Δtop) repeat more frequently in the GM sets with the asymmetric tolerances than the symmetric tolerances (Figure 3.3.3).

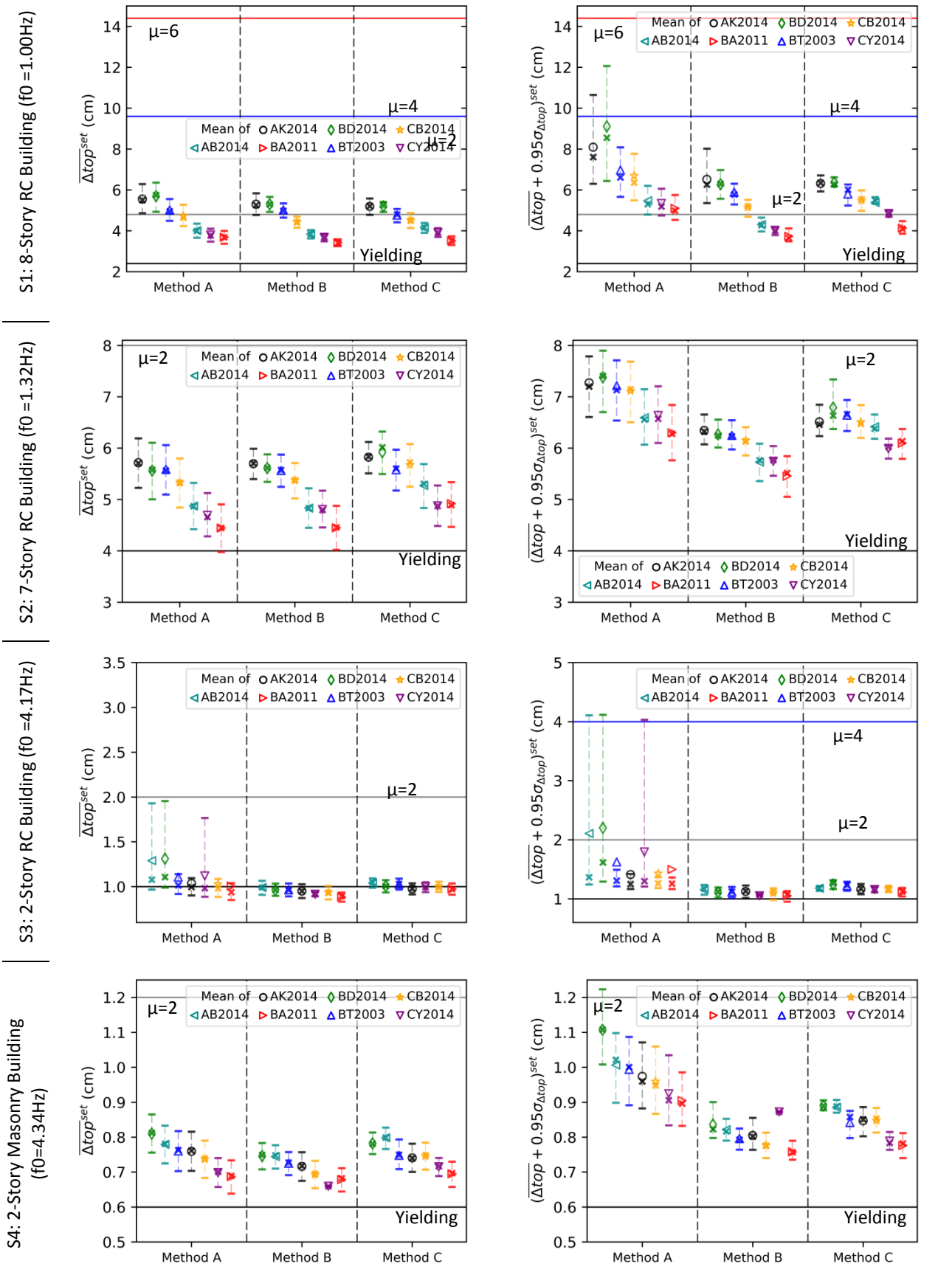

➔ Figure C.2.5, Continued, 1/3

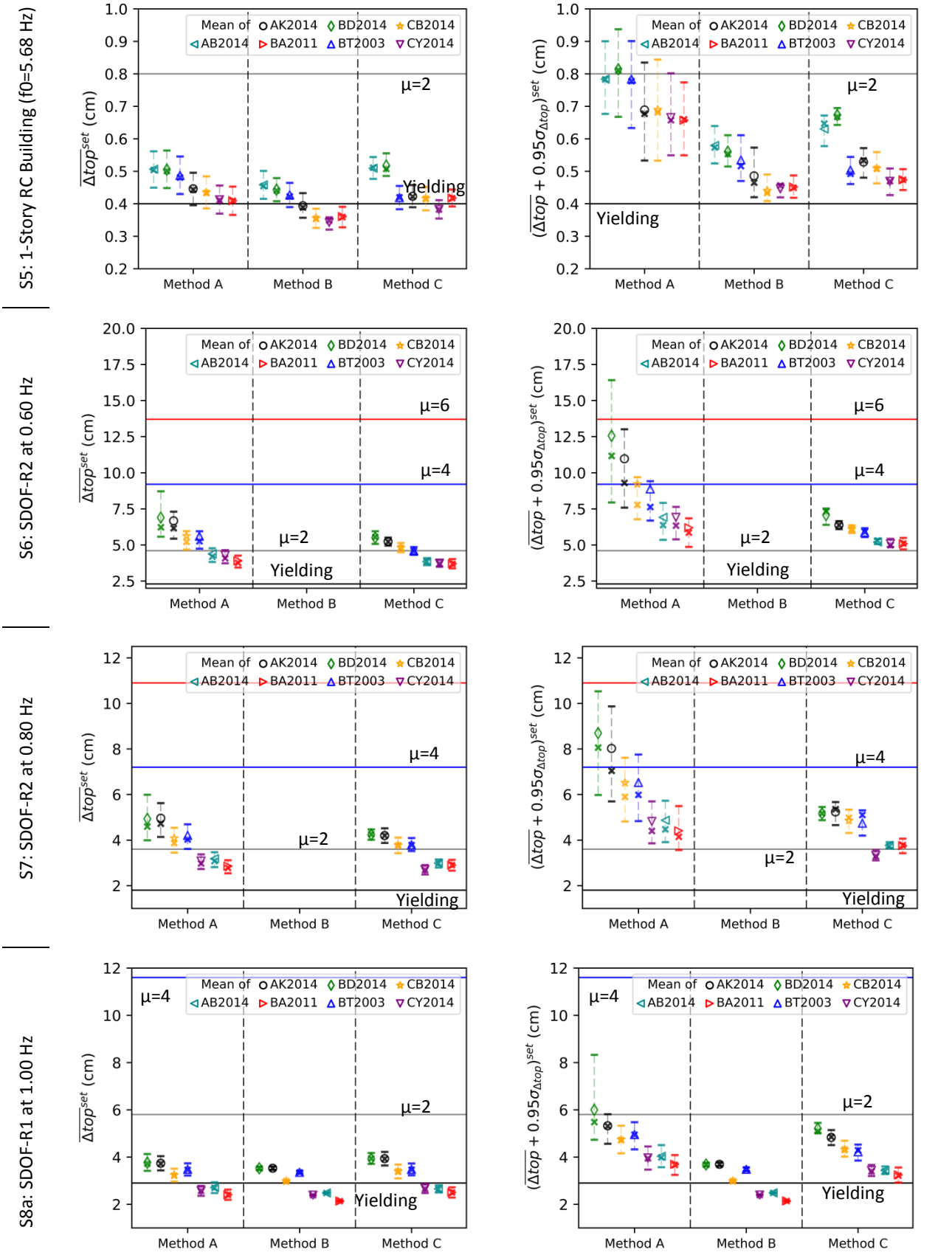

➔ Figure C.2.5, Continued, 2/3

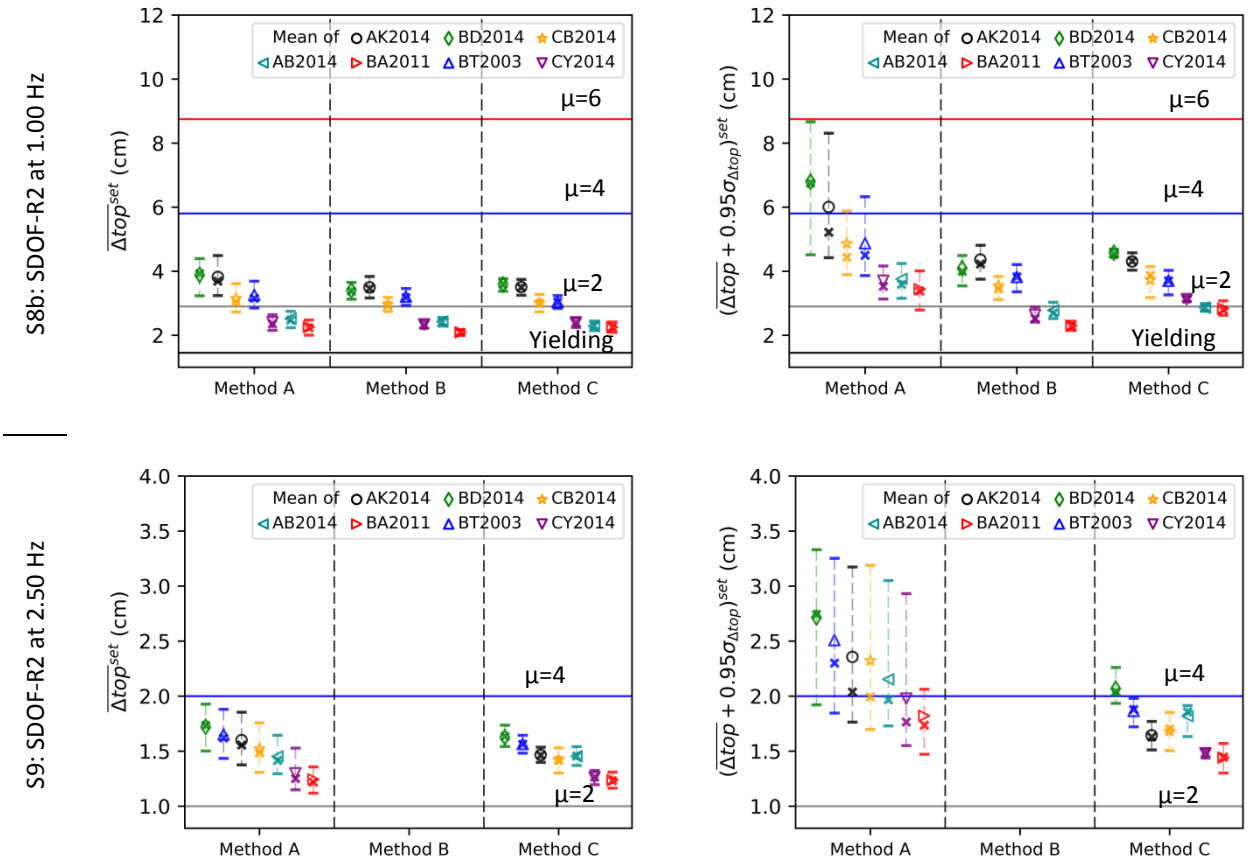

Figure C.2.5: Distribution of roof (or lateral) displacements (Δtop) with all GM sets considering intraset variability with the asymmetric tolerances. Each set includes five ground motions. The upper and lower amplitude tolerances are -5% and +50% of the target for Methods A, B, and C. The frequency range is from 0.50 Hz and 20.0 Hz. The target is obtained for the scenario of M7.0R40, Vs450, and normal fault as explained in Section 1.4. In column-wise, distributions of each set's average are shown in (a), and the distributions of each set's average-plus-95%-standard-deviation are shown in (b). In row-wise, the responses of structural models are listed. Means are demonstrated with the markers and colors in the legend box for the corresponded GMPEs. Medians are shown with the cross markers. The 16th and 84th percentiles are plotted with the horizontal bars. The yielding limit and the ductility demands (μ) of 2, 4, and 6 are shown with a horizontal solid line with black, grey, blue, and red, respectively. For some simple structures, Method B selection is not available.

C.2.3 Impact on Base Shear Forces (Vbase)

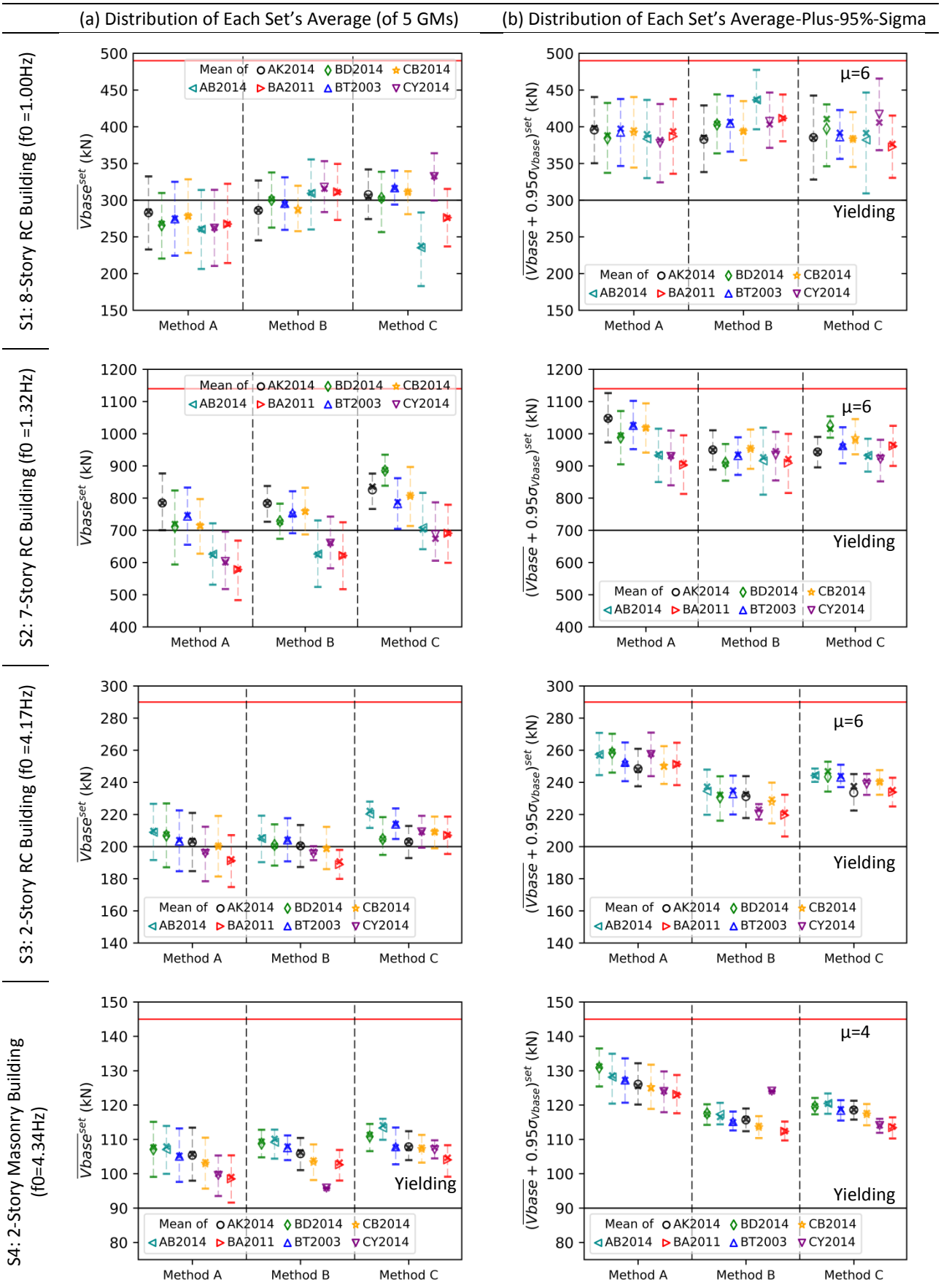

➔ Figure C.2.6, Continued, 1/3

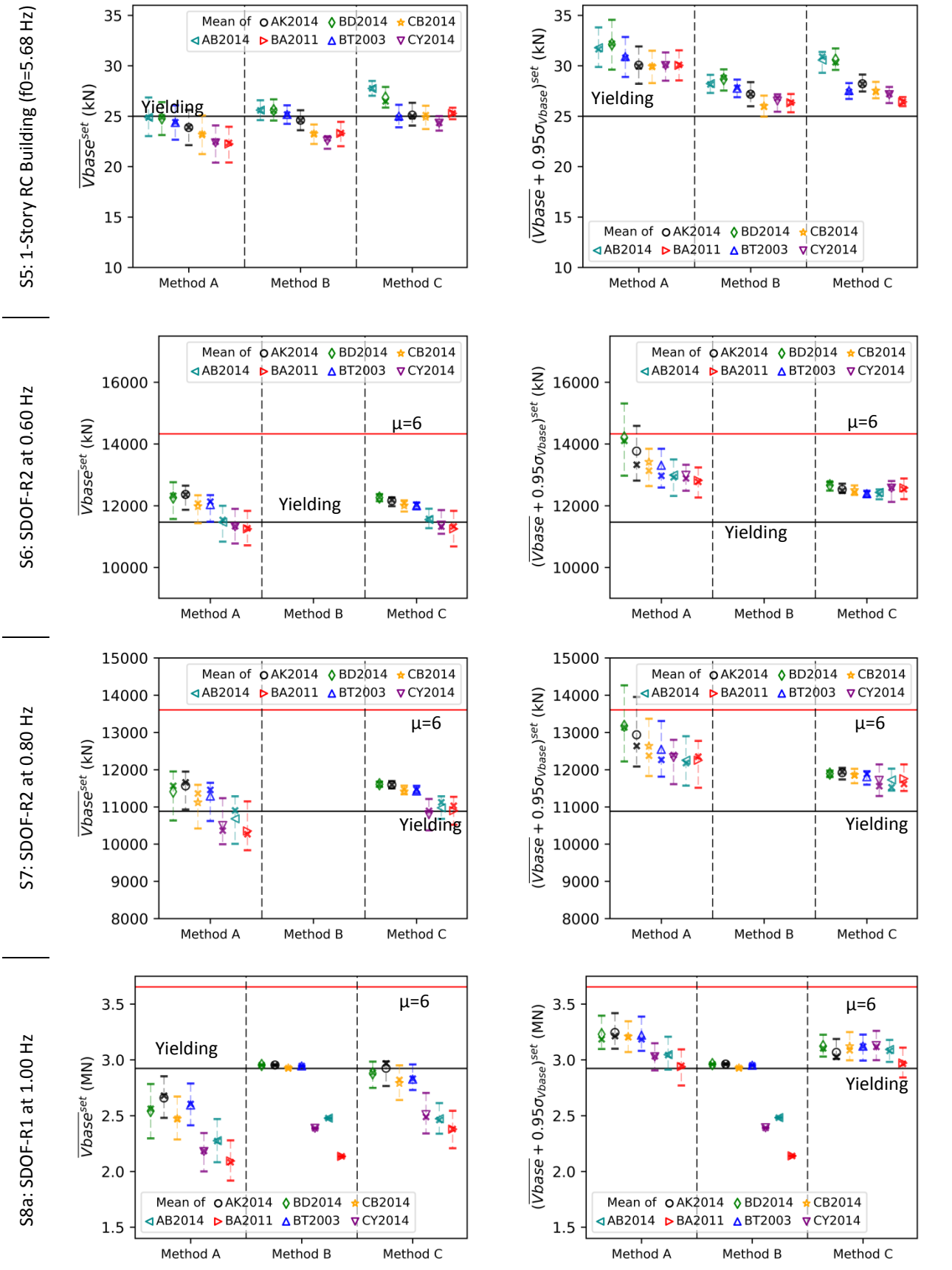

➔ Figure C.2.6, Continued, 2/3

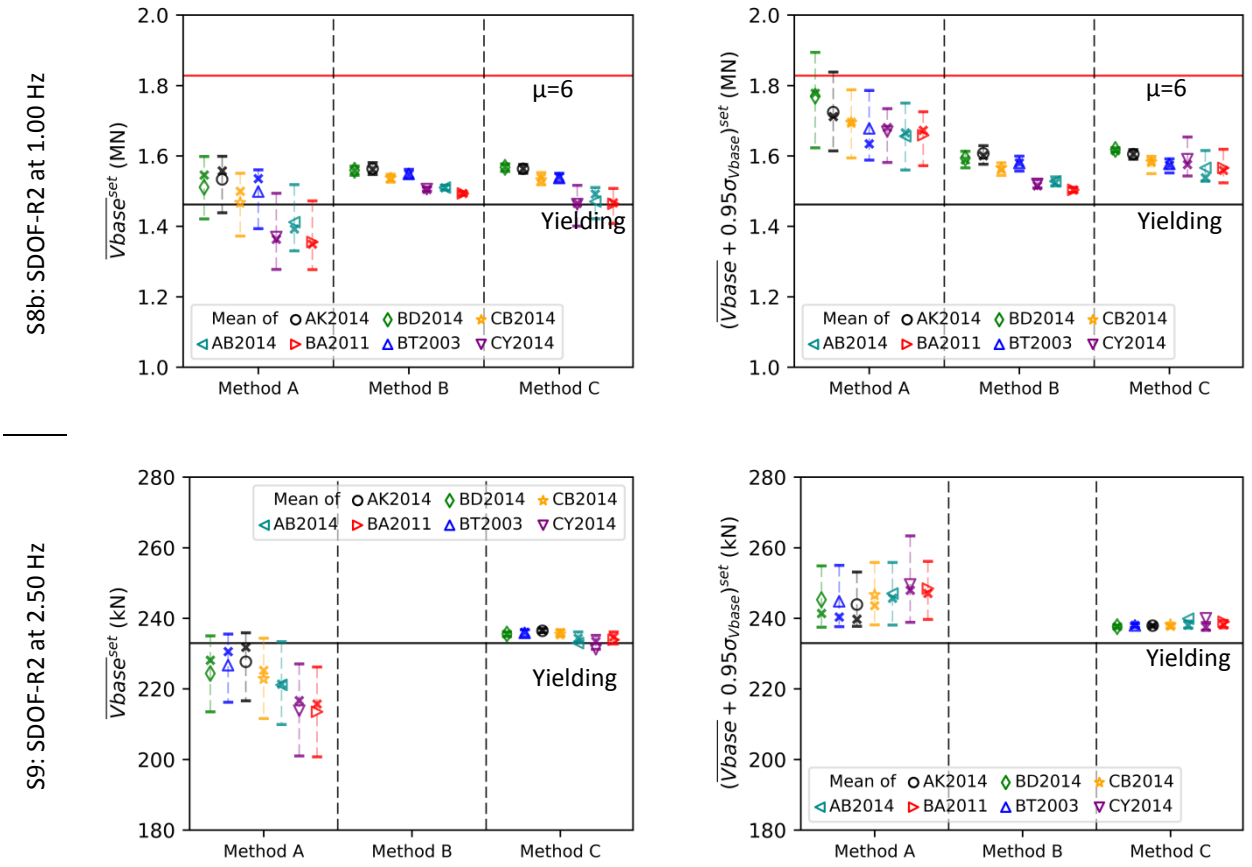

Figure C.2.6: Distribution of base shear forces (Vbase) with all GM sets considering intraset variability with the asymmetric tolerances. Each set includes five ground motions. The upper and lower amplitude tolerances are -5% and +50% of the target for Methods A, B, and C. The frequency range is from 0.50 Hz and 20.0 Hz. The target is obtained for the scenario of M7.0R40, Vs450, and normal fault as explained in Section 1.4. In column-wise, distributions of each set's average are shown in (a), and the distributions of each set's average-plus-95%-standard-deviation are shown in (b). In row-wise, the responses of structural models are listed. Means are demonstrated with the markers and colors in the legend box for the corresponded GMPEs. Medians are shown with the cross markers. The 16th and 84th percentiles are plotted with the horizontal bars. The yielding limit and ductility demands (μ) are shown with a horizontal solid line of black and red, respectively. Vbase is obtained at the response time when the absolute maximum of Δtop is obtained. For some simple structures, Method B selection is not available.

C.2.4 Impact on Intensity Drift Ratio (IDR)

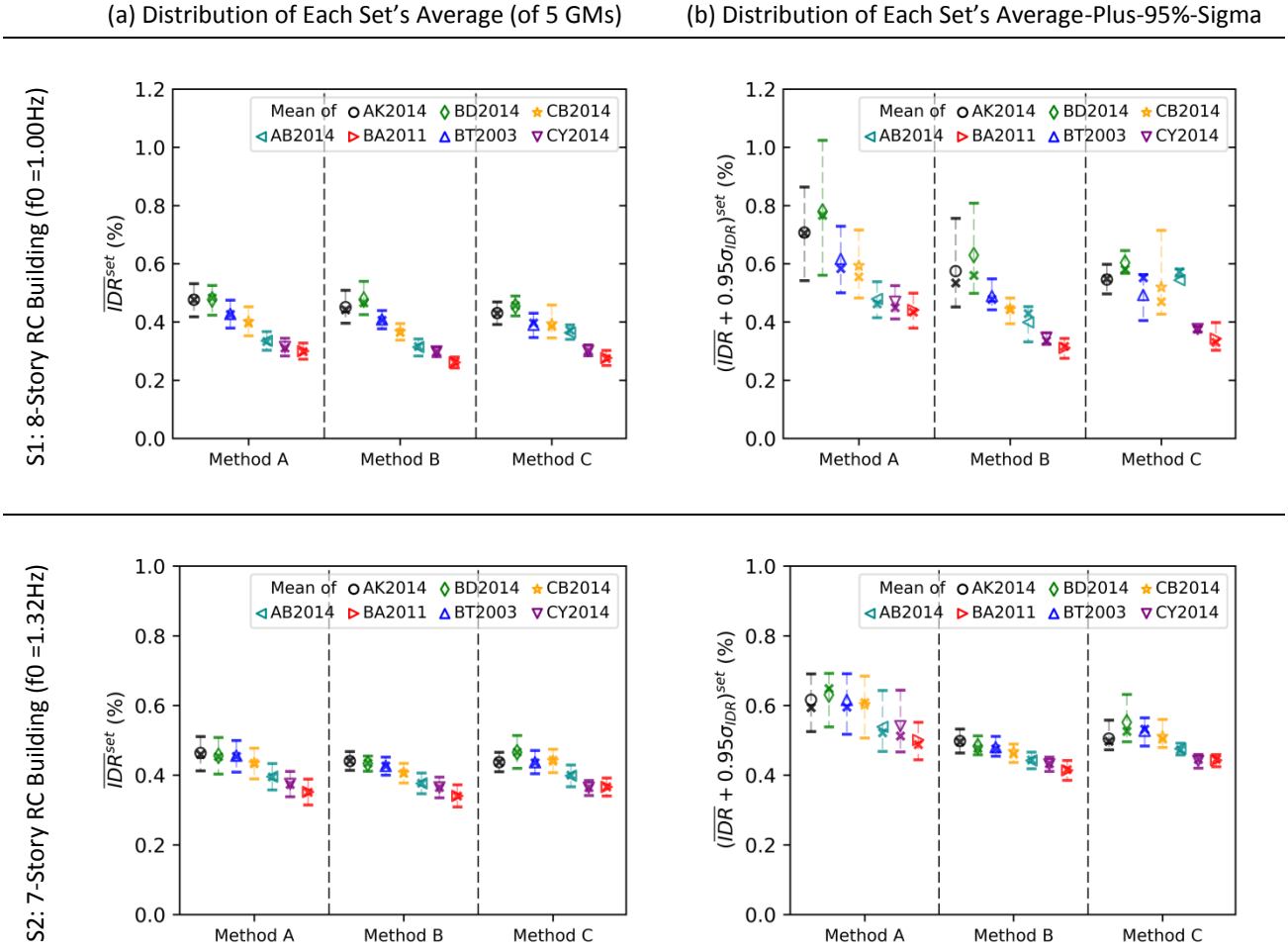

Figure C.2.7: Distribution of interstory drift ratio (IDR) with all GM sets considering intraset variability with the asymmetric tolerances. Each set includes five ground motions. The upper and lower amplitude tolerances are -5% and +50% of the target for Methods A, B, and C. The frequency range is from 0.50 Hz and 20.0 Hz. The target is obtained for the scenario of M7.0R40, Vs450, and normal fault as explained in Section 1.4. In column-wise, distributions of each set's average are shown in (a), and the distributions of each set's average-plus-95%-standard-deviation are shown in (b). In row-wise, the responses of structural models are listed. Means are demonstrated with the markers and colors in the legend box for the corresponded GMPEs. Medians are shown with the cross markers. The 16th and 84th percentiles are plotted with the horizontal bars. IDR is obtained at the response time when the absolute maximum of Δtop is obtained.

C.2.5 Impact on Damage Index (DI)

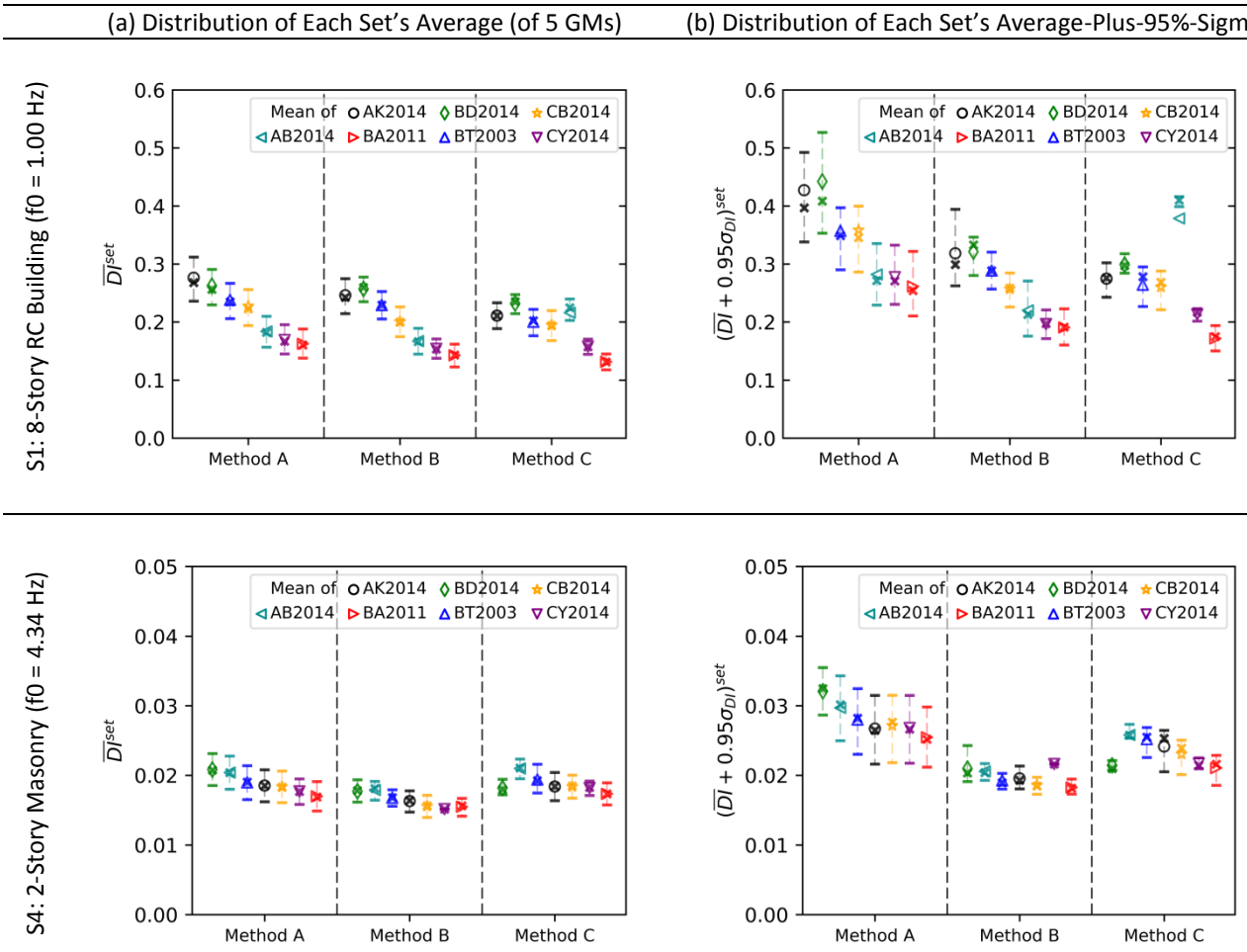

Figure C.2.8: Distribution of global damage index (DI) with all GM sets considering intraset variability with the asymmetric tolerances. Each set includes five ground motions. The upper and lower amplitude tolerances are -5% and +50% of the target for Methods A, B, and C. The frequency range is from 0.50 Hz and 20.0 Hz. The target is obtained for the scenario of M7.0R40, Vs450, and normal fault as explained in Section 1.4. In column-wise, distributions of each set's average are shown in (a), and the distributions of each set's average-plus-95%-standard-deviation are shown in (b). In row-wise, the responses of structural models are listed. Means are demonstrated with the markers and colors in the legend box for the corresponded GMPEs. Medians are shown with the cross markers. The 16th and 84th percentiles are plotted with the horizontal bars. Global DI is obtained at the response time when the absolute maximum of Δtop is obtained.

C.2.6 Quantification of Impact due to the Intraset and Interset Variability

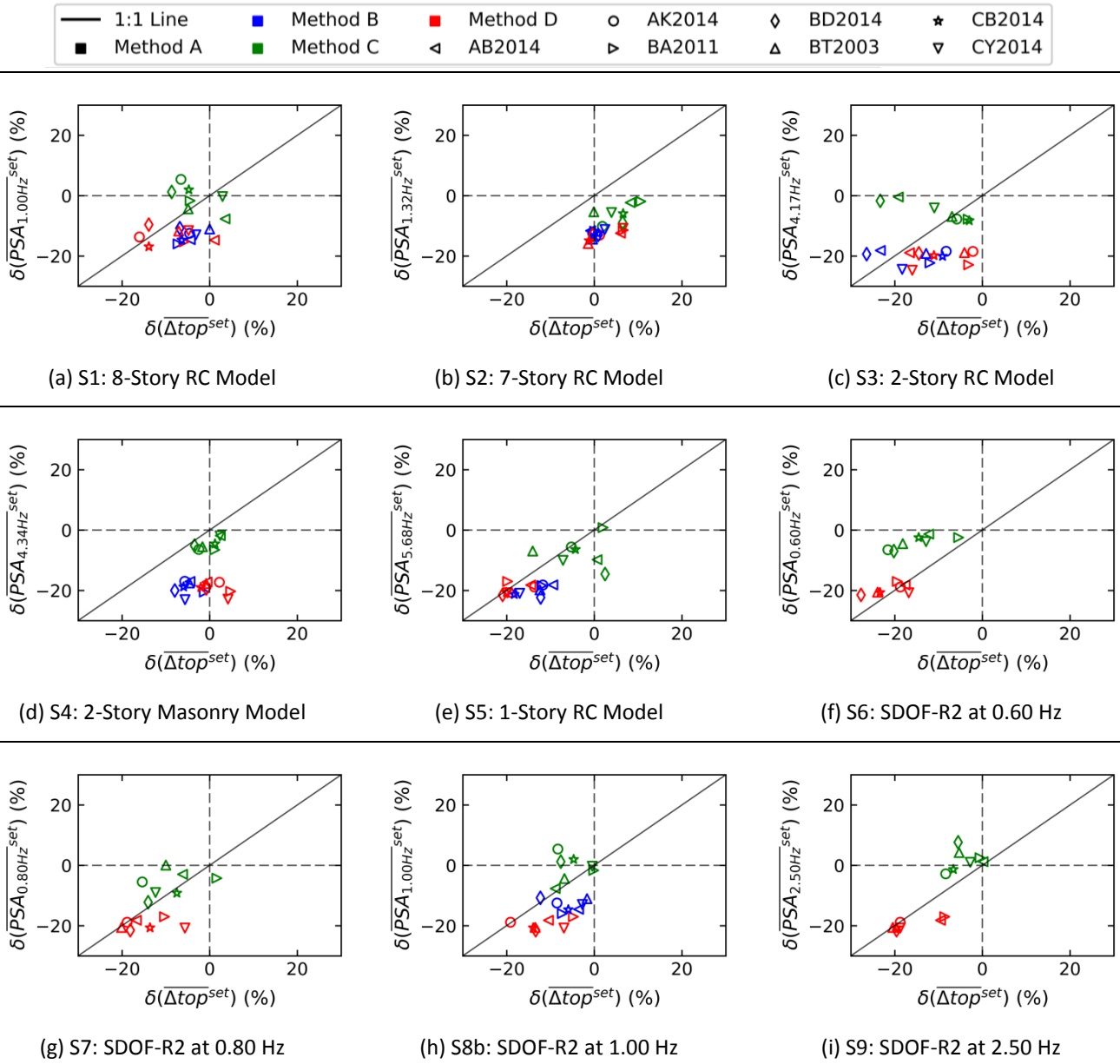

(a) S1: 8-Story RC Model (b) S2: 7-Story RC Model (c) S3: 2-Story RC Model

(d) S4: 2-Story Masonry Model (e) S5: 1-Story RC Model (f) S6: SDOF-R2 at 0.60 Hz

(g) S7: SDOF-R2 at 0.80 Hz (h) S8b: SDOF-R2 at 1.00 Hz (i) S9: SDOF-R2 at 2.50 Hz

Figure C.2.9: The difference in mean of input PSAs at f0 versus the difference in mean of output lateral structural displacements (Δtop) with respect to Method A for seven GMPEs. The x-axis illustrates the difference in the mean of Δtop distributions. The y-axis illustrates the differences in the mean of input PSAs at f0. The solid black line is the equality line. The earthquake scenario is M7.0R40, Vs450, and normal fault. GMPEs such as AB2014, AK2014, BA2011, BD2014, BT2003, CB2014, and CY2014 are shown with the marker in the legend. Methods B, C, and D are represented with black, blue, green, and red, respectively. The spectrum selection is made with each set including five ground motions. The upper and lower amplitude tolerances are -5% and +50% of the target for Methods A, B, and C, and between-5% and +5% of the target for Method D. The frequency range is from 0.50 Hz and 20.0 Hz. For some simple structures, Method B selection is not available. The negative values represent underprediction relative to Method A and vice versa.

1: 8-Strory RC f0 = 1.00 Hz	**2**: 7-Story RC f0 = 1.32 Hz	**3**: 2-Story RC f0 = 4.17 Hz	**4**: 2-Story Masonry f0 = 4.34 Hz	**5**: 1-Story RC f0 = 5.68 Hz
6: SDOF-R2 f0 = 0.60 Hz	**7**: SDOF=R2 f0 = 0.80 Hz	**8**(a): SDOF-R1 f0 = 1.00 Hz	(8)**b**: SDOF-R2 f0 = 1.00 Hz	**9**: SDOF-R2 f0 = 2.50 Hz

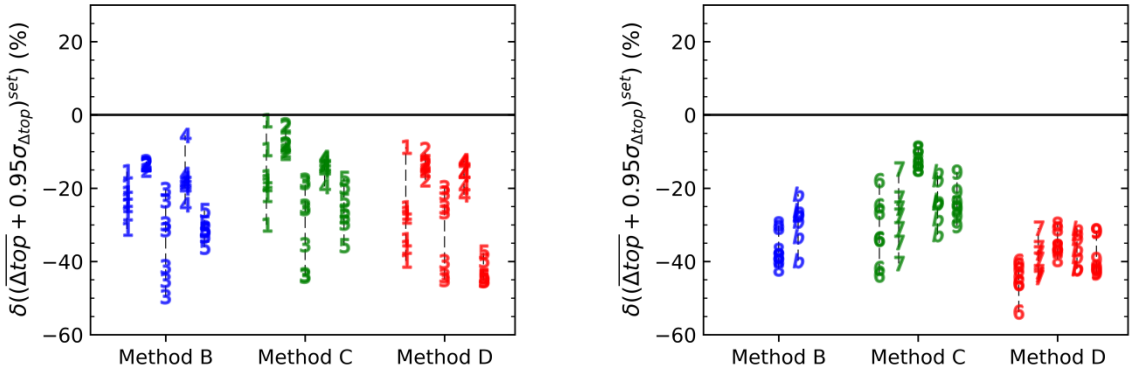

Figure C.2.10: The difference in mean of lateral structural displacements (Δtop) distributions at each set's average-plus-95%-standard-deviation. The spectrum compatible selection is made as explained in the caption of Figure C.2.9. The markers are shown with the ID of the structural model given in the legend above the subfigures. The differences are quantified according to Equation 3.4.2. Methods B, C, and D are shown with blue, green, and red colors, respectively. The negative values represent the underprediction relative to Method A and vice versa.

1: 8-Strory RC f0 = 1.00 Hz	**2**: 7-Story RC f0 = 1.32 Hz	**3**: 2-Story RC f0 = 4.17 Hz	**4**: 2-Story Masonry f0 = 4.34 Hz	**5**: 1-Story RC f0 = 5.68 Hz

Complex Models

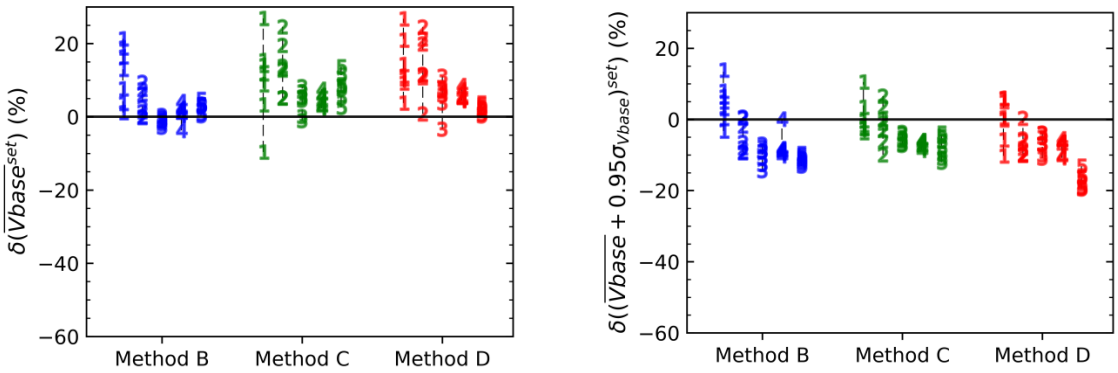

6: SDOF-R2 f0 = 0.60 Hz	**7**: SDOF=R2 f0 = 0.80 Hz	**8**(a): SDOF-R1 f0 = 1.00 Hz	(8)**b**: SDOF-R2 f0 = 1.00 Hz	**9**: SDOF-R2 f0 = 2.50 Hz

Simple Models

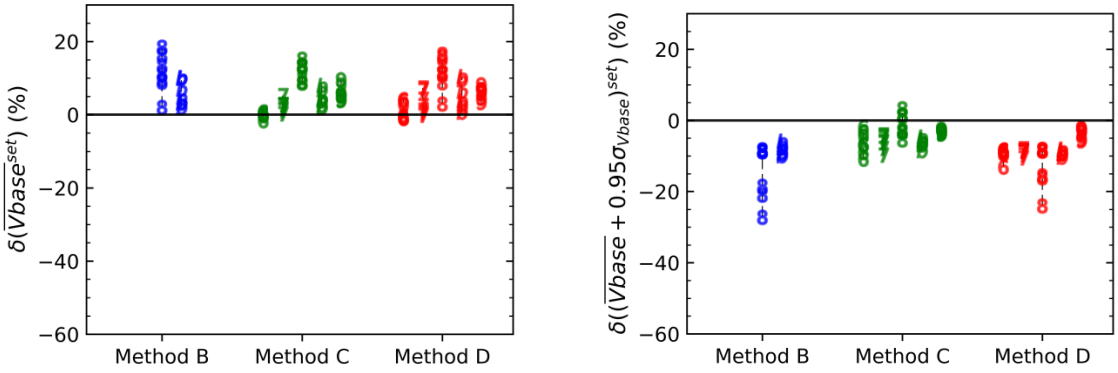

Figure C.2.11: The difference in mean of base shear force (Vbase) distributions with asymmetric tolerances. The spectrum compatible selection is made as explained in the caption of Figure C.2.9. The markers are shown with the ID of the structural model given in the legend above the subfigures. The differences are quantified according to Equations 3.4.1 and 3.4.2. Methods B, C, and D are shown with blue, green, and red colors, respectively. The negative values represent the underprediction relative to Method A and vice versa.

1: 8-Strory RC f0 = 1.00 Hz	**2**: 7-Story RC f0 = 1.32 Hz

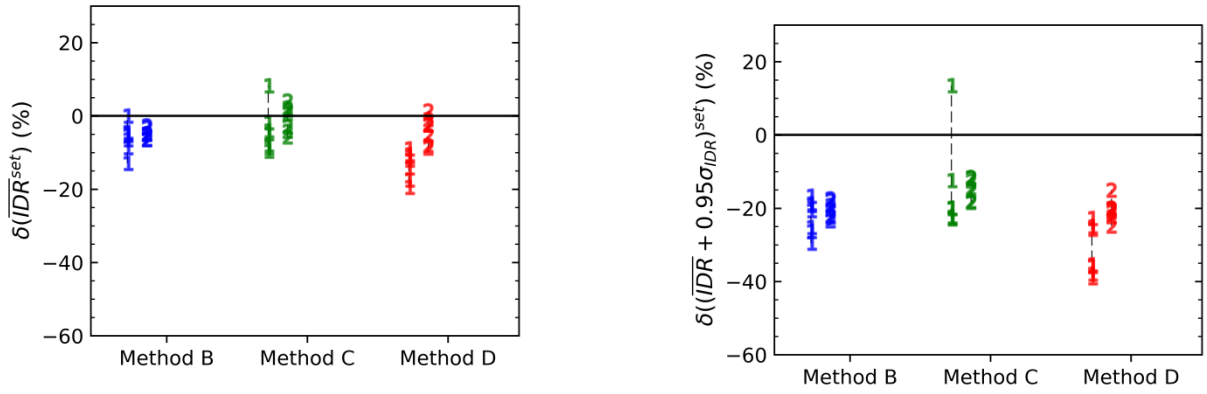

Figure C.2.12: The difference in mean of interstory drift ratio (IDR) distributions with asymmetric tolerances. The same graphical elements are used in the previous figure.

1: 8-Strory RC f0 = 1.00 Hz	**4**: 2-Story Masonry f0 = 4.34 Hz

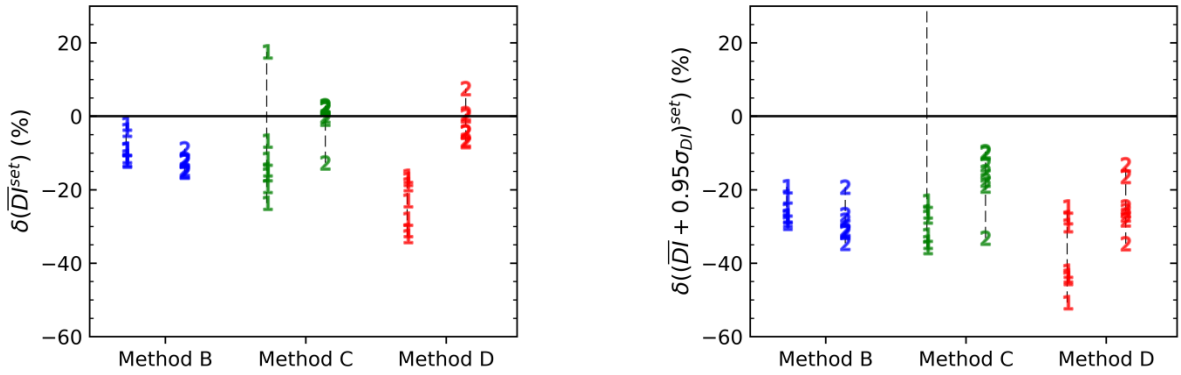

Figure C.2.13: The difference in mean of global damage index (DI) distributions with asymmetric tolerances. The same graphical elements are used in the previous figure.

C.2.7 Quantification with Logic Tree

1: 8-Strory RC f0 = 1.00 Hz	**2**: 7-Story RC f0 = 1.32 Hz	**3**: 2-Story RC f0 = 4.17 Hz	**4**: 2-Story Masonry f0 = 4.34 Hz	**5**: 1-Story RC f0 = 5.68 Hz

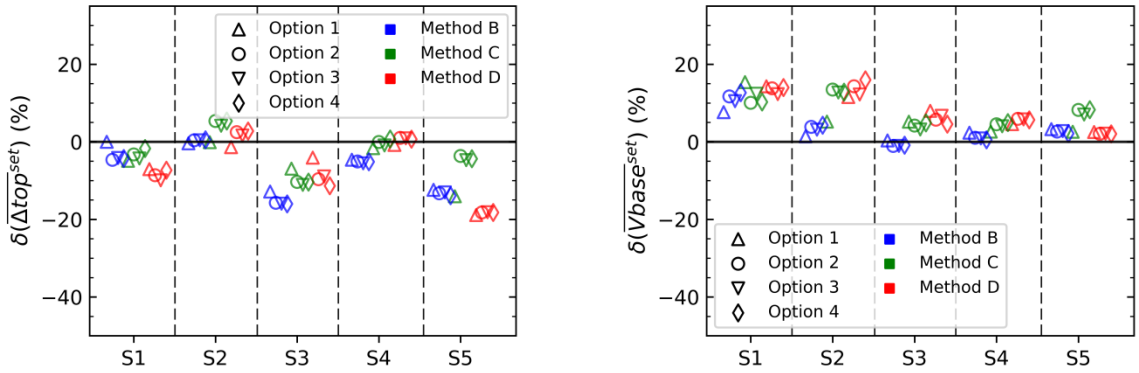

Figure C.2.14: The difference in structural response distributions relative to Method A with the logic tree approach and asymmetric tolerances. The differences in distributions of each set's average are shown. The spectrum compatible selection is made as explained in the caption of Figure C.2.9. The differences are quantified according to Equation 3.4.1. The labels in y-axis show the ID of the structural model given in the legend above the subfigure. Methods B, C, and D are shown with blue, green, and red colors, respectively. The negative values represent the underprediction relative to Method A and vice versa. The GMPE weight options are provided in Table 3.4.1.

C.3 Perspective

C.3.1 Code-Based Design Spectra and GMPE Spectrum

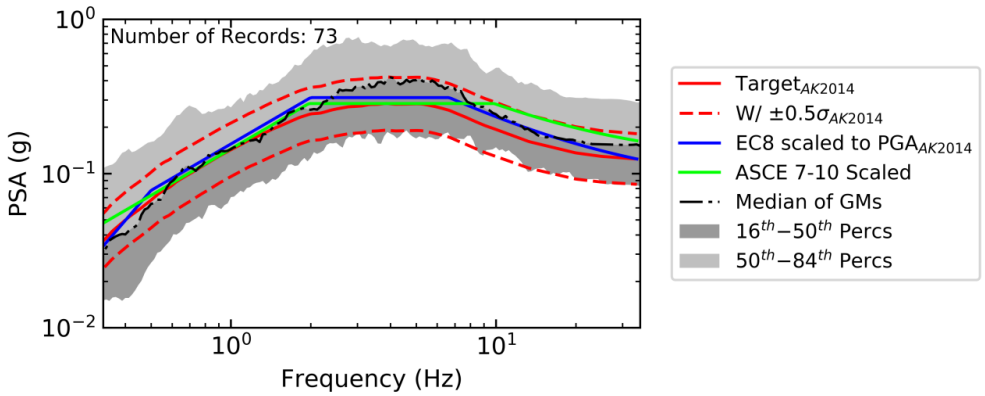

Figure C.3.1. Response spectrum of GMs and alternative target spectra. The AK2014 spectrum is shown by the solid red line and the half-sigma-around-median spectra are shown with the dashed red lines. It is obtained for the scenario of M7.0, Rhypo 40.0 km, Vs30 450 m/s, and normal fault. The EC8 spectrum is scaled to the PGA of the AK2014 spectrum. The ASCE 7-10 spectrum is scaled to the AK2014 spectrum at 1.00 Hz and 4.00 Hz.

The EC8 and ASCE 7-10 spectra reach similar amplitudes with the AK2014 spectrum from the low frequencies to 1.00 Hz. The EC8 and ASCE7-10 spectra are above the AK2014 spectrum with a sharp curve change at around 2.00 Hz. The ASCE 7-10 spectrum has the largest amplitudes at high frequencies (beyond 9.00 Hz). It is expected to have similar (and slightly higher) structural responses distributions with the code-based design spectra for the structural models in this study.

C.3.2 Earthquake Scenario of M5.5R20 and Vs450

A different earthquake scenario with M5.5R20 and Vs450 is tested in this subsection. The collected and modified GMs are shown in Figure C.3.2. The median spectrum in the unscaled earthquake records (MA) is mostly above the target. The loosely spectrum-matched waveforms (MC) result in the median spectrum around the target with reduced spectral variability at higher frequencies (above 5.0 Hz). The tightly spectrum-matched waveforms (MD) reveal the closest spectra to the target with a peak at higher frequencies (out of criteria). The linearly scaling method is not considered.

The GMs, which are refined with respect to the PSAs at 4.34 Hz, are compared between the input PSAs at 4.34 Hz and the roof displacements of the S4 model (introduced in Section 2.4.2) in Figure C.3.3. The structural responses mostly remain in the elastic range and each method reveals similar responses. For MC and MD, the input PSA variability is reduced, and the output structural variability is considerable.

Then, the spectrum compatible selection is performed for the target spectrum of AK2014 and the scenario. The set distributions of the IMs are given in Figure C.3.4. The variability in the GM characteristics is reduced by MC and MD except for SCAV. The means of the IM distributions are underpredicted by the modified GMs relative to MA.

The impact on the set distribution of the PSAs at 4.34 Hz and the structural responses are shown in Figure C.3.5. In this example, the upper and lower amplitude tolerances are tight between +20% and -5% for MA and MC (which are roughly between 0.30σ and -0.05σ in Figure 1.10.1). They are between ±5% for MD. The set variability in the structural responses remains small. Therefore, a single set likely represents the all-GM-set distribution. The differences among the GMSM methods are slight.

The analyses are repeated for other GMPEs with the use of the equivalent GMPE parameters in Figure C.3.5. The differences in PSAs and the structural responses are significant due to the choice of a GMPE. The use of intraset approach with some standard deviation increases the mean of the response distributions about 50%. The structural responses remain mostly in the elastic range.

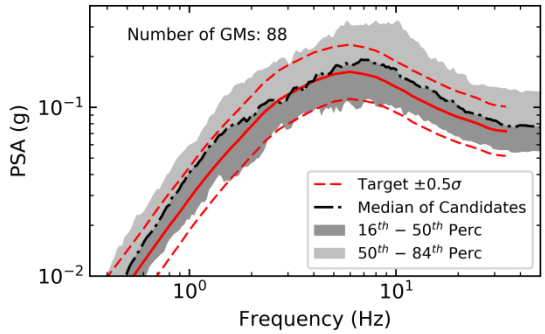

(a) Method A: Unscaled Real Records

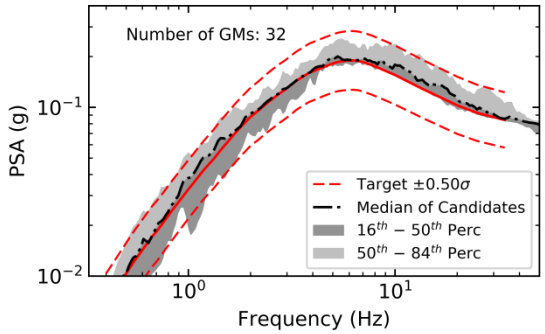

(c) Method C: Loosely Matched Waveforms

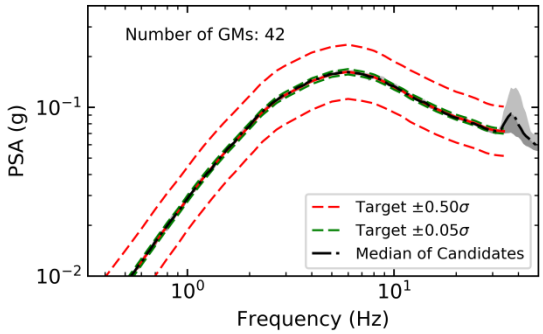

(d) Method D: Tightly Matched Waveforms

Figure C.3.2: The median of AK2014 for the defined scenario and the 16th, 50th and 84th percentiles of pseudo-spectral accelerations (PSAs) of ground motions (GMs) in Methods A, C, and D. The GMs are obtained from magnitude distance bin of M5.5R20 and the signal processing is applied as explained in Section 1.2.1. The modifications in Methods C and D are applied according to the target, which is the median of AK2014 for the earthquake scenario of M5.5R20, Vs450, and normal fault. The red dashed lines show half sigma around the median of AK2014. The amount of GMs is given for the methods.

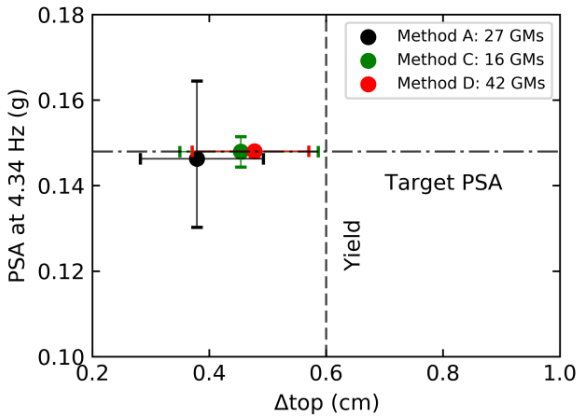

(e) S4: 2-Story Masonry Model

Figure C.3.3: Distribution of PSAs at f0 in Methods A, B, C, and D and the corresponding roof displacements (Δtop) of the complex models. PSAs at f0 are shown on the y-axis. The target PSA at f0 is plotted in the horizontal dashed line. The x-axis illustrates the maximum absolute of Δtop. The yielding limit is plotted with the vertical dashed lines. The 16th and 84th percentiles of the distributions are shown with the horizontal bars (for PSAs at f0) and the vertical bars (for Δtop). The mean of the distribution is shown with the filled circle. The target is the median of AK2014 for the scenario of M5.5R20, Vs450, and normal fault. The color code represents the method as in the legend. GMs in MA and MC are selected if they are within ±15% of the target PSA at 4.34 Hz (horizontal dashed line). GMs in MD have PSAs at f0 between ±20% of the target PSA at f0. The amount of data is given in the legend.

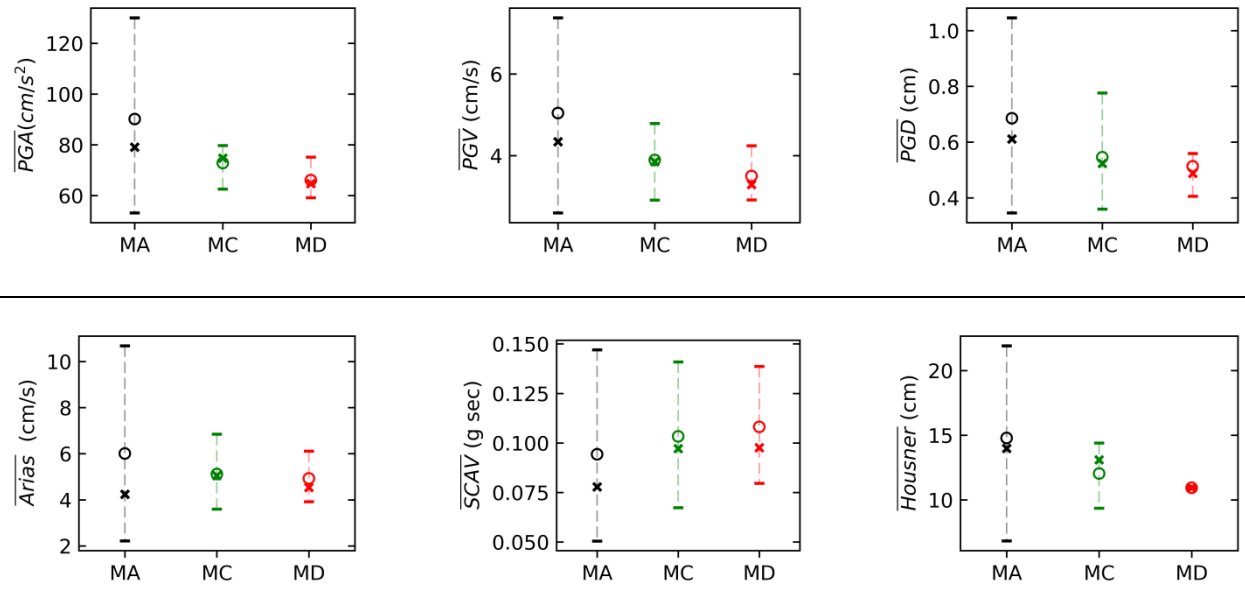

Figure C.3.4: Intensity measures obtained by Method A in black, Method C in green, and Method D in red. The spectrum compatible selection is performed with +20% and -5% tolerances around the median target spectrum for MA and MC and ±5% tolerances for MD. The frequency range is from 0.50 Hz to 20.0 Hz. Each GM set is composed of 5 GM. All possible GM sets are collected. The target is the median of AK2014 for the scenario of M5.5R20 and Vs450. The y-axes plot intensity measures (IMs). The x-axes show the different methods. The 16th and 84th percentiles of the distributions are shown with the horizontal bars. The mean of the distribution is shown with the unfilled circle. The median is plotted with the cross marker.

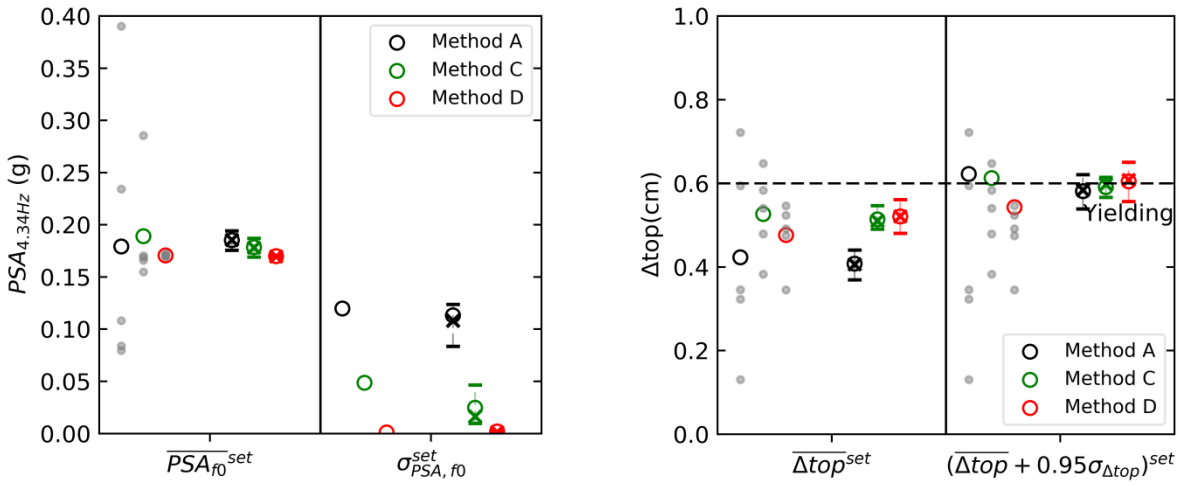

Figure C.3.5: Distribution of PSAs at 4.34 Hz and Δtop with a single set versus all sets for each GMSM method. The spectrum compatible selection is explained in Figure C.3.4. The single sets are obtained according to the RMS distance in Equation 1.8.1. Each grey dot shows the value of a GM. The mean of the set distribution is plotted with the unfilled circles. The median is shown with the cross markers. The 16th and 84th percentiles are plotted with the horizontal bars. The color code shows the method in the legend box.

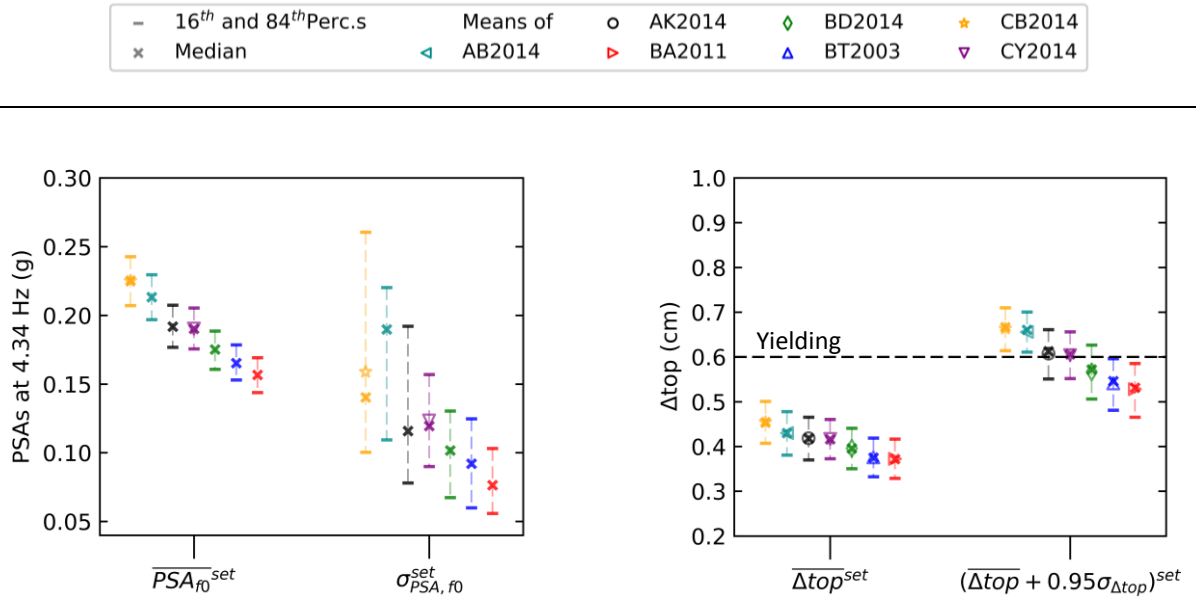

(a) PSAs at 1.00 Hz

(b) Δtop of the S4 model

Figure C.3.6: Impact of GMPEs on the distributions of PSAs at 4.34 Hz and Δtop of S4 Model. The spectrum compatible selection is explained in Figure C.3.4. The 16th and 84th percentiles are plotted with horizontal line markers. Medians are shown with cross markers. Means are demonstrated with the markers and colors in the legend box for corresponded GMPEs. The average of 5 GMs per set is shown. The average with 95% of standard deviation per set is also shown. The equivalent GMPE parameters are obtained in a similar way in Section 1.4.

BIBLIOGRAPHY

AASHTO (2010). *AASHTO LRFD Bridge Design Specifications.* American Association of State Highway and Transportation Officials (AASHTO), Washington D.C.

Abrahamson, N. A. (1992). Non-stationary spectral matching. *Seismological research letters*, 63(1):30.

Abrahamson, N. A., Coppersmith, K. J., Koller, M., Roth, P., Sprecher, C., Toro, G. R., & Youngs, R. (2004). Probabilistic seismic hazard analysis for Swiss nuclear power plant sites (PEGASOS Project). *Final Report prepared for the Unterausschuss Kernenergie (UAK) der Überlandwerke (UeW)*, 1–6.

Abrahamson N. A., Silva W. J., and Kamai R. (2014). Summary of the ASK14 Ground Motion Relation for Active Crustal Regions. *Earthquake Spectra*, Vol 30, No 3.

Akkar, S., Sandıkkaya, M. A., Şenyurt, M., Sisi, A. A., Ay, B. Ö., Traversa, P., ... & Godey, S. (2014). Reference database for seismic ground-motion in Europe (RESORCE). *Bulletin of earthquake engineering*, *12*(1), 311–339.

Akkar S., Sandikkaya M. A., and Bommer J. J. (2014). Empirical Ground-Motion Models for Point- and Extended- Source Crustal Earthquake Scenarios in Europe and the Middle East. *Bulletin of Earthquake Engineering* ,2014, 12(1): 359–387.

Al Atik, L. & Abrahamson, N. A., (2010). An improved method for nonstationary spectral matching. *Earthquake Spectra*, 26 (3), 601-617: doi: http://dx.doi.org/10.1193/1.3459159

Ambraseys N. N., Douglas J., Rinaldis D., Berge-Thierry C., Suhaloc P., Costa G., et al. (2004). Dissemination of European strong-motion data, vol. 2, CD-ROM collection. *Engineering and Physical Sciences Research Council*, UK.

Applied Technical Council (ATC). (1995*). Technical Report 19: Structural Response Modification.* Redwood City, CA.

Applied Technical Council (ATC). (2011). *Seismic Performance Assessment of Buildings, 90% Draft*, ATC-58-1. Redwood City, CA.

Arias, A. (1970). *A measure of earthquake intensity. in seismic design for nuclear power plants*, pages 438–483. R.J. Hansen. MIT Press. Cambridge, Mass.

ASCE (2005). *Seismic Design Criteria for Structures, Systems, and Components in Nuclear Facilities.* ASCE/SEI 43-05, American Society of Civil Engineers, Reston, VA.

ASCE (2007). *Seismic Rehabilitation of Existing Buildings.* ASCE/SEI 41-06, American Society of Civil Engineers, Reston, VA.

ASCE (2010). *Minimum Design Loads for Buildings and Other Structures.* ASCE/SEI 7-10, American Society of Civil Engineers, Reston, VA.

ASN/2/01 Guide. (2006). *Prise en compte du risque sismique à la conception des ouvrages de génie civil d'installations nucléaires de base à l'exception des stockages à long terme des déchets radioactifs* (Consideration of seismic risk for the design of civil engineering buildings of nuclear plants excepted long duration radioactive wastes disposal), published by Autorité de Sûreté Nucléaire (The French Nuclear Safety Authority).

Atkinson G. M. and Boore D. (2011). Modifications to Existing Ground-Motion Prediction Equations in Light of New Data. *Bulletin of the Seismological Society of America*, Vol 101, No. 3, p. 1121–1135.

Aubry D, Chouvet D, Modaressi A, Modaressi H. (1986) GEFDYN: Logiciel d'Analyse de Comportement Mécanique des Sols par Eléments Finis avec Prise en Compte du Couplage Sol-Eau-Air. Manuel Scientifique. Ecole Centrale Paris: LMSS-Mat.

Aubry, D., & Modaressi, A. (1996). GEFDYN, Manuel Scientifique.

Ay, B. Ö., & Akkar, S. (2012). A procedure on ground motion selection and scaling for nonlinear response of simple structural systems. *Earthquake Engineering & Structural Dynamics*, *41*(12), 1693-1707.

Ay, B. Ö., & Akkar, S. (2013). Evaluation of a recently proposed record selection and scaling procedure for low-rise to mid-rise reinforced concrete buildings and its use for probabilistic risk assessment studies. *Earthquake Engineering & Structural Dynamics*, *43*(6), 889-908.

Baker, J. W. (2007). Probabilistic structural response assessment using vector-valued intensity measures. *Earthquake Engineering & Structural Dynamics*, *36*(13), 1861-1883.

Baker, J. W. (2011). Conditional mean spectrum: Tool for ground-motion selection. *Journal of Structural Engineering*, *137*(3), 322–331.

Baker, J. W., & Cornell, CA. (2005). A vector-valued ground motion intensity measure consisting of spectral acceleration and epsilon. *Earthquake Engineering & Structural Dynamics*, *34*(10), 1193-1217.

Baker, J. W., & Lee, C. (2017). An Improved Algorithm for Selecting Ground Motions to Match a Conditional Spectrum. *Journal of Earthquake Engineering*, 1-16.

Bazzurro P, & Cornell CA. (1994a). Seismic hazard analysis of nonlinear structures, I: methodology. *Journal of Structural Engineering*, 120(11):3320–44.

Bazzurro P, & Cornell CA. (1994b). Seismic hazard analysis of nonlinear structures, II: applications. *Journal of Structural Engineering*, 120(11):3345–65.

Berge-Thierry C., Cotton F., Scotti O., Griot-Pommera D. A., Fukushima Y. (2003). New empirical response spectral attenuation laws for moderate European earthquakes. *Journal of Earthquake Engineering*, vol. 7, n° 2, 2003, p. 193–222.

Berge-Thierry, C., Hollender, F., Guyonnet-Benaize, C., Baumont, D., Ameri, G., & Bollinger, L. (2017). Challenges ahead for nuclear facility site-specific seismic hazard assessment in France: The alternative energies and the Atomic Energy Commission (CEA) Vision. *Pure and Applied Geophysics*, *174*(9), 3609-3633.

Beyer, K., & Bommer, J. J. (2007). Selection and scaling of real accelerograms for bi-directional loading: a review of current practice and code provisions. *Journal of Earthquake Engineering*, *11*(S1), 13–45.

Bindi D., Massa M., Luzi L., Ameri G., Pacor F. , Puglia R. and Augliera P. (2014). Pan-European ground motion prediction equations for the average horizontal component of PGA, PGV and 5 %-damped PSA at spectral periods of up to 3.0 s using the RESORCE dataset. *Bulletin of Earthquake Engineering*, 12(1), 391–340.

Bommer, J. J. (2002). Deterministic vs. probabilistic seismic hazard assessment: an exaggerated and obstructive dichotomy. *Journal of Earthquake Engineering*, *6*, 43-73.

Bommer, J. J., & Acevedo, A. B. (2004). The use of real earthquake accelerograms as input to dynamic analysis. *Journal of Earthquake Engineering*, *8*, 43–91.

Boore D. M. (2001). Effect of Baseline Corrections on Displacements and Response Spectra for Several Recordings of the 1999 Chi-Chi, Taiwan, Earthquake. *Bulletin of the Seismological Society of America*, **91** (5): 1199–1211.

Boore, D. M., & Akkar, S. (2003). Effect of causal and acausal filters on elastic and inelastic response spectra. *Earthquake engineering & structural dynamics*, *32*(11), 1729–1748.

Boore, D., and Atkinson G. (2008). Ground-motion prediction equations for the average horizontal component of PGA, PGV, and 5%-damped PSA at spectral periods between 0.01 s and 10.0 s. *Earthquake Spectra,* 24, 99–138

Boore D. M. and Bommer J. J. (2005). Processing of strong-motion accelerograms: needs, options and consequences. *Soil Dynamics and Earthquake Engineering*, **25**: 93–115.

Bradley, B. A., Dhakal, R. P., MacRae, G. A. and Cubrinovski, M. (2010). Prediction of spatially distributed seismic demands in specific structures: Ground motion and structural response. *Earthquake Engng. Struct. Dyn*., 39: 501–520. doi:10.1002/eqe.954

Buratti N, Stafford PJ, Bommer JJ. (2011). Earthquake accelerogram selection an scaling procedures for estimating the distribution of drift response. *J Struct Eng,* 137(3):345–57.

Burks L. S. and Baker J. W. (2014). Fling in near-fault ground motions and its effect on structural collapse capacity. *Tenth U.S. National Conference on Earthquake Engineering Frontiers of Earthquake Engineering*, July 21–25, Anchorage, Alaska.

Burks L. S. and Baker J. W. (2016). A predictive model for fling-step in near-fault ground motions based on recordings and simulations. *Soil Dynamics and Earthquake Engineering,* **80**: 119–126.

Campbell K. W. and Bozorgnia Y. (2014). NGA-West2 Ground Motion Model for the Average Horizontal Components of PGA, PGV, and 5 % Damped Linear Acceleration Response Spectra. *Earthquake Spectra*, Volume 30, Number 3, p. 1087 - 1115.

Carballo, J. E. and Cornell, C. A. (2000). *Probabilistic seismic demand analysis: Spectrum matching and design*. Report No. RMS-41, Department of Civil and Environmental Engineering, Reliability of Marine Structures Program, Stanford University, Stanford, CA.

Causse, M., Laurendeau A., Perrault M., Douglas J., Bonilla L. F., and Guéguen P. (2013). Eurocode 8-compatible synthetic time-series as input to dynamic analysis. *Bulletin of Earthquake Engineering*; **12 (***2)*.

CEA (2007). *Calculs Dynamiques Des Portiques IRSN Sous Chargements Sismiques*. CEA Report SEMT/EMSI/RT/07-026/A. Commissariat à l'énergie atomique (CEA).

CEA (2015). Cast3M v15 web site via http://www-cast3m.cea.fr/ .Commissariat à l'énergie atomique (CEA).

CEN (2004). Eurocode 8: Design of Structures for Earthquake Resistance, Part 1: General Rules, Seismic Actions and Rules for Buildings. European Norms 1998.

Chiou, B. S. J., & Youngs, R. R. (2014). Update of the Chiou and Youngs NGA model for the average horizontal component of peak ground motion and response spectra. *Earthquake Spectra*, *30*(3), 1117–1153.

Chopra A. (2012). *Dynamics of Structures: Theory and Applications to Earthquake Engineering*. Fourth Edition, Upper Saddle River, NJ: Prentice-Hall, 844 p.

De Biasio, M., Grange, S., Dufour, F., Allain, F., & Petre-Lazar, I. (2014). A simple and efficient intensity measure to account for nonlinear structural behavior. *Earthquake Spectra*, *30*(4), 1403–1426.

Dobry, R., Idriss I. M. and E. Ng (1978). Duration characteristics of horizontal components of strong-motion earthquake records. *Bull. Seis. Soc. Am.*, Vol. 68, No. 5, pp. 1487–1520.

Douglas J. (2017). Ground Motion Prediction Equations 1964-2017, 5th December 2017, Glasgow, United Kingdom, (accessed via http://gmpe.org.uk/gmpereport2014.pdf).

Douglas J., Akkar S., Ameri G., Bard P.Y., Bindi D., Bommer J.J., Bora S.S., Cotton F., Derras B., Hermkes M., Kuehn N.M., Luzi L., Massa M., Pacor F., Riggelsen C., Sandıkkaya M.A., Scherbaum F., Stafford P.J., Traversa P. (2014). Comparisons among the five ground-motion models developed using RESORCE for the prediction of response spectral accelerations due to earthquakes in Europe and the Middle East. *Bulletin of earthquake engineering*, *12*(1), 341-358.

Douglas, J., & Aochi, H. (2008). A survey of techniques for predicting earthquake ground motions for engineering purposes. *Surveys in Geophysics*, *29*(3), 187.

Electrical Power Research Institute (EPRI) (1991). *Standardization of the Cumulative Absolute Velocity*. EPRI TR-100082, Palo Alto, CA.

Electrical Power Research Institute (EPRI) (2006). *Program on Technology Innovation: Use of Cumulative Absolute Velocity (CAV) in Determining Effects of Small Magnitude Earthquakes on Seismic Hazard Analyses*. EPRI 1014099, Palo Alto, CA.

FEMA (2009). "*Effects of Strength and Stiffness Degradation on Seismic Response"*, FEMA P440A, Prepared by the Applied Technology Council for the Federal Emergency Management Agency, Washington, D.C.

FEMA (2012). "*Seismic Performance Assessment of Building",* FEMA P-58-1, Prepared by the Applied Technology Council for the Federal Emergency Management Agency, Washington, D.C.

Ferrario, E., Pedroni, N., Zio, E., & Lopez-Caballero, F. (2017). Bootstrapped Artificial Neural Networks for the seismic analysis of structural systems. *Structural Safety*, *67*, 70-84.

Gasparini, D. A. and Vanmarcke, E. H. (1976). *SIMQKE: A Program for Artificial Motion Generation*. Technical report, Cambridge, MA.

Giberson M. (1969). Two non-linear beams with definitions of ductility. *J Struct Div ASCE*, 95(2):137–57.

Grant, D. N. and Diaferia, R. (2013). Assessing adequacy of spectrum-matched ground motions for response history analysis. *Earthquake Engineering & Structural Dynamics*, 42(9):1265–1280.

Grigoriu, M. (2011). To Scale or Not to Scale Seismic Ground Acceleration Records. *Journal of Engineering Mechanics*, 137(4) : 284–293.

Haddadi H., Shakal A., Huang M. , Parrish J. , Stephens C. , Savage W. U. , and Leith W. S. (2012). Report on progress at the Center for Engineering Strong Motion Data (CESMD). *The 15th World Conference on Earthquake Engineering*, Portugal, September 24–28, 2012.

Hancock J, Bommer J. J. (2006). Using matched records to explore the influence of strong-motion duration on inelastic structural response. *Soil Dynamics and Earthquake Engineering*; 27:291–9.

Hancock, J., Bommer, J. J., and Stafford, P. J. (2008). Numbers of scaled and matched accelerograms required for inelastic dynamic analyses. *Earthquake Engineering & Structural Dynamics*, 37(14):1585–1607.

Hancock, J., Watson-Lamprey, J., Abrahamson, N., Bommer, J. J., Markatis, A., McCoy, E., and Mendis, R. (2006). An improved method of matching response spectra of recorded earthquake ground motion using wavelets. *J. Earth. Eng*., 10:67–89.

Haselton, C. B., Baker, J. W., Bozorgnia, Y., Goulet, C. A., Kalkan, E., Luco, N., ... & Watson-Lamprey, J. (2009). Evaluation of ground motion selection and modification methods: Predicting median interstory drift response of buildings. *PEER Report 2009*, *1*.

Heo, Y., Kunnath, S., and Abrahamson, N. (2011). Amplitude-Scaled versus Spectrum-Matched Ground Motions for Seismic Performance Assessment. *Journal of Structural Engineering*, 137(3):278–288.

Housner, G. W., & Jennings, P. C. (1964). Generation of artificial earthquakes. *Journal of the Engineering Mechanics Division*, *90*(1), 113–152.

Huang, Y.-N., Whittaker, A. S., Luco, N., and Hamburger, R. O. (2011). Scaling Earthquake Ground Motions for Performance-Based Assessment of Buildings. *Journal of Structural Engineering*, 137(3):311–321.

Iervolino, I., & Cornell, C. A. (2005). Record selection for nonlinear seismic analysis of structures. *Earthquake Spectra*, *21*(3), 685–713.

Iervolino, I., De Luca, F., and Cosenza, E. (2010a). Spectral shape-based assessment of SDOF nonlinear response to real, adjusted and artificial accelerograms. *Engineering Structures*, 32(9):2776–2792.

Iervolino, I., Galasso, C., & Cosenza, E. (2010b). REXEL: computer-aided record selection for code-based seismic structural analysis. *Bulletin of Earthquake Engineering*, *8*(2), 339-362.

Isbiliroglu, L. (2016). “Strategy for selecting input ground motion for structural seismic demand analysis: Rapport de première année de thèse”, *IRSN Report,* RT 2016-00004.

Jayaram N, Lin T, Baker J. (2011). A computationally efficient ground-motion selection algorithm for matching a target response spectrum mean and variance. *Earthquake Spectra*, 27:797–815.

Kaklamanos, J., Baise L. G., and Boore D. M. (2011). Estimating Unknown Input Parameters When Implementing the NGA Ground-Motion Prediction Equations in Engineering Practice, *Earthquake Spectra,* Volume 27, Number 4, p. 1219 - 1235.

Kalkan, E., & Chopra, A. K. (2011). Modal-pushover-based ground-motion scaling procedure. *Journal of structural engineering*, *137*(3), 298-310.

Kanlı, A. I., Tildy, P., Prónay, Z., Pınar, A., & Hermann, L. (2006). VS 30 mapping and soil classification for seismic site effect evaluation in Dinar region, SW Turkey. *Geophysical Journal International*, *165*(1), 223-235.

Kappos, A. (2001). *Dynamic loading and design of structures*. CRC Press.

Katsanos, E. I., Sextos, A. G., & Manolis, G. D. (2010). Selection of earthquake ground motion records: A state-of-the-art review from a structural engineering perspective. *Soil Dynamics and Earthquake Engineering*, *30*(4), 157-169.

Katsanos, E. I., & Sextos, A. G. (2013). ISSARS: An integrated software environment for structure-specific earthquake ground motion selection. *Advances in Engineering Software*, *58*, 70–85.

Kaul, M. K. (1978). Spectrum-consistent time-history generation. *Journal of the Engineering Mechanics Division*, 104(4):781–788.

Kohrangi, M., Bazzurro, P., & Vamvatsikos, D. (2016). Vector and scalar IMs in structural response estimation, Part II: Building demand assessment. *Earthquake Spectra*, *32*(3), 1525–1543.

Kottke A, Rathje EM. (2008). A semi-automated procedure for selecting and scaling recorded earthquake motions for dynamic analysis. *Earthquake Spectra,* 2008;24(4):911–32.

Krinitzsky, E. L. (1995). Deterministic versus probabilistic seismic hazard analysis for critical structures. *Engineering Geology*, *40*(1-2), 1-7.

Krinitzsky, E. L. (2002). How to obtain earthquake ground motions for engineering design. *Engineering Geology*, *65*(1), 1-16.

Kwon, O. S., & Elnashai, A. (2006). The effect of material and ground motion uncertainty on the seismic vulnerability curves of RC structure. *Engineering Structures*, *28*(2), 289-303.

Kwong, N. S. and Chopra A. K. (2015). *Selection and scaling of ground motions for nonlinear response history analysis of buildings in performance-based earthquake engineering*. PEER Report No. 2015/11, University of California, Berkeley.

Lai C. G., Corigliano M., Rota M., Strobbiad C. L. (2012). ASCONA: Automated Selection of COmpatible Natural Accelerograms, *Earthquake Spectra* 28, 3, p. 965–987.

Lancieri, M., Renault, M., Berge-Thierry, C., Gueguen, P., Baumont, D., & Perrault, M. (2015). Strategy for the selection of input ground motion for inelastic structural response analysis based on naïve Bayesian classifier. *Bulletin of Earthquake Engineering*, *13*(9), 2517-2546.

Lilhanand, K. and Tseng, W. S. (1988). Development and application of realistic earthquake time histories compatible with multiple-damping design spectra. In *9th World Conference on Earthquake Engineering*, Tokyo, Japan.

Lopez-Caballero, F., Modaressi-Farahmand-Razavi, A., & Tabbakhha, M. (2011). Effects of soil foundation on the performance of masonry buildings. In *Proceedings of the 8th International Conference on Structural Dynamics, EURODYN*.

Luco N., & Bazzurro P. (2007). Does amplitude scaling of ground motion records result in biased nonlinear structural drift responses?, *Earthq Eng Struct Dyn* ;36 (13): 1813–35.

Luzi, L., Puglia, R., Russo, E., D'Amico, M., Felicetta, C., Pacor, F., ... & Duni, L. (2016). The Engineering Strong-Motion Database: A Platform to Access Pan-European Accelerometric Data. *Seismological Research Letters*.

Marante M, Suárez L, Quero L, Redondo J, Vera J, Uzcátegui M, Delgado S, León L, Núñez L, Flórez-López J. (2005). Portal of damage: a web-based finite element program for the analysis of framed structures subjected to overloads. *Adv Eng Softw,* 36(5):346–58.

Mazzoni, S., McKenna, F., Scott, M. H., & Fenves, G. L. (2006). The Open System for Earthquake Engineering Simulation (OpenSEES) User Command-Language Manual.

McGuire, R. K. (1995). Probabilistic seismic hazard analysis and design earthquakes: closing the loop. *Bulletin of the Seismological Society of America*, *85*(5), 1275-1284.

Naeim, F., Alimoradi, A., & Pezeshk, S. (2004). Selection and scaling of ground motion time histories for structural design using genetic algorithms. *Earthquake Spectra*, *20*(2), 413-426.

NIST (2011). *Selecting and Scaling Earthquake Ground Motions for Performing Response-History Analyses*. NIST GCR 11-917-15, Prepared by the NEHRP Consultants Joint Venture: A Partnership of the Applied Technology Council and the Consortium of Universities for Research in Earthquake Engineering, Gaithersburg, Maryland.

Padgett, J. E., & DesRoches, R. (2007). Sensitivity of seismic response and fragility to parameter uncertainty. *Journal of Structural Engineering*, *133*(12), 1710-1718.

Pagani M., Monelli D., Weatherill G., Danciu L., Crowley H., Silva V., Henshaw P., Butler L., Nastasi M., Panzeri L., Simionato M., and Vigano D. (2014). OpenQuake Engine: An Open Hazard (and Risk) Software for the Global Earthquake Model, *Seismological Research Letters, 85 (3).*

Park, Y. and Ang, A. (1985). Mechanistic seismic damage model for reinforced concrete, *Journal of Structural Engineering*, ASCE, 111(4):722–739.

Park Y. J, Ang A. H-S & Wen Y.K. (1987). Damage-limiting aseismic design of buildings. *Earthquake Spectra*: 3(1): 1–26.

PEER (2013). *PEER NGA-West2 Database*, prepared for the Pacific Earthquake Engineering Research Center, University of California, Berkeley.

PEER (2014). *PEER NGA-East Database*, prepared for the Pacific Earthquake Engineering Research Center, University of California, Berkeley.

Prakash V, Powel G, Campbell S. (1993). DRAIN 2D-X: base program description and user guide. Dept. of Civil Engineering, University of California, Berkeley; 1993.

Reiter, L. (1991). *Earthquake hazard analysis: issues and insights*. Columbia University Press.

RFS 2001-01 (2001). *Règle fondamentale de sûreté n°2001-01* (French Safety Rule), published by Autorité de Sûreté Nucléaire (The French Nuclear Safety Authority).

Rizzo, P. C., Shaw, D. E., and Jarecki, S. J. (1975). Development of real/synthetic time histories to match smooth design spectra. *Nuclear Engineering and Design*, 32(1):148–155.

Sáez E. (2009). Dynamic non-linear soil-structure interaction. *Ph.D. thesis*, Ecole Centrale Paris, Châtenay-Malabry, FR.

Sáez, E., Lopez-Caballero, F., & Modaressi-Farahmand-Razavi, A. (2011). Effect of the inelastic dynamic soil-structure interaction on the seismic vulnerability assessment. *Structural safety*, *33*(1), 51-63.

Sáez, E., Lopez-Caballero, F., & Modaressi-Farahmand-Razavi, A. (2013). Inelastic dynamic soil-structure interaction effects on moment-resisting frame buildings. *Engineering structures*, *51*, 166-177.

Scherbaum F., Schmedes J., Cotton F. (2004). On the Conversion of Source-to-Site Distance Measures for Extended Earthquake Source Models, *Bulletin of the Seismological Society of America*; **94** (3): 1053–1069.

Scordilis, E. M., (2006). Empirical global relations converting MS and mb to moment magnitude, *J. Seismology*. 10, 22–236.

Seifried, A. E. (2013). Response spectrum compatibilization and its impact on structural response assessment, *Ph.D. Thesis*, Dept. of Civil and Environmental Engineering, Stanford University, Stanford, CA.

Seifried, A. E., & Baker, J. W. (2016). Spectral variability and its relationship to structural response estimated from scaled and spectrum-matched ground motions. *Earthquake Spectra*, *32*(4), 2191-2205.

Sextos, A. G., Katsanos, E. I., & Manolis, G. D. (2011). EC8-based earthquake record selection procedure evaluation: Validation study based on observed damage of an irregular R/C building. *Soil Dynamics and Earthquake Engineering*, *31*(4), 583-597.

Sextos, A. G. (2014). Selection of Ground Motions for Response History Analysis. *Encycl Earthq Eng*, 1-11.

Shome, N., & Cornell, C. A. (1998). Normalization and scaling accelerograms for nonlinear structural analysis. In *Sixth US national conference on earthquake engineering, Seattle, WA*.

Shome, N., Cornell, C. A., Bazzurro, P., & Carballo, J. E. (1998). Earthquakes, records, and nonlinear responses. *Earthquake Spectra*, *14*(3), 469-500.

Silva, W. J., & Lee, K. (1987). *State-of-the-Art for Assessing Earthquake Hazards in the United States. Report 24. WES RASCAL Code for Synthesizing Earthquake Ground Motions*. Walnut Creek, CA.

Singh, J. P. (1985). Earthquake ground motions: implications for designing structures and reconciling structural damage. *Earthquake Spectra*, *1*(2), 239-270.

Smerzini, C., Galasso, C., Iervolino, I., & Paolucci, R. (2014). Ground motion record selection based on broadband spectral compatibility. *Earthquake Spectra*, *30*(4), 1427-1448.

Stewart JP, Chiou SJ, Bray RW, Graves P, Somerville G, Abrahamson NA. Ground motion evaluation procedures for performance-based design. *PEER report 2001/09,* Pacific Earthquake Engineering Research Center, University of California, Berkeley, 2001.

Trifunac M. D. (2003). 70th Anniversary Of Biot Spectrum, *ISET Journal of Earthquake Technology,* Paper No. 431, Vol. 40, No. 1, March 2003, pp. 19-50.

Trifunac, M. D. (2012). Earthquake response spectra for performance-based design—A critical review. *Soil Dynamics and Earthquake Engineering*, *37*, 73-83.

Vanmarcke E. H. (1979). State-of-the-art for assessing earthquake hazards in the United States: representation of earthquake ground motion: scaled accelerograms and equivalent response spectra. *Miscellaneous paper* S-73-1, Report 12, US Army Corps of engineers waterways experiment station, Vicksburg, Mississippi.

Von Thun, J. L., Rochim, L. H., Scott, G. A., and Wilson, J. A. (1988). Earthquake ground motions for design and analysis of dams, *Earthquake Eng. Soil Dyn. II—Recent Advances in Ground-Motion Evaluation (GSP 20),* ASCE, New York, 463–481.

Wang, Z. (2010). Seismic hazard assessment: issues and alternatives. *Pure and Applied Geophysics*, *168*(1-2), 11-25.

Wang, G. (2011). A ground motion selection and modification method capturing response spectrum characteristics and variability of scenario earthquakes. *Soil Dynamics and Earthquake Engineering*, 31(4):611–625.

Wang, G., Youngs, R., Power, M., & Li, Z. (2015). Design ground motion library: an interactive tool for selecting earthquake ground motions. *Earthquake Spectra*, *31*(2), 617–635.

Watson-Lamprey, J. and Abrahamson, N. (2006). Selection of ground motion time series and limits on scaling. Soil Dynamics and Earthquake Engineering, 26(5):477–482.

Youngs, R., Power, M., Wang, G., Makdisi, F., & Chin, C. C. (2007). Design ground motion library (DGML)–tool for selecting time history records for specific engineering applications. In *SMIP07 Seminar on Utilization of Strong-Motion Data* (pp. 109-110). Sacramento, CA: California Geological Survey.

Zentner, I. (2014). A procedure for simulating synthetic accelerograms compatible with correlated and conditional probabilistic response spectra. *Soil Dynamics and Earthquake Engineering*, *63*, 226-233.

Zhai, C., Chang, Z., Li, S., & Xie, L. (2013). Selection of the most unfavorable real ground motions for low-and mid-rise RC frame structures. *Journal of Earthquake Engineering*, *17*(8), 1233-1251.

Zhu, T. J., Heidebrecht, A. C., & Tso, W. K. (1988). Effect of peak ground acceleration to velocity ratio on ductility demand of inelastic systems. *Earthquake engineering & structural dynamics*, *16*(1), 63-79.